Technical Report
RAL-TR-2000-020

CLRC

Vesuvio Workshop Proceedings

A L Fielding

19th June 2000

COUNCIL FOR THE CENTRAL LABORATORY OF THE RESEARCH COUNCILS

VESUVIO WORKSHOP

The Cosener's House, Abingdon

26/27 th November 1999

Speakers Notes

Edited by A.Fielding

Contents

VESUVIO Workshop Program

Friday 26th November 1999

11:00 Coffee and Registration.

11:30 Session 1. Introduction
Chair W G Stirling

11:30 Welcome.
A.D.Taylor (ISIS Facility, UK)

11:45 History of Neutron Compton Scattering.
H.R. Glyde, (University of Delaware, USA)

12:10 Description of the current eVS instrument.
J.Mayers (ISIS Facility, UK)

12:35 Introduction to the VESUVIO project.
C. Andreani (Universitá di Tor Vergata, Rome, Italy)

12:50 Lunch

14:00 Session 2. Examples of eVS Measurements.
Chair R Simmons

14:00 eVS measurements on the kinetic energy of helium
M.Zoppi (CNR-IEQ, Florence, Italy).

14:20 eVS measurements on Catalysts
P Mitchell (Department of Chemistry, Reading University, UK)

14:40 Final State Effects and anharmonicity in Graphite
D Timms (Department of Physics, Portsmouth University, UK)

15:00 eVS measurements and neutron spectroscopy.
F Fillaux (CNRS, Paris, France)

15:20 eVS Measurements on Glasses and high T_c superconductors
F Mompean (Instituto de Ciencias de Materiales de Madrid, Spain)

15:40 Measurements and Calculations on H2/D2
D.Colognesi (CNR,GNSM Rome, Italy)

16:00 Coffee

16:30 Session 3: Instrument Hardware and Software. Chair C Andreani

16:30 Critical review of eVS data analysis.
D Sivia (ISIS Facility, UK)

16:50 Multiple scattering corrections and instrument resolution calibration.
A Fielding (Liverpool University,UK)

17:10 Planned improvements in count rate. Description of detector tests. Limitations of current eVS detectors. How these will be improved.
R Senesi (Universitá di Tor Vergata, Rome,Italy)

17:40 Panel Discussion: (*J Mayers, ,J Tomkinson, J Norris, N Rhodes, M Zoppi, C Andreani, R Simmons, W G Stirling)*

18:30 End of Session

20:00 Dinner.

Saturday 27th November 1999

9:00 "Adventurous" experiments and new possibilities. Chair H Glyde

09:00 Measurement of Atomic Kinetic Energies using synchrotron radiation
A Cunsolo, (ESRF, Grenoble, France)

09:30 Quantum Correlations in condensed matter revealed by Neutron Compton scattering.
E. Karlsson (Department of Physics, Uppsala University, Sweden)

10:05 Reconstruction of proton momentum distributions and wave functions from eVS data
G. Reiter (University of Houston, USA)

10:35 Coffee.

11:05 Panel Discussion. (*G Reiter, H Glyde, R Simmons, W G Stirling, J Mayers, C Andreani, J Tomkinson)*

12:30 Lunch.

Vesuvio Workshop

Cosener's House, Abingdon. 26/27 November 1999

Friday 26th November Session 1

Chair: W.G. Stirling

The morning session began with a warm welcome and introduction from John Tomkinson to over 30 participants who had travelled from the UK, Europe and the USA. The first session, chaired by Bill Stirling from the University of Liverpool, began with an introduction to the technique of neutron Compton scattering (NCS) by Henry Glyde from the University of Delaware. He introduced the concepts of the impulse approximation (IA) and Final State effects (FSE) and how expanding the scattering function can give direct information on the momentum distribution n(p), as well as FSE. Finally he gave a brief historical sketch of the key theories and measurements that have brought the technique to where it is today.

This was followed by a talk by Jerry Mayers, the instrument scientist of the eVS spectrometer. He described the current status of the instrument describing the filter difference technique and how eVS can measure J(y) and mean kinetic energies. He gave illustrations of some key measurements on molecular hydrogen and ^{4}He. He concluded by introducing the VESUVIO project.

Carla Andreani concluded the morning session by describing in more detail the VESUVIO project and what it aims to deliver. This includes

- Improvement of count rate.
- Improvement of resolution.
- Developing a theoretical framework for NCS.
- Test experiments quantum fluids and molecular systems.
- Possibility of measuring eV magnetic and electronic excitations.
- Training of young scientists.

Afternoon Session 2

Chair: R. Simmons

The first afternoon session was chaired by Ralph Simmons from the University of Illinois and included a series of talks that reported the results of some of the successful eVS measurements that have been performed over the last 5 years. Marco Zoppi from CNR-IEQ in Florence showed the results of his groups work on the study of the kinetic energy of solid and liquid helium as a function of density. Phil Mitchell of the University of Reading talked about the information that the NCS technique can give chemists with particular emphasis on his measurements on hydrogen in catalysts and xenon in catalysts. Dave Timms from the University of Portsmouth presented results of a series of measurements that have been carried out on pyrolytic graphite. Pyrolytic graphite has a highly anisotropic momentum distribution and this was measured as a function of temperature. An anisotropy in the $\langle\nabla^2 V\rangle$ was also measured from the final state effects. Francois Fillaux of the CNRS, Paris, gave a talk that showed how eV spectroscopy can complement other neutron spectroscopy techniques in helping chemists understand the hydrogen bond. Federico Mompean of the Institute of Materials Sciences, Madrid presented results of a series of measurements on glass systems and also the high T_c superconductor PrBaCuFeO that were made using the eVS. Daniele Colognesi of CNR, GNSM , Rome and ISIS gave a talk on work that has been carried out on molecular hydrogen and deuterium. He compared experimental data with existing theories on these systems and also new theories that have recently been developed. Finally, to conclude the session Aris Dreismann of T.U. Berlin gave an impromptu presentation of some new results on the quantum entanglement of the proton and deuteron in the H_2/D_2 system that showed significant anomalies in the measured cross-section of the proton.

The final session of the afternoon was given over to talks on instrument hardware and software and was chaired by Carla Andreani. Davinder Sivia from the ISIS Facility gave a critical review of the eVS data analysis procedures in the Bayesian framework. Andrew Fielding of the University of Liverpool and ISIS gave a presentation describing the procedures that are used to calibrate the eVS. This included the calibration of detector positions as well as the instrument resolution and energies of

the analyser foils. Roberto Senesi from the Universita di Tor Vergata, Rome gave an account of work that is currently ongoing regarding the development of the new detector bank as part of the VESUVIO workshop. Tests that have already been carried out as well as planned tests that will explore the possibilities for optimisation of all aspects of the detectors and electronics in eV neutron spectroscopy were discussed.

Saturday 27th November

Morning Session

The title of this session, chaired by Henry Glyde, was *Adventurous experiments and new possibilities*. The first speaker was Alessandro Cunsolo from the ESRF, Grenoble who spoke about the technique of measuring atomic kinetic energies using inelastic x-ray scattering. Results were shown of measurements made on ^{3}He and ^{4}He as a function of temperature and density in the q range 7.8 – 24 $Å^{-1}$. Erik Karlsson from Uppsala University spoke of recent results on quantum correlation's in condensed matter that have been revealed using the technique of NCS. Anomalies in the measured cross-sections made on H_2O-D_2O mixtures and Nb Hydrides/Deuterides have been observed. He spoke of new work to develop a possible theory to explain the anomalies. The final talk of the morning was given by George Reiter of the University of Houston on recent developments in the work he has carried out with Jerry Mayers in developing the technique of reconstructing n(p) from measurements made on eVS. Software is now available that allows the n(p) to be reconstructed from eVS J(y) measurements by fitting a sum of Hermite polynomials to the data. The n(p) can then be simply reconstructed from the fit coefficients.

Panel Discussion

A lively open discussion rounded off the two day workshop during which a number of issues were discussed.

The reproducibility of eVS measurements was discussed at various times through the two days. In particular it should be possible to have the detectors in a few fixed positions so that measurements can be easily reproduced. However, the point was made that measurements on the inert gases/solids taken over many years, with slightly different detector geometry's have shown good consistency.

The question of how well the resolution function is known for measurements on helium was raised and discussed. The question seemed to be, is the resolution obtained using the eVS calibration procedures understood well enough to allow lineshape analysis and accurate kinetic energies or is a more complicated calculation of the lineshape of the instrumental resolution required. It was agreed that more work on simulating the instrument response would be useful.

A number of talks during the workshop showed the potential of electron volt spectroscopy for measurements on oxygen and carbon. The point was made that for such measurements vanadium and niobium cans (rather than the standard aluminium) would simplify the data analysis due to the better mass separation between the background and carbon/oxygen peaks.

VESUVIO WORKSHOP - List of Participants

Name and Address	e-mail
C. Andreani Dipartimento di Fisica Universito di Roma Tor Vergata Via R. Scientifica 1 00133 Roma Italy	Andre@roma2.infn.it
C.A. Dreismann I.N. Stranski Institute T.U. Berlin Strasse des 17 Juni 112 D-10623 Berlin Germany	Dreismann@chem.tu-berlin.de
W.G. Stirling Department of Physics University of Liverpool Liverpool L69 7ZE UK	Stirling@liv.ac.uk
D.K. Ross Joule Physics Laboratory University of Salford Salford M5 4WT UK	d.k.ross@salford.ac.uk
Henry Glyde Department of Physics & Astronomy University of Delaware Newark Delaware 19711 USA Tel: 302-831-3361 Fax: 302-831-1637	glyde@udel.edu
F. Fillaux LADIR-CNRS Rue H. Dunant 94320 Thiais France	fillaux@gest.cnrs.fr
John Tomkinson ISIS Facility Rutherford Appleton Laboratory Chilton Didcot Oxfordshire OX11 0QX UK	j.tomkinson@rl.ac.uk

Jerry Mayers ISIS Facility Rutherford Appleton Laboratory Chilton Didcot Oxfordshire OX11 0QX UK	j.mayers@rl.ac.uk
George Reiter Department of Physics University of Houston	Greiter@uh.edu
Davinder Sivia ISIS Facility Rutherford Appleton Laboratory Chilton Didcot Oxfordshire OX11 0QX UK	dss@isise.rl.ac.uk
Roberto Senesi INFM Roma Tor Vergata Via R. Scientifica 1 00133 Roma Italy	Senesi@roma2.infn.it
Daniele Colognesi CNR (Italy) c/o ISIS Facility Rutherford Appleton Laboratory Chilton Didcot Oxfordshire OX11 0QX UK	Dc@isise.rl.ac.uk
Alessandro Cunsolo Dipartimento di Fisica, Universita' di Roma Tre Via della Vasca Navale 84 00146 Roma Italy Tel: +39-06-55177229 Fax: +39-06-5579303	Cunsolo@amaldi.fis.uniroma3.it
Friedrich Streffer Hahn Meitner Institut Abt. NI Glienicker Str. 100 14109 Berlin Germany fon: +49 30 8062 3076 fax: +49 30 8062 2523	Streffer@hmi.de

Mark Telling ISIS Facility Rutherford Appleton Laboratory Chilton Didcot Oxfordshire OX11 0QX UK	m.telling@rl.ac.uk
Richard Azuah Department of Physics University of Liverpool Liverpool L69 7ZE UK	Azuah@liv.ac.uk
Jon Pearce Department of Physics University of Liverpool Liverpool L69 7ZE UK	Jvpearce@liv.ac.uk
Andrew Fielding Department of Physics University of Liverpool c/o ISIS Facility Rutherford Appleton Laboratory Chilton Didcot Oxfordshire OX11 0QX UK	a.fielding@rl.ac.uk
A.J. Ramirez-Cuesta Department of Chemistry University of Reading Reading RG6 6AD UK	a.j.ramirez-cuesta@reading.ac.uk
Christine Uffindell UMIST c/o ISIS Facility Rutherford Appleton Laboratory Chilton Didcot Oxfordshire OX11 0QX UK	Chu01@isise.rl.ac.uk
Phillip Mitchell Department of Chemistry University of Reading Reading RG6 6AD UK	p.c.h.mitchell@reading.ac.uk

Bruce Hudson Department of Chemistry Centre for Science and Technology Syracuse University Syracuse, NY 13244-4100 USA	Bshudson@syr.edu
Federico J. Mompean Instituto de Ciencia de Materiales de Madrid (ICMM) CSIC Campus de Cantoblanco ES-28049 MADRID (Spain) Tel.: +34 91 334 89 90 Fax: +34 91 372 06 23	Mompean@icmm.csic.es
Robert Delaplane The Studsvik Neutron Research Laboratory Uppsala University S-61182 Nykoping Sweden tel: +46 (0)155 22 18 43	Rgd@studsvik.uu.se
Kristina Edstrom Inorganic Chemistry Angstrom Laboratory Uppsala University Box 538 S - 751 21 Uppsala Sweden tel: +46 18 4713713	Eke@kemi.uu.se
Dave Timms Department of Physics University of Portsmouth St Michael's Building Portsmouth PO1 2DT UK	David.timms@port.ac.uk
Marco Zoppi CNR-IEQ Firenze Italy	Zoppi@ieq.fi.cnr.it
Ralph Simmons Department of Physics University of Illinois Urbana IL 61801 USA	Ros@uiuc.edu

Neutron Compton Scattering Concepts and History

Henry R. Glyde
University of Delaware

Collaborators:

Richard Azuah — The University of Liverpool

Ken Andersen — ISIS, Rutherford Appleton Lab

Massimo Boninsegni — San Diego State University

William Stirling — The University of Liverpool

Paul Sokol — Pennsylvania State University

Steve Bennington — ISIS, Rutherford Appleton Lab

eVS Workshop
November 26, 1999

Aim:

- Introduce Concepts
- Impulse Approximation, $J_{IA}(y)$
- Final State Effects, R(Q,y)
- Expressions for J(q,y)
- Determining Momentum Distribution
- Magnitudes of R(Q,y)
- The Condensate
- Historical Highlights

Condensate, Momentum Distribution and Final-State Effects in Liquid ^{4}He

R.T. Azuah and W.G. Stirling

Department of Physics, Oliver Lodge Laboratory, University of Liverpool, Liverpool L69 3BX, U.K.

H.R. Glyde

Department of Physics and Astronomy, University of Delaware, Newark, Delaware 19716

Abstract

We present high precision measurements of the dynamic structure factor $J(Q,y)$ of liquid ^{4}He at several temperatures over a wide wavevector transfer range, $15 \leq Q \leq 29$ Å. The data show that $J(Q,y)$ is very similar at temperatures $T = 3.5$ K and $T = 2.3$ K in the normal liquid phase ($T > T_\lambda = 2.17$ K). It is also quite similar at temperatures $T = 0.5$ K, 1.3 K and $T = 1.6$ K in the superfluid phase ($T < T_\lambda$). However, $J(Q,y)$ is very different above and below T_λ. Below T_λ, $J(Q,y)$ contains a pronounced additional contribution near $y = 0$ that is asymmetric about $y = 0$ reflecting a condensate contribution modified by asymmetric final-state (FS) effects. We analyze the data at all T using the same model of $J(Q,y)$ consisting of a condensate fraction n_0, a momentum distribution $n^*(\mathbf{k})$ for states $k > 0$ above the condensate and a FS broadening function $R(Q,y)$. With data at many Q values all seven adjustable parameters in the model can be determined. We find a condensate fraction $n_0 = 7 \pm 1\%$ at $T = 0.5$ K, and $n_0 = 0$ for $T > T_\lambda$. The $n^*(\mathbf{k})$ is narrower than a Gaussian in both superfluid and normal ^{4}He and somewhat narrower in normal ^{4}He where $n_0 = 0$. The final state function is the same within precision above and below T_λ, but better determined below T_λ. The precise form of $R(Q,y)$ is important in determining the value of $n_0(T)$ below T_λ, but less critical in determining $n^*(\mathbf{k})$ above T_λ where $n_0 = 0$.

Condensate and final-state effects in superfluid ^{4}He

R. T. Azuah* and W. G. Stirling†
Department of Physics, University of Keele, Keele ST5 5BG, United Kingdom

H. R. Glyde and M. Boninsegni‡
Department of Physics and Astronomy, University of Delaware, Newark, Delaware 19716

P. E. Sokol
Department of Physics, Pennsylvania State University, University Park, Pennsylvania 16802

S. M. Bennington
ISIS Division, Rutherford Appleton Laboratory, Didcot OX11 0QX, United Kingdom
(Received 15 April 1997; revised manuscript received 11 August 1997)

We present high-precision measurements of the dynamics of single atoms in superfluid ^{4}He at $T=1.6$ K and saturated vapor pressure. The measurements were taken on the MARI instrument at the ISIS neutron-scattering facility, Rutherford-Appleton Laboratory. From the measurements we obtain a condensate fraction $n_0=6.0 \pm 2.0\%$ at $T=1.6$ K. The final-state effects (FSE's) in the atomic response are also determined from the data in the form of a final-state broadening function, $R(Q,y)$. We find that this FS function is the same in the superfluid at $T=1.6$ K as that determined previously in normal ^{4}He at $T=2.3$ K. If we reanalyze the data assuming that the superfluid has no condensate, i.e., $n_0=0$, then the data requires that the normal $n(\mathbf{k})$ change dramatically between $T=2.3$ K and $T=1.6$ K. Since such a change in $n(\mathbf{k})$ is physically unexpected, given that kT is much less than the zero-point energy, the data requires that a new contribution, such as a condensate, enter $n(\mathbf{k})$ in the superfluid. [S0163-1829(97)04946-1]

Reprinted from JOURNAL OF LOW TEMPERATURE PHYSICS Vol. 109, Nos. 1/2, October 1997
Printed in Belgium

Momentum Distribution and Final State Effects in Liquid Neon

R. T. Azuah,[1,*] W. G. Stirling,[1,†] H. R. Glyde,[2] and M. Boninsegni[2]

[1]*Department of Physics, University of Keele, Keele ST5 5BG, UK*
[2]*Department of Physics and Astronomy, University of Delaware, Newark, Delaware 19716, USA*

(Received December 23, 1996; revised June 13, 1997)

We report high precision inelastic neutron scattering measurements in liquid Neon at a temperature of 25.8 K and saturated vapour pressure. The data covers a wide range of energy and momentum transfer ($2\,\text{Å}^{-1} \leqslant Q \leqslant 13\,\text{Å}^{-1}$). The atomic momentum distribution, $\mathbf{n}(\mathbf{p})$, and final state effects (FSE) can be readily extracted from this intermediate wavevector transfer data provided a suitable method of analysis is used. We find that the momentum distribution in liquid Neon is marginally sharper than a Gaussian and that final state effects contribute predominantly an antisymmetric component to the the dynamic structure factor. The width of $\mathbf{n}(\mathbf{p})$ and the kinetic energy are increased by 37% above the classical values due to quantum effects. The experimental results are in agreement with theoretical values obtained by a Path Integral Monte Carlo simulation.

NEUTRON SCATTERING

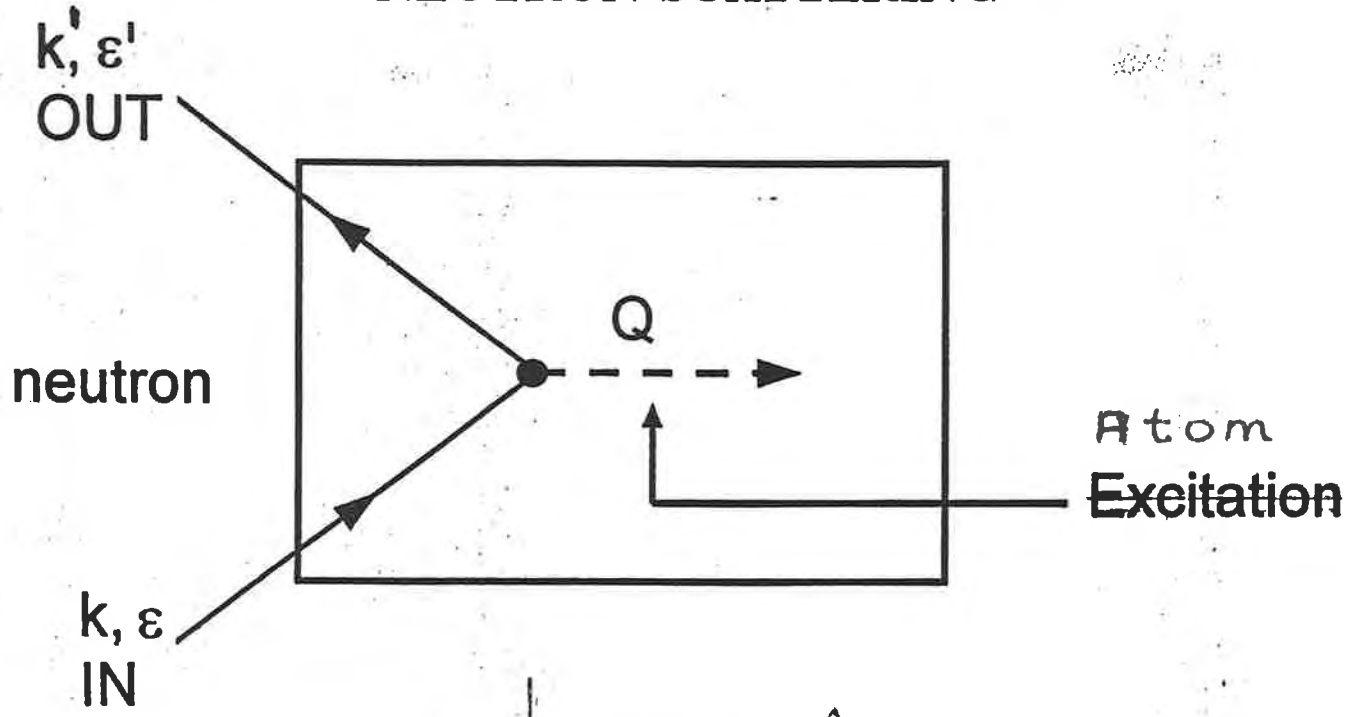

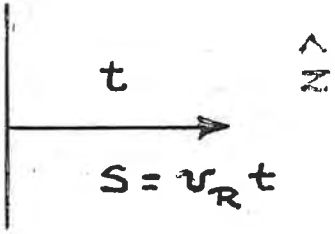

t - scattering time.

S - distance that atom travels.

I A ⇒ S → 0

Excitations in Liquid and Solid Helium

Henry R. Glyde

Department of Physics and Astronomy
University of Delaware

OXFORD SERIES ON NEUTRON SCATTERING IN CONDENSED MATTER

General Editors
S. W. Lovesey, E. W. J. Mitchell

CLARENDON PRESS • OXFORD
1994

IMPULSE APPROXIMATION

$$Q \to \infty$$

$$t \to 0$$

Free atom: $\omega = (\mathbf{k}+\mathbf{Q})^2/2m - k^2/2m$

$$S_{IA}(Q,\omega) = \int d\mathbf{k}\; n(\mathbf{k})\; \delta(\omega - \omega_R - \mathbf{k}\cdot\mathbf{v}_R)$$

$n(\mathbf{k})$ – momentum distribution

$$v_R = \frac{\hbar Q}{M} \quad \text{– Recoil velocity}$$

$$\omega_R = \frac{\hbar Q^2}{2M} \quad \text{– Recoil energy}$$

e.g. $n(\mathbf{k}) = n_0\delta(\mathbf{k})$ $\quad S_{IA}(Q,\omega) = \delta(\omega - \omega_R)$

S_{IA} – "Doppler Broadened" by $n(\mathbf{k})$

Observe $n(\mathbf{k})$ in S_{IA}

DEFINE y - scaling

$$y = (\omega - \omega_R)/v_R \quad \text{"wavevector"}$$
$$s = v_R t \quad \text{"length"}$$

$$J_{IA}(y) = v_R S_{IA}(Q,\omega) = \int d\mathbf{k}\; n(\mathbf{k})\; \delta(y - k_Q)$$

$$= \int dk_x dk_y n(k_x, k_y, y)$$

$$= n(k_Q) \quad \hat{\mathbf{z}} \text{ parallel to } \mathbf{Q}$$

– Longitudinal momentum distribution. 1D

e.g. $n(\mathbf{k})$ – Gaussian, MB

$$J_{IA}(y) = n(y) \sim e^{-y^2/2\overline{\alpha}_Q} \qquad \overline{\alpha}_2 = \langle k_Q^2 \rangle = \sigma^2$$

1D Gaussian centred at $y = 0$.

MOMENTUM DISTRIBUTION

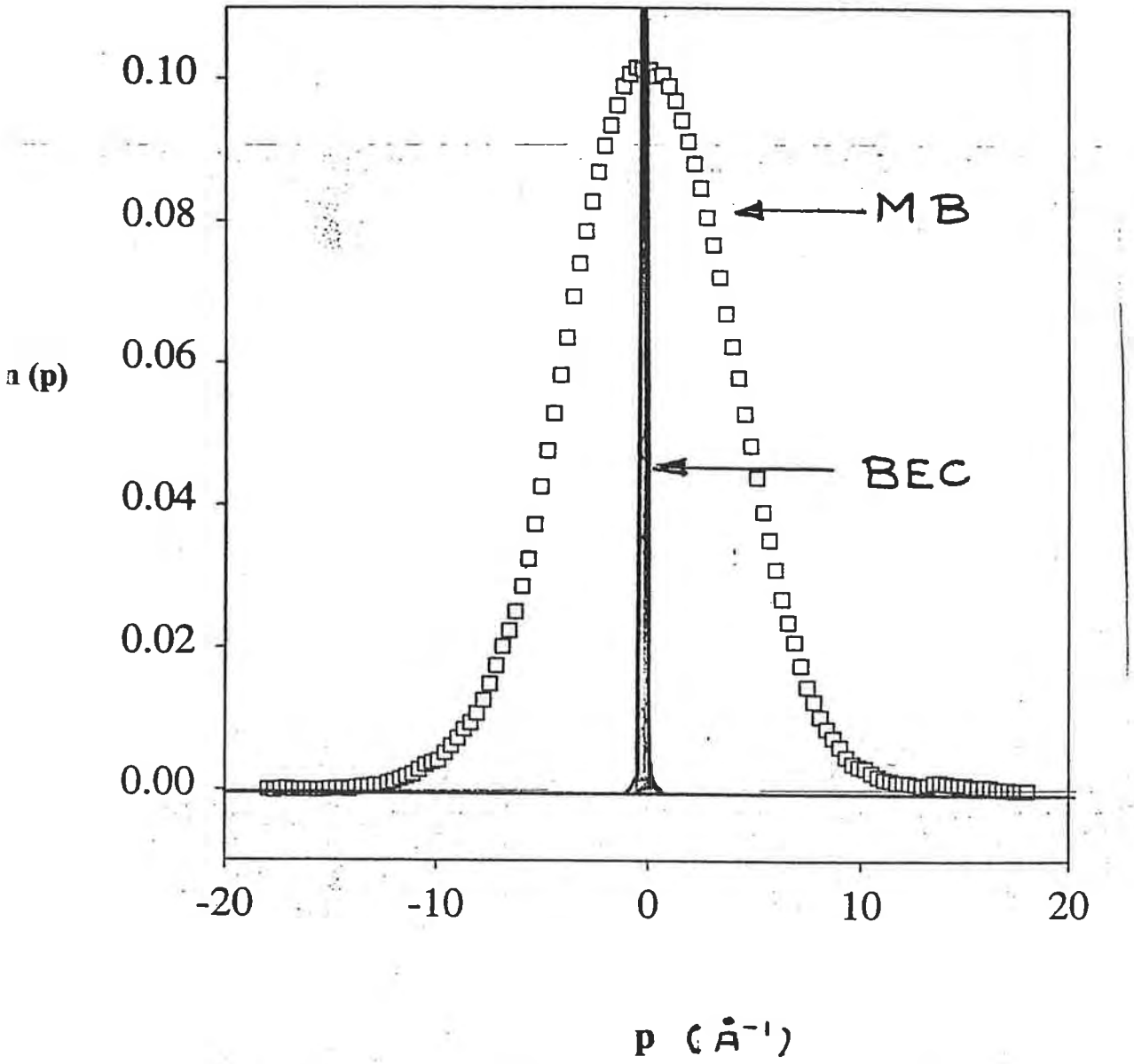

□ **Classical Maxwell — Boltzmann**

— **Bose — Einstein Condensation**

INCLUDE FINAL STATE EFFECTS

– struck atom recoils and
collides with neighbours

Observe:

$$J(Q,y) = \int dy' J_{IA}(y') R(Q, y - y')$$

$$\uparrow \qquad \uparrow$$

IA FS

– definition of $R(Q,y)$
FS Broadening Function

S(Q,t) , J(Q,s) $\qquad s = v_R t$

s – distance travelled in time t

$$S(Q,\omega) = \int dt\ e^{i\omega t} S_i(Q,t)$$

$$S_i(Q,t) = \langle e^{-iQ\cdot r(t)} e^{iQ\cdot r(0)} \rangle \quad Q \gtrsim 10\ \text{Å}^{-1}$$

$$J(Q,y) = \int ds\ e^{iys} J(Q,s)$$

$$J(Q,s) = J_{IA}(s) R(Q,s)$$

$$\uparrow \qquad \uparrow$$

IA FS

Gersch & Rodriguez (1973)

DYNAMIC STRUCTURE FACTOR

$Q, \omega \rightarrow$ Large $\quad s, t \rightarrow 0 \qquad\qquad s = v_R t$

short time (t), short distance (s)
representation of $S(Q,t)$

INCOHERENT $S(Q,t) \qquad\qquad S(Q) = 1$

$$\begin{aligned} S(Q,t) &= \langle e^{-i\mathbf{Q}\cdot\mathbf{r}(t)} e^{i\mathbf{Q}\cdot\mathbf{r}(0)} \rangle \\ &= \langle e^{iHt} \left[e^{-i\mathbf{Q}\cdot\mathbf{r}} e^{-iHt} e^{i\mathbf{Q}\cdot\mathbf{r}} \right] \rangle \\ &= \langle e^{iHt} e^{-iH'(\mathbf{k}+\mathbf{Q})t} \rangle \\ &= \langle T_t e^{-v_R \int_0^t dt' k_Q(t')} \rangle e^{-i\omega_R t} \end{aligned}$$

r – position of struck atom

k – momentum of struck atom

$$J(Q,s) = e^{i\omega_R t} S(Q,t)$$

$$J(Q,s) = \langle T_s e^{-i \int_0^s ds' k_Q(s')} \rangle$$

$k_Q(s')$ – struck atom momentum
after it has travelled
a distance s'.

DYNAMIC STRUCTURE FACTOR

$$J(Q,y) = \frac{1}{2\pi}\int_{-\infty}^{\infty} ds\; e^{iys} J(Q,s)$$

$$J(Q,s) = \left\langle T_s\; e^{-i\int_0^s ds' k_Q(s')} \right\rangle \quad - \text{ Exact}$$

$y = \frac{1}{v_R}(\omega - \omega_R)$ — y scaling variable

$v_R = \frac{\hbar Q}{m}$ — free atom recoil velocity

$\omega_R = \frac{\hbar Q^2}{2m}$ — free atom recoil energy

$s = v_R t$ — conjugate to y, distance traveled by "struck" atom

k_Q — momentum of the "struck" atom along wavevector Q, $k_Q = \mathbf{k}\cdot\widehat{\mathbf{Q}}$

IMPULSE APPROXIMATION

$$Q, s) = \langle T_s\, e^{-i\int_0^s ds' k_Q(s')} \rangle$$ — Exact

— assume that the "struck" atom is "free", does not strike neighbours

$$s = v_R t$$ — atom travels only a short distance; s small, t short

$$k_Q(s) = k_Q(0) + \dot{k}_Q s + \cdots .$$

$$\simeq k_Q(0) = k_Q$$ — initial momentum.

$$I_A(s) = \langle e^{-ik_Q s} \rangle$$ — Impulse Approximation

$$I_A(y) = \frac{1}{2\pi} \int ds\; e^{iys} \langle e^{-ik_Q s} \rangle$$

$$= \int d\mathbf{k}\; n(\mathbf{k})\; \delta(y - k_Q)$$

$$I_A(y) = \int dk_x\; dky\; n(k_x, k_y, y) = n(y)$$

Longitudinal momentum distribution

ONE-BODY DENSITY MATRIX (OBDM)

OBDM - Fundamental Property

$$\rho_1(\mathbf{r},0) = \langle e^{-i\mathbf{k}\cdot\mathbf{r}} \rangle \qquad (\rho_1(\mathbf{r},0) \equiv \langle \psi^+(\mathbf{r}_1+\mathbf{r})\psi(\mathbf{r}_1) \rangle)$$

$$\rho_1(s,0) = \langle e^{-ik_Q s} \rangle = J_{IA}(s) \quad \mathbf{r} = s\widehat{\mathbf{Q}}$$

$J_{IA}(s)$ – OBDM for displacements s along $\hat{Q}$

Momentum Distribution

$$n(\mathbf{k}) = \frac{1}{2\pi} \int d\mathbf{r} e^{i\mathbf{k}\cdot\mathbf{r}} \rho_1(\mathbf{r},0)$$

$$n(y) = n(k_Q) = \frac{1}{2\pi} \int ds e^{iys} \rho_1(s,0)$$

$$= \int dk_x dk_y n(k_x, k_y, k_Q)$$

$n(y)$ – Longitudinal momentum distribution

EXPANSION OF DYNAMIC STRUCTURE FACTOR

Expand $J(Q,s)$ and $J_{IA}(s)$ in powers of s (small).

Determine expansion coefficients by fitting expansion to data.

Determine $n(s)$, $R(Q,s)$ as a series.

IA – OBDM, n(k)

Normal Fluid

$$n^*(s) = J_{IA}(s) = \langle e^{-ik_Q s} \rangle$$

$$J_{IA}(s) = \exp\left[-\frac{\overline{\alpha}_2 s^2}{2!} + \frac{\overline{\alpha}_4 s^4}{4!} - \frac{\overline{\alpha}_6 s^6}{6!} + \cdots\right]$$

$$\simeq e^{-\frac{1}{2}\overline{\alpha}_2 s^2}\left[1 + \frac{\overline{\alpha}_4 s^4}{4!} - \frac{\overline{\alpha}_6 s^6}{6!} + \cdots\right]$$

$$\overline{\alpha}_2 = \langle k_Q^2 \rangle = \sigma^2,$$

$$\overline{\alpha}_4 = \langle k_Q^4 \rangle - 3\langle k_Q^2 \rangle^2,$$

$$\overline{\alpha}_6 = \langle k_Q^6 \rangle - 15\langle k_Q^4 \rangle\langle k_Q^2 \rangle + 30\langle k_Q^2 \rangle^3$$

– valid for a normal fluid/solid.

Bose Condensate

$$n(s) = n_0\,[1 + f(s)] + n^*(s)$$

n_0 – Condensate Fraction

IMPULSE APPROXIMATION: VALIDITY

$$J_{IA}(s) = \langle e^{-ik_Q s} \rangle \simeq e^{-\frac{1}{2}\langle k_Q^2 \rangle s^2}$$

IA obtained using

$$\begin{aligned} k_Q(s) &= k_Q(0) + \dot{k}_Q s + \tfrac{1}{2}\cdots \\ &\simeq k_Q(0) = k_Q \end{aligned}$$

Require

$$\dot{k}_Q s \ll k_Q$$

$$s^2 \lesssim \langle k_Q^2 \rangle^{-1} \qquad\qquad \dot{k}_Q = \frac{F_Q}{\hbar v_R}$$

$$\frac{F_Q}{\lambda Q \langle k_Q^2 \rangle} \ll 1$$

F_Q — "average" Force on struck atom.

$$\langle k_Q^2 \rangle = \overline{\alpha}_2 = \sigma^2, \quad \langle K \rangle = \tfrac{3}{2}\lambda \langle k_Q^2 \rangle$$

$$\lambda = \hbar^2/m$$

$s^2 \lesssim \langle k_Q^2 \rangle^{-1}$ $\qquad$ $\tau = \frac{s}{v_R} \lesssim \frac{m}{\hbar Q \langle k_Q^2 \rangle^{1/2}}$

- scattering time

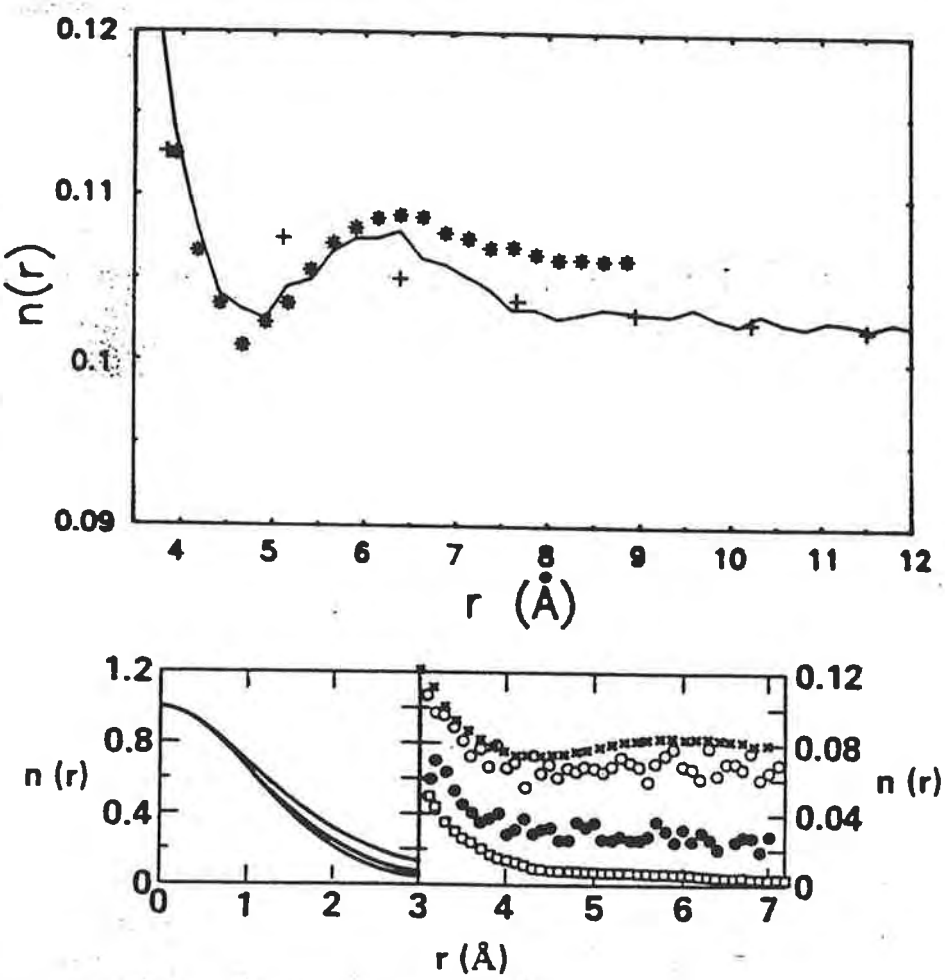

FIG. 7.5. One-body density matrix (7.26) in liquid ^{4}He. Upper: at $T = 0$ K calculated by Whitlock and Panoff (1987). Lower: at finite temperature calculated by Ceperley and Pollock (1986); upper curve and open circles, 1.18 K, lowest curve and open squares, 3.33 K.

NORMAL ^4He

$$n^*(s) = \exp\left[-\alpha_2 \frac{s^2}{2!} + \alpha_4 \frac{s^4}{4!} - \alpha_6 \frac{s^6}{6!}\right]$$

$$\alpha_2 = \langle k_Q^2 \rangle \qquad \alpha_4 = \langle k_Q^2 \rangle - 3\langle k_Q^2 \rangle^2$$

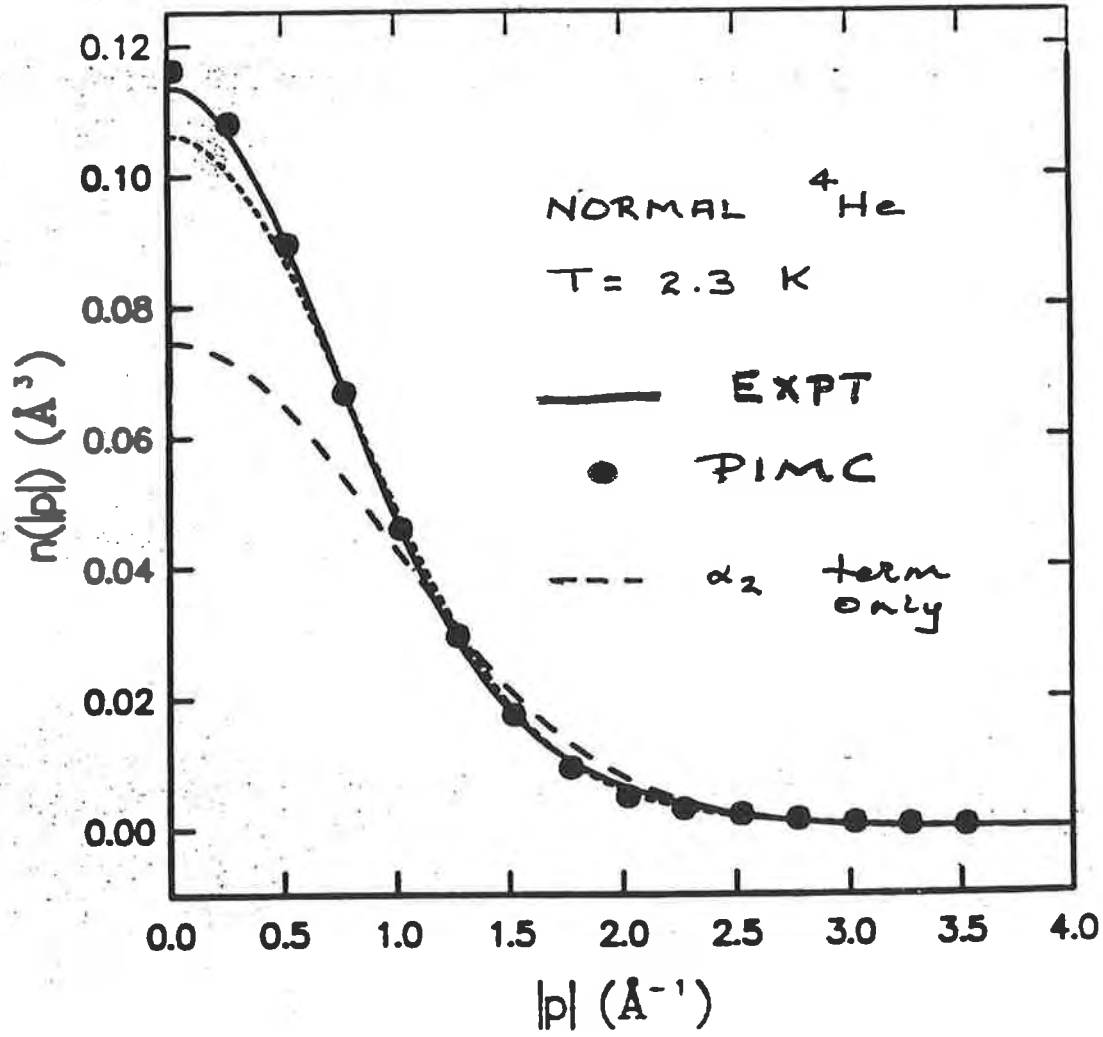

EXPT : $\langle K \rangle = \frac{3}{2}\alpha_2 = 16.3 \pm 0.35$ K

PIMC : $\langle K \rangle = 16.0$ K

Ceperley & Pollock

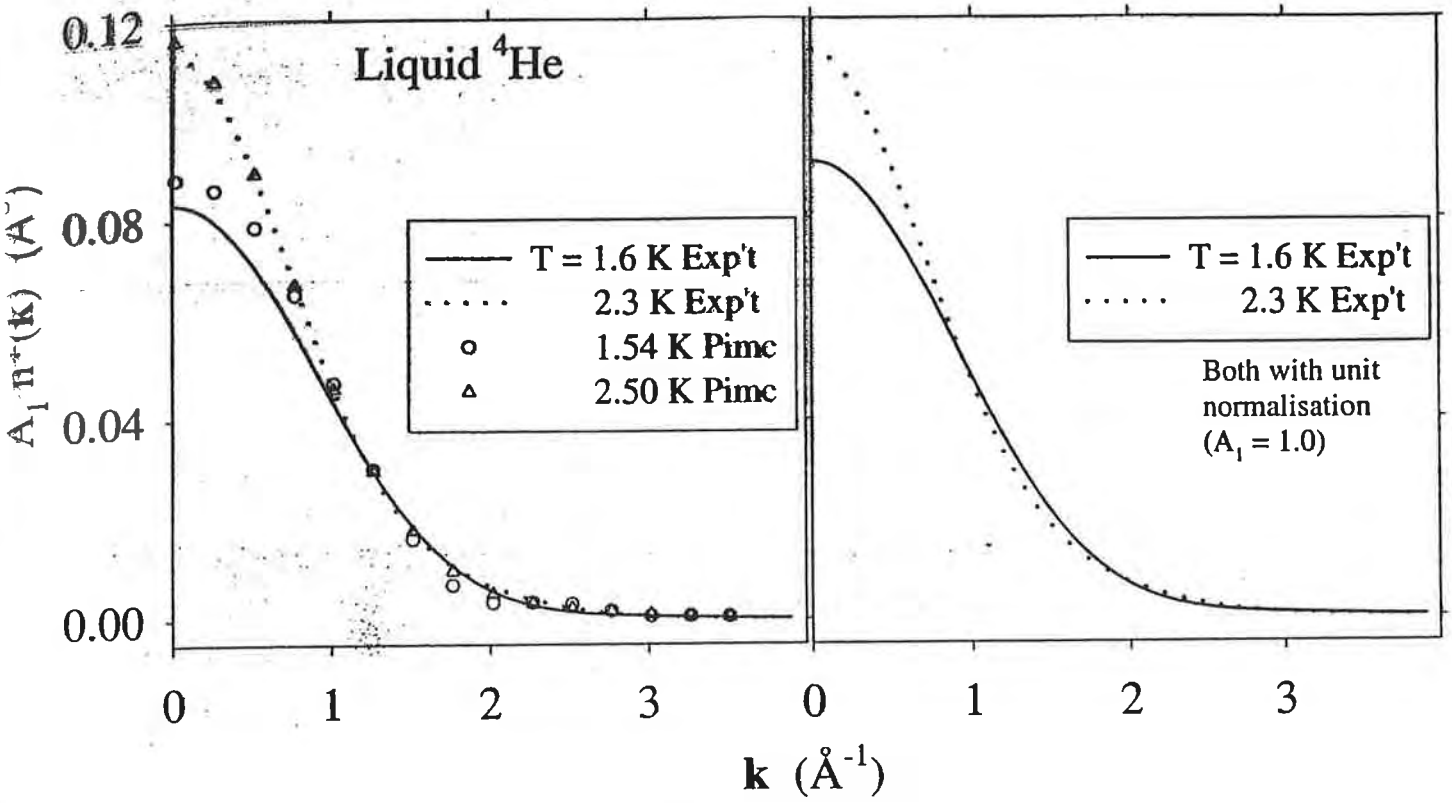
Liquid ^{4}He
0.12
0.08
0.04
0.00
$A_1 n^*(k)$ (Å^3)
T = 1.6 K Exp't
2.3 K Exp't
1.54 K Pimc
2.50 K Pimc
T = 1.6 K Exp't
2.3 K Exp't
Both with unit normalisation (A_1 = 1.0)
0
1
2
3
k (Å^{-1})

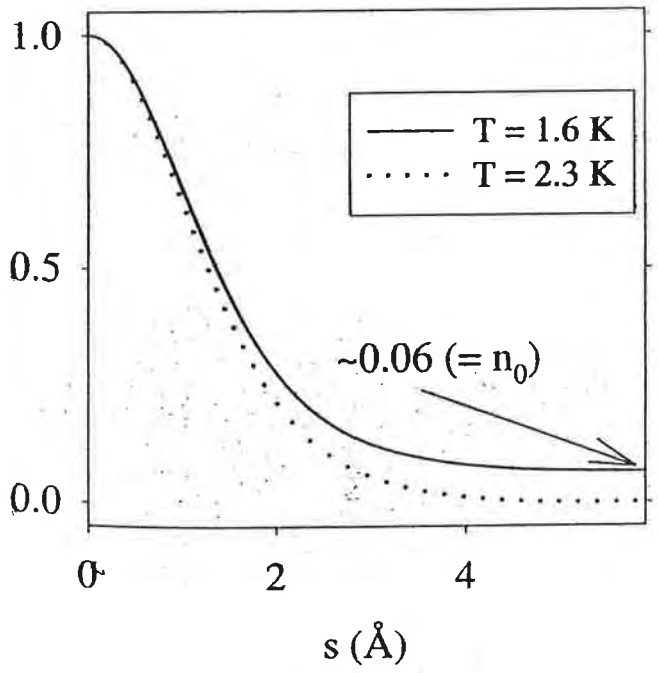
1.0
0.5
0.0
T = 1.6 K
T = 2.3 K
~0.06 (= n_0)
0
2
4
s (Å)

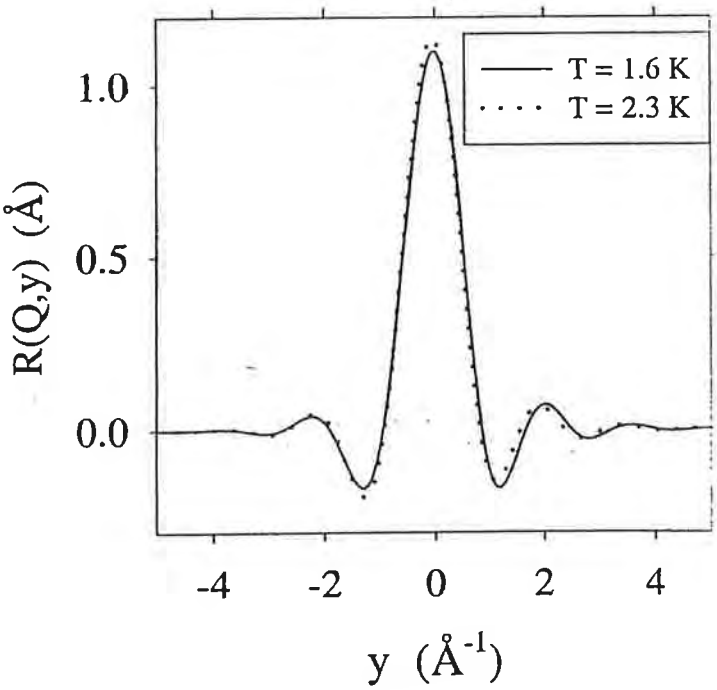
1.0
0.5
0.0
R(Q,y) (Å)
T = 1.6 K
T = 2.3 K
-4
-2
0
2
4
y (Å^{-1})

Fig. 5

Physics &
Astronomy

Liquid Neon T = 25.8 K

Momentum Distribution

- Full n(k)
- Gaussian Component

n(k) - Nearly Gaussian,

$\langle KE \rangle = 52.9 \pm 2.5$ K $3/2\ k_B T = 38.7$ K

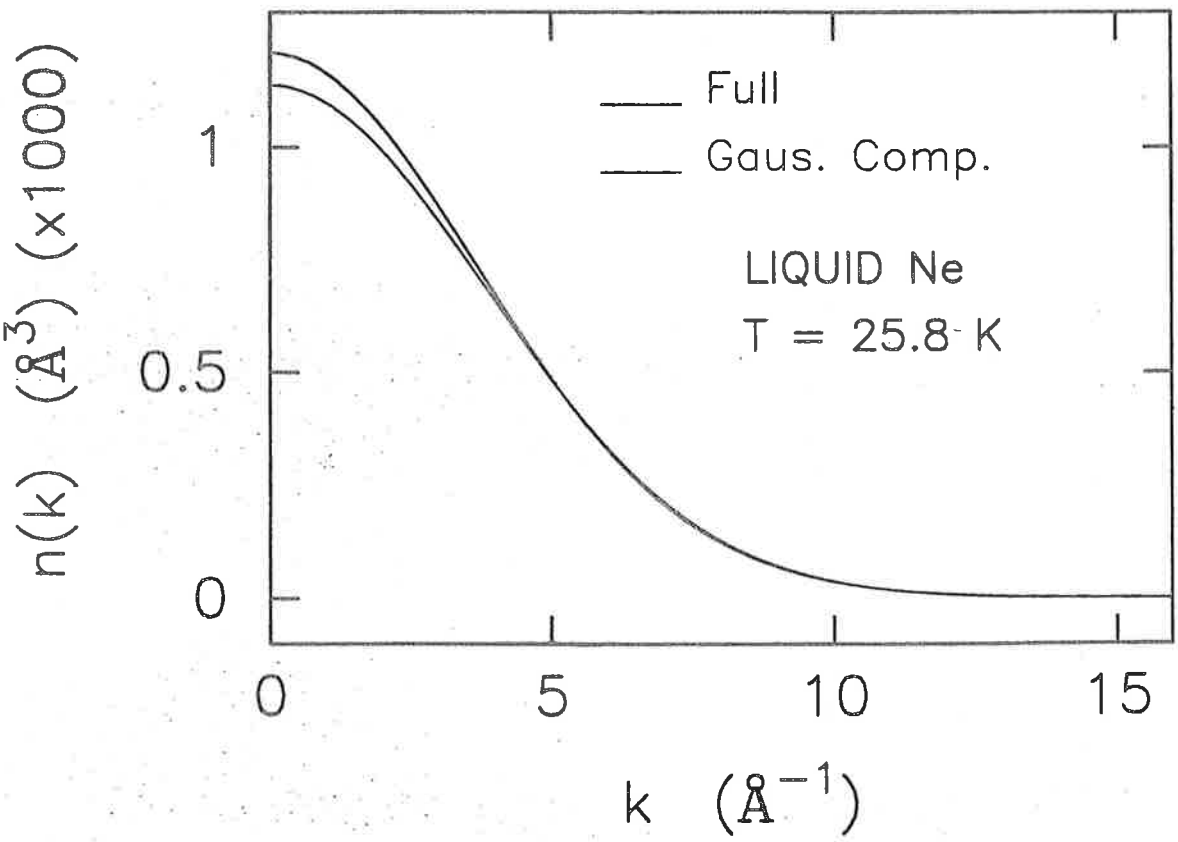

S(Q,ω) AND FINAL STATE FUNCTION

$$J(Q,s) = \exp\left[-\frac{\overline{\mu}_2 s^2}{2!} + i\frac{\overline{\mu}_3 s^3}{3!} + \frac{\overline{\mu}_4 s^4}{4!} - i\frac{\overline{\mu}_5 s^5}{5!} - \frac{\overline{\mu}_6 s^6}{6!} + \cdots\right],$$

$v_R = \frac{\hbar Q}{m}$

$$\overline{\mu}_2 = \overline{\alpha}_2 = \langle k_Q^2 \rangle \quad - \quad IA$$

$$\overline{\mu}_3 = \overline{a}_3 / v_R \quad - \quad FS$$

$$\overline{\mu}_4 = \overline{a}_4 / v_R + \overline{\alpha}_4 \quad - \quad FS + IA$$

$$\overline{\mu}_5 = \overline{a}_{52} / v_R^3 + \overline{a}_{54} / v_R \quad - \quad FS$$

$$\overline{\mu}_6 = \overline{a}_{62} / v_R^4 + \overline{a}_{64} / v_R^2 + \overline{\alpha}_6 \quad - \quad FS + IA$$

$$\overline{a}_3 = \langle \nabla^2 v \rangle / 6\hbar \qquad \overline{a}_4 = \langle F_Q^2 \rangle / \hbar^2$$

$$J(Q,s) = \exp[\overline{\alpha} + \overline{\beta}] = \exp[\overline{\alpha}] \exp[\overline{\beta}]$$

Final State Function

$$J(Q,s) \equiv J_{IA}(s)\ R(Q,s)$$

$$R(Q,s) = \exp\left[\sum_{n=3}^{\infty} \frac{\overline{\beta}_n}{n!} (-is)^n\right]$$

$$\overline{\beta}_n = \overline{\mu}_n \qquad -n \text{ odd}$$

$$\overline{\beta}_n = \overline{\mu}_n - \overline{\alpha}_n \quad -n \text{ even}$$

FINAL STATE FUNCTION

$$J(Q,s) = J_{IA}(s)R(Q,s)$$

$$J(Q,s) = \exp\left[\overline{\alpha}\right]\exp\left[\overline{\beta}\right]$$

$$R(Q,s) = \exp\left[\frac{is^3}{3!}\frac{\overline{a}_3}{v_R} + \frac{s^4}{4!}\frac{\overline{a}_4}{v_R^2} - \frac{is^5}{5!}\left(\frac{\overline{a}_{54}}{v_R} + \frac{\overline{a}_{52}}{v_R^3}\right) - \frac{s^6}{6!}\left(\overline{a}_{64}/v_R^2 + \overline{a}_{62}/v_R^4\right)\right]$$

$$v_R = \frac{\hbar Q}{m}$$

FINAL STATE FUNCTION R(Q,y)

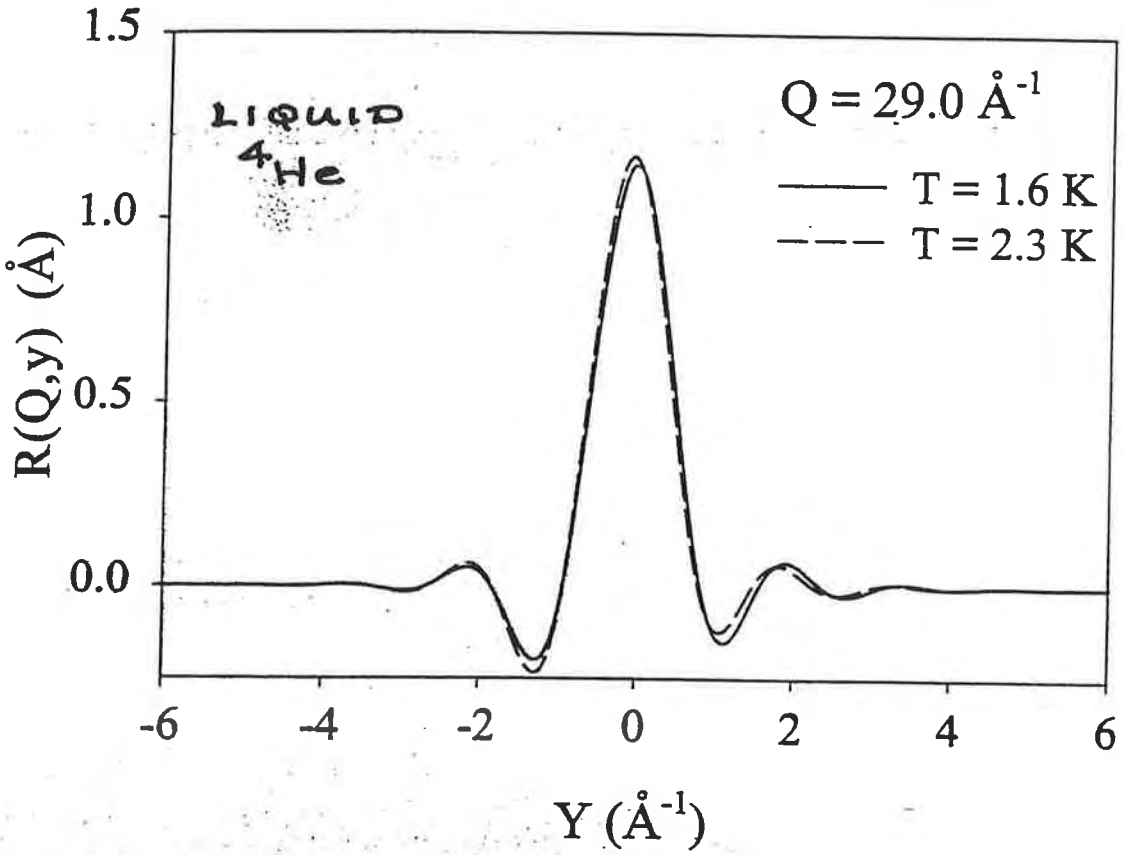

$$R(Q,s) = \exp\left[i\bar{\beta}_3 \frac{s^3}{3!} + \bar{\beta}_4 \frac{s^4}{4!} - i\bar{\beta}_5 \frac{s^5}{5!} - \bar{\beta}_6 \frac{s^6}{6!} \right]$$

$$\bar{\beta}_3 = \bar{\mu}_3 \sim 1/Q$$

$$\bar{\beta}_5 = \bar{\mu}_5 \sim 1/Q^3 + 1/Q$$

$$\bar{\beta}_6 = \bar{\mu}_6 - \bar{\alpha}_6 \sim 1/Q^4 + 1/Q$$

THREE PARAMETERS $\bar{\beta}_3, \bar{\beta}_5, \bar{\beta}_6$

$\bar{\beta}_4 = 0$

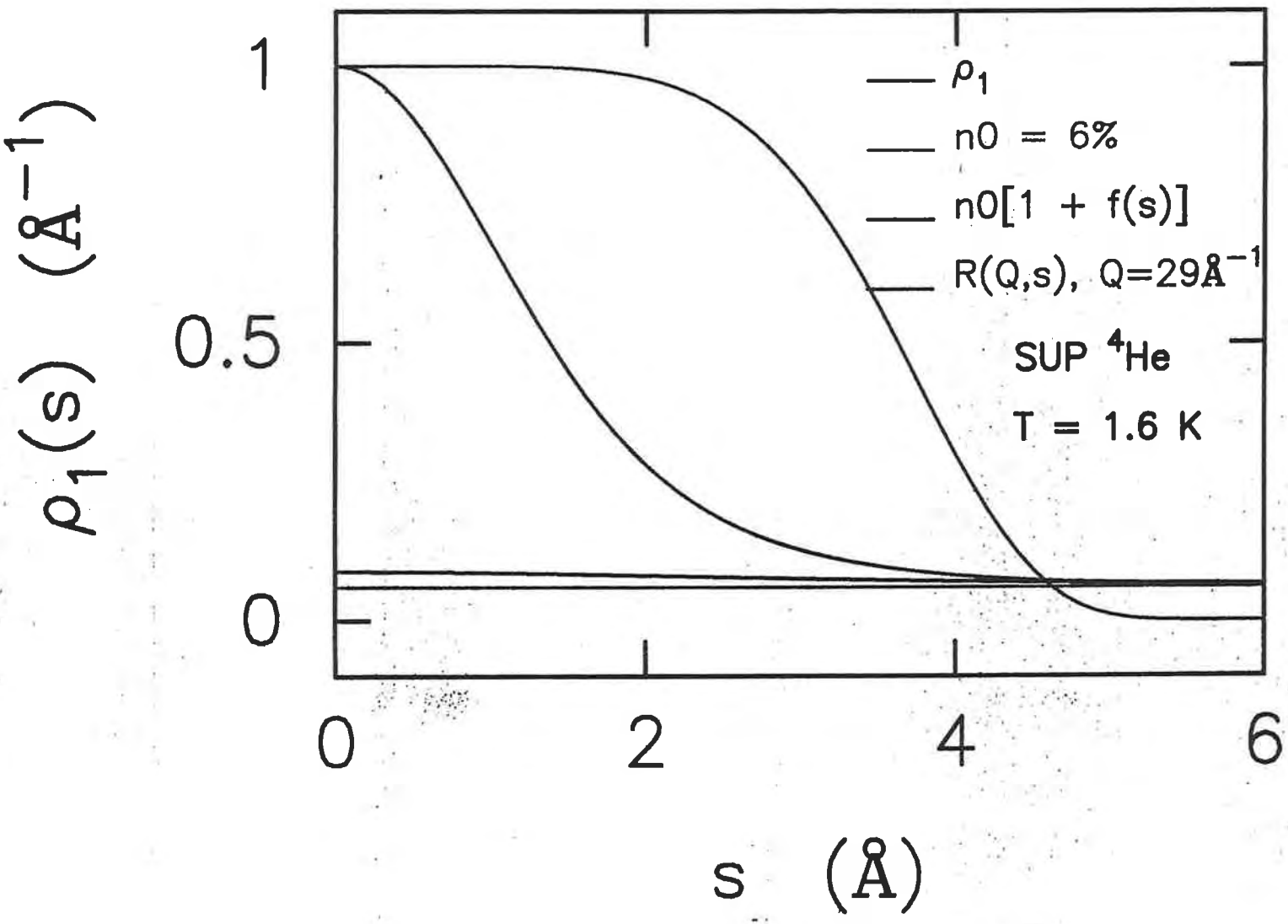

R(Q,Y) (A)

LIQUID ^3He $T = 1.4\ K$

$$R(Q,s) = \exp\left[\frac{i}{3!}\bar{B}_3 s^3 + \frac{1}{4!}\bar{B}_4 s^4 - \frac{i}{5!}\bar{B}_5 s^5 - \frac{1}{6!}\bar{B}_6 s^6\right]$$

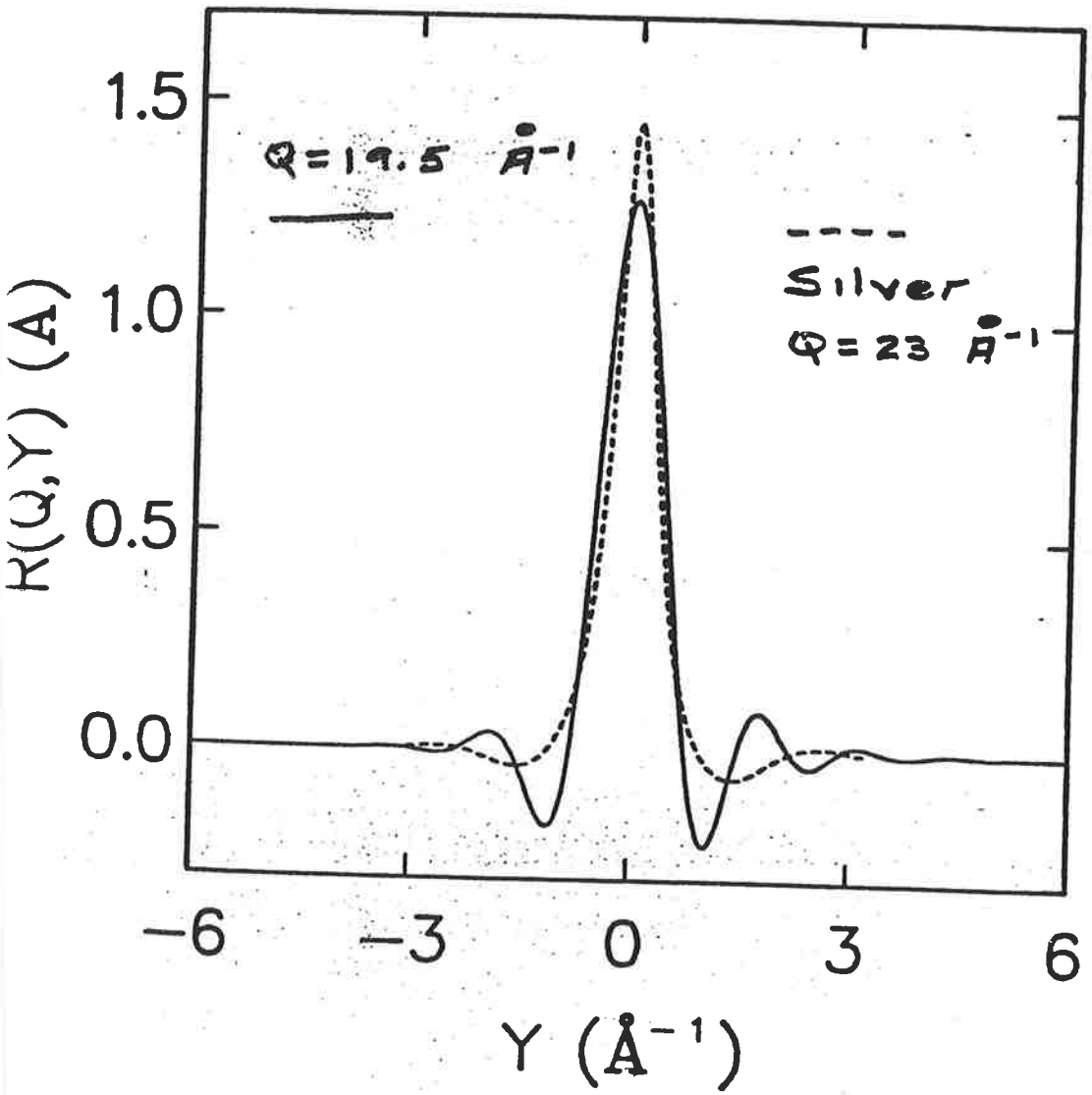

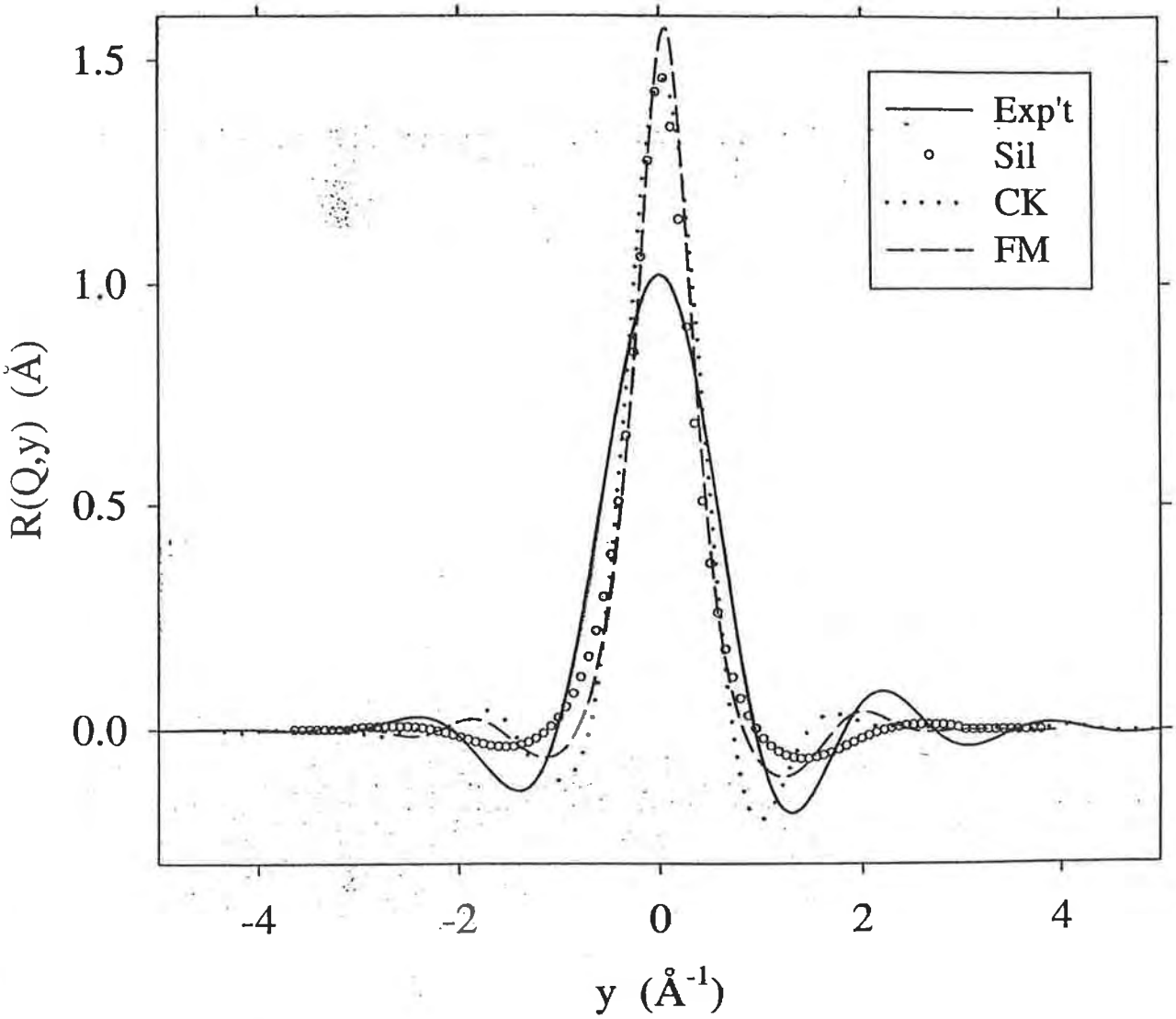

FIG. 9

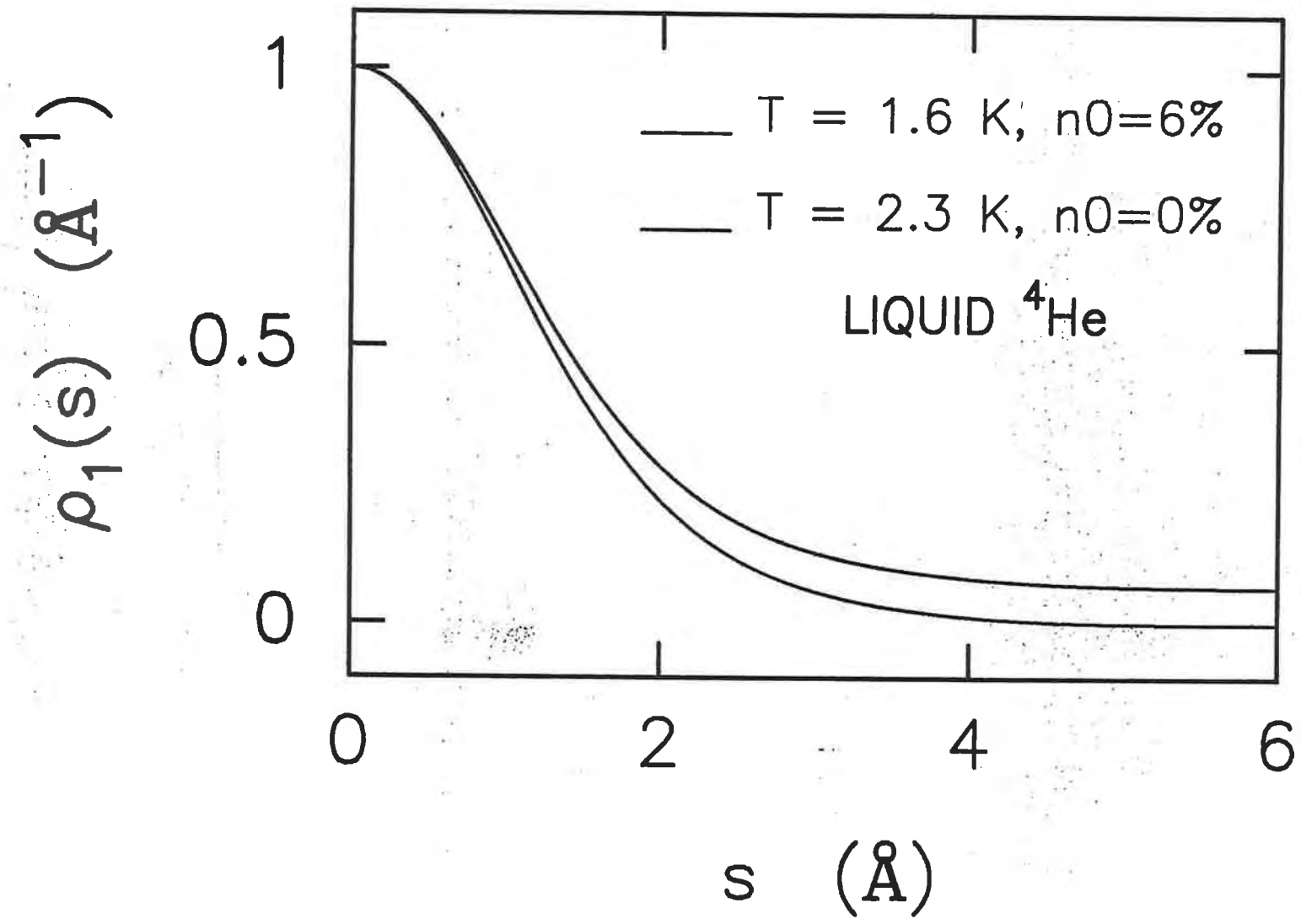
1
0.5
0
0
2
4
6
$\rho_1(s)$ (Å^{-1})
s (Å)
T = 1.6 K; n0=6%
T = 2.3 K, n0=0%
LIQUID ^{4}He

$\rho_1(s)$ $(Å^{-1})$
0
0.5
1
0
2
4
6
s (Å)
$\rho_1 \times R(Q,s)$, Q = 29Å^{-1}
T = 1.6 K, n0=6%
T = 2.3 K, n0=0%
LIQUID ^{4}He

DYNAMIC STRUCTURE FACTOR

$$, s) = \exp\left[-\frac{\overline{\mu}_2 s^2}{2!} + i\frac{\overline{\mu}_3 s^3}{3!} + \frac{\overline{\mu}_4 s^4}{4!} - i\frac{\overline{\mu}_5 s^5}{5!} - \frac{\overline{\mu}_6 s^6}{6!} + \cdots\right],$$

$$\overline{\mu}_2 = \overline{\alpha}_2 = \langle k_Q^2 \rangle = \sigma^2 \qquad - \quad n(k)$$

$$\overline{\mu}_3 = \overline{a}_3 / v_R \qquad - \quad FS$$

$$\overline{\mu}_4 = \overline{a}_4 / v_R + \overline{\alpha}_4 \qquad - \quad FS + n(k)$$

$$\overline{\mu}_5 = \overline{a}_{52} / v_R^3 + \overline{a}_{54} / v_R \qquad - \quad FS$$

$$\overline{\mu}_6 = \overline{a}_{62} / v_R^4 + \overline{a}_{64} / v_R^2 + \overline{\alpha}_6 \qquad - \quad FS + n(k)$$

$$\overline{a}_3 = \langle \nabla^2 v \rangle / 6\hbar \qquad\qquad \overline{a}_4 = \langle F_Q^2 \rangle / \hbar^2$$

$$J(Q,y) = \left[1 + \frac{\overline{\mu}_3}{2\alpha_2^{3/2}}\left(x - \frac{x^3}{3}\right) + \frac{\overline{\mu}_4}{8\overline{\alpha}_2^2}\left(1 - 2x^2 + \frac{x^4}{3}\right) + \frac{\overline{\mu}_5}{8\overline{\alpha}^{5/2}}\left(x - \frac{2}{3}x^3 + \frac{1}{15}x^5\right)\right] J_G(x)$$

$$x = y / \langle k_Q^2 \rangle$$

$$J_G(x) = \left(2\pi \langle k_Q^2 \rangle\right)^{-\frac{1}{2}} e^{-\frac{1}{2}x^2}$$

$$J(Q,y) = J_G(y) + J_1(Q,y) + J_2(Q,y) + J_3(Q,y)$$

FINAL STATE EFFECTS: MAGNITUDE

$$J(Q,z) = e^{-\frac{1}{2}z^2}\left[1 + \frac{i}{3!}\frac{\bar{\mu}_3}{\sigma^3}z^3 + \frac{1}{4!}\frac{\bar{\mu}_4}{\sigma^4}z^4 - \frac{i}{5!}\frac{\bar{\mu}_5}{\sigma^5}z^5 + \cdots\right]$$

$$z^2 = \bar{\alpha}_2 s^2 = \sigma^2 s^2 \qquad - \text{ dimensionless}$$

$$\frac{\bar{\mu}_3}{\sigma^3} = \frac{\bar{a}_3}{\sigma^3 v_R} = \frac{\langle \nabla^2 v\rangle}{6\lambda\sigma^3}\frac{1}{Q}$$

$$\frac{\bar{\mu}_4}{\sigma^4} = \frac{\bar{\alpha}_4 + \bar{a}_4/v_r^2}{\sigma^4} = \delta + \frac{\langle F_Q^2\rangle}{\lambda^2\sigma^4}\frac{1}{Q^2}$$

$$\delta = \frac{\langle k_Q^4\rangle - 3\langle k_Q^2\rangle^2}{\langle k_Q^2\rangle^2} \qquad \text{"IA validity"}$$

Liquid ^{4}He

$$\lambda = 1.0443 \text{ meV}$$
$$\sigma^2 = 0.897 \text{ Å}^{-2}$$
$$\bar{a}_3/\lambda = 2.8 \pm 1.0 \text{ Å}^{-4}$$
$$\bar{a}_4/\lambda^2 \lesssim 50 \text{ Å}^{-6}$$

$$\frac{\bar{\mu}_3}{\sigma^3} \simeq 1.8/Q \simeq 0.1 \qquad Q = 25 \text{ Å}^{-1}$$

$$\frac{\bar{a}_4}{\lambda^2\sigma^2 Q^2} \leq 50/Q^2 \leq 0.1$$

$$\delta \simeq 0.50$$

$$\frac{\bar{\mu}_6}{\sigma^6} \simeq 175/Q^2 \simeq 0.2$$

Andersen et al.
1997

NORMAL ^4He

$$S = S_{IA} + S_1 + S_2$$

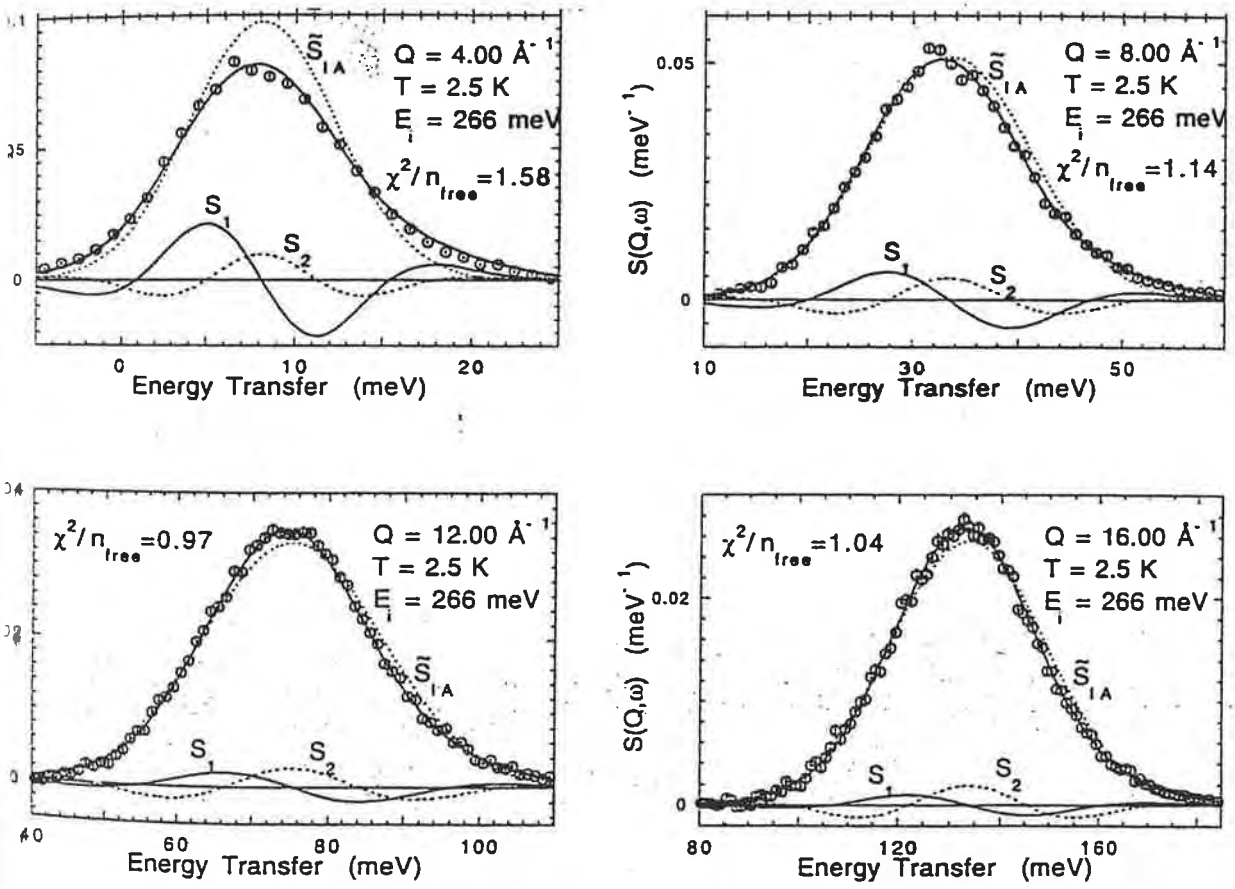

$$\mu_m = \bar{\mu}_m Q^m$$

$$\mu_4 = \bar{\alpha}_4 Q^4 + \bar{\alpha}_4 Q^2$$

$$\begin{matrix} | & | \\ n(k) & FS \end{matrix}$$

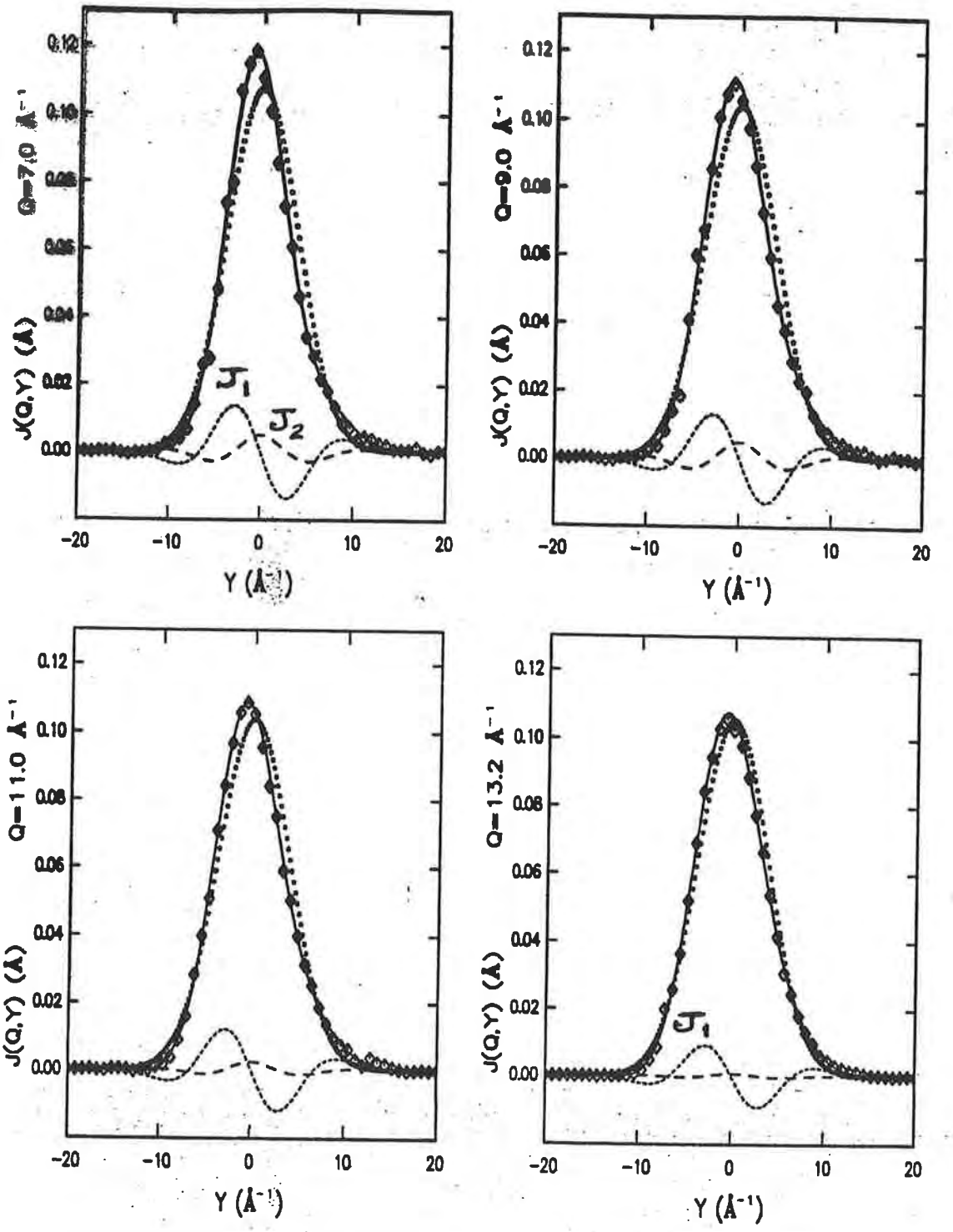

$$J(Q,y) = \tilde{J}_{IA}(y) + J_1(Q,y) + J_2(Q,y)$$

Figure 4.8: AA fits for liquid neon at T=25.8K. The magnitude of $J_1(Q,Y)$ is considerable. This is essential as a result of the long tails on the high Y side of the peaks. The symmetric term $J_2(Q,Y)$ decays systematically with Q. Symbols same as in figure ??

STORICAL SKETCH:

- In the beginning
  — Miller, Pines and Nozières (1962), Hohenberg and Platzman (1966) propose measuring $n(\mathbf{k}), n_0$ by neutron scattering at high Q.

- Many "measurements" of n_0 using reactor neutrons at $5 \leq Q \leq 10$ Å^{-1}. Wide range of n_0 obtained (see Martel *et al.*, JLTP (1976) for a review). $(2 \leq n_0 \leq 17\%)$

- Sears (1969) — expressions for $S(Q,\omega)$ at high Q. Additive Expansion.

- Gerch and Rodriguez (1973) — PR **A8**, 905
  — define FS function R(Q,y) as a convolution.

- Sears *et al.* (1982) — PRL
  — first systematic and results for n_0; reduce coherent, FS effects account for f(k) term.
  $10 \leq n_0 \leq 13\%$

- Sokol and Collaborators (1995-91)
  - $n_0 = 10\%$, $n_0(T)$, $n_0(p)$
  - higher Q , IDNS
  - convolution $R(Q,y)$ (Silver)

  Momentum Distributions (1989)
  Silver and Sokol
  Sosnick et al. (1991)

- Sears (1984)
  - expressions for $S(Q,\omega)$
    expansion of $J(Q,y)$

- Simmons and Collaborators
  - $\langle K \rangle$, FS terms J_1 , J_2

  Ne, Ar, Kr, He Solid & liquid
  Fradkin et al. (1994)

- Mayers et al. (1996)
  - $\langle K \rangle$, FS terms J_1 , J_2

  e.g. H in Zr

- $\langle K \rangle$ in Liquid & Solid ^4He
  e.g. Bafile et al. (1995) H
  Andreani et al. (1994)
  Zoppi et al. (1998)

- Azuah et al. (1995, 1997, ...)
  - $n(k)$, normal / superfluid ^4He
  - $R(q,y)$ "
  - $n_0(T)$

- Reiter and Mayers (preprint)
  - $n(k)$, anisotropic
  - method for obtaining $n(k)$.

Reviews

Watson (1995)
Mayers (1998)
(1997)
(1996)

GOALS

$\langle K \rangle$, n_0 — ^3He and ^4He mixtures

$n(k)$ — in many systems
— bulk, disordered

H — in materials

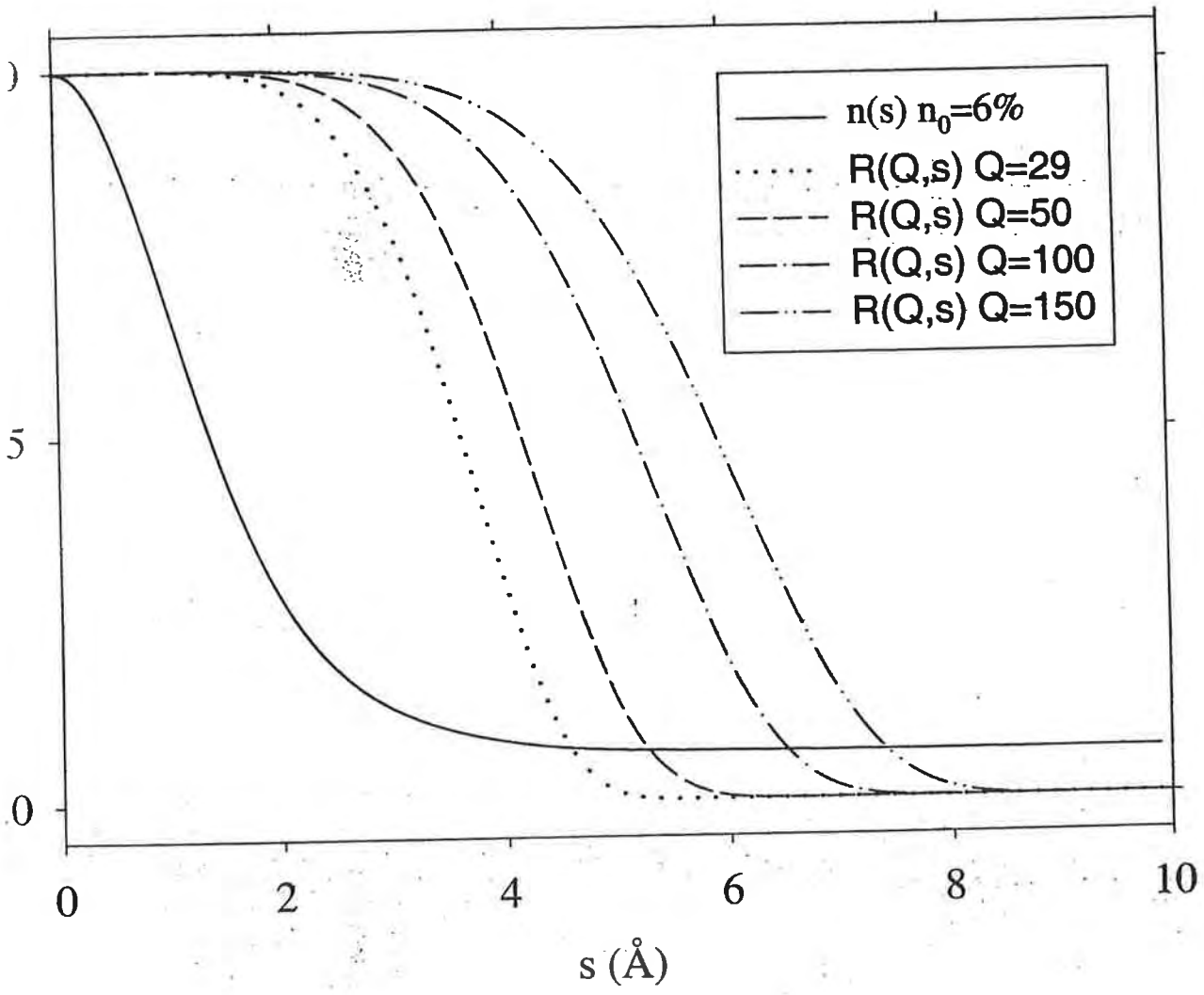
n(s) n0=6%
R(Q,s) Q=29
R(Q,s) Q=50
R(Q,s) Q=100
R(Q,s) Q=150
0
2
4
6
8
10
s (Å)

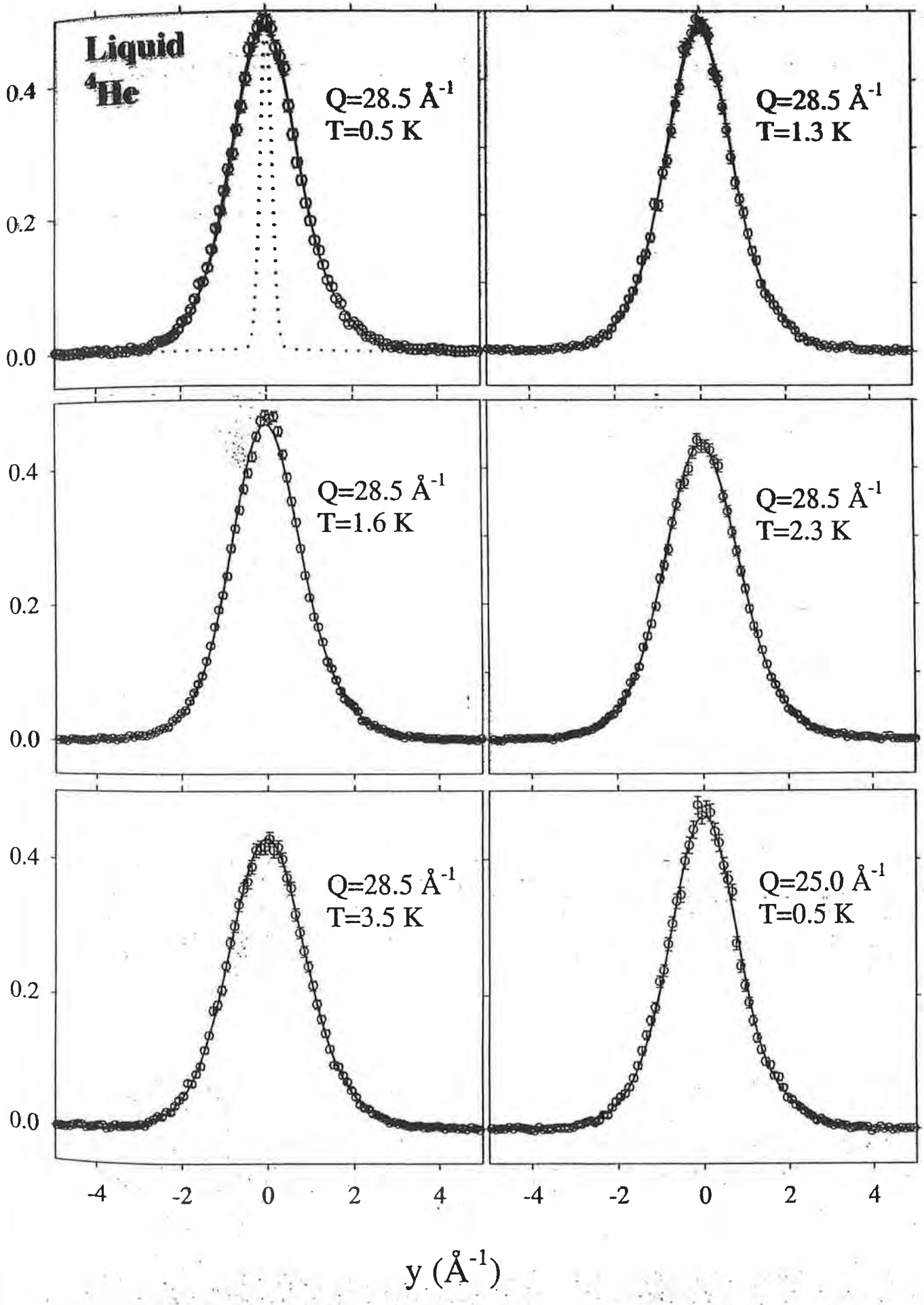
Liquid
4He
Q=28.5 Å-1
T=0.5 K
Q=28.5 Å-1
T=1.3 K
Q=28.5 Å-1
T=1.6 K
Q=28.5 Å-1
T=2.3 K
Q=28.5 Å-1
T=3.5 K
Q=25.0 Å-1
T=0.5 K
0.0
0.2
0.4
-4
-2
0
2
4
y (Å-1)

FIG. 3

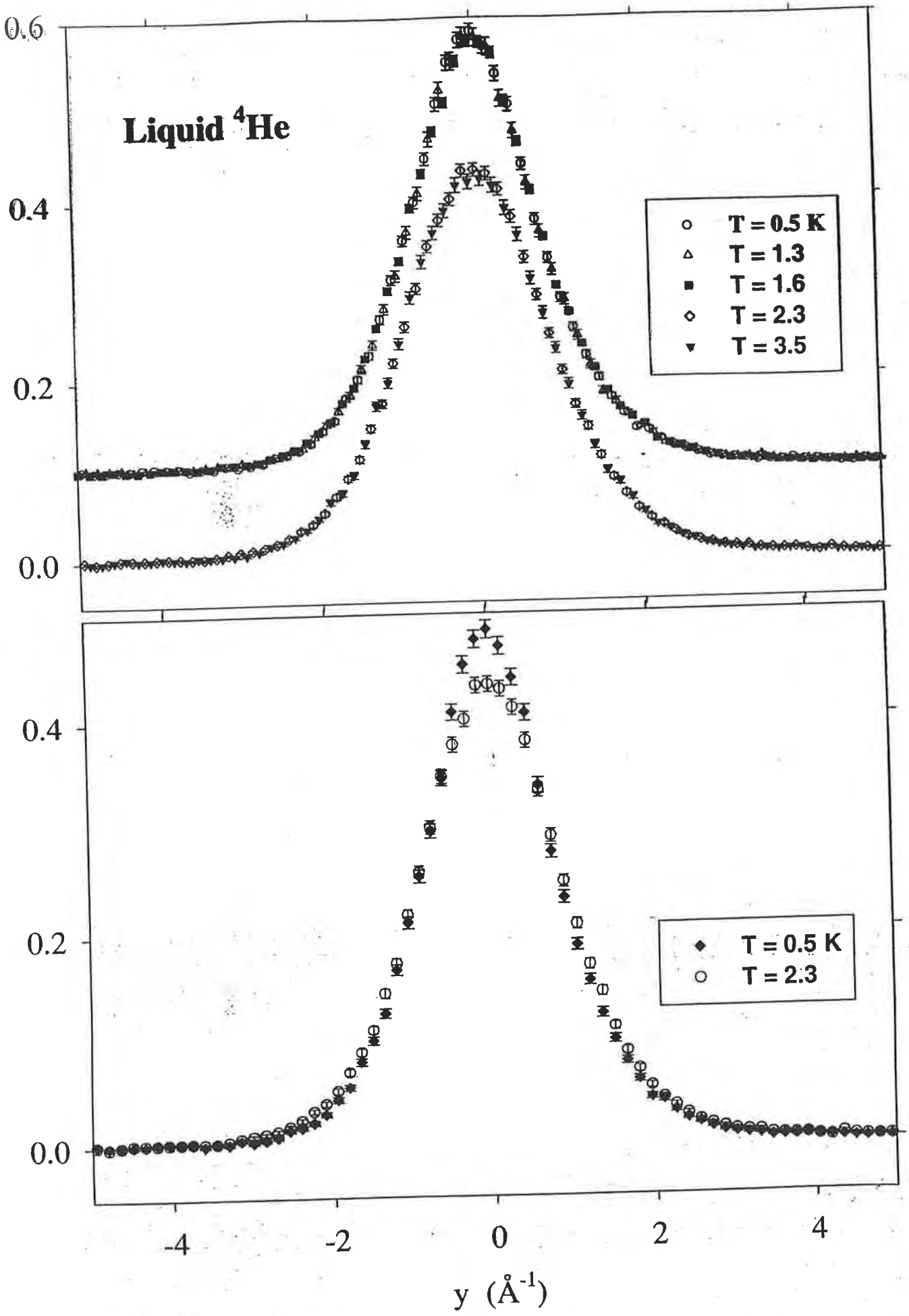
Liquid ^{4}He
T = 0.5 K
T = 1.3
T = 1.6
T = 2.3
T = 3.5
T = 0.5 K
T = 2.3
0.6
0.4
0.2
0.0
0.4
0.2
0.0
-4
-2
0
2
4
y (Å^{-1})

Fig.

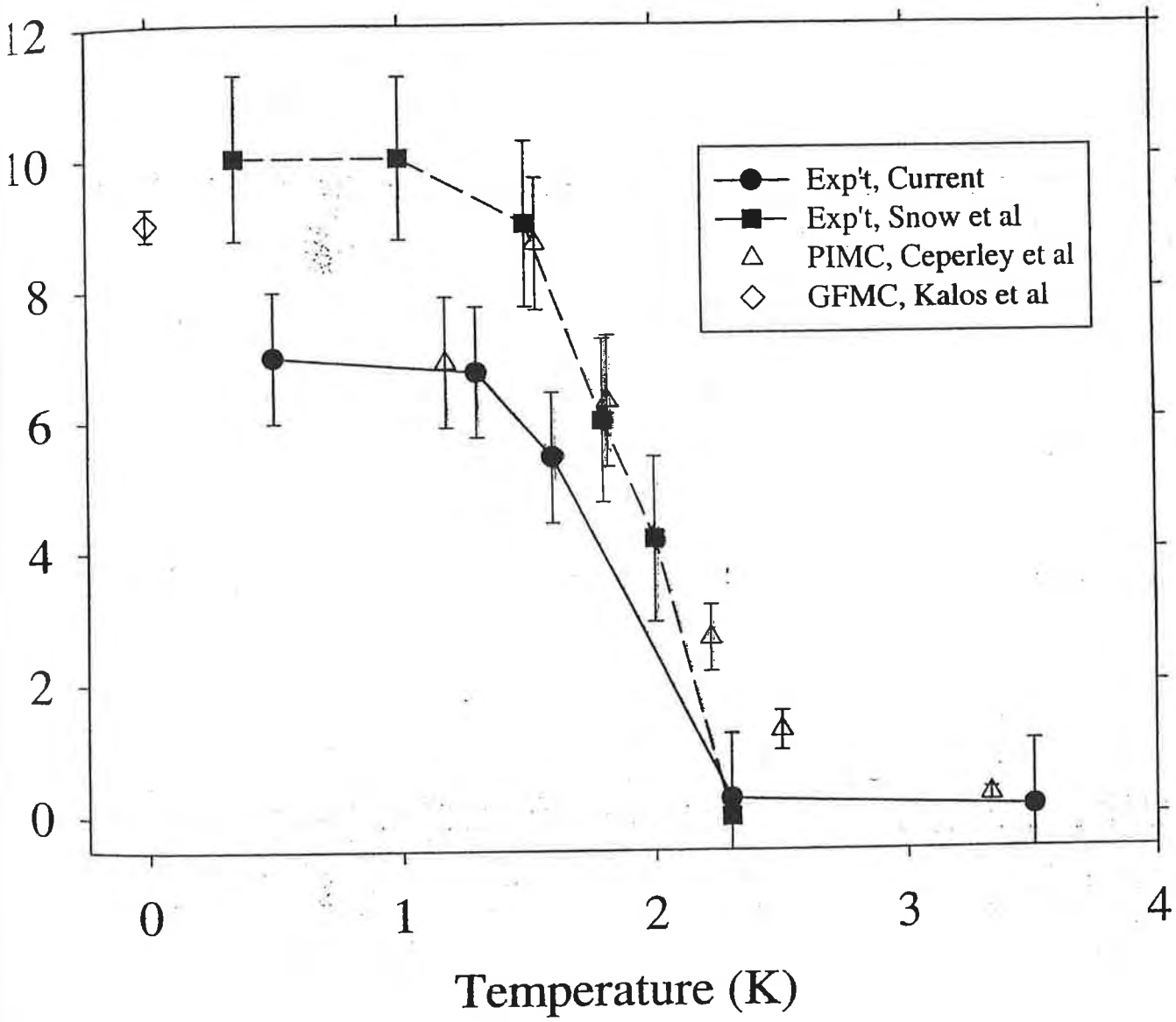
12
10
8
6
4
2
0
0
1
2
3
4
Temperature (K)
Exp't, Current
Exp't, Snow et al
PIMC, Ceperley et al
GFMC, Kalos et al

FIG.

C. Andreani

VESUVIO

A novel instrument for neutron spectroscopy at eV energies

CLRC- RAL (UK), INFM (IT), Univ. of Liverpool (UK)

J. Tomkinson (ISIS-UK, Coordinator)

C. Andreani (INFM-Italy)

D. Colognesi (CNR and INFM-Italy)

• A. Fielding (Liverpool Univ. -UK)

• E. Degiorgi (INFM-Italy)

J. Mayers (ISIS-UK)

M. Nardone (INFM-Italy)

E. Pace (INFN and INFM-Italy)

M. Praitano (Ditta RMP ROMA-Italy)

• R. Senesi (INFM-Italy)

W.G. Stirling (Liverpool Univ. -UK)

C. Uden (ISIS-UK)

- NEUTRON SCATTERING
  $20\ A^{-1} < q < 200\ A^{-1}$ and $\hbar w > 1eV$

- EXPERIMENTAL TECHNIQUE

- PROJECT DELIVERALES

- EXAMPLE OF APPLICATIONS

Deep Inelastic Neutron Scattering
(DINS)

- High **q**: $20\,\text{Å}^{-1} < q < 200\,\text{Å}^{-1}$

Incoherent approximation:

If $q >> \frac{2\pi}{d}$ then $\sigma_i \rightarrow \sigma$ and:

$$\left(\frac{d^2\sigma}{d\Omega dE'}\right) = \frac{k'}{k} \mid \bar{b} \mid^2 S_i(\mathbf{q},\omega)$$

where:

$$S_i(\mathbf{q},\omega) = \sum_I \sum_F p_I \mid < F \mid \exp(i\mathbf{q}\cdot\mathbf{r}) \mid I > \mid^2 \delta(\hbar\omega + E_I - E_F)$$

- High **ω: $\hbar\omega > 1$ eV**

Impulse approximation

$\mathbf{r}(t) = \mathbf{r}(0) + \mathbf{q}\frac{t}{M}$ e:

$$S_i^{IA}(\mathbf{q},\omega) = \sum_I p_I < I \mid \delta(\hbar\omega - \overbrace{\frac{\hbar^2 q^2}{2M}}^{\omega_R} - \frac{\hbar\mathbf{q}\cdot\mathbf{p}}{M}) \mid I >$$

$$S_i^{IA}(\mathbf{q},\omega) = \int d\vec{p}\; \underbrace{n(\vec{p})}_{\downarrow} \delta[\hbar\omega - \frac{(\vec{p} + \hbar\vec{q})^2}{2M} - \frac{\hbar\mathbf{p}^2}{2M}]$$

of the initial state

(energy conservation in a free system:
$E_I = \frac{p^2}{2M} \rightarrow E_F = \frac{(\mathbf{p}+\hbar\mathbf{q})^2}{2M}$)

- West scaling:

$$y = \frac{M}{\hbar^2 q}\left(\hbar\omega - \frac{\hbar^2 q^2}{2M}\right)$$

$q < \infty \rightarrow F(y,q) = \frac{\hbar q}{M} S_i(q,\omega) \rightarrow_{q\rightarrow\infty} F^{IA}(y) = n_z(y)$

where:

$$n_z(p_z) = \int_{-\infty}^{\infty} dp_x \int_{-\infty}^{\infty} dp_y n(\mathbf{p})$$

but for $q < \infty$ (final state interaction):

$$F(y,q) = F^{IA}(y) \otimes R^{FSI}(y,q)$$

- Molecular fluid (decoupling)

If:

$$\Psi = \Phi(\mathbf{R}_1, ..., \mathbf{R}_N) \prod_{i=1}^{N} \phi_i(\mathbf{r}_i)$$

then:

$$S(q,\omega) = S_{CM}(q,\omega) \otimes S_r(q,\omega)$$

$$F(q,y) = F_{CM}(q,y) \otimes F_r(q,y)$$

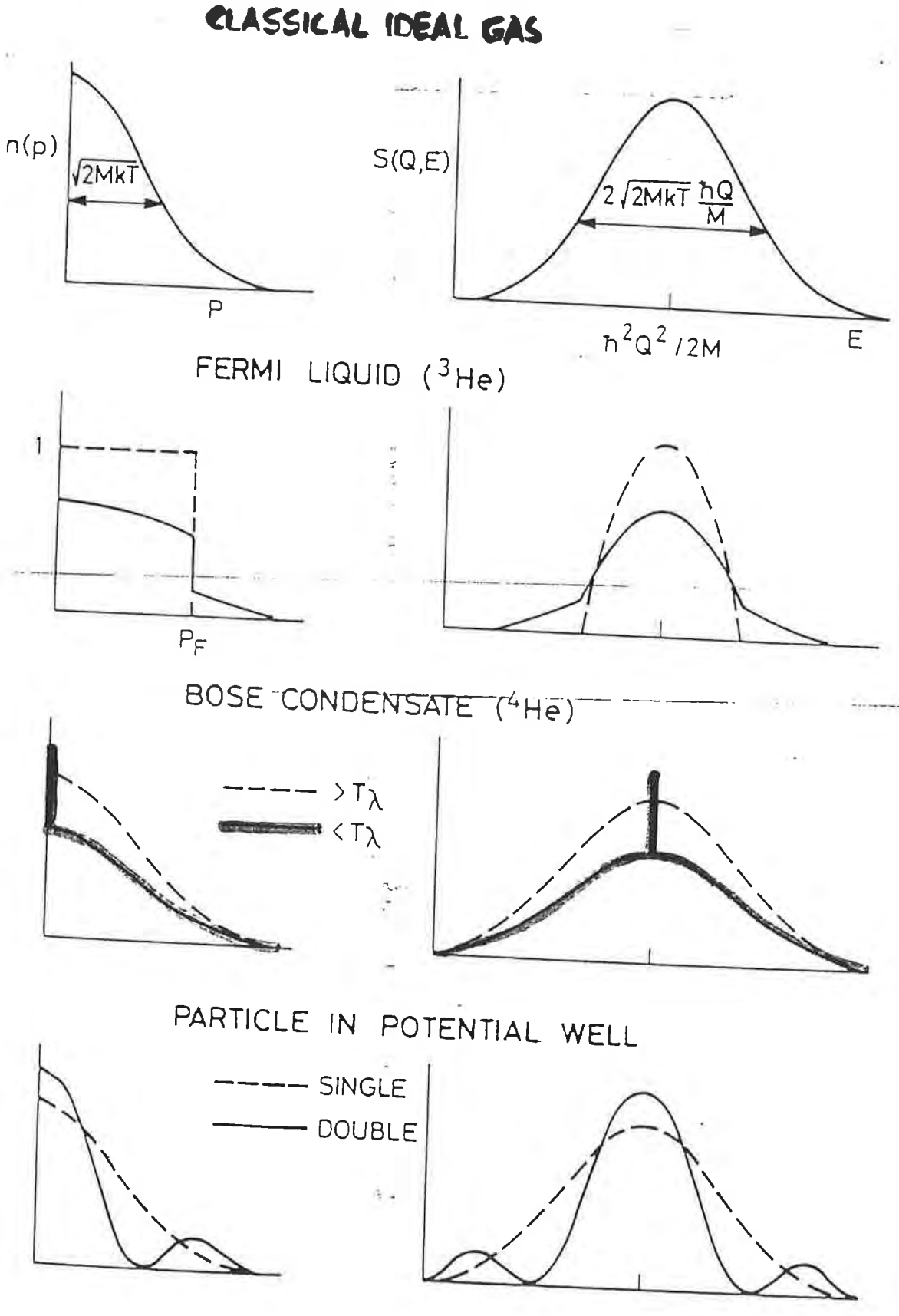

FIG 1. n(p) and S(Q,E) for four cases.

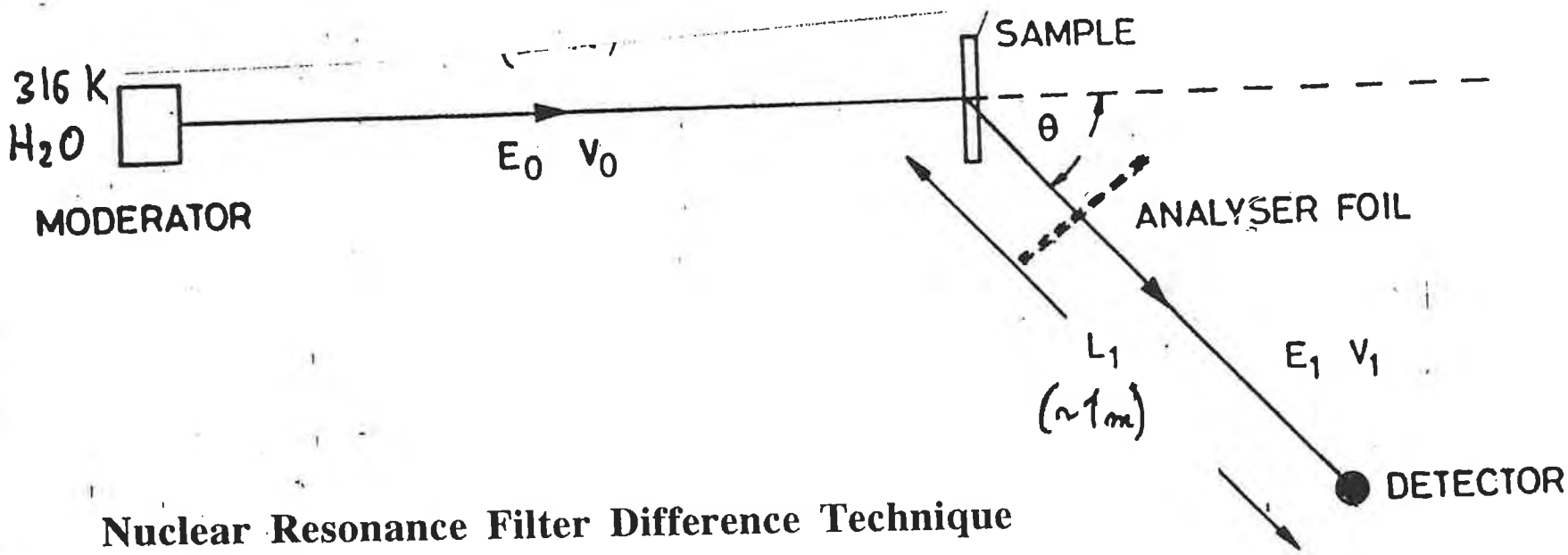

Nuclear Resonance Filter Difference Technique

- U foil absorbs neutrons
- Difference between two measurements (one with U foil in and one with U foil out) gives:
  - number of neutrons captured by U foil
  - defines E_1 of the scattered neutrons

eVS Spectrometer

- **eVS:** epithermal time of flight spectrometer

inverse geometry $\longrightarrow$ nuclear resonance

$$^{238}U: \ (6671 \pm 106)\ meV$$

$$Au: \ (4906 \pm 182)\ meV$$

beam: $\phi = 30$ mm

detectors (Li glass): #32, $\Delta\theta = 30^o \div 69^o$

range: $\hbar\omega = (2 \div 32.4)\ eV$, $q = (32 \div 126)$ Å^{-1}

resolution (H): $\simeq (1 \div 1.5)$ Å^{-1}

RESOLUTION CONPONENT

- Geometrical conponent ⟶ Gaussian
- Energy conponent ⟶ Gaussian and Lorentzian

First development : single difference technique

Au, U foils

U resonances : 6.7 eV, 20.7 eV, 37 eV

- FWHM (intrinsic width at 6.7 eV) → 0.04 eV
- Doppler broadning at RT → 0.11 eV
- Doppler broadning at 70 K → 0.06 eV

Second development : double difference technique

Reduction factor 0.75

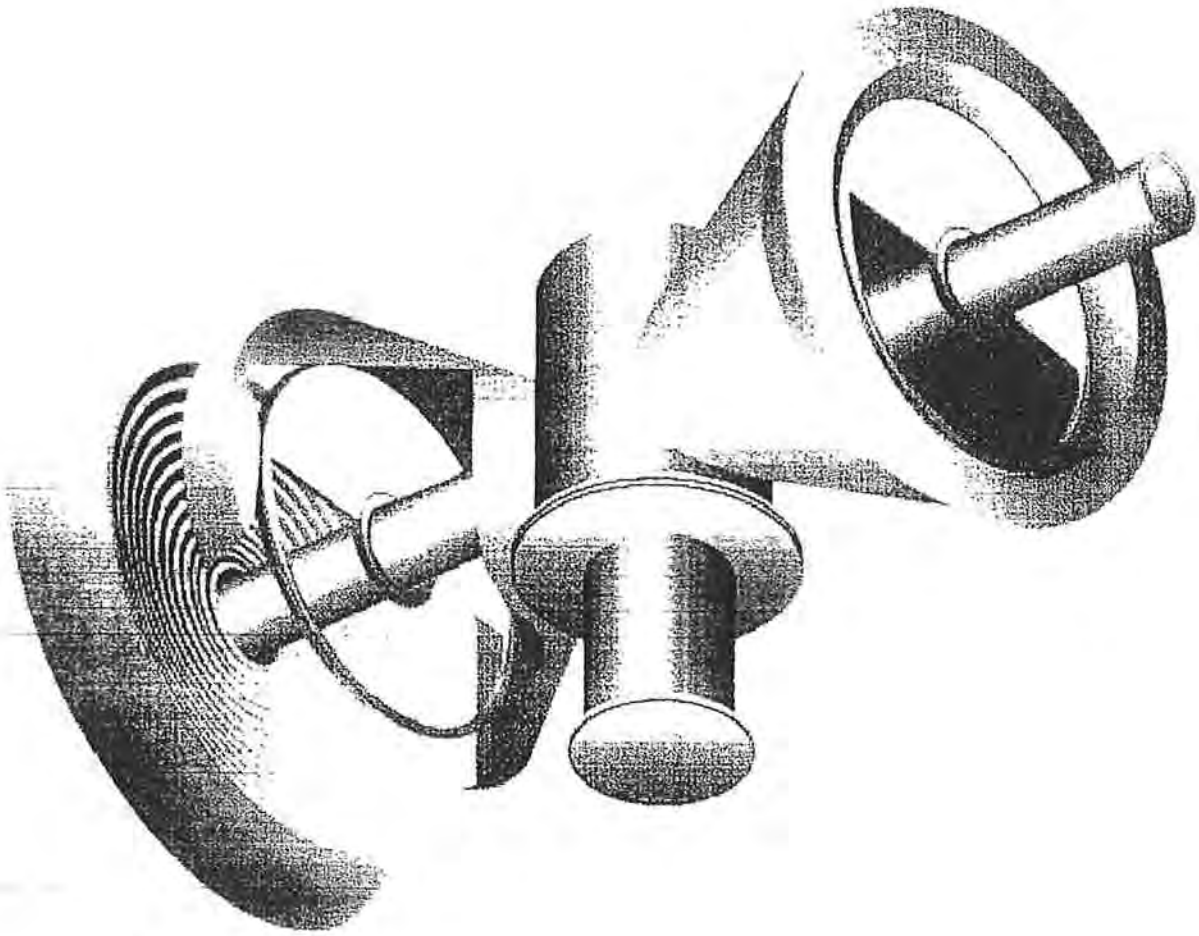

Deliverables of the project

- **New instrument tank**
  cold filter analysers
  double difference techniques
- **New Detectors for eV energies**
  Cerium-activated lithium glass scintillators $^{6}Li(n, \alpha)^{3}H$
  Boron-loaded liquid scintillators $^{10}B(n, \alpha)^{7}Li$
- **Neutron scattering formalism**

  $20\ A^{-1} < q < 200\ A^{-1} \qquad \omega > 1\ eV$
- **Specific goal in experimental physics**
  - **Chemistry/biology**
    hydogen-bonded polycristalline and single crystals
  - **Atomic and molecular quantum systems**

  Materials Science:
  amorphous materials,
  polymers,
  catalysts
  metal hydrides.

- **Magnetic and electronic transitions:**
  transition metal spin-waves,
  intermultiplet transitions in rare-earths and actinides,
  interband electronic transitions.

- **Training of Young Scientists**

- **Workshop**
  26/27 November ISIS

http://www.roma2.infn.it/infm/vesuvio

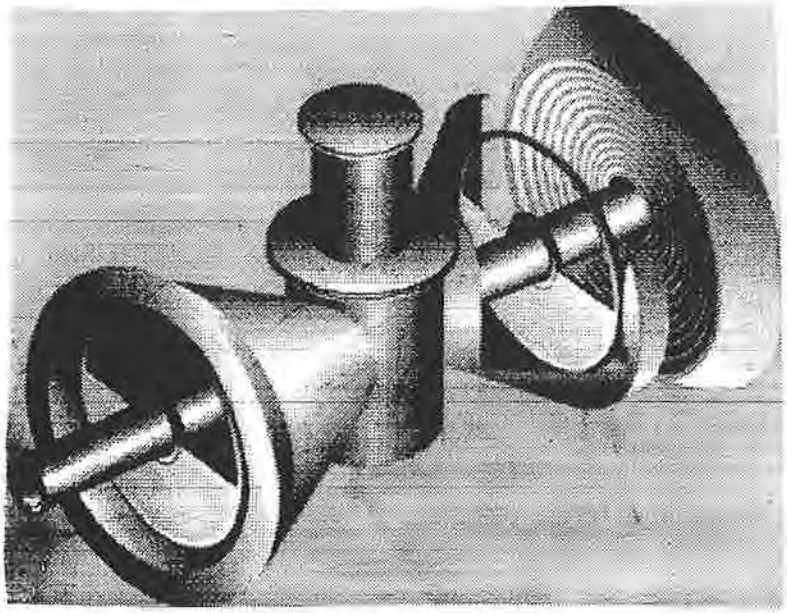

PARA - H_2

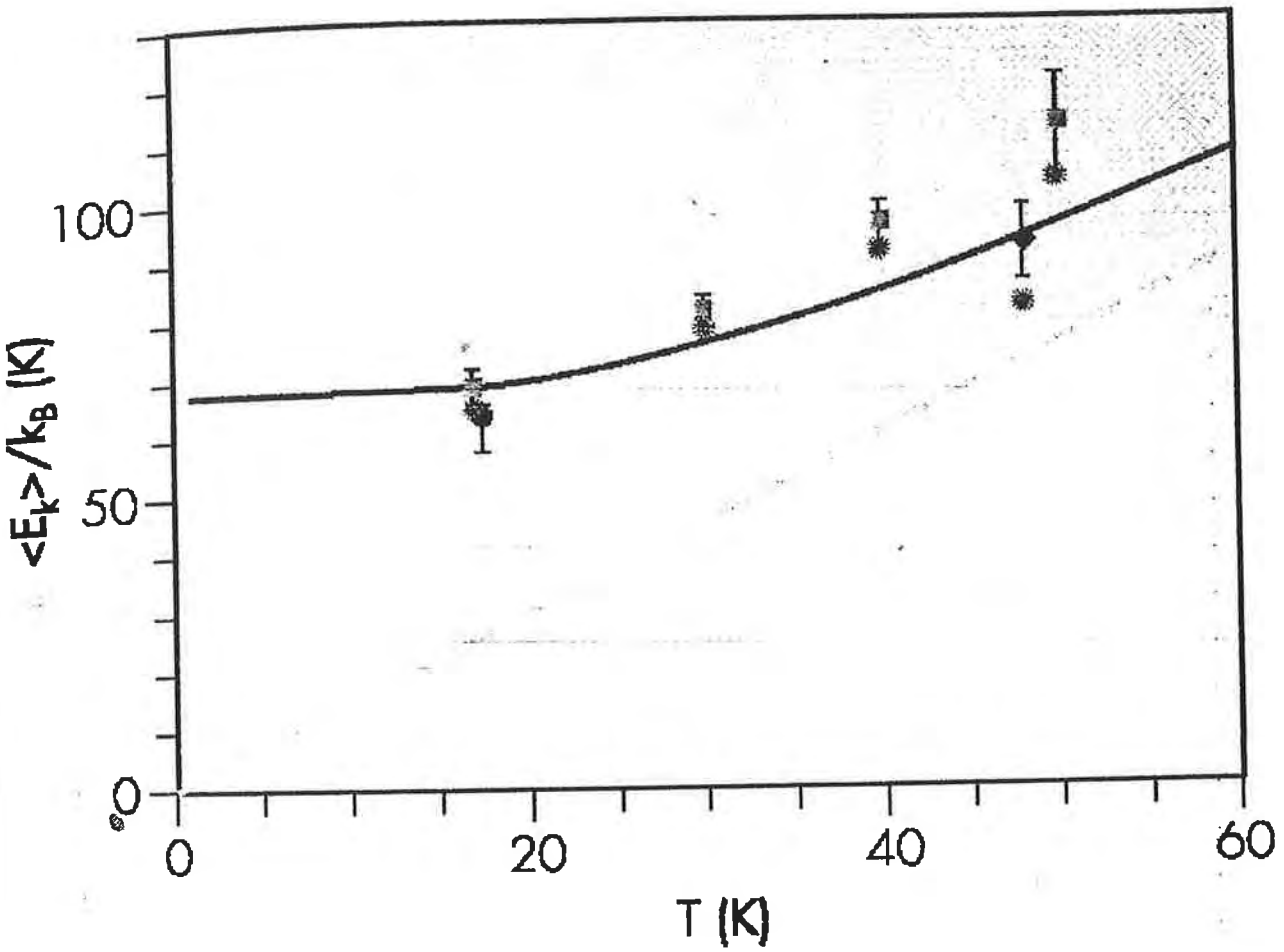

Translational kinetic energy <Ek> as a function of temperature T for parahydrogen. Squares: ρ=22.41 molecules.nm^{-3}; diamond: ρ=10.45 molecules·nm^{-3}; circle: previous measurement by other workers; stars: Path Integral Monte Carlo simulation; dashed line: classical behavior; full line: harmonic oscillator model with a zero-point energy corresponding to 68 K.

^{4}He

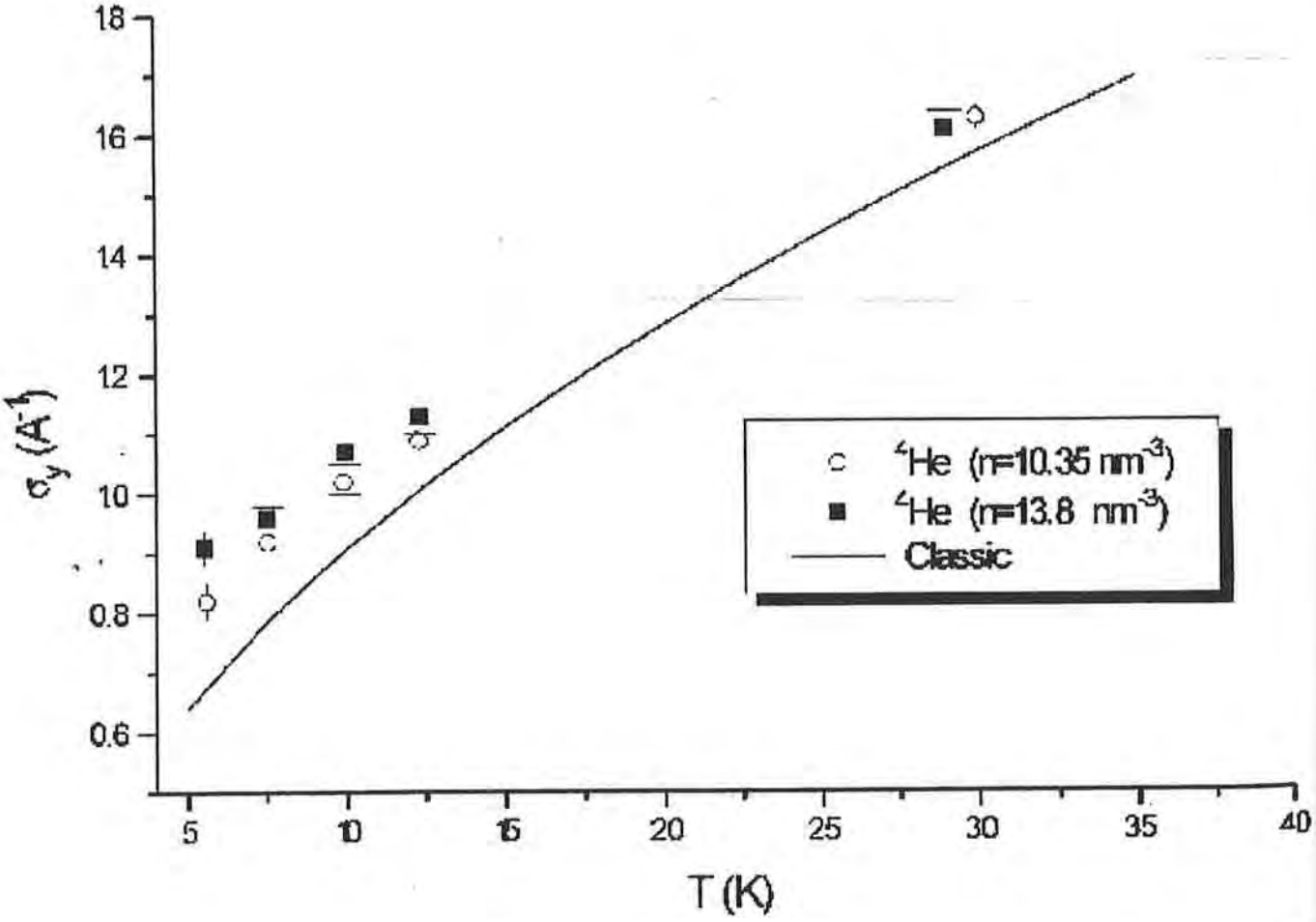
18
16
14
12
10
0.8
0.6
σ_y (Å^{-1})
5
10
15
20
25
30
35
40
T (K)
^{4}He (n=10.35 nm^{-3})
^{4}He (n=13.8 nm^{-3})
Classic

Exp (n=10.35nm⁻³)
Exp. (n=13.8 nm⁻³)
RMC (n=10.0 nm⁻³)
[Capehart et al., 1995]
RMC (n=13.8 nm⁻³)
FIL ΔVT₀₂ (n=10.0 nm⁻³)
FIL ΔVT₀₂ (n=13.8 nm⁻³)
<ΔE^K> (K)
T (K)
0
10
20
30
40
1
2
3
4
5
6
7
8

^4He $T = 2.5\,K$

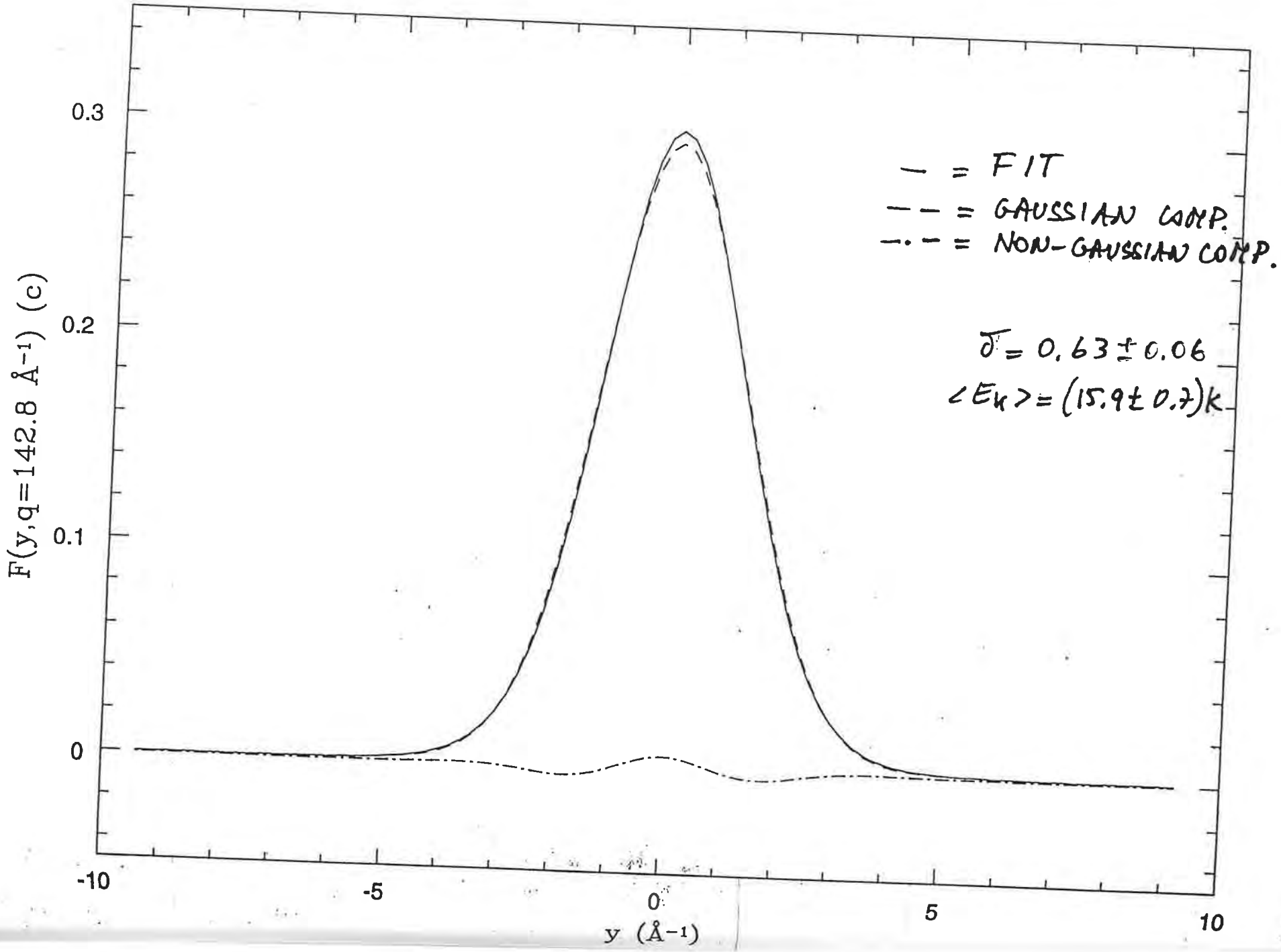

^4H $T = 2.5\,K$

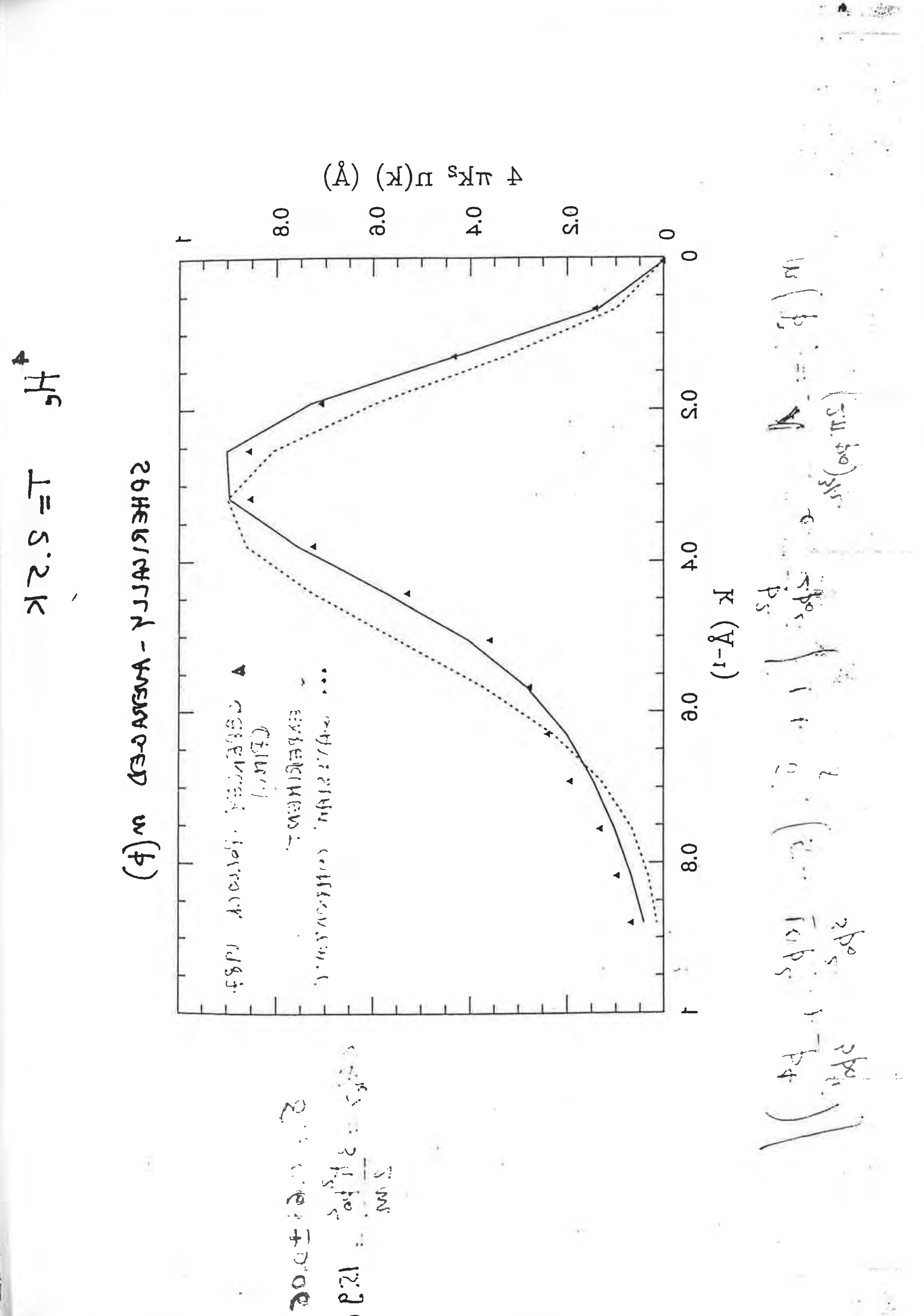
SPHERICALLY - AVERAGED n(p)
T = 2.2 K
k (Å⁻¹)
4 πk² n(k) (Å)
EXPERIMENT
12.9 K

Scattering Angle (°)	Resonance foil	Resonance energy E_I (eV)	Resonance width ΔE_I (eV)	Momentum transfer q (Å^{-1})	Energy transfer ω (eV)	Δy_E (Å^{-1})	Δy_I (Å^{-1})
106	Au	4.908	0.128	94	4.58	1.86	0.71
123	U	6.671	0.063	125	8.15	0.79	0.72
137	U	6.671	0.063	136	9.64	0.75	0.75
152	U	6.671	0.063	152	10.96	0.73	0.65
148	cooled U	6.671	0.045	143	10.59	0.57	0.67

Temperature (K)	σ(Au) (Å^{-1})	σ(U) (Å^{-1})	κ(Au) (K)	κ(U) (K)	n_0
1.3	0.875 ± 0.008	0.881 ± 0.011	13.9 ± 0.3	14.1 ± 0.4	15 ± 4
1.7	0.889 ± 0.009	0.899 ± 0.011	14.4 ± 0.3	14.7 ± 0.4	12 ± 4
1.9	0.903 ± 0.009	0.907 ± 0.011	14.8 ± 0.3	15.0 ± 0.4	10 ± 4
2.5	0.963 ± 0.009	0.945 ± 0.011	16.9 ± 0.3	16.2 ± 0.4	0
1.5		—		13.5 ± 0.7	11.6 ± 3.3
2.5		0.935 ± 0.019		15.9 ± 0.7	0

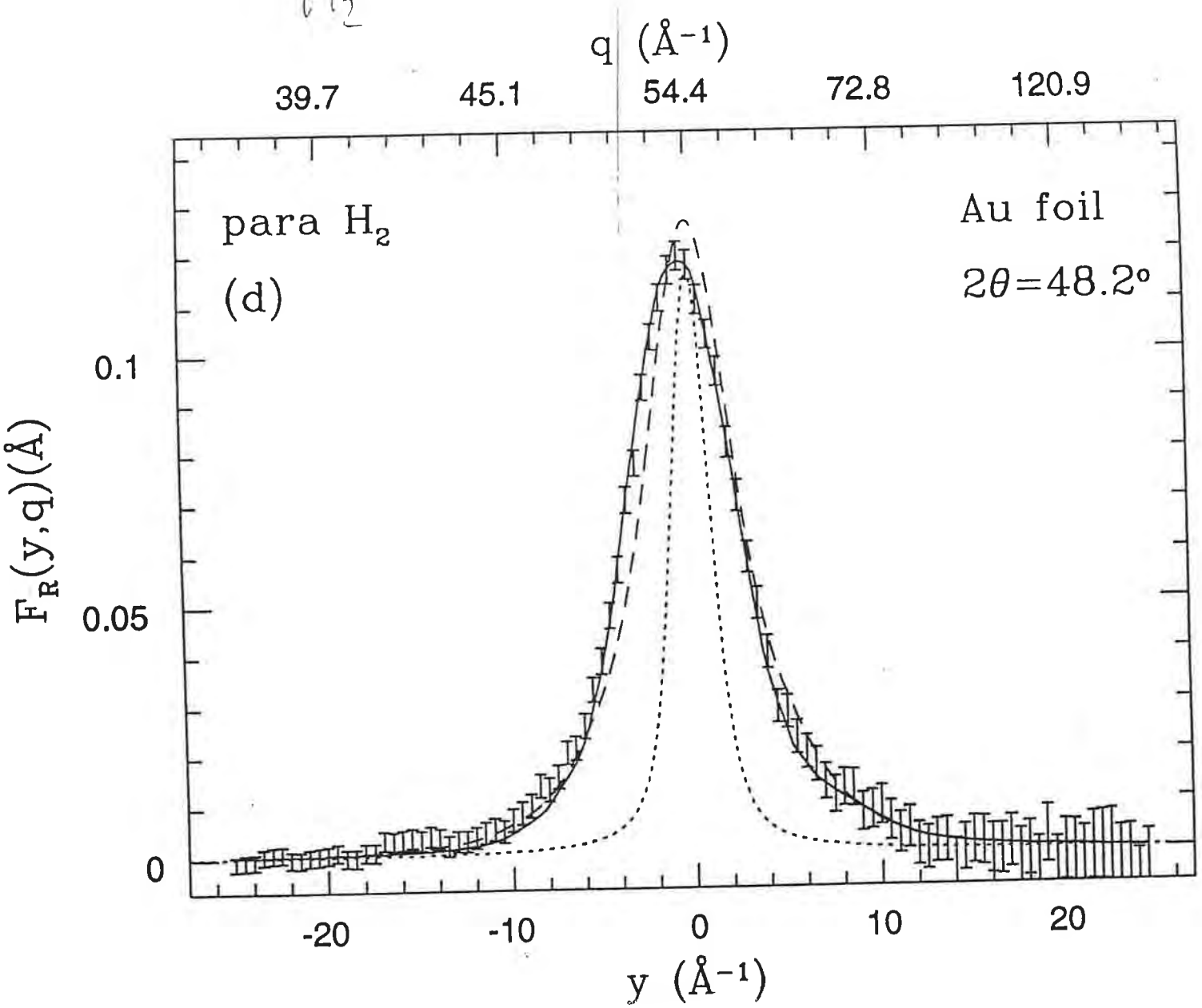

H2

--- IA

—— WKB

III DATA

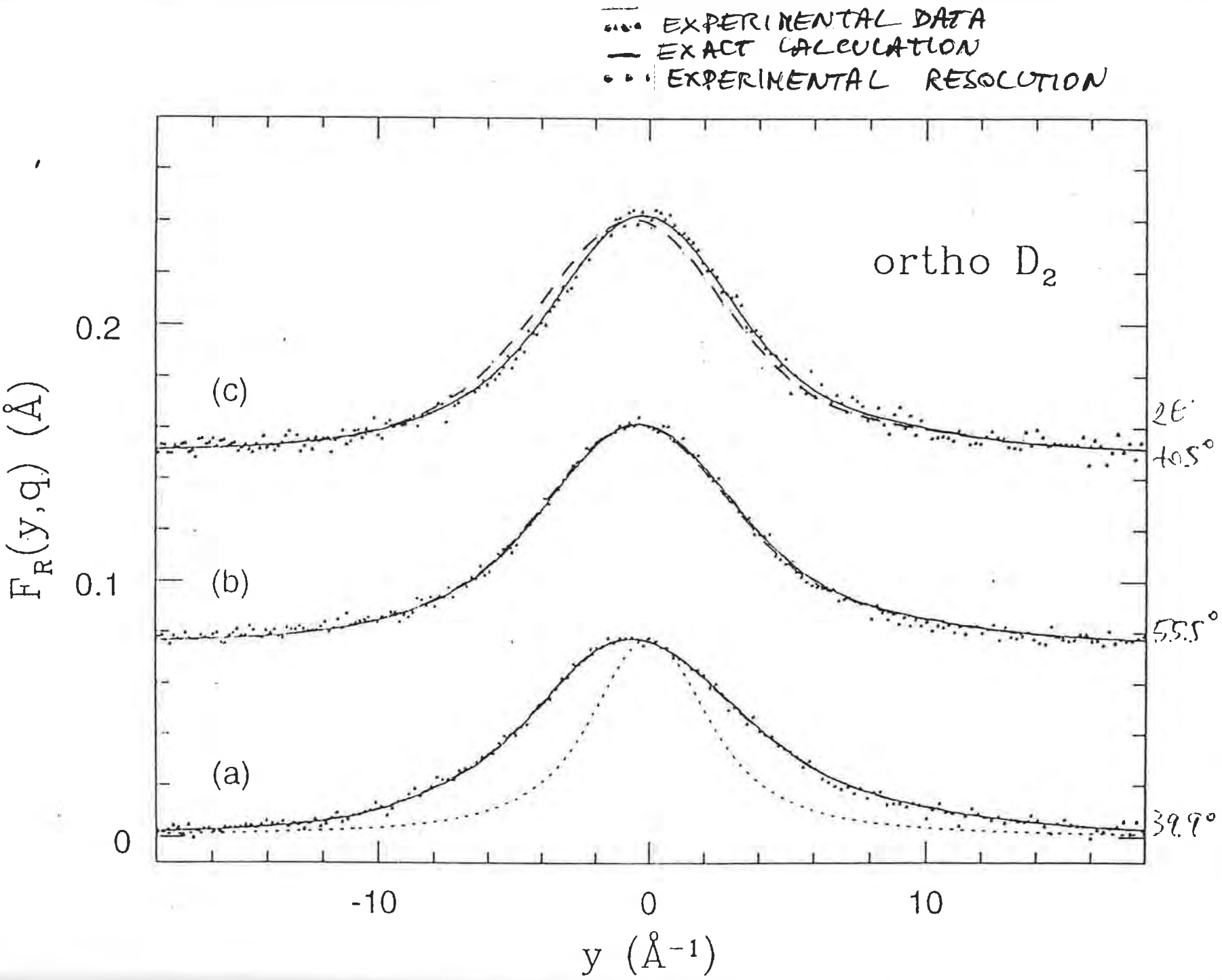
EXPERIMENTAL DATA
EXACT CALCULATION
EXPERIMENTAL RESOLUTION
ortho D_2
(c)
(b)
(a)
2E
40.5°
55.5°
39.9°
0.2
0.1
0
-10
0
10
$F_R(y,q)$ (Å)
y (Å^{-1})

y (A^{-1})

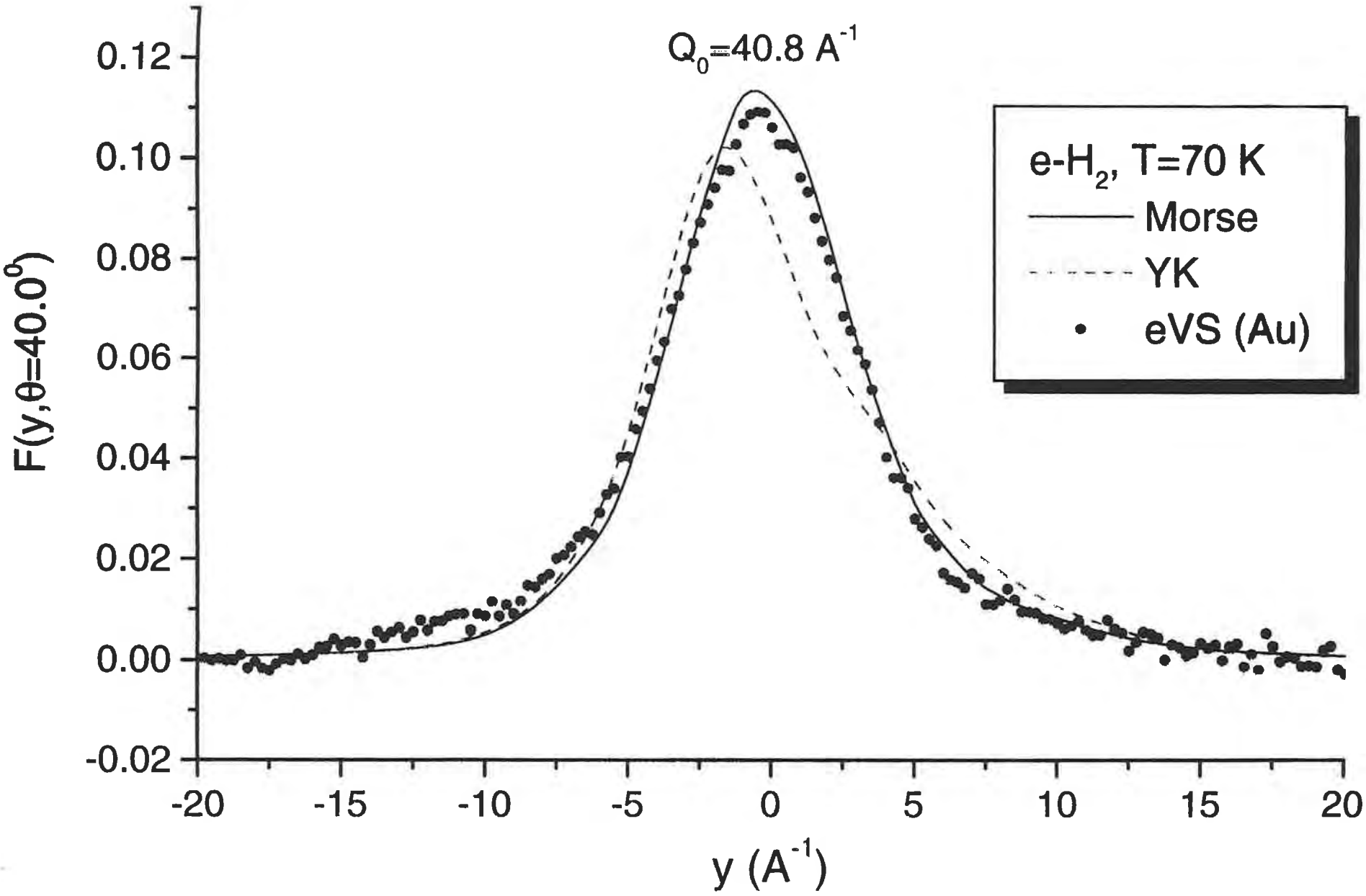
Q_0=40.8 A^{-1}
e-H_2, T=70 K
Morse
YK
eVS (Au)
F(y,θ=40.0°)
0.12
0.10
0.08
0.06
0.04
0.02
0.00
-0.02
-20
-15
-10
-5
0
5
10
15
20
y (A^{-1})

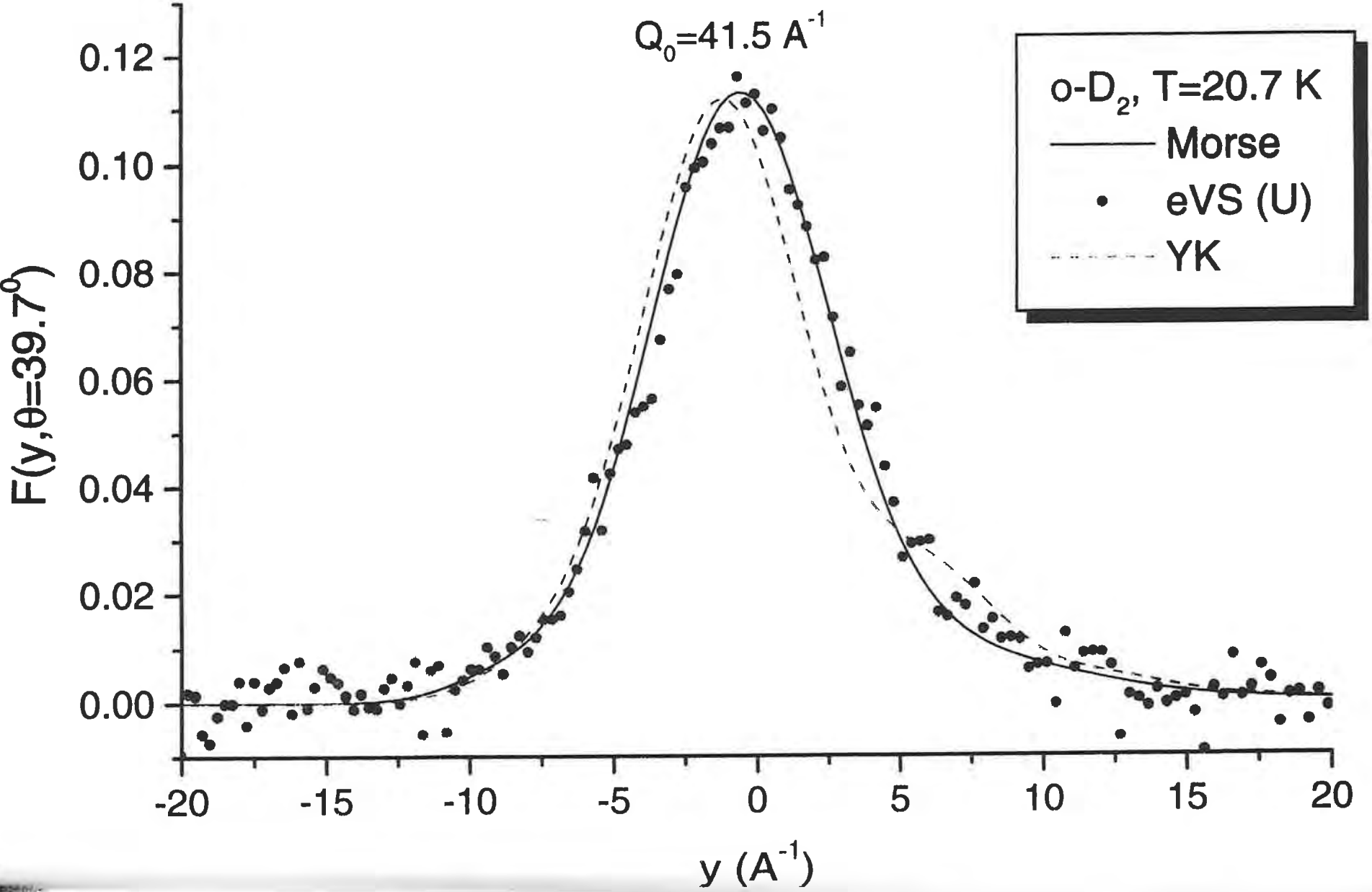
Q_0=41.5 A^{-1}
o-D_2, T=20.7 K
Morse
eVS (U)
YK
F(y,θ=39.7°)
0.12
0.10
0.08
0.06
0.04
0.02
0.00
-20
-15
-10
-5
0
5
10
15
20
y (A^{-1})

y (A^{-1})

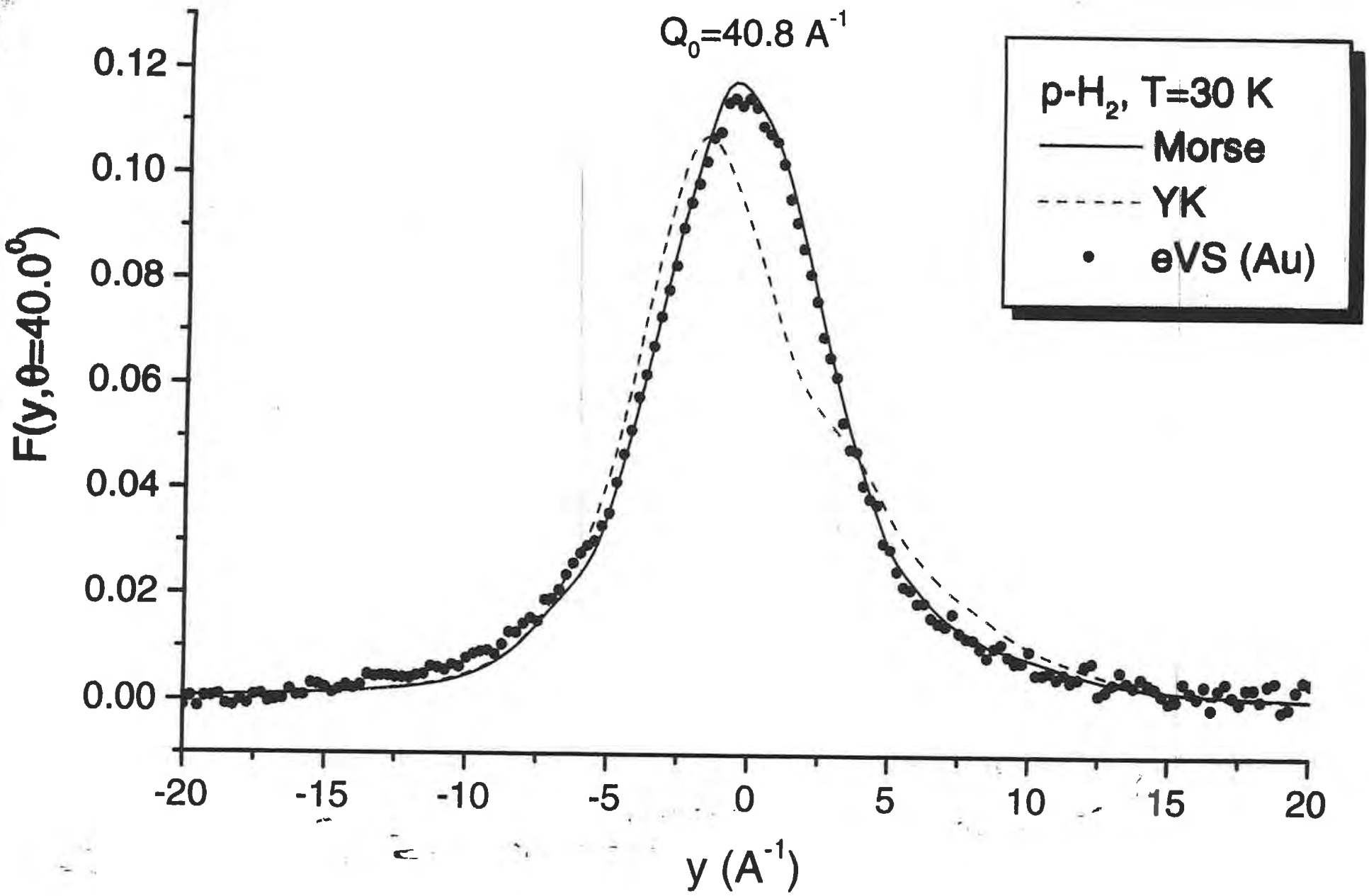
Q_0=40.8 A^{-1}
p-H_2, T=30 K
Morse
YK
eVS (Au)
F(y,θ=40.0°)
0.12
0.10
0.08
0.06
0.04
0.02
0.00
-20
-15
-10
-5
0
5
10
15
20
y (A^{-1})

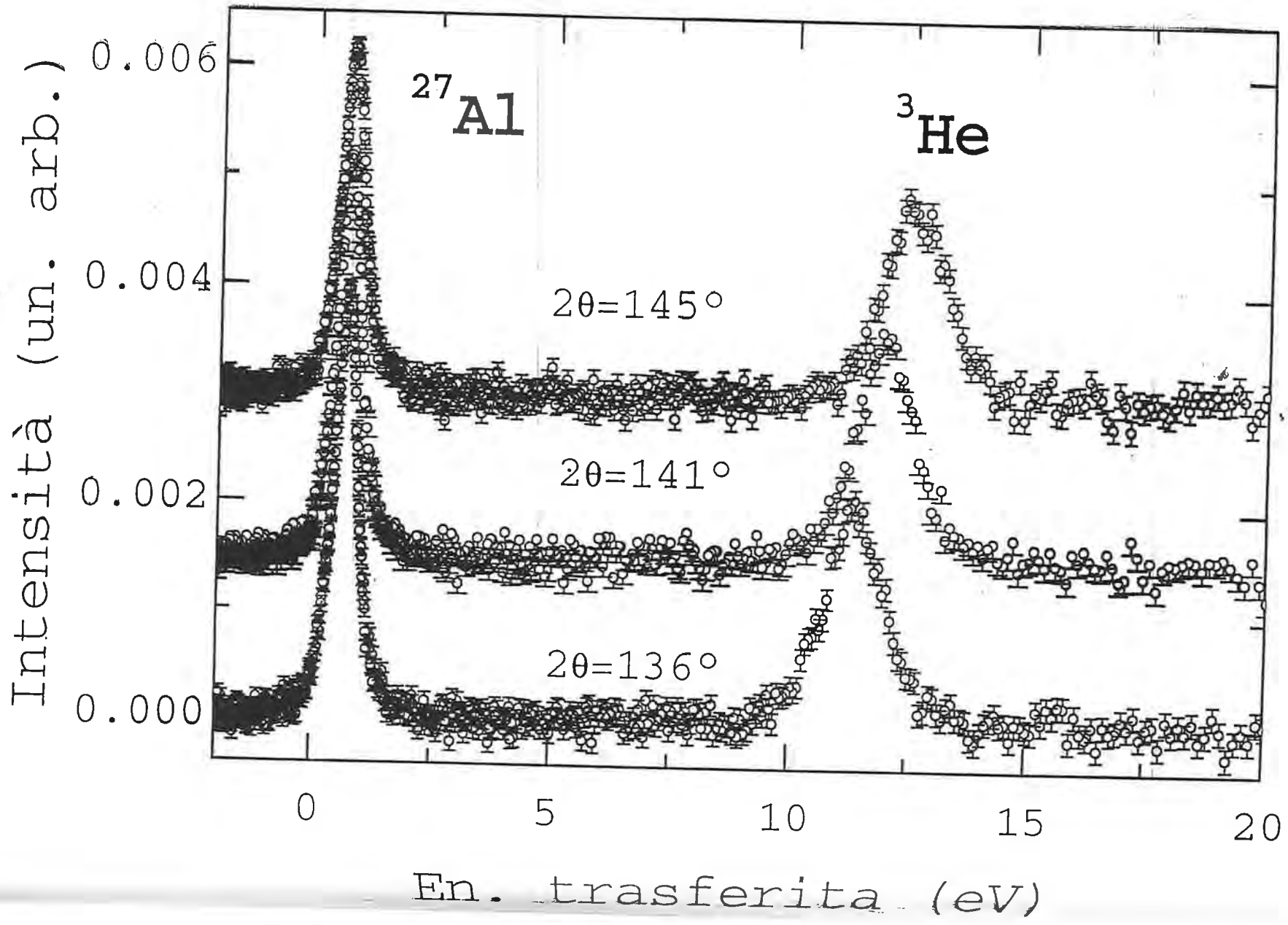
Intensità (un. arb.)
0.006
0.004
0.002
0.000
^{27}Al
^{3}He
2θ=145°
2θ=141°
2θ=136°
0
5
10
15
20
En. trasferita (eV)

En. trasferita (eV)

$<E_K>$(K)	T(K)	$\rho(nm^{-3})$	Ref	note
$8.1^{+1.7}_{-1.3}$	0.2	16.306	Sokol et al. (1985)	esp
10.7	1.2	16.173	Mook (1985)	esp
10.4±1.5	1.4	16.070	Azuah et al (1995)	esp
10.2±0.9	0.5	16.304	Dimeo et al (1998)	esp
12.9±0.7	1.5	15.990	**PRESENTE LAV. (1999)**	**ESP**
13	0	16.350	Usmani et al (1983)	teor
12.5±0.3	0	16.350	Whithlock et al. (1987)	teor
12.02±0.02	0	16.350	Moroni et al (1997)	teor

Tabella 1: **$<E_K>$ in ^{3}He liquido**

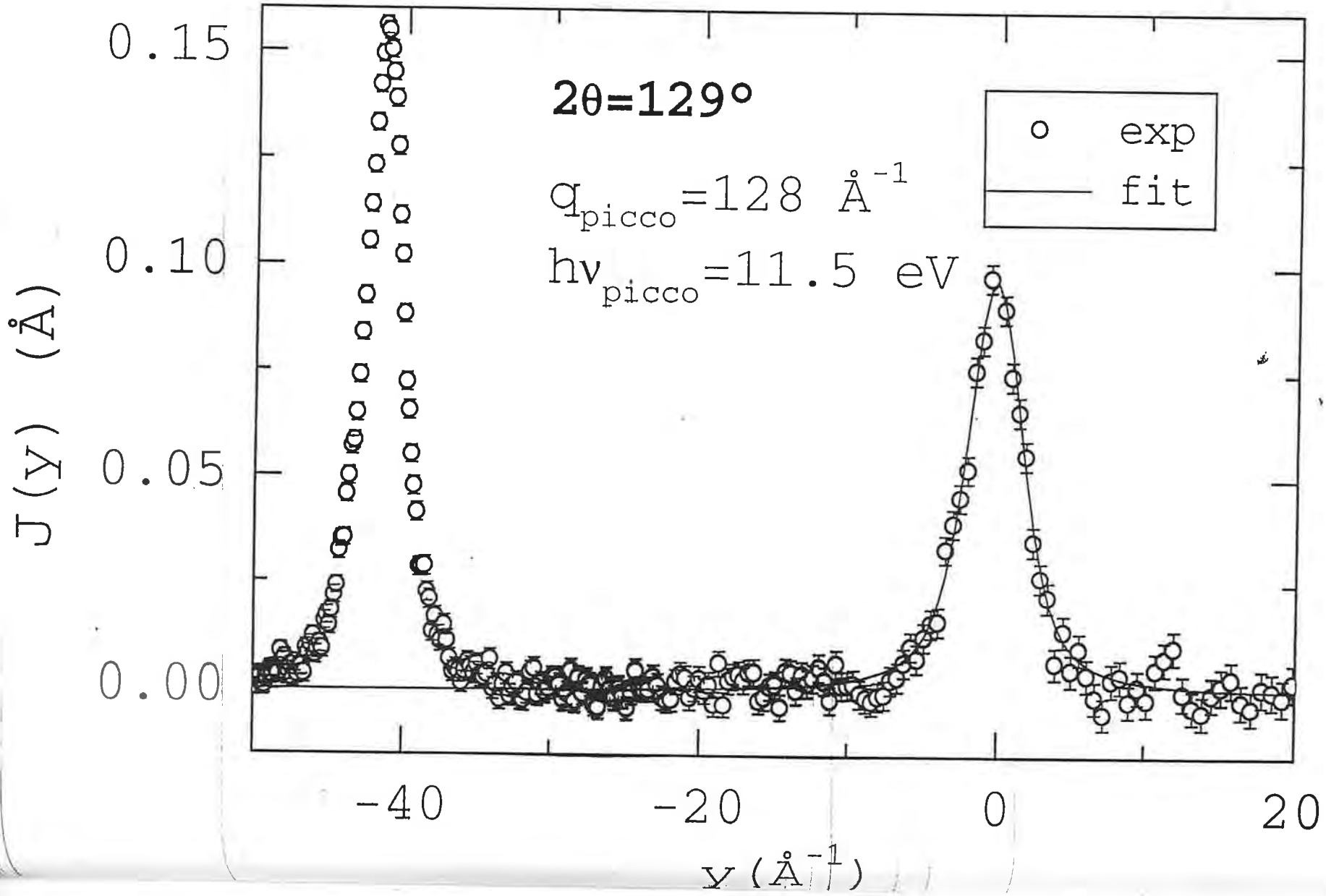
2θ=129°
q_{picco}=128 Å^{-1}
$h\nu_{picco}$=11.5 eV
exp
fit
J(y) (Å)
0.15
0.10
0.05
0.00
-40
-20
0
20
y (Å^{-1})

H_2S

y (Å^{-1})

H_2S

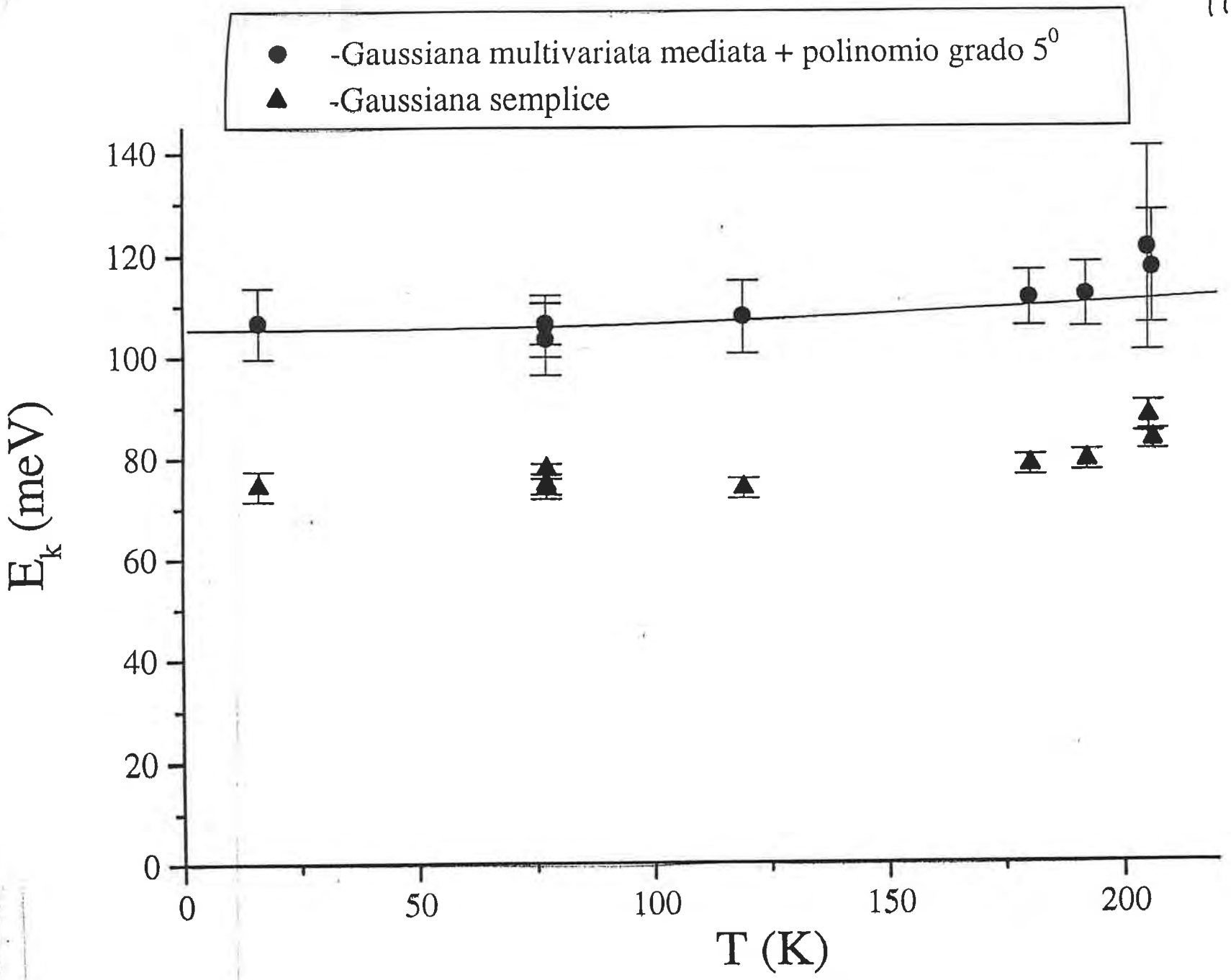
-Gaussiana multivariata mediata + polinomio grado 5^0
-Gaussiana semplice
140
120
100
80
60
40
20
0
0
50
100
150
200
E_k (meV)
T (K)

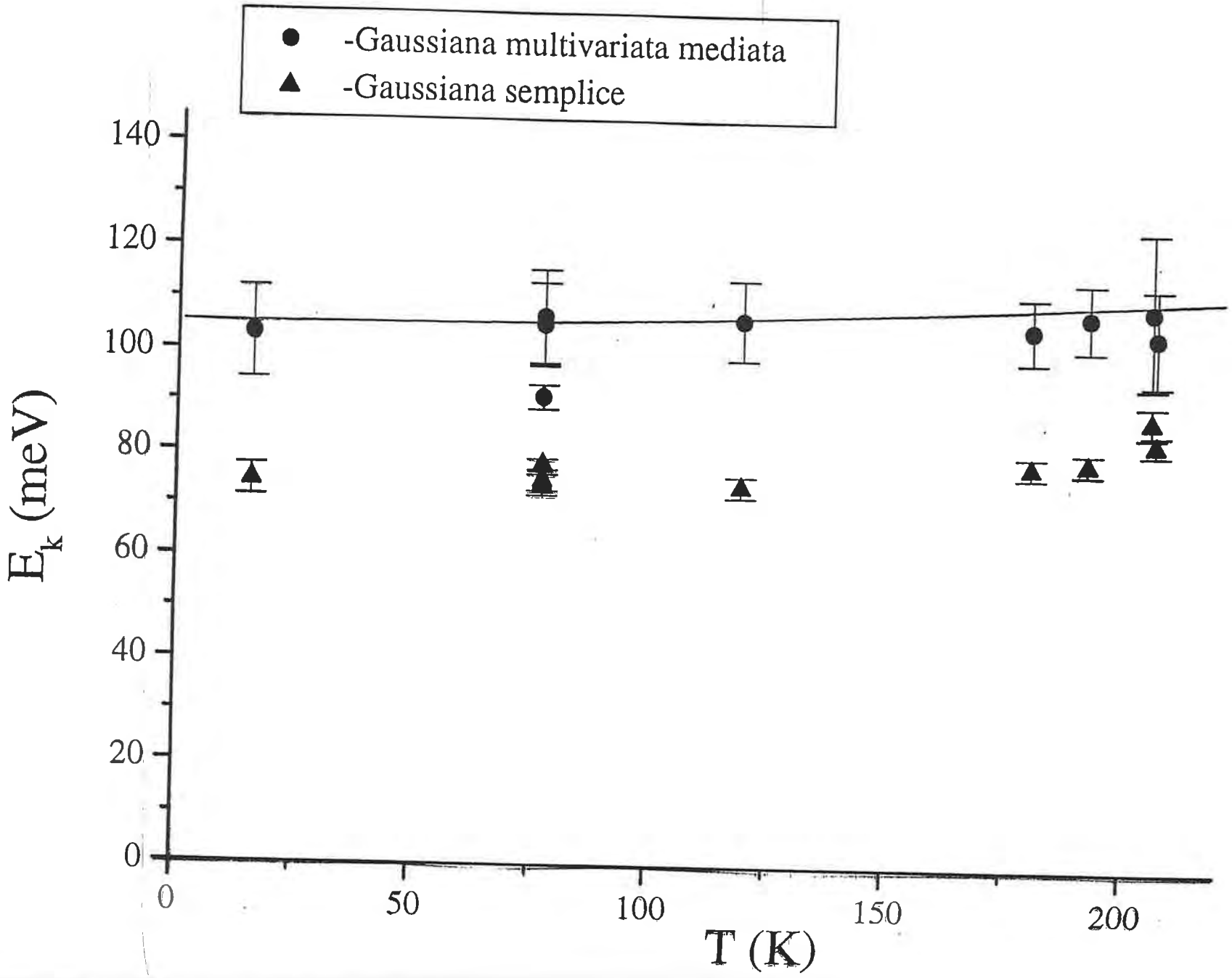
-Gaussiana multivariata mediata
-Gaussiana semplice
140
120
100
80
60
40
20
0
E_k (meV)
0
50
100
150
200
T (K)

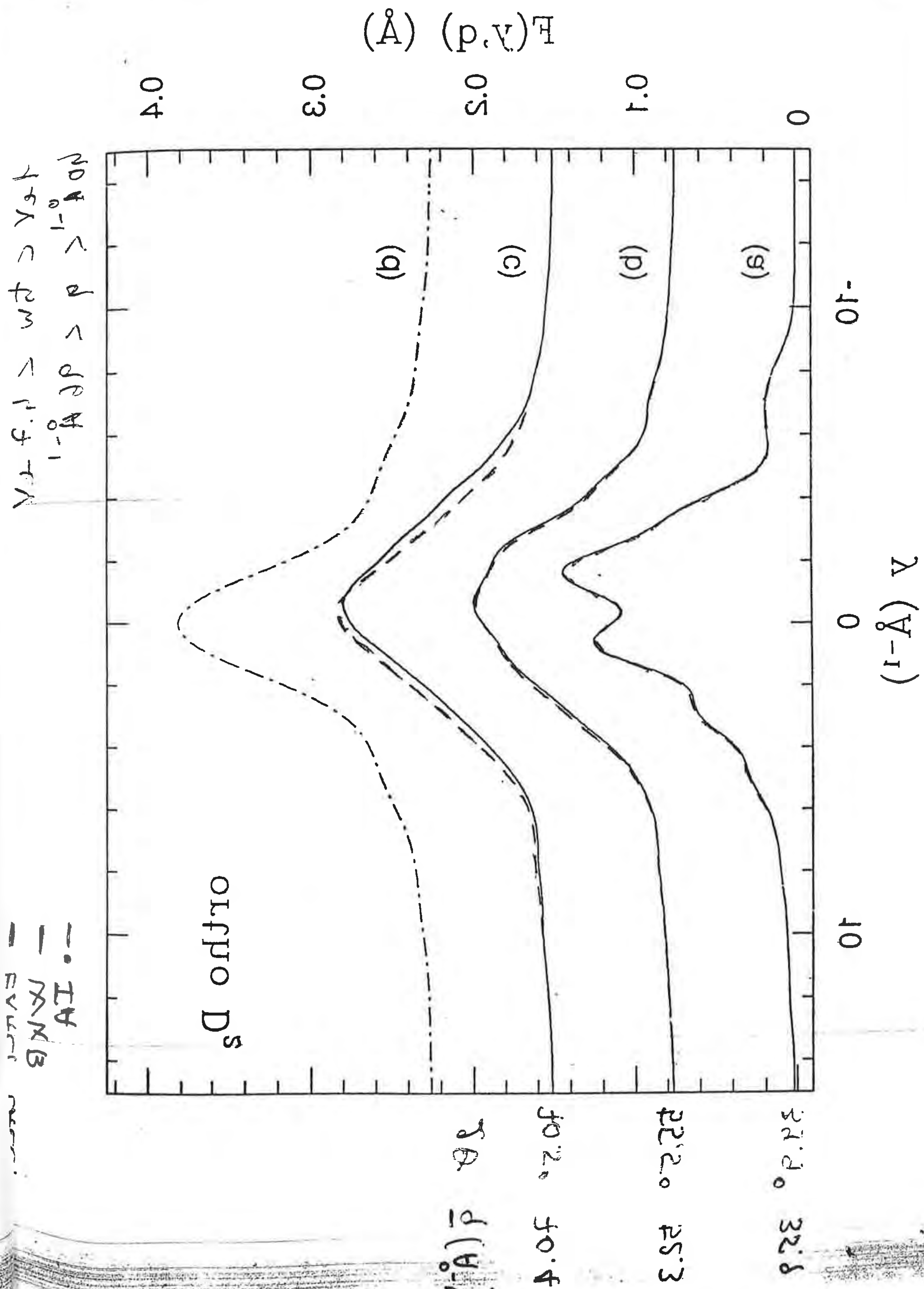

ortho D_s
(a)
(b)
(c)
(d)
λ (Å^{-1})
F(λ,d) (Å)

T(λ,θ) (A)
0.00
0.05
0.10
0.15
0.20
0.25
0.30
0.35
λ (Å)
-10
-5
0
5
10
T=17 K
θ=30°
θ=20°
θ=0°
Al
(a)
(b)
(c)
(d)
(e)

J. MAYERS

J. MAYERS

ISIS

"DESCRIPTION OF THE CURRENT eVS INSTRUMENT"

CLRC

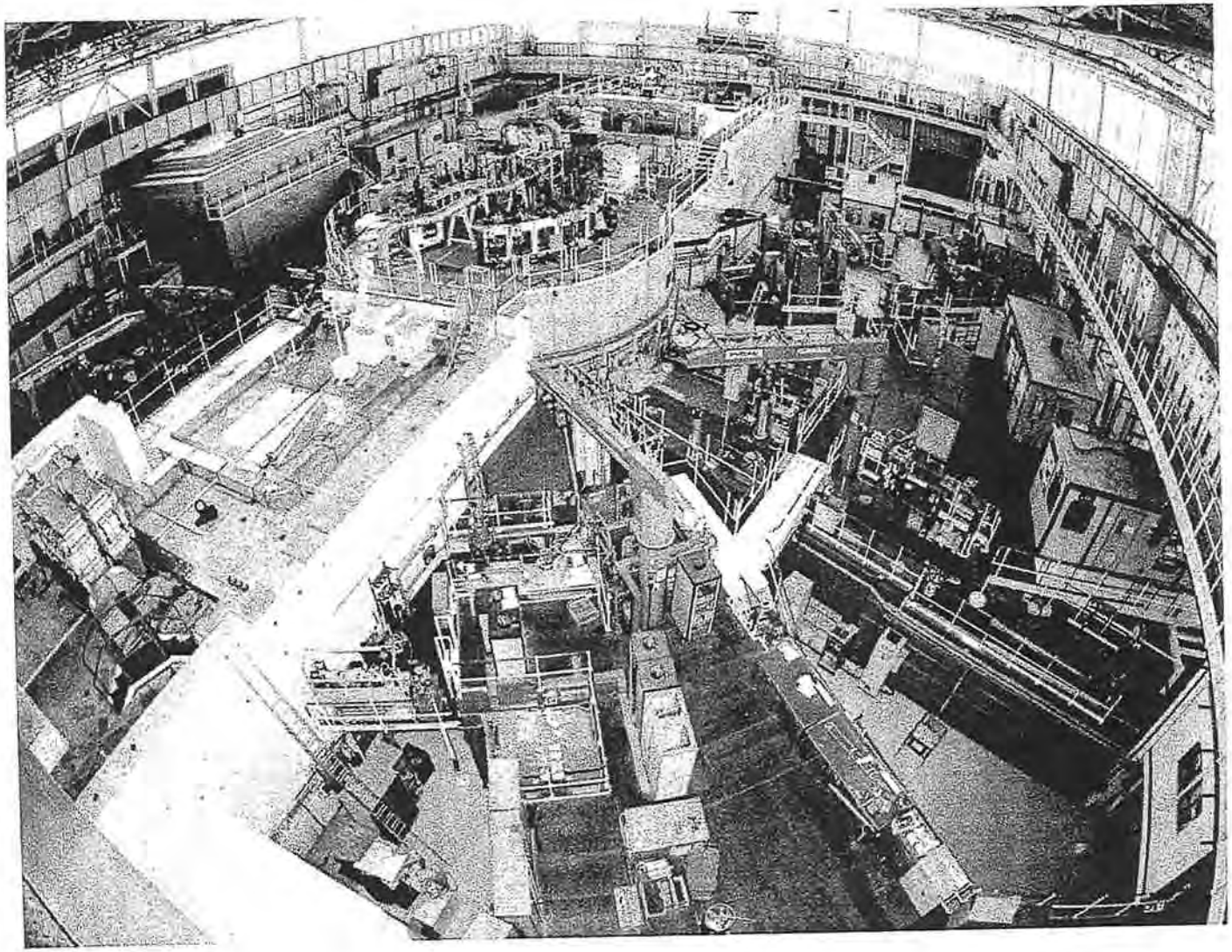

ISIS

CLRC

The Electron Volt Spectrometer (eVS)

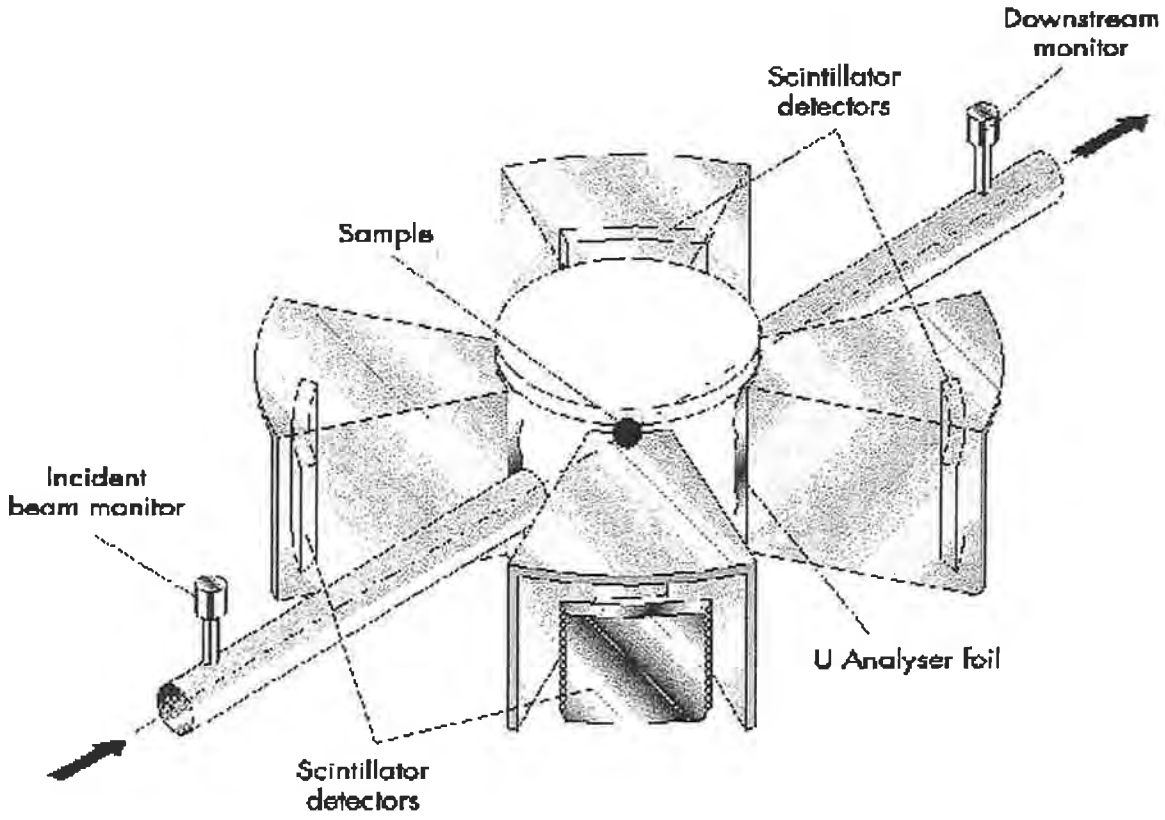

ISIS

Impulse Approximation

CLRC

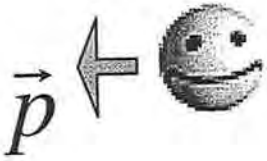

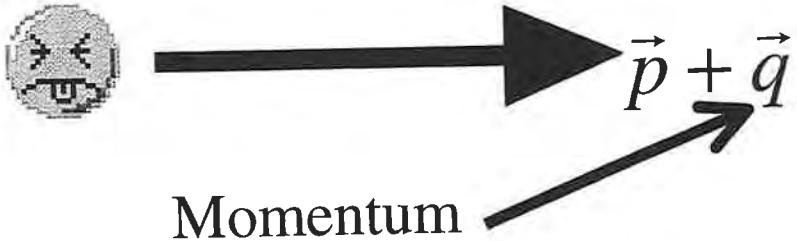

$$\kappa_i = p^2 / 2M$$

$$\kappa_f = (\vec{p}+\vec{q})^2 / 2M$$

$$\omega = \frac{(\vec{p}+\vec{q})^2}{2M} - \frac{p^2}{2M}$$

Energy transfer

$$y = \vec{p}.\hat{\vec{q}} = \frac{M}{q}\left(\omega - \frac{q^2}{2M}\right)$$

Momentum along $\hat{q}$

ISIS

CLRC

The Filter Difference Method

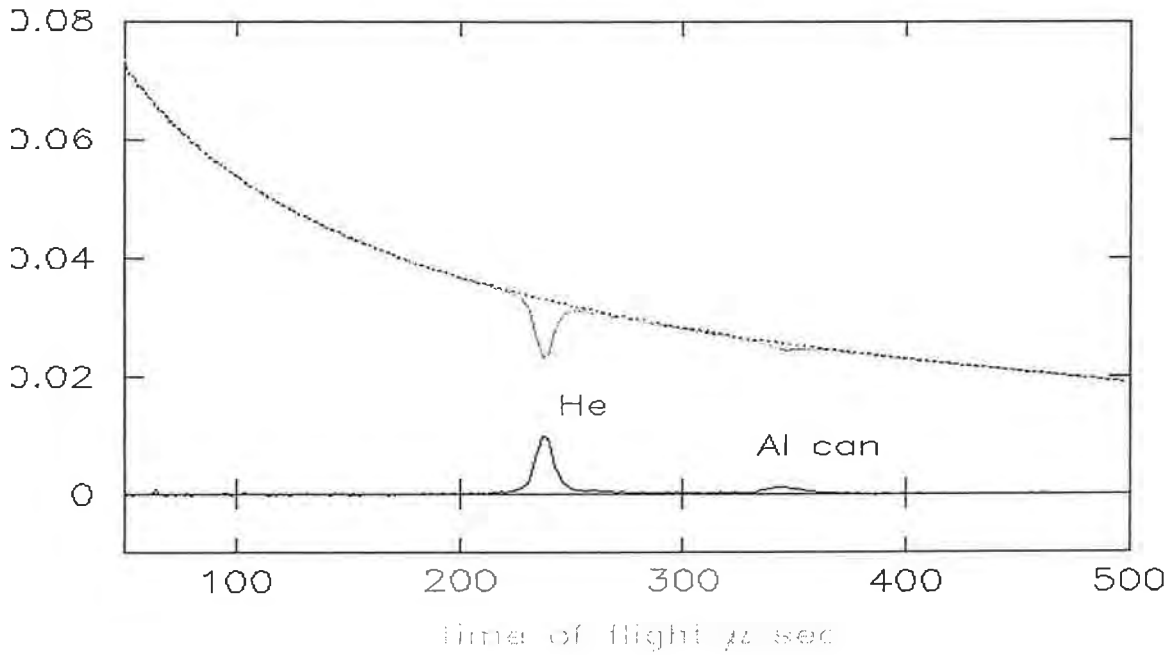

eVS Measurements on Liquid H_2

J Mayers (PRL **71** 1553 (1993)

Figure 3a

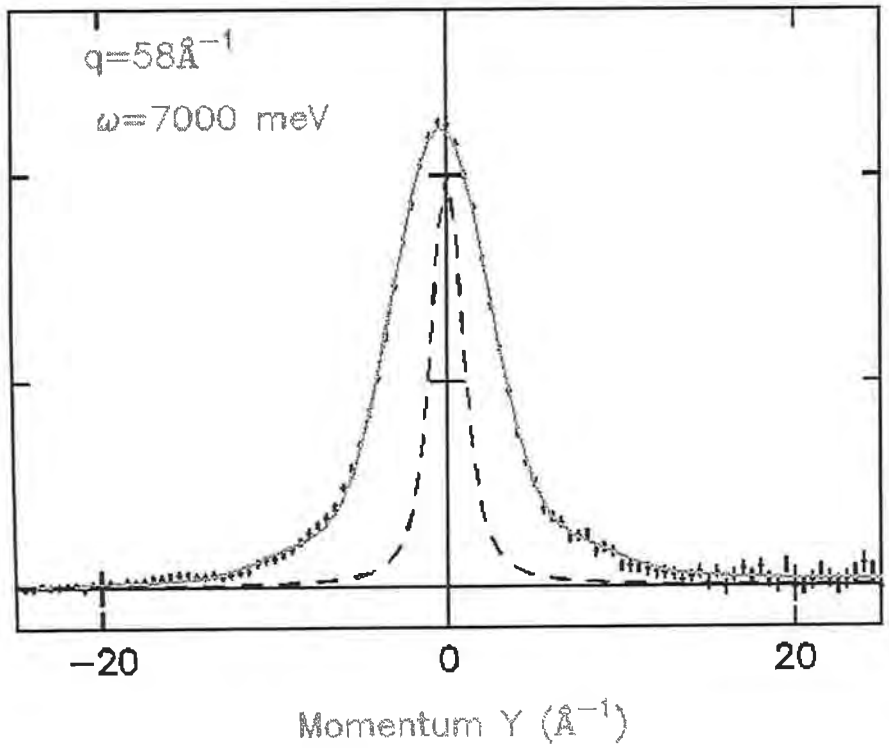

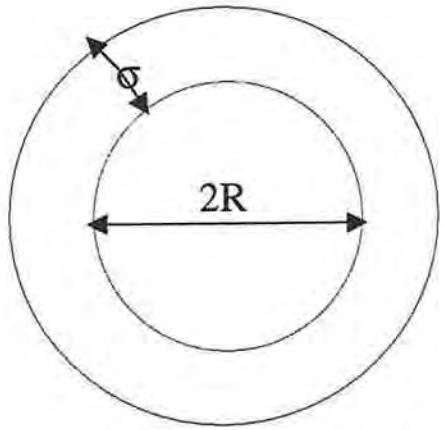

$$\psi(\vec{r}) = C \exp\left[\frac{-(r-R)^2}{2\sigma^2}\right]$$

ISIS

CLRC

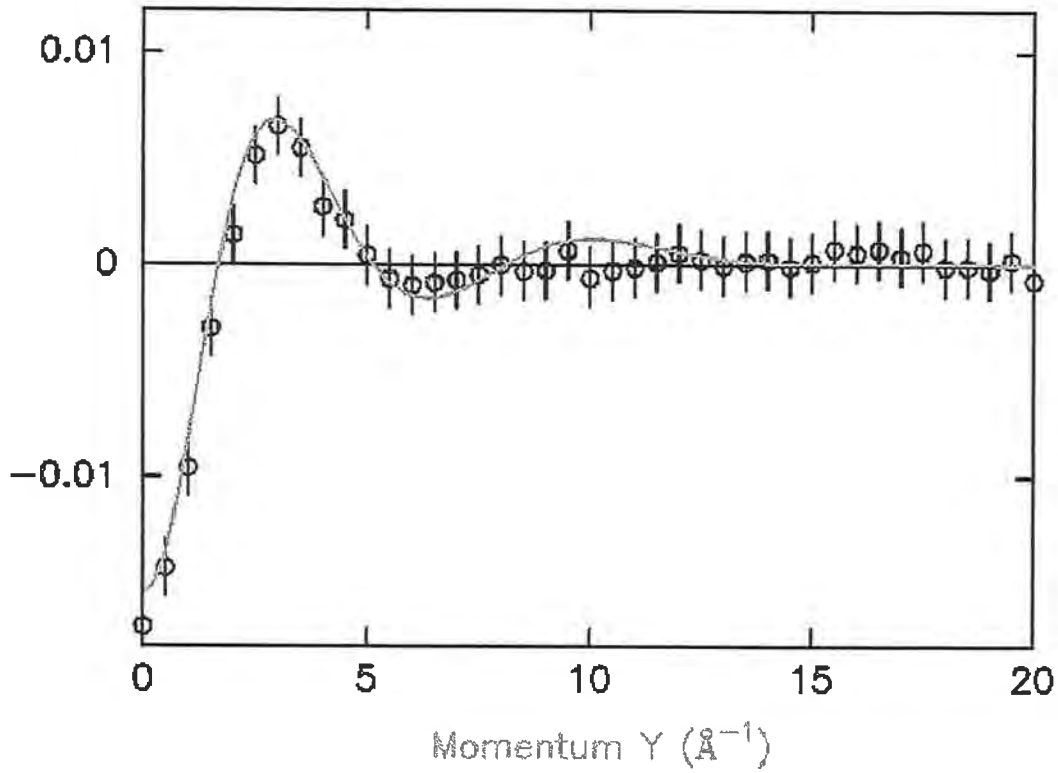

Quantum model

$$n(\vec{p}) = \left| \int \psi(\vec{r}) \exp(i\vec{p}.\vec{r}) d\vec{r} \right|^2$$

$$n(p) = \left(p\sigma^2 \cos pR + R \sin pR \right)^2 \times \frac{C_2}{p^2} \exp\left(-\sigma^2 p^2\right)$$

Classical model

$$n(p) = \frac{C_3}{p^2} \exp\left(-\sigma^2 p^2\right)$$

ISIS

Kinetic Energy of ^{4}He

ISIS

CLRC

Kinetic Energy of ^{4}He

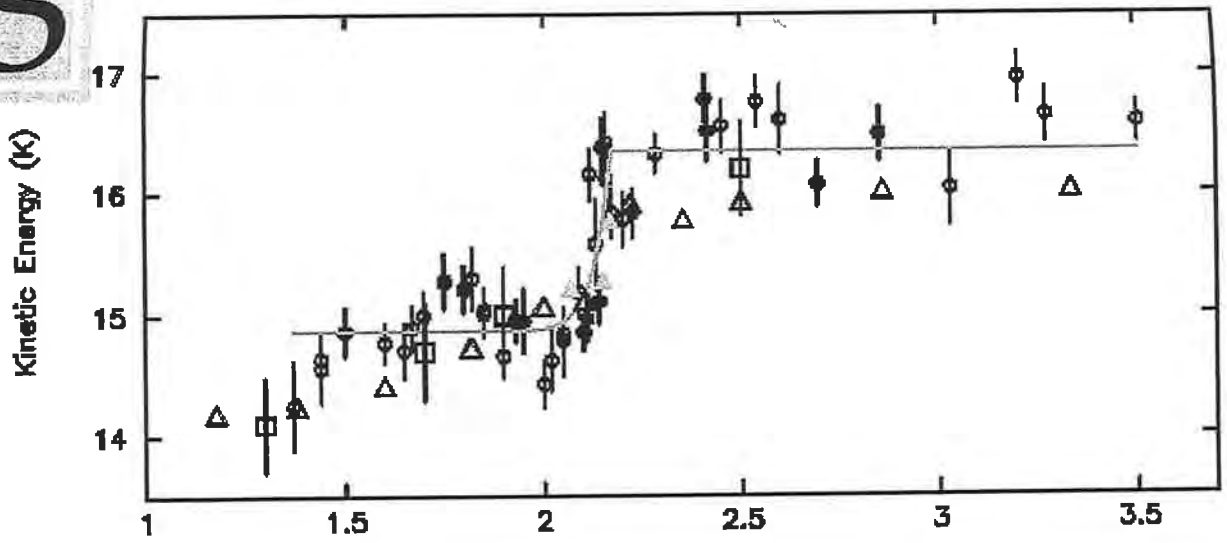

Potential Energy of ^{4}He

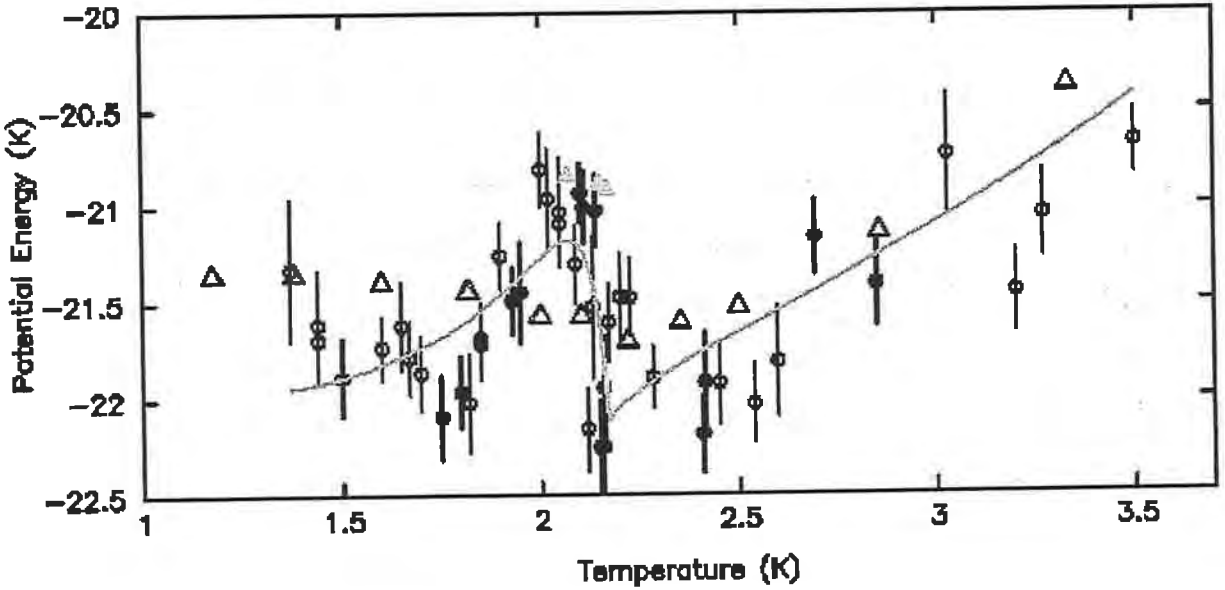

ISIS

CLRC

VESUVIO MODIFICATIONS

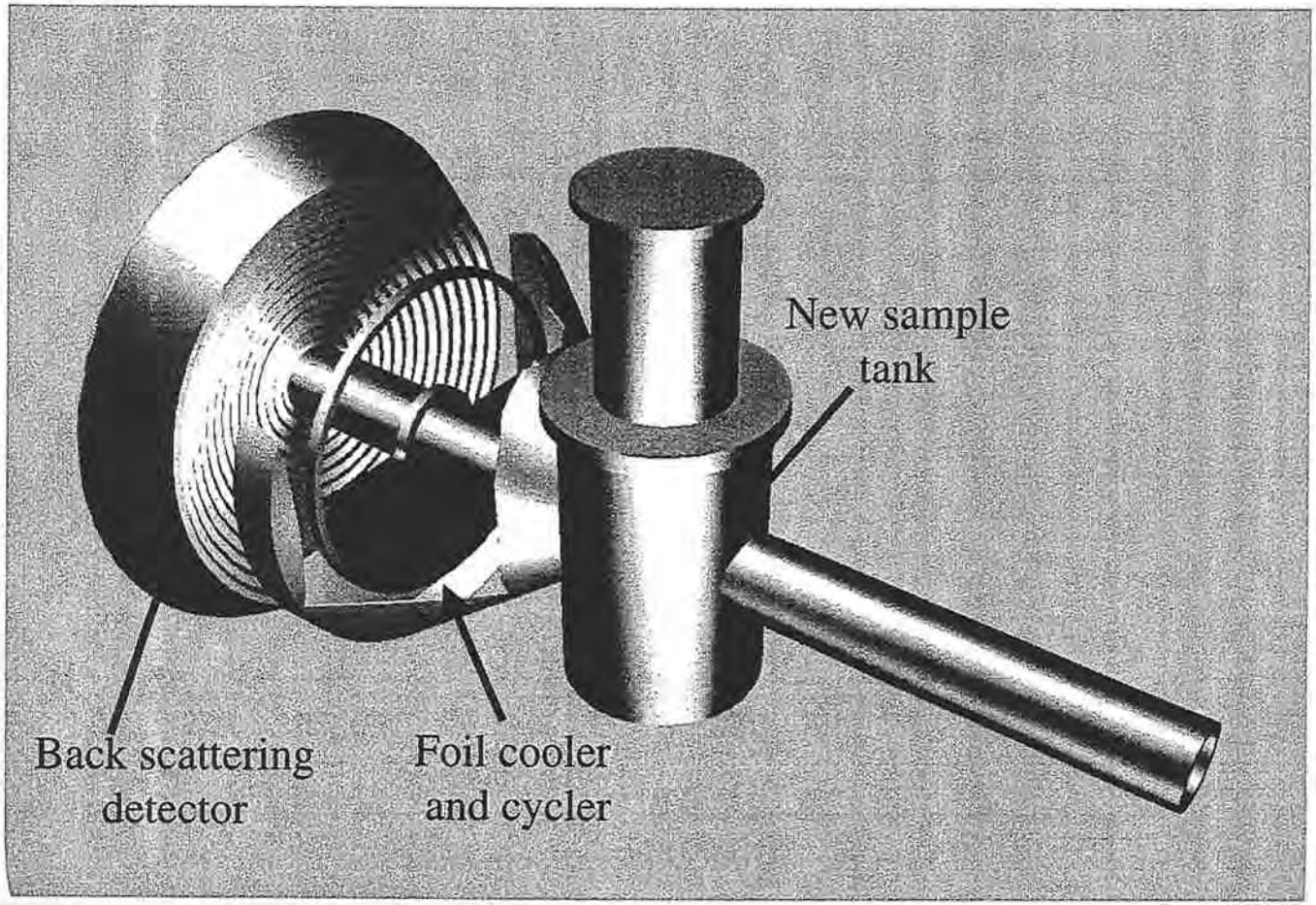

ISIS

CLRC

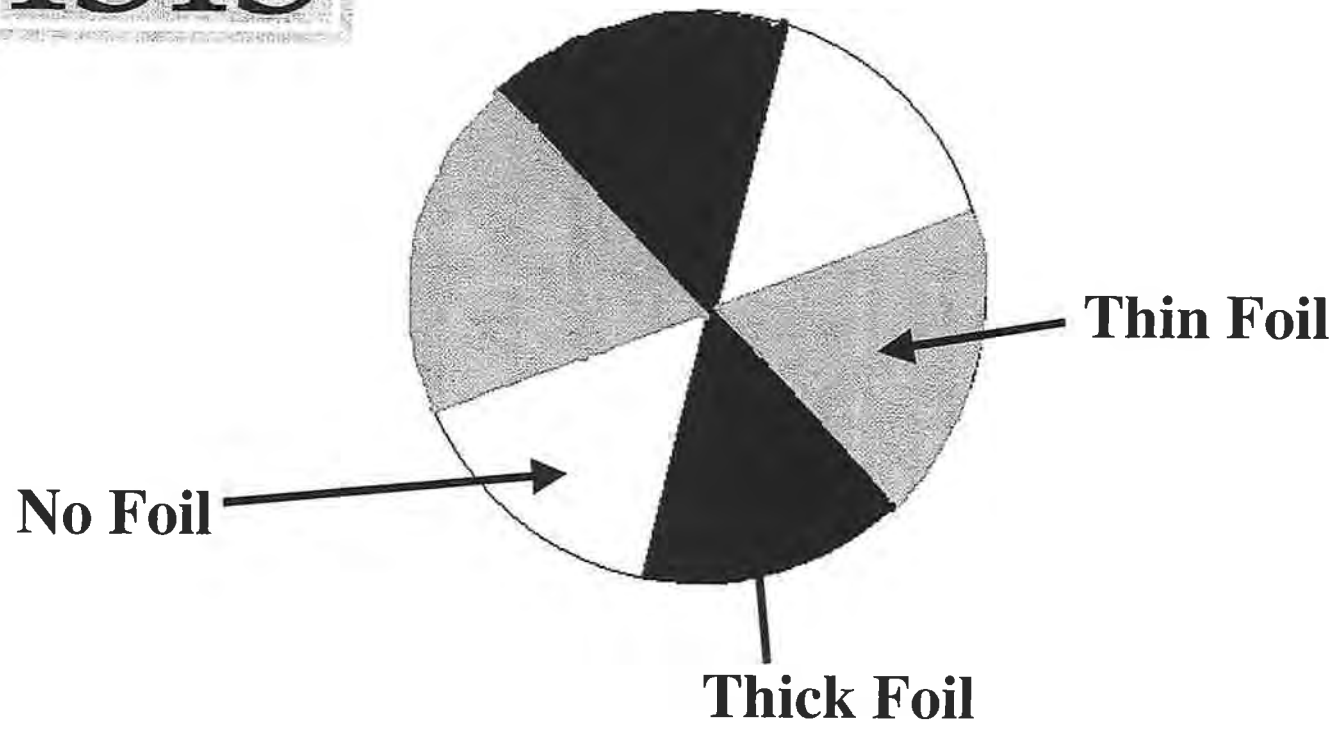

ISIS

CLRC

DOUBLE DIFFERENCE TECHNIQUE

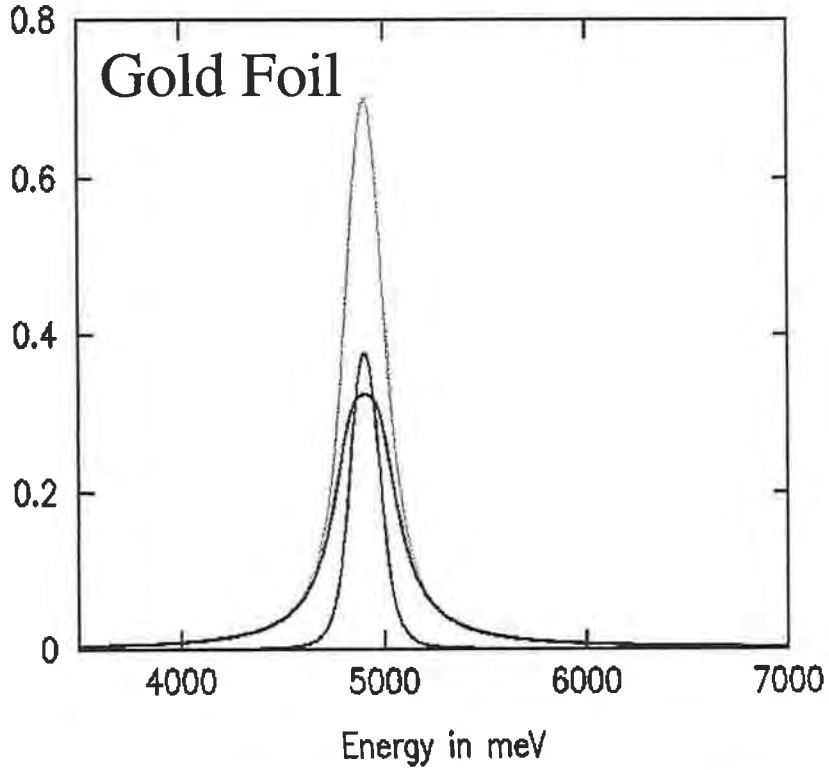

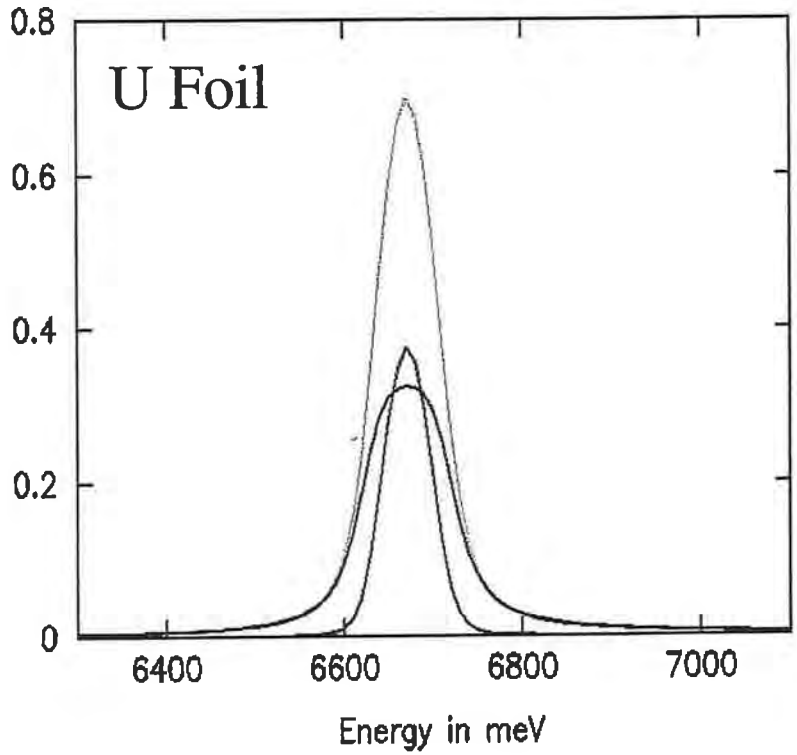

Vesuvio Workshop, 26-27 November 1999
The Cosener's House, Abingdon (UK)

eVS and the quantum fluids: the kinetic energy of helium

by

Marco Zoppi

Consiglio Nazionale delle Ricerche
Istituto di Elettronica Quantistica
Firenze, Italy

and

Ubaldo Bafile	**CNR-IEQ, Firenze, Italy**
Fabrizio Barocchi	**INFM, Firenze, Italy**
Milva Celli	**CNR-IEQ, Firenze, Italy**
Renato Magli	**INFM, Firenze, Italy**
Jerry Mayers	**ISIS, UK**
Martin Neumann	**Universität Wien, Austria**

The neutron cross section

$$\frac{d^2\sigma}{d\Omega\, dE} = N\frac{b^2}{\hbar}\frac{k_1}{k_0}S(k,\omega)$$

where:

- b = nuclear scattering length.
- k_0 , k_1 = incident and scattered neutron wave-vector.
- $S(k,\omega)$ = the Van Hove dynamic structure factor:

$$S(\mathbf{k},\omega) = \left(\frac{1}{2\pi}\right) \int_{-\infty}^{+\infty} dt \int d\mathbf{r}\, \exp\left\{i\left[\mathbf{k}\cdot\mathbf{r} - \omega t\right]\right\} G(\mathbf{r},t)$$

- $G(\mathbf{r},t)$ = time-dependent pair correlation function:

$$G(\mathbf{r},t) = \left(\frac{1}{2\pi}\right)^3 \int d\mathbf{k}\, \exp\left(i\mathbf{k}\cdot\mathbf{r}\right) F(\mathbf{k},t)$$

- $F(\mathbf{k},t)$ = intermediate scattering function:

$$F(\mathbf{k},t) = \left(\frac{1}{N}\right) \sum_{i,j} \left\langle \exp\left[-i\mathbf{k}\cdot\mathbf{r}_i(0)\right] \exp\left[+i\mathbf{k}\cdot\mathbf{r}_j(t)\right] \right\rangle$$

As the momentum transfer increases…

$$F(\mathbf{k},t) \cong \left(\frac{1}{N}\right) \sum_i \left\langle \exp\left[-i\mathbf{k}\cdot\mathbf{r}_i(0)\right] \exp\left[+i\mathbf{k}\cdot\mathbf{r}_i(t)\right] \right\rangle$$

i.e. : the incoherent approximation applies.

If the momentum transfer increases more…

...we reach the so-called:

Impulse Approximation (I.A.) Regime

$$F(\mathbf{k},t) \cong F_{IA}(\mathbf{k},t) = \exp\left\{ i \frac{E_r}{\hbar} t \right\} \left\langle \exp\left\{ i\mathbf{k}\cdot\mathbf{v}\, t \right\} \right\rangle$$

where:

$E_r = \dfrac{\hbar^2 k^2}{2m} =$ Recoil Energy

$\mathbf{v} = \mathbf{v}(0) =$ velocity of the target particle at $t = 0$

and ...

... the statistical average <···> is now ***independent*** of the intermolecular potential.

The scattering function within the I.A.

$$S(\mathbf{k},\hbar\omega) = \int d\mathbf{p}\, n(\mathbf{p})\, \delta(\hbar\omega - E_R - \hbar\, \mathbf{k}\cdot\mathbf{p}/m)$$

where:

$n(\mathbf{p})$ = the momentum distribution of the particles

In conclusion:

if *high momentum* transfer is available.....
then, it becomes possible to measure, *directly*,
the *momentum distribution*.

IF the momentum distribution has a Gaussian shape
(true for classical liquids and solids, quantum solids)

and IF the momentum distribution is *isotropic*

$$n(p) = C\exp(-p^2/\sigma_p^2)$$

$$S(\mathbf{k},\hbar\omega) = C\exp\left\{-\frac{m(\hbar\omega - E_R)^2}{2\,E_R\,\sigma_p^2}\right\}$$

where:

σ_p = **width** of the momentum distribution
i.e.: the **average translational kinetic energy**

The momentum distribution of Helium.

- First experiments, aiming to determine the momentum distribution of superfluid helium and, from that, to derive the **condensate fraction** of the **superfluid** phase, date back to **1982**
  (V.F. Sears, E.C. Svensson, P. Martel, A.D.B. Woods)

- In 1990, a **density dependence** of the **kinetic energy** of liquid helium was observed *(K.W. Herwig, P.E. Sokol, T.R. Sosnick, W.N. Snow, R.C. Blasdell).*

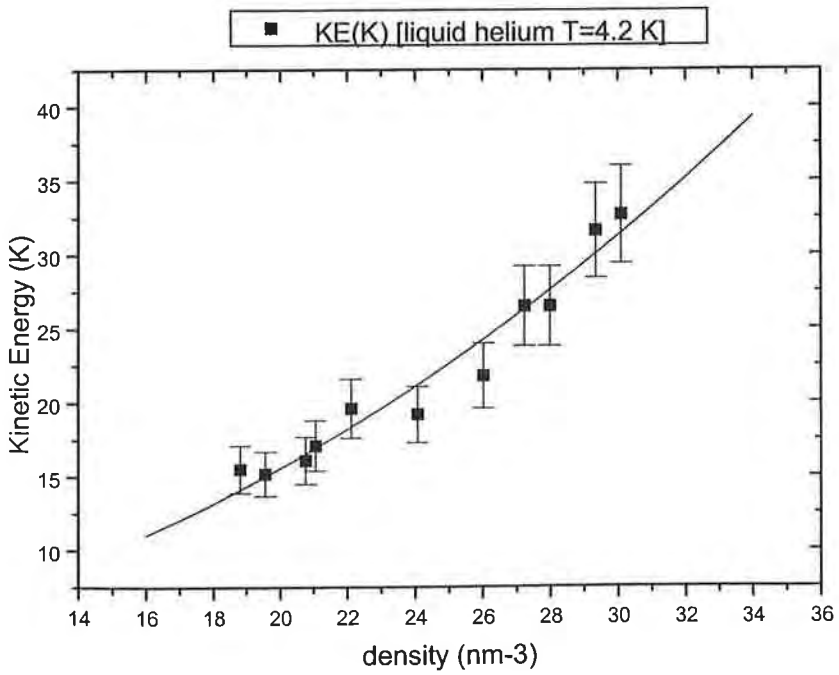

Reminder:

For a *classical* liquid the kinetic energy is:

$$E_K = \frac{3}{2} k_B T$$

i.e. *independent* of density.

What is the origin of the density dependence?

Consider a dense system (e.g. a liquid):

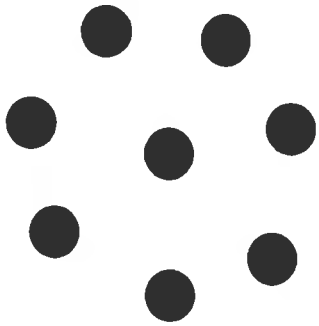

.... and an interaction potential

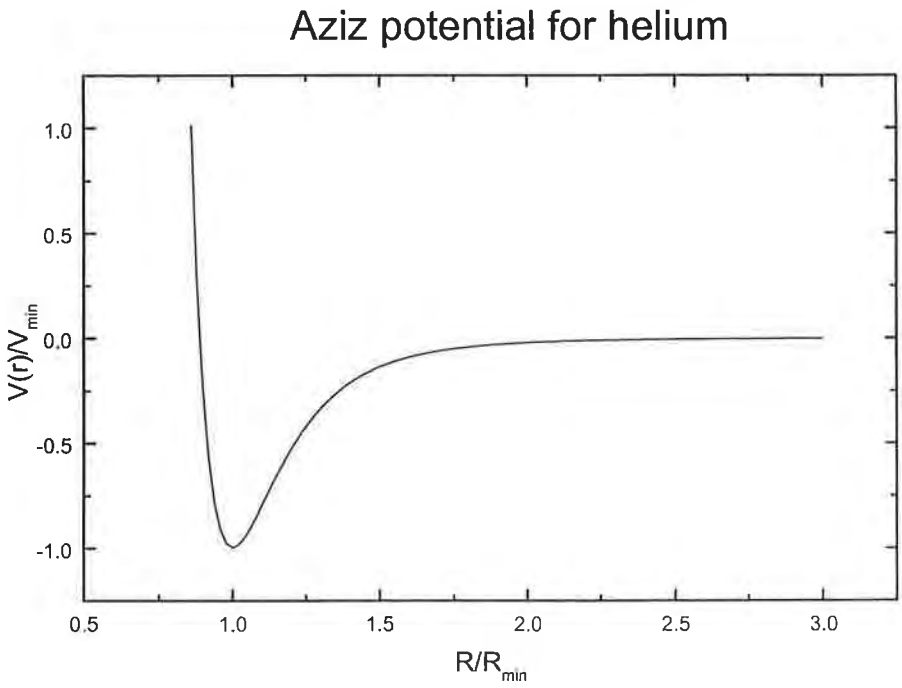

V_{min}= 10.8 K
R_{min}=2.967 A

At high density, the repulsive component plays the main role....

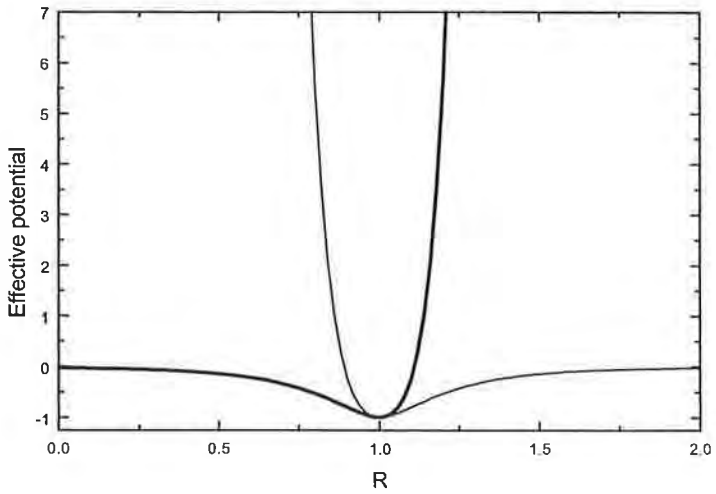

as density increases, the effective potential becomes steeper and steeper...

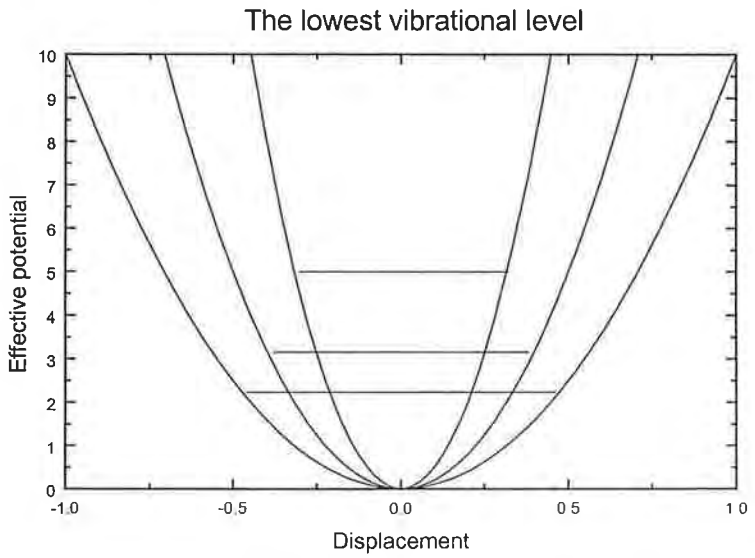

According to the Heisemberg uncertainty principle:

$$\Delta r \cdot \Delta p \cong \hbar$$

The *density increase* of the translational kinetic energy is a *common* characteristics of quantum liquids

- In 1988, a ***change*** in the **translational kinetic energy** was observed going from liquid to solid **hydrogen** *(W. Langel, D.L. Price, R.O. Simmons, P.E. Sokol)*

- In 1990, a ***density dependence*** of the **kinetic energy** of solid **hydrogen** was measured *(K.W. Herwig, J.L. Gavilano, M.C. Schmidt, and R.O. Simmons)*

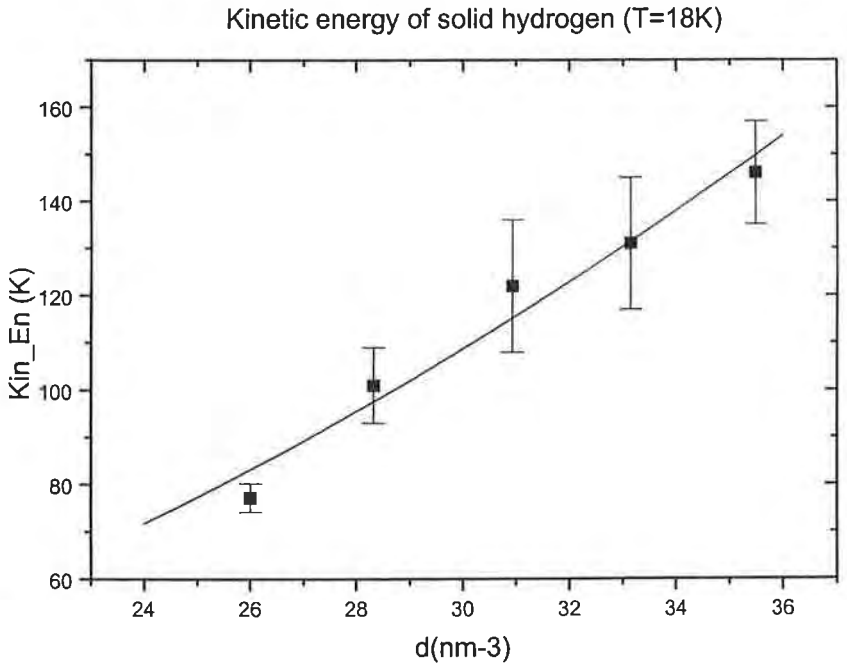

- An *almost parabolic* increase of the **kinetic energy** (translational) of solid hydrogen was confirmed by PIMC simulations *(M. Zoppi and M. Neumann, 1991)*

A high energy- and momentum-transfer inelastic spectrometer: eVS

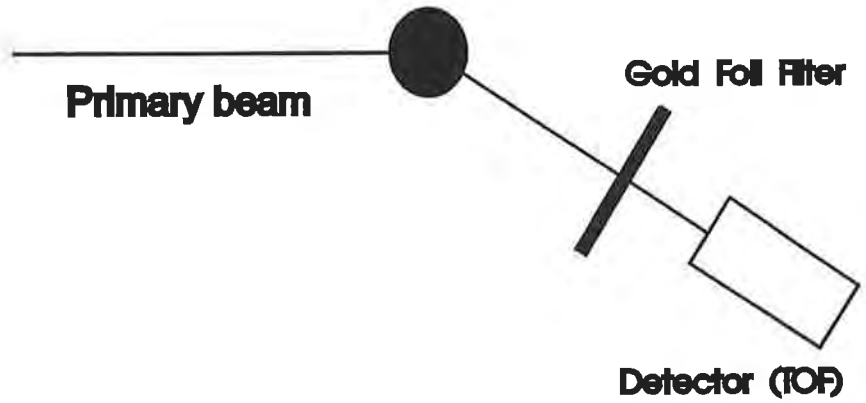

Gold-foil resonance: $E = 4.912\ eV$ ($\delta E = 138\ meV$)

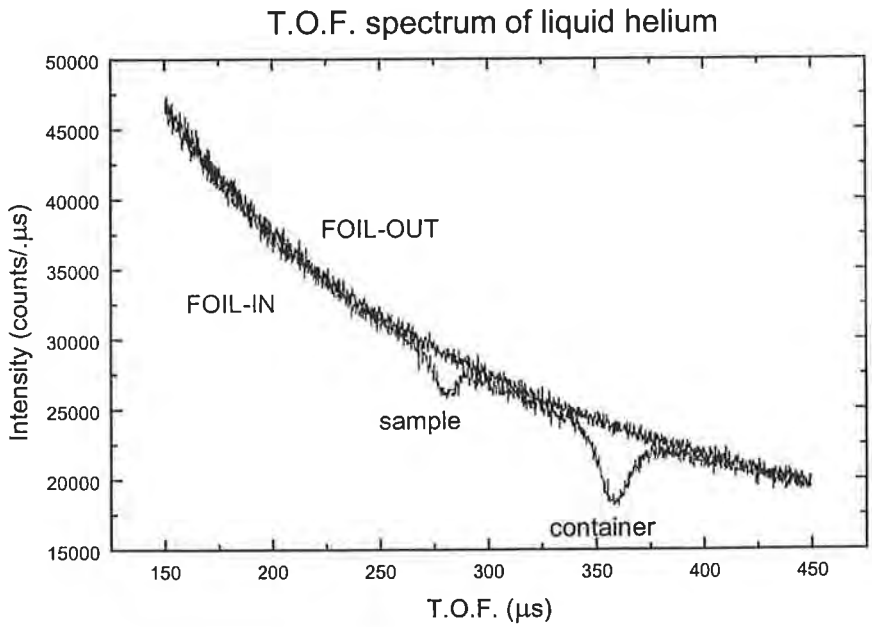

The recoil spectrum is obtained from the difference of the two spectra:

The eVS spectrum of liquid helium

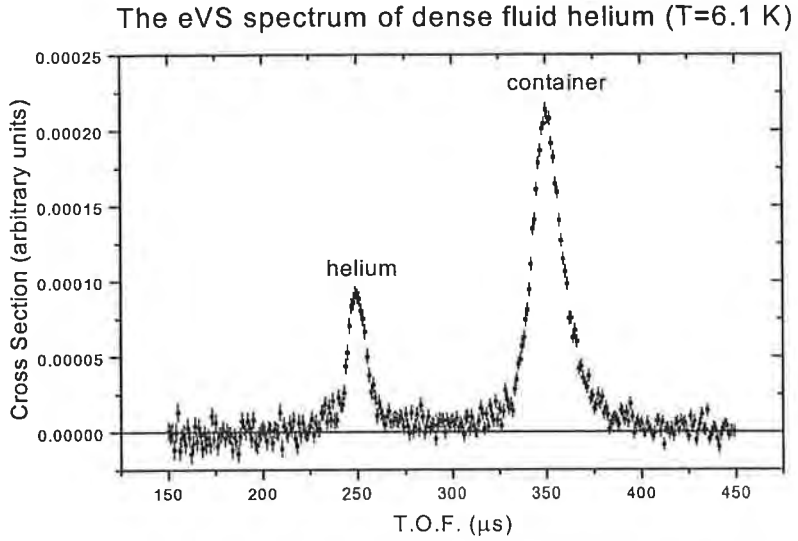

32 detectors ⇒ **32 independent spectra**
32 different scattering angle
32 different values for *k*-distribution

Adavantages of the I.A.

the various spectra, even taken at different *k*-values, can be recast together if one uses a scaling variable, y.

$$y = \left(\frac{M}{\hbar^2 k}\right)\left(\hbar\omega - \frac{\hbar^2 k^2}{2M}\right) = \text{reduced variable}$$

Then, the scattering function can be expressed by means of the scaling variable, y, as:

$$S(\mathbf{k},\omega) = \frac{M}{\hbar k} J(\hat{\mathbf{k}}, y)$$

where:

$\hat{\mathbf{k}}$ is the *unit vector* of $\mathbf{k}$ and

$J(\hat{\mathbf{k}}, y)$ is the so-called ***Compton Profile***.

The Compton Profile of liquid helium

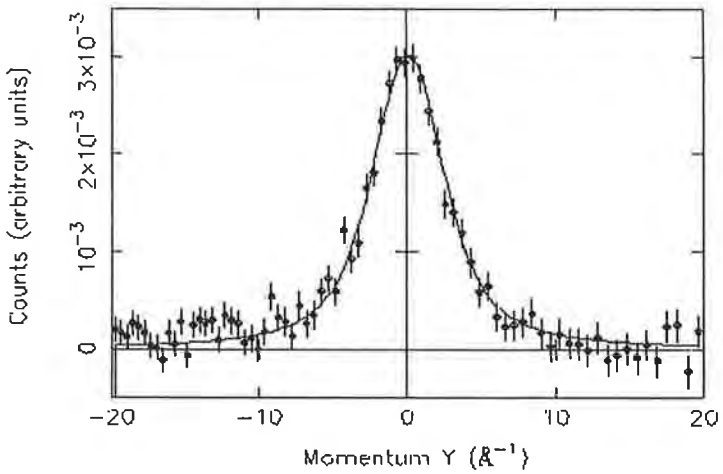

Using the ***scaling variable,*** the spectra could be added together with a sensible reduction of the statistical error.

How good is the I.A. for helium?

Range of the momentum transfer depends both:
on ***sample*** (recoil energy) and on the ***scattering angle.***

For **helium:**
$83.5° < \theta < 148.7°$
implies:
$73.6\ A^{-1} < k < 122.6\ A^{-1}$

Density dependence.

(U. Bafile, M. Zoppi, F. Barocchi, R. Magli, J. Mayers, PRL 1995)

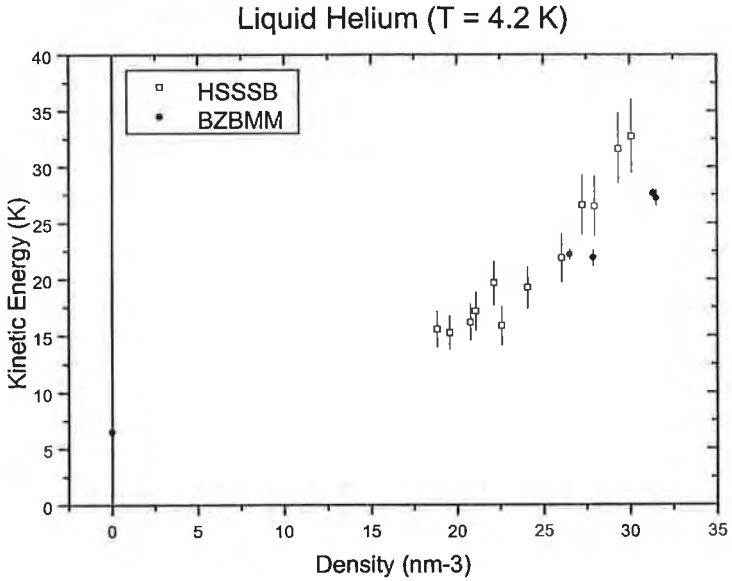

- The error-bars are much smaller than in previous experiments....

but

- ....a large region of densities is not covered.

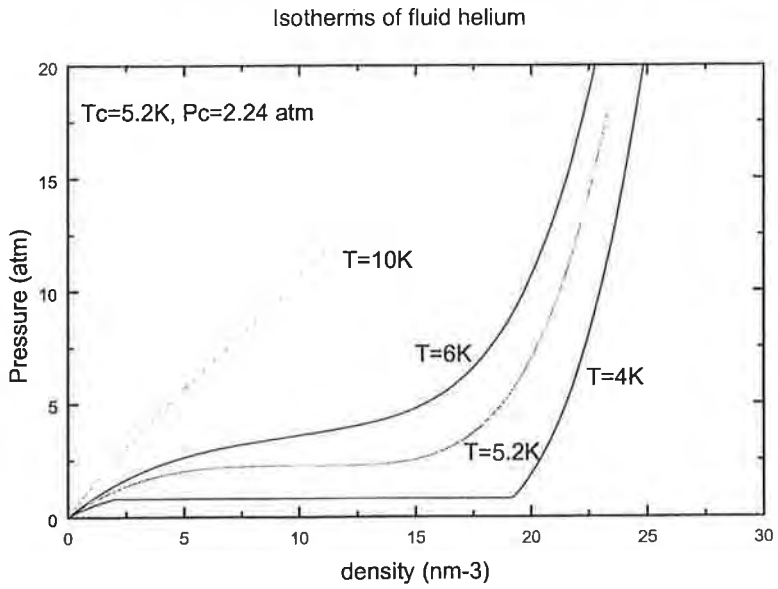

Crossing the liquid-solid phase transition.

(U. Bafile, M. Zoppi, F. Barocchi, R. Magli, J. Mayers, PRB 1996)

(M. Celli, M. Zoppi, J. Mayers, PRB 1998)

The kinetic energy of liquid and solid helium at T=6.1K

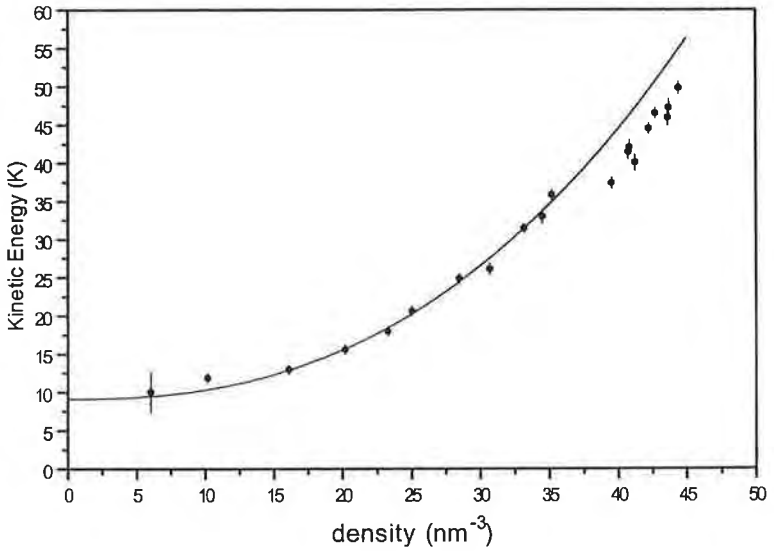

Fitting the **fluid** data with a **parabola**: $(\chi^2)_R$=**4.02**

Fitting the **fluid** data with a **power-law** $(\chi^2)_R$=**1.56**

Most likely, the fitting function is ***not*** a parabola but a power-law of exponent **2.46**

If this is the case:

The data points for the kinetic-energy, in the solid phase, lay ***below*** the extrapolation of the liquid phase

Is this behavior peculiar of helium?

check on other systems!

- ***However,***

- Quantum features of ***neon*** are too small.
- The only reliable check can be carried out on ***hydrogen***

.... but ...

eVS is not accurate enough
for measuring the
translational kinetic energy of hydrogen
(too much energy-momentum transfer).

the solution:

TOSCA

..... but this is another story
for another time.

eVS Measurements on Catalysts

P.C.H. Mitchell
A.J. Ramirez-Cuesta
University of Reading
Vesuvio Workshop 26-27/11/99

Topics

- H species in $CoMoS_2$ desulfurisation catalysts
- H species in RuS_2 catalysts
- H species in Pt alloy fuel cell catalysts
- H species in Ce/NiO catalysts
- H in Pd/SnO_2 sensors
- Hydrocarbon species on $FeSbO_4$ catalysts
- Xenon as a probe in zeolites

People

- Timmy Ramirez-Cuesta
- David Timms
- Edman Tsang
- Edmond Payen
- Jerry Mayers
- Andrew Fielding
- Stewart Parker
- John Tomkinson

Probing the Internal Structure of a Zeolite With Xenon

- Porous aluminosilicates used as
  - Catalyts
  - Molecular sieves
  - Drying agents
- Shape selectivity determined by the size and shape of the internal channels

Xe as a Probe Atom
^{129}Xe nmr

- Xe interactions change chemical shift.
  - Xe-Xe and Xe-zeolite
  - LJ PE curves
- Electric fields
  - Mg^{2+}, Zn^{2+}
  - Paramagnetic Co^{2+} and Ni^{2+}
    - Broadening
    - Shift

Xe as a Probe Atom
eVS

- Neutron Compton scattering
- Final state effects in spectrum
  - Xe-zeolite potential
  - Statistics not good enough

Xenon in Na zeolite-Y

- Zeolite in cylindrical vanadium can
- Dehydrated 673 K in vacuo overnight
- Dosed xenon in situ to saturation at 293 K
- Mass of zeolite 8.90 g
- Mass of Xe 2.64 g

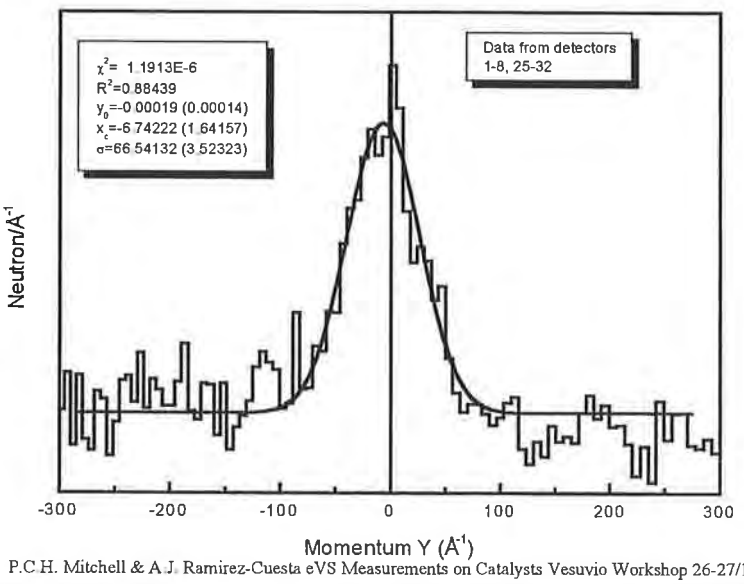

Xe in Na Zeolite-Y Kinetic Energy

- Recoil scattering
  - U foil
  - Two back scattering detectors
- 41.9 +/- 7.5 meV
  - 486.4+/-87.3 K
  - 450.8+/-80.9 cm^{-1}
- Ideal gas value at 293 K 37.9 meV

Xe Neutron Absorption Resonance Doppler Broadening

$$\Delta\lambda_{1/2} = const.\lambda\sqrt{\frac{T}{M}}$$

Xe Neutron Absorption Resonance Doppler Broadening

Gaussian fit

$$I(\lambda) = const. e^{\frac{-(\lambda - \lambda_m)^2}{2\Delta\lambda_{1/2}^2}}$$

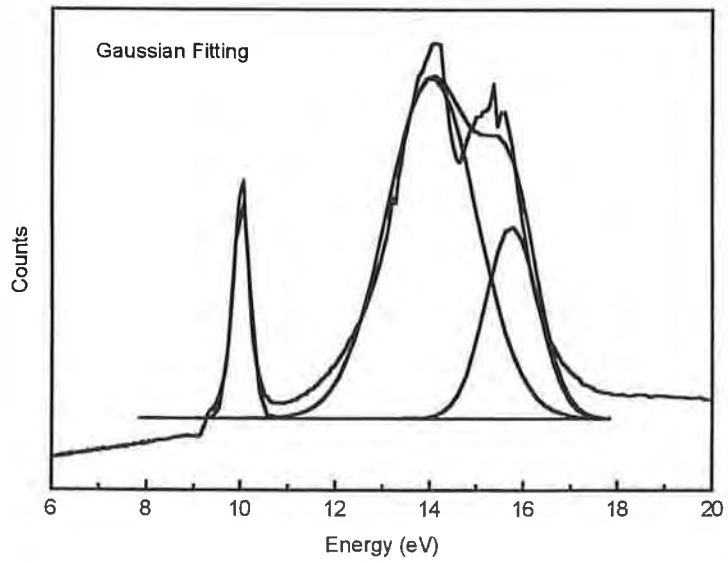

Xe Neutron Absorption Resonance

- 10 eV line
- Doppler broadening
- Gaussian fit
- Chi^2 2.18 x 10^6
- R^2 0.983
- Centre 10.01+/- 0.006 eV
- Half width 0.323+/- 0.014 eV
- KE 38.1+/- 1.1 meV

Xe Neutron Absorption Resonance Doppler Broadening

Lorentzian fit

$$I(\lambda) = const. \left[1 + \left(\frac{\Delta \lambda_{1/2}}{\lambda} \right)^2 \right]^{-1}$$

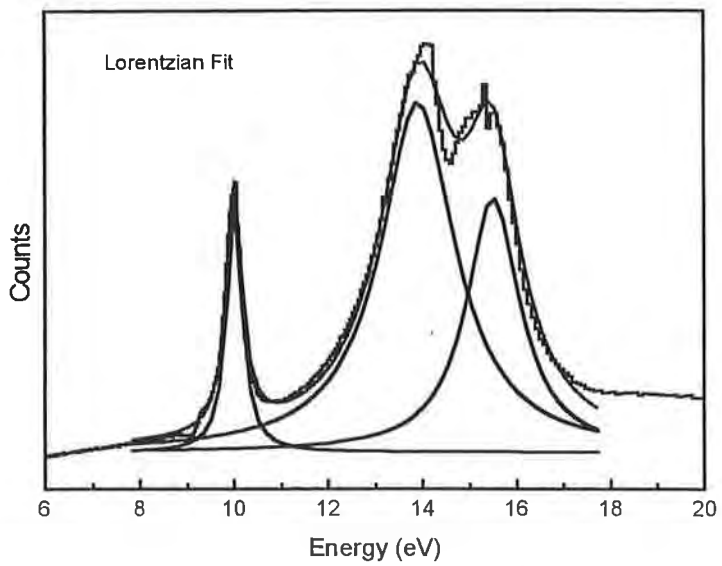

Xe Neutron Absorption Resonance Doppler Broadening

- Lorentzian fit
- Chi^2 0.65 10^6
- R^2 0.995
- Broadening due to intermolecular collisions/diffusion
- Appropriate for condensed phase

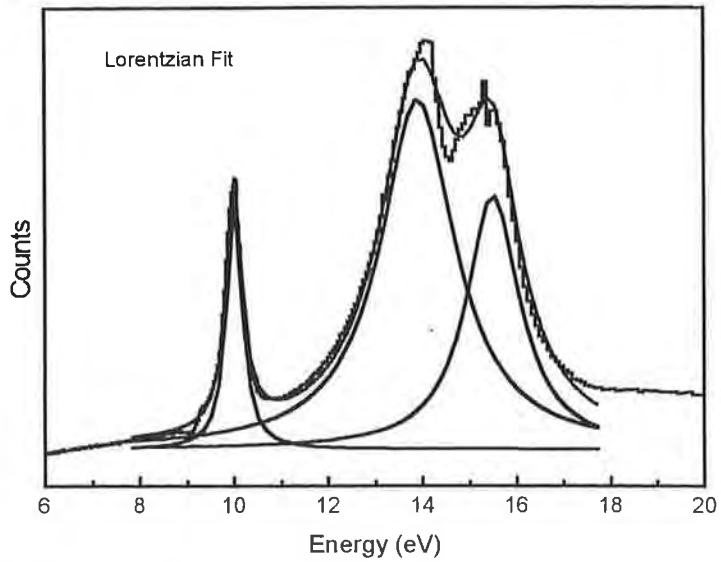

Xe Neutron Absorption Resonance Doppler Broadening

- Lorentzian fit
- Chi^2 0.65 10^6
- R^2 0.995
- Broadening due to intermolecular collisions/diffusion
- Appropriate for condensed phase

Pt and Ru Fuel Cell Catalysts

- Speed up the H_2/O_2 reaction
- Ru reduces susceptibility to CO poisoning
- ? Nature of H and CO species on catalyst and concentrations
- ? Mode of action of Ru
- With eVS measure actual surface species: do not rely on deductions from gas measurements.

Pt + Hydrogen + CO

- Catalyst
  - Pt 20 w/w % on C
  - Pt black
- Ca 20 g
- Dosed with hydrogen in situ at 20 K
- Warmed to r.t.
- H from forward scattering
- Pt from back scattering
- From intensities (+/- < 5%) give atomic ratios
- Kinetic energies (+/10-20%) give species & binding

$Pt + H_2 + CO$

Catalyst	$+H_2$	$+H_2+CO$
Pt/C		
Atomic ratios	3H/60C/1Pt	
Kinetic energies/cm^{-1}	H 1307 Pt 900	
Pt black		
Atomic ratios	0.3H/1Pt	0.2H/0.02CO/1Pt
Kinetic energies/cm^{-1}	H 1300	H 871

$Pt + H_2 + CO$ Deductions

- Much higher H on C supported catalyst
  - Pt higher dispersion?
  - KE corresponds to Pt-H
- Effect of CO
  - Fewer H atoms per Pt
  - Weaker H binding

Pt black + H_2

- In situ
- Pt black (13.6 g) loaded into Al can and pumped down at r.t.
- Sample reduced in situ with H_2 at r.t.
- Intensities give relative atomic ratios
  - H/Pt = 0.309

Pt black + H_2 + CO

- From intensities (+/- < 5 %)
  - H/CO/Pt = 0.22/0.017/1
- Kinetic energies (+/- 10 - 20%)
  - H 871 cm^{-1}
  - Pt 908 cm^{-1}

Ru black with hydrogen

- Ru black 10 g in flat Al cell
- In situ dosing

Ru black with hydrogen

Treatment	Atomic ratios		Kinetic energies/cm^{-1}	
	Ru	H	Ru	H
Initial reduced	1	0.13	1205	1605
H2 170 mbar 20 K	1	0.15	1177	1324
H2 Saturated 10 K	1	0.20	1736	1017
H2 373 K	1	0.085	2170	1415

Ru black with hydrogen Deductions

- H content from intensities
  - Increases with dose at first
  - But decreases after reduction
    - sintering?
- H KE gives species
  - Bound H atoms not H_2 (627 cm^{-1})
- Ru KE
- Much higher after higher temperature reduction
  - Ru sintered?
- Different Ru second two: bulk Ru sintering.

PtRu black + H_2 + CO

- CO not detected
- Ru inhibits binding of CO

Next Steps

- Improve resolution
- Improve sensitivity
- Develop sample handling
- End electronics/detector saturation
- Computational modelling of eVS data
  - Kinetic energies of species
  - Intensities = concentrations

University of Portsmouth

Final State Effects (FSE) and anharmonicity in graphite

D.N. Timms[a], A.L. Fielding[b,c], J. Mayers[c]

[a]Division of Physics, University of Portsmouth

[b]Department of Physics, University of Liverpool

[c]ISIS Facility, Rutherford Appleton Laboratory

University of Portsmouth

1 Final State Effects

2 Correcting for FSE

3 Using eVS to study FSE

4 Graphite

5 Summary

University of Portsmouth

INITIAL & FINAL STATE EFFECTS

•**Initial State Effects** - result from quantum nature of atom in its initial state. Deviation from free particle behaviour.

•**Final State Effects** - Atom does not recoil freely in final state. At finite q , inter-atomic potential slows recoiling atom.

•Any deviations from Impulsive scattering are generically known as final state effects (FSE).

•Manifests as an asymmetry in the measured J(y).

•J(y) no longer Gaussian.

University of Portsmouth

THEORETICAL TREATMENTS FOR FINAL STATE EFFECTS

The Sears expansion

$$J(y) = J_{IA}(y) - \frac{m\langle \nabla^2 V \rangle}{36\hbar^2 q}\frac{d^3 J_{IA}(y)}{dy^3} + \frac{m^2\langle F^2 \rangle}{72\hbar^4 q^2}\frac{d^4 J_{IA}(y)}{dy^4} - \cdots$$

where

$$A_3 = \frac{M\langle \nabla^2 V \rangle}{36\hbar^2 q} \quad \text{and} \quad A_4 = \frac{M^2\langle F^2 \rangle}{72\hbar^4 q^2}$$

- FSE represented as additive corrections to IA consisting of symmetric and asymmetric terms.
- Relates FSE to physical parameters, V and F

University of Portsmouth

The Glyde [redacted] approach

- FSE represented by final state broadening function.
- Shown to be most appropriate in quantum systems where inter-atomic interactions are strong
- Reduces to Sears in systems where FSE are small.

Azuah, Stirling, Glyde, Soköl, Bennington, Phys Rev B 51, 1, 605, 1995

University of Portsmouth

Do **you** need to worry about FSE?

- FSE have predominantly 1/q dependence
- Minimised at high q's
- Still noticeable in:

  Strongly bound systems incorporating light atoms

  e.g. Hydrides, beryllium etc

To avoid FSE

- Maximise **q** by using back scattering
- Correct using symmetrisation or fitting with Sears'

To study FSE

- Intermediate detectors

  best combination of resolution and **q**

  gold analyser to maximise statistics

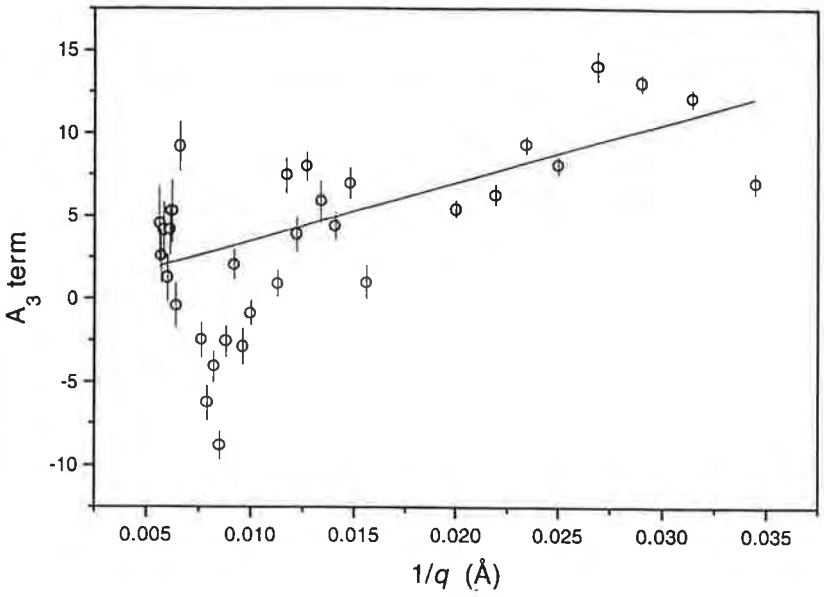

Figure 4.12 *A plot of A_3 against 1/q extracted from the measured Compton profiles (circles). The line is a least-squares straight line fit to the data allowing $\langle\nabla^2 V\rangle$ of the D in ZrD_2 to be extracted from the gradient.*

University of Portsmouth

Simulation for beryllium at room temperature

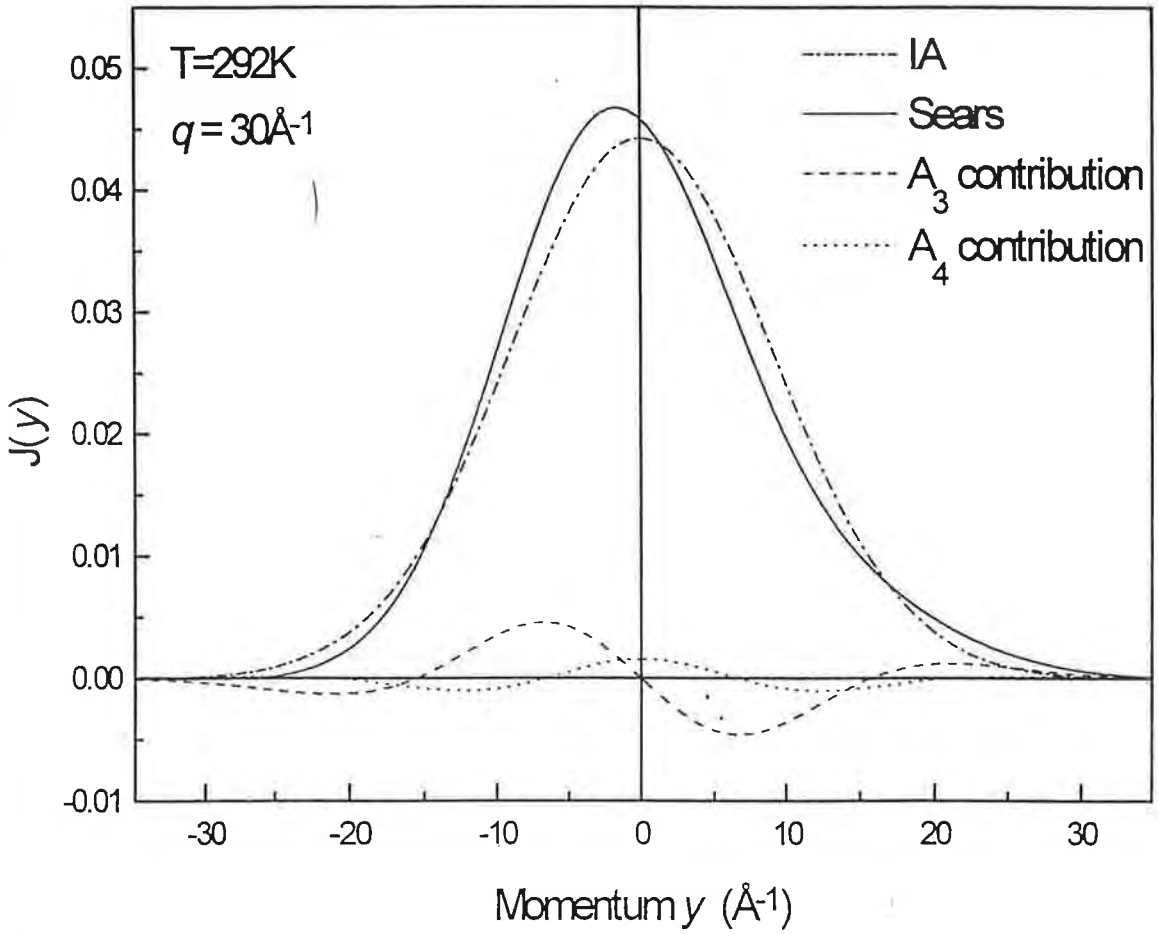

IA - 8.17(0.07)

A_3 - 8.39(0.07)

Sym. - 8.32(0.06)

Sim. - 8.33

Fitting Procedure

- Fit includes A_0, y_0, σ, $\langle \nabla^2 V \rangle$
- A_0 Scale factor
- y_0 peak position
- σ profile width
- $\langle \nabla^2 V \rangle$ incorporates Sear's A_3 term
- $$\langle E_k(q) \rangle = \frac{3\hbar^2\sigma^2}{2M}$$

Simulation for basal plane

Parallel to basal plane

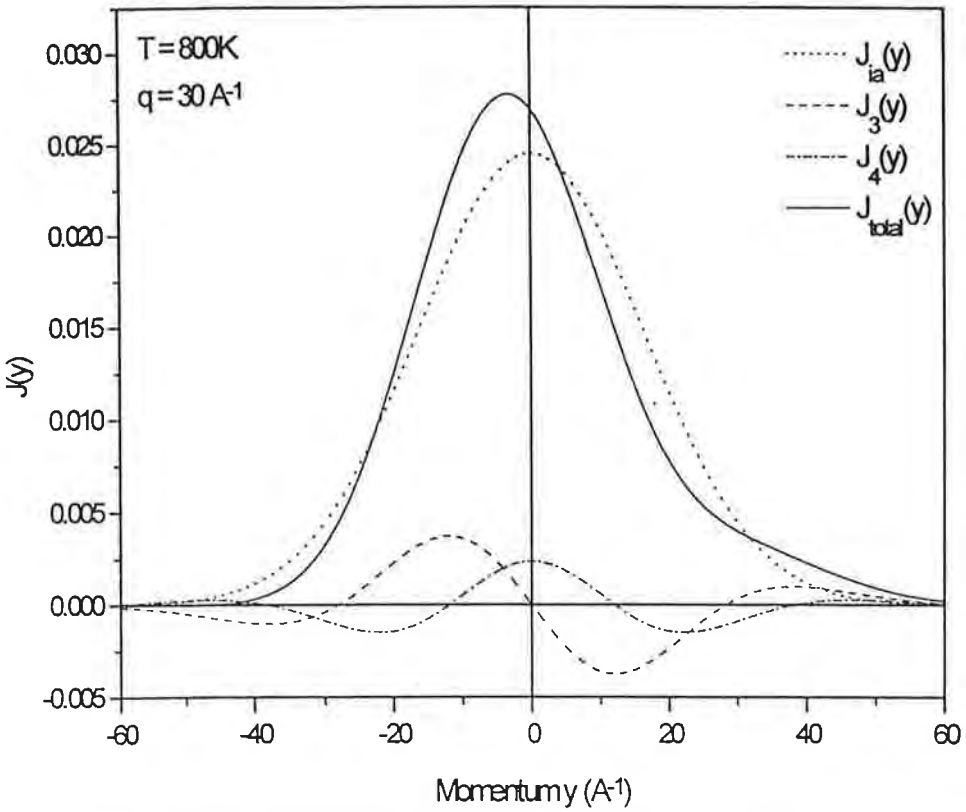

Parallel to the basal plane

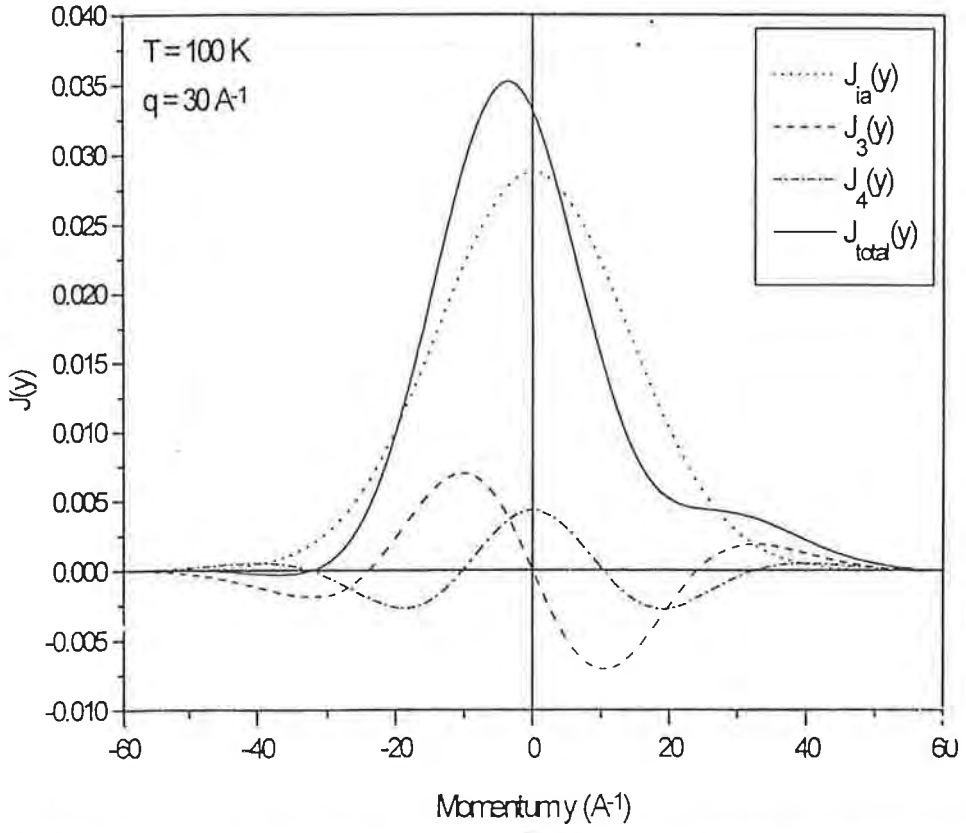

Zirconium Deuteride

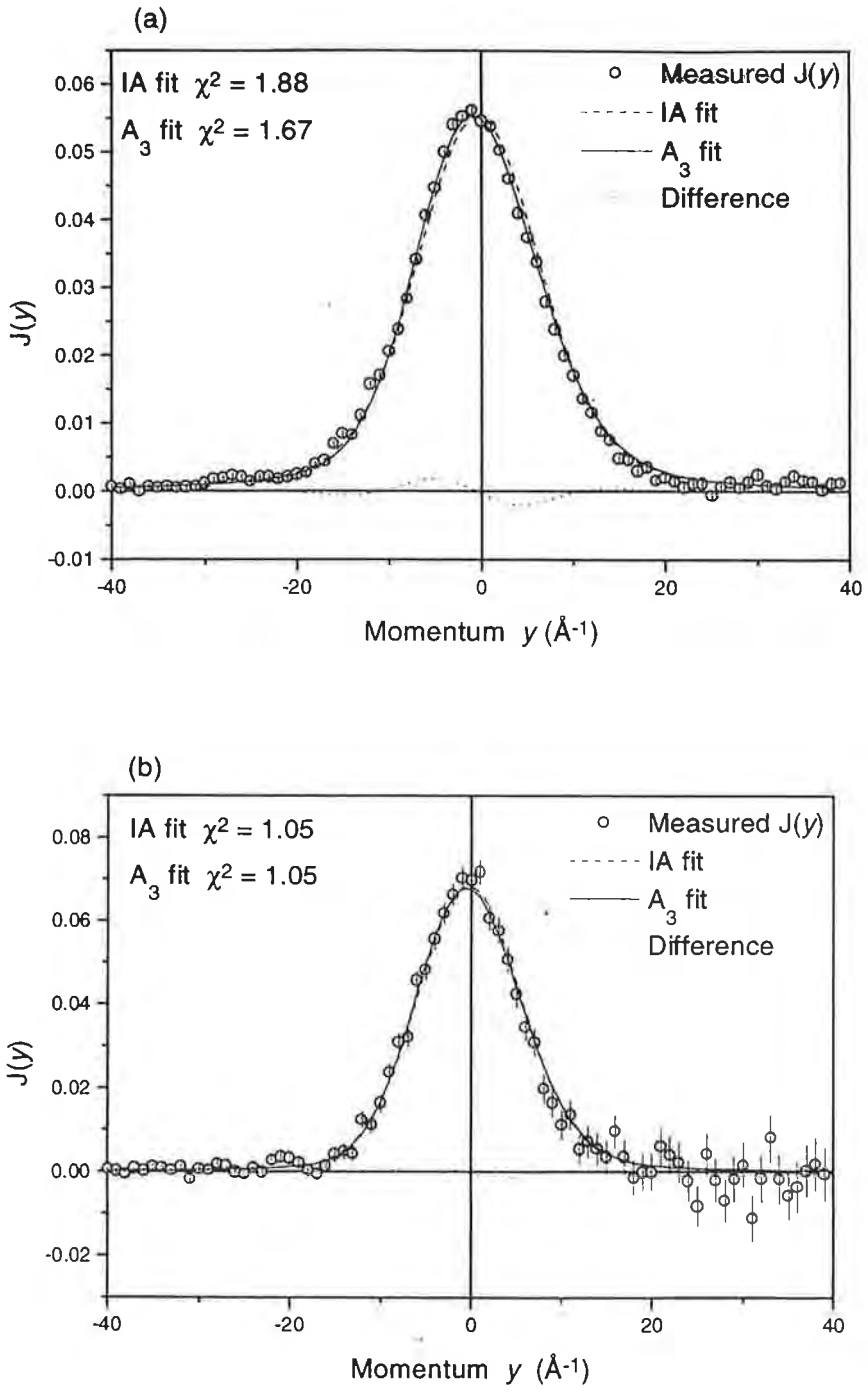

Figure 4.10 *The measured data and the A_3 fits (procedure 4) obtained for the Compton profiles at (a) q=29.1 Å^{-1} and (b) q=177.9 Å^{-1}. Also plotted is the IA fit (procedure 2) along with the difference between the two fits.*

University of Portsmouth

PYROLYTIC GRAPHITE

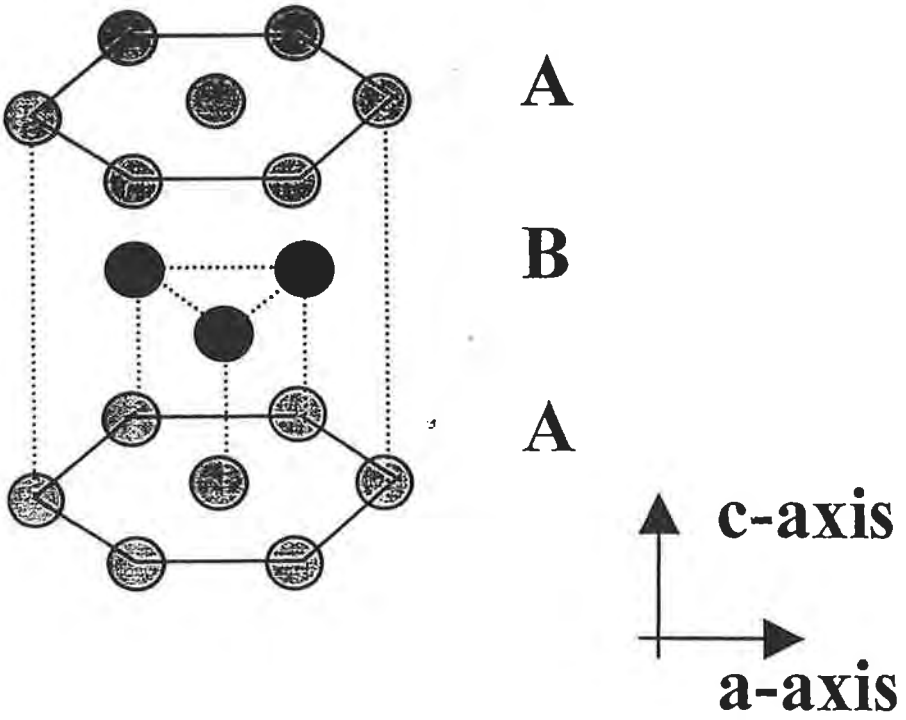

- Small atom, tightly bound - FSE large
- Anisotropic momentum distribution:<Ek> in planes greater than <Ek> between planes
- Anisotropy in FSE

Experimental Conditions.

- Pyrolytic graphite at room temperature in thin aluminium holder
- Sample size 10mm × 10mm × 1mm
- Gold resonance foils
- 32 simultaneous projections of n(**p**)
- 3 measurements to study anisotropy over range of **q**
- Simultaneous diffraction and recoil scattering
- Powder sample

University of Portsmouth

Typical detector positions for measuring anisotropy and FSE

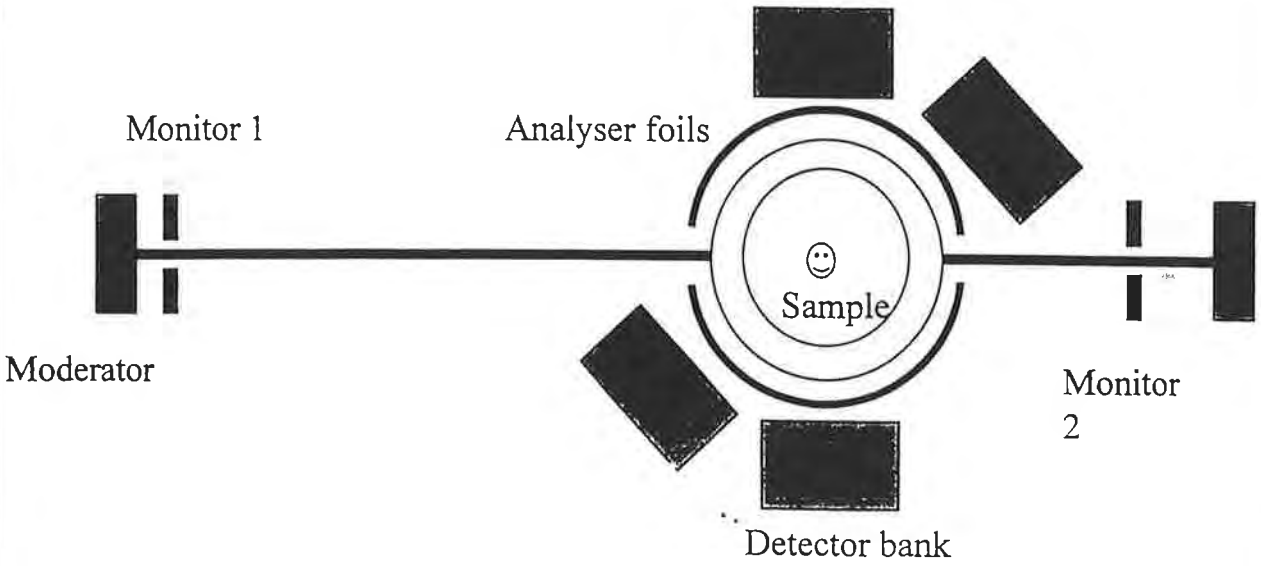

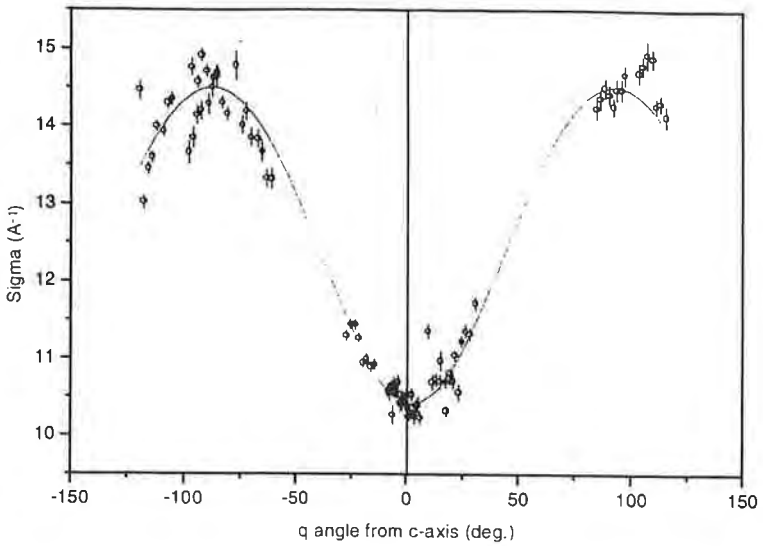

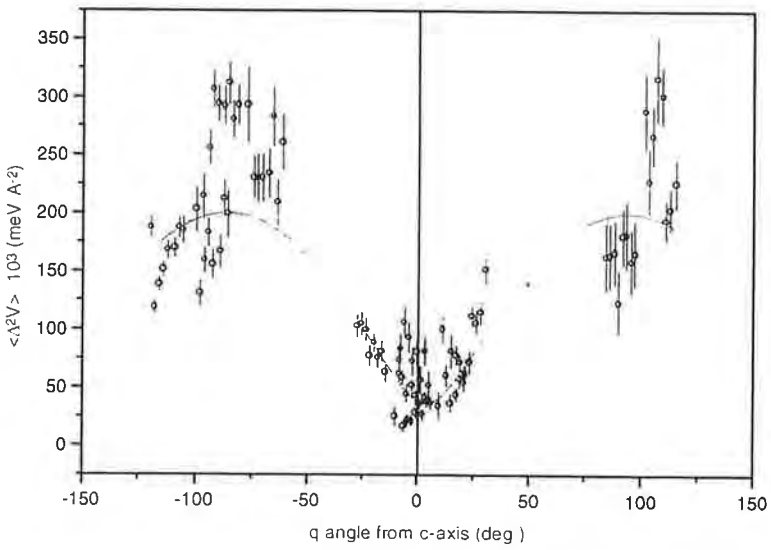

- ***Plots of σ and $\langle\nabla^2 V\rangle$ as a function of angle between the q vector and the c-axis direction. The solid line is a fit of an ellipse function to the data points***

Observations

- Excellent agreement with average $\langle E_k \rangle$ from powder
- Agree with powder result of Mayers, Burke, Newport
- Weighted sum for $\left\langle \nabla^2 V \right\rangle$ agrees
- Disagreement with earlier work
  - Poor statistics
  - Significant ms & background
  - scale of anisotropy similar

- From DOS can calculate $\langle E_k \rangle$ per atom using Harmonic Approximation
- calculated $\left\langle \nabla^2 V \right\rangle$ agrees for basal but inadequate for c-axis
- Potential of atoms in basal plane is harmonic
- Evidence of anharmonicity perpendicular to planes

Pyrolytic graphite at 10K and 1100K

University of Portsmouth

T=10 K

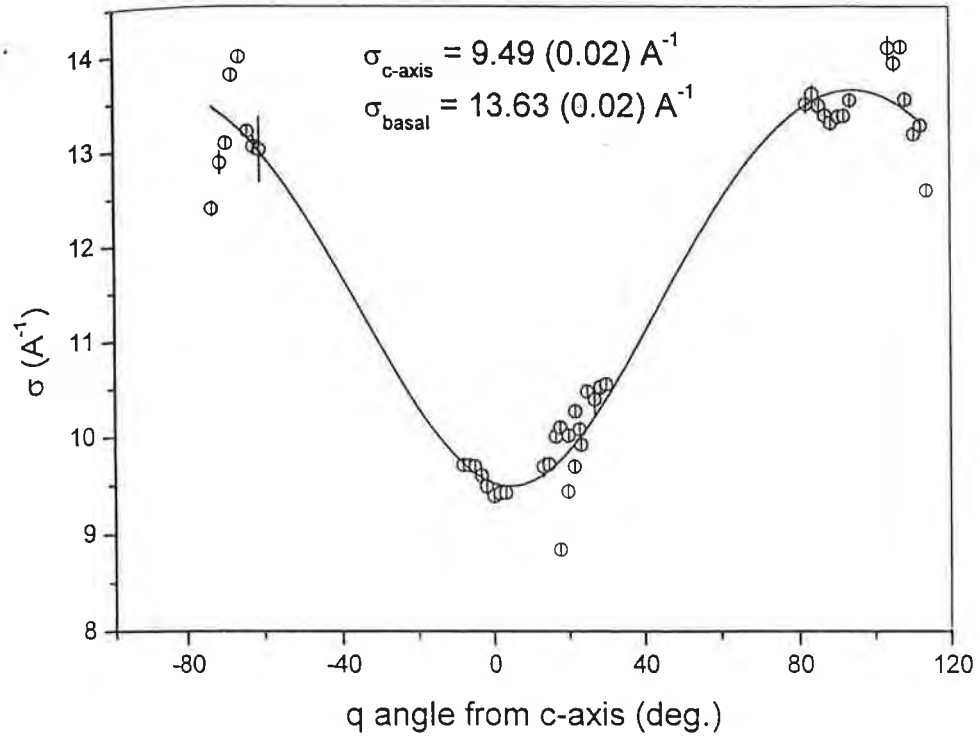

T = 1100 K

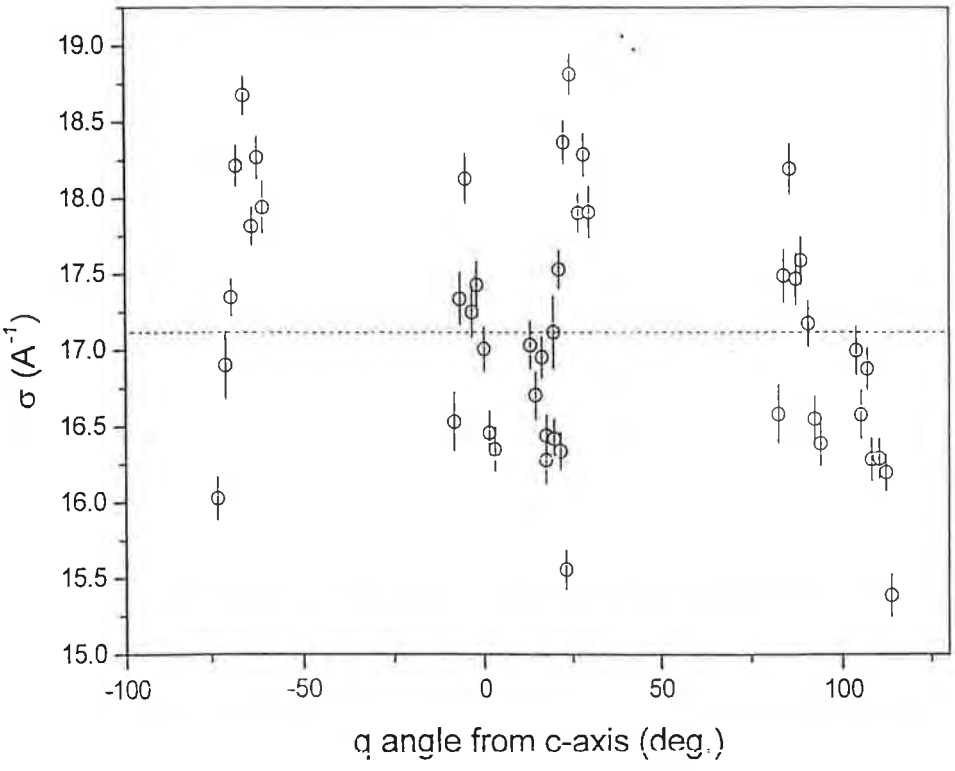

Expt.	$\langle E_k \rangle_\perp$(K)	$\langle E_k \rangle_{//}$ (K)	$\langle E_k \rangle$ (K)	$\langle \nabla^2 V \rangle_\perp$ 10^3 meV Å^{-2}	$\langle \nabla^2 V \rangle_{//}$ 10^3 meV Å^{-2}	$\langle \nabla^2 V \rangle$ 10^3 meV Å^{-2}
eVS pyro.	662±2(4)	1282±4(15)	1075±3(11)	35.6±1.4(3.4)	200.0±2(8)	144.8±2(8)
eVS poly.	---	---	1059±13	---	---	124.8 ±8
DOS[1]	828	1185	1024	75.7	173.5	141.5
Ref.[2]	837±30	1500±70	1279±48	---	---	---
Ref. [3]	825±49	1575±121	1325±82	---	---	---
Ref.[4]	---	---	1104±49	---	---	---

1. Young J and Koppel JU J. Chem. Phys. **42** 357 (1965)
2. Paoli MP and Holt RS J. Phys. C: Solid State Physics **21** 3633 (1988)
3. Rauh H and Watanbe N Phys. Lett. **100A** 244 (1984)
4. Mayers J, Burke TM and Newport RJ J. Phys.: Condens. Matter **6** 641 (1994)

	DOS			**Measured**		
TEMP	c-axis	Ave.	Basal	c-axis	Average	Basal
10K	770	995	1176	545(6)	932(22)	1125(15)
300K	828	1069	1185	662(4)	1075(11) 1059(13)	1282(15)
1100K	1734	1817	1898	1613(200)	1802(200)	1927(200)

University of Portsmouth

SUMMARY

- FSE can be routinely corrected by **fitting with A_3** or **symmetrisation.**

- NCS provides information on single atom properties $\langle E_k \rangle$ and $\langle \nabla^2 V \rangle$

- $\langle \nabla^2 V \rangle$ provides a new and sensitive probe of anharmonicity in condensed matter

- FSE may become more significant with Vesuvio

VESUVIO
&
FSE

University of Portsmouth

Back scattering bank

Resolution improvements

Improved count rates

Also need:

Multiple scattering developments:

cylindrical and plane geometry

cryostat and furnace scattering

MS within detector banks

F. Fillaux

EVS MEASUREMENTS AND NEUTRON VIBRATIONAL SPECTROSCOPY

1. Band Assignment Schemes

2. Proton Transfer

VESUVIO Workshop 26-27 November 1999

N-METHYLACETAMIDE
$CH_3CONHCH_3$

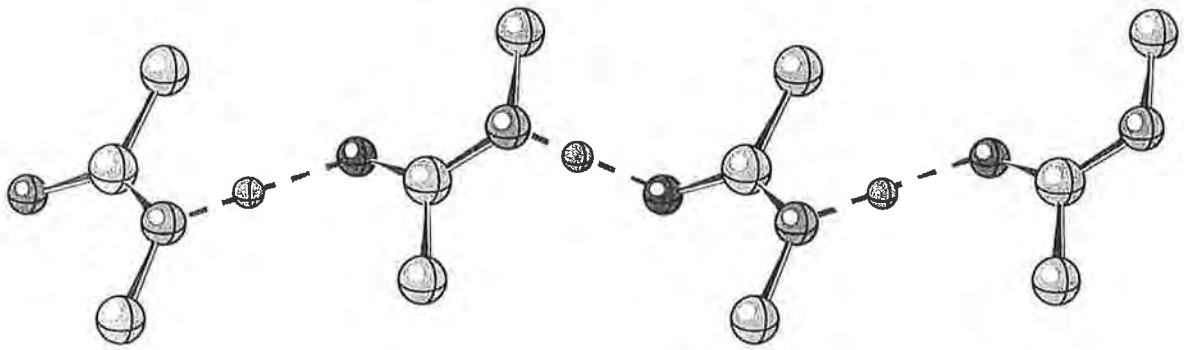

C N O H

Localized Modes

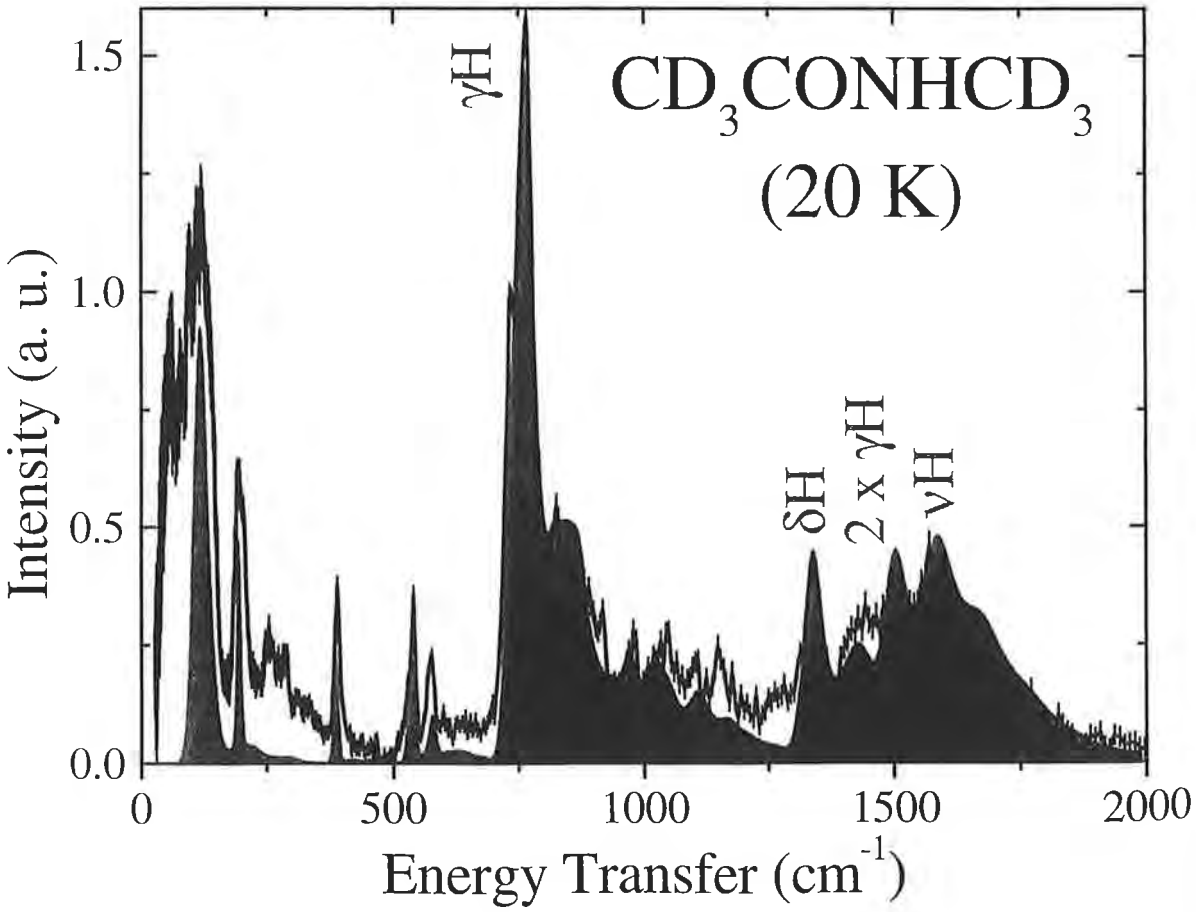

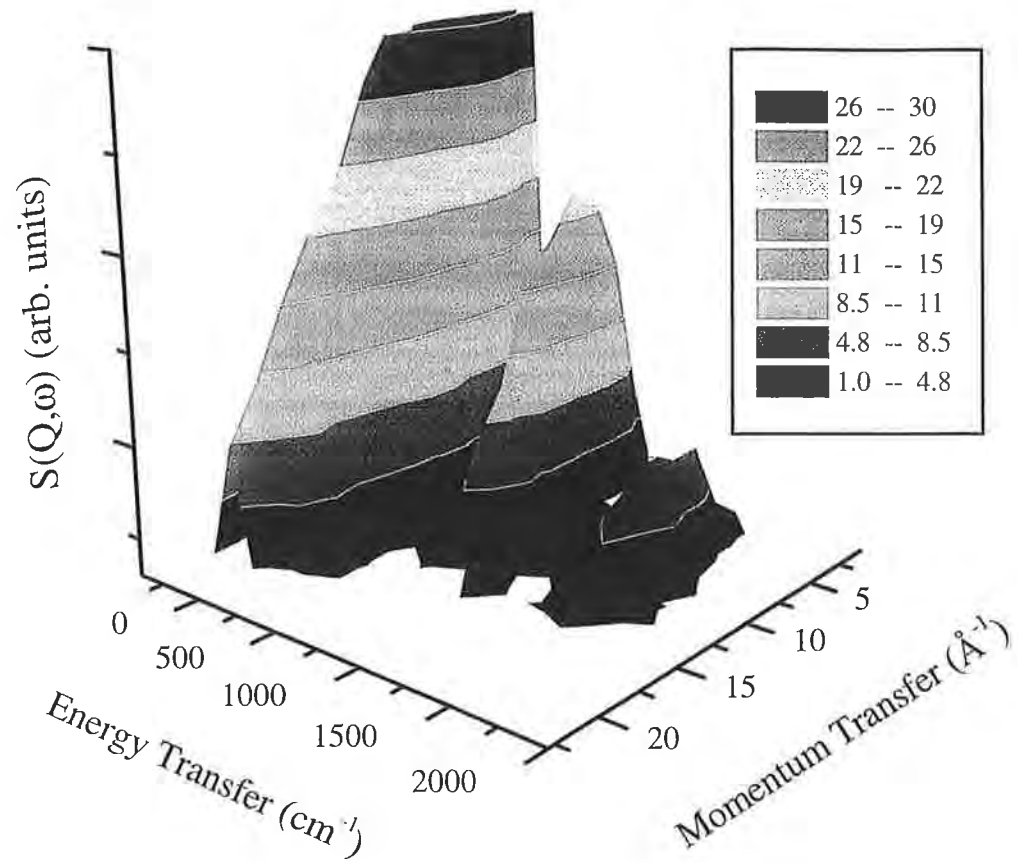

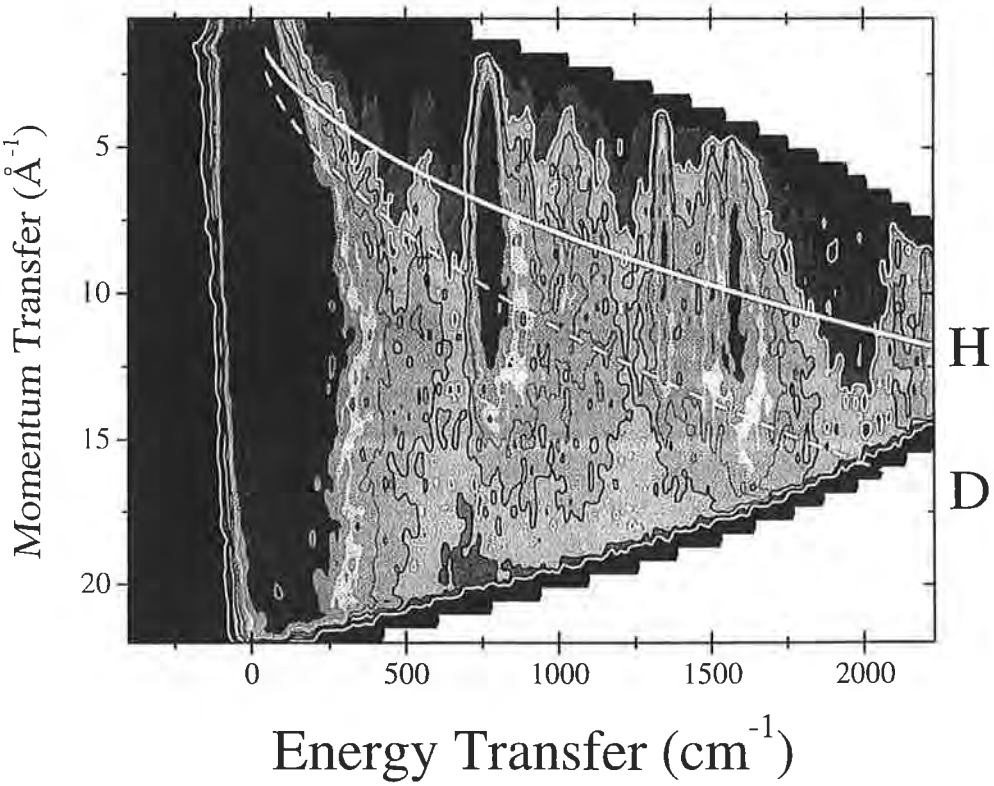

$CD_3CONHCD_3$ 30 K

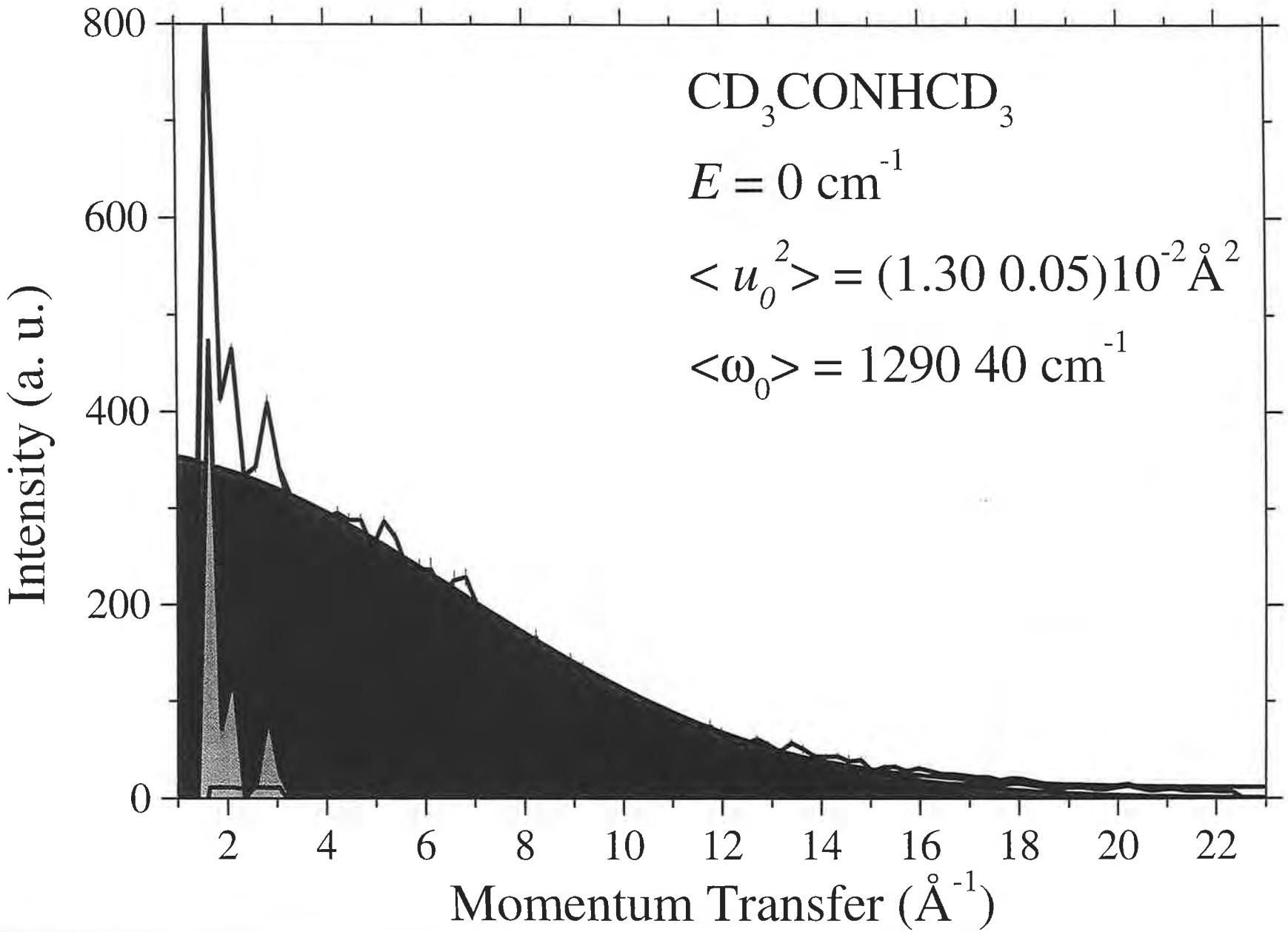
$CD_3CONHCD_3$
$E = 0\ cm^{-1}$
$< u_0^2 > = (1.30\ 0.05)10^{-2} Å^2$
$<\omega_0> = 1290\ 40\ cm^{-1}$
Intensity (a. u.)
Momentum Transfer ($Å^{-1}$)
0
200
400
600
800
2
4
6
8
10
12
14
16
18
20
22

N-METHYLACETAMIDE

Band assignment schemes and mean frequency values (cm^{-1}).

	MARI			TFXA	IR & Raman		NCS
	Elastic	Harmonic	Phonon-wings	Ref. [1]	Ref. [2]	Ref. [3]	Ref. [4]
ν	--	1610±90	1610±90	1575	3193	3146	--
δ	--	1350±50	1350±50	1347	1367	1327	--
γ	--	870±20	760±20	766	728	645	--
$\langle\hbar\omega\rangle$	1290±50	1280±50	1240±50	1229	1763	1706	1457±38

1 F.Fillaux, J.P.Fontaine, M.-H.Baron, G.J.Kearley and J.Tomkinson, Chem.Phys., 176 (1993) 249.
2 M.Rey-Lafon, M.T.Forel and C.Garrigou-Lagrange, Spectrochim. Acta, A **29** (1973) 471.
3 T.C.Cheam and S.Krimm, J.Chem.Phys., **82** (1985) 1631.
4 F.Fillaux, M.-H.Baron, J.Mayers and J.Tomkinson, Chem.Phys.Letters, **240** (1995) 114.

eVS measurements on glasses and (non) high-T_c superconductors

F J Mompeán
ICMM CSIC Madrid

A Srinivasan, IEM CSIC
C Prieto, ICMM CSIC
U Amador, USP - CEU Madrid
J Mayers, ISIS
A Evans, ISIS

OUTLINE

1. EXPERIMENTS ON GLASSES

A) Molecular glass : methanol

B) Metallic glass : $Ni_{0.83}{}^{11}B_{0.17}$

(J. Dawidowski et al.)

C) Conclusions

2. EXPERIMENT ON $PrBaFeCuO_{5+\delta}$

A) Interest (related to $YBa_2Cu_3O_{7-x}$)

B) Experiments on eVS

C) Conclusion

3. POSSIBLE TOPICS FOR DINS IN 'NOVEL' OXIDE MATERIALS

A. MOLECULAR GLASS : METHANOL

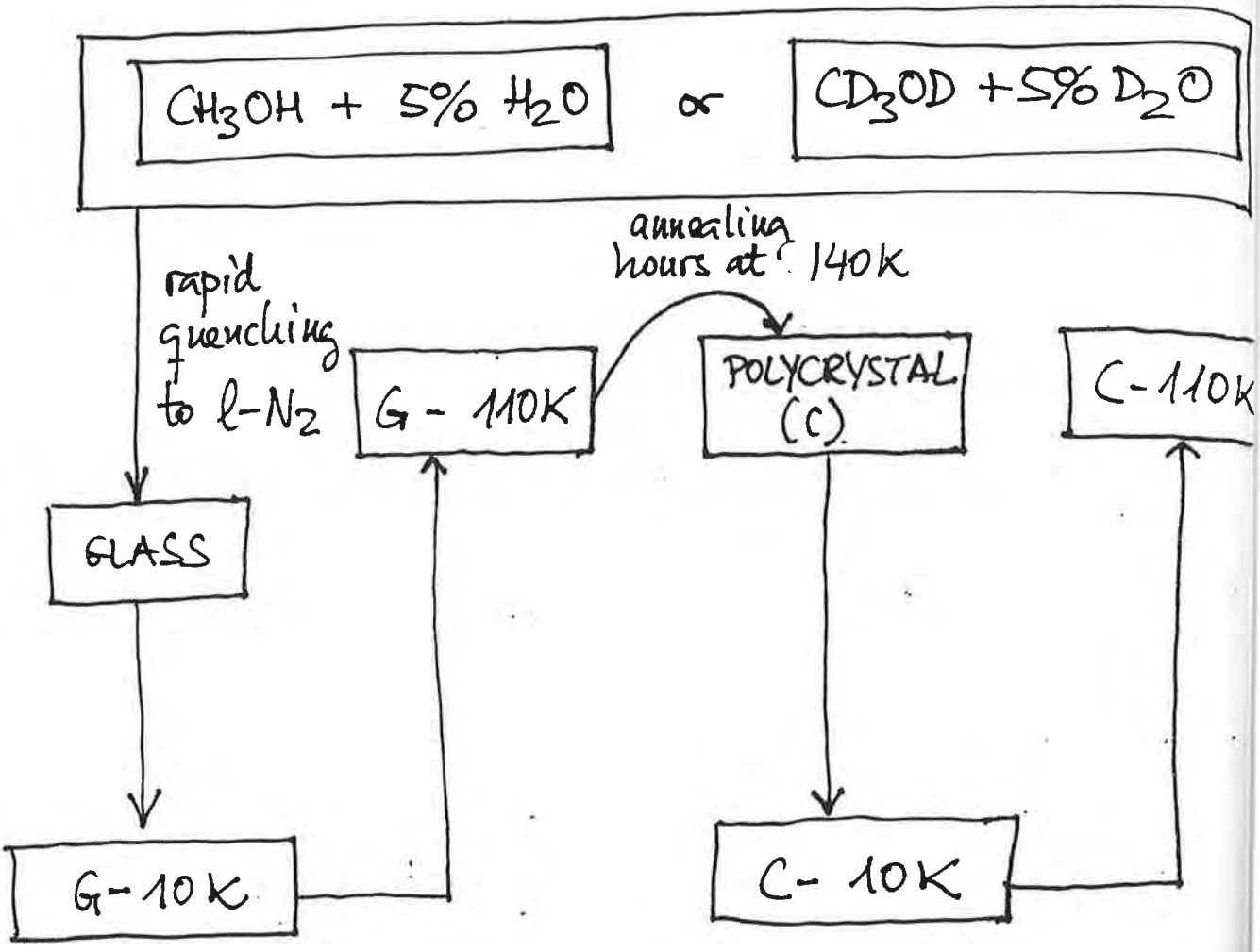

eVS Aim:

$n(p)$ for H (D), C, O

at T = 10, 110 K

for Glass and poly(C) cryst

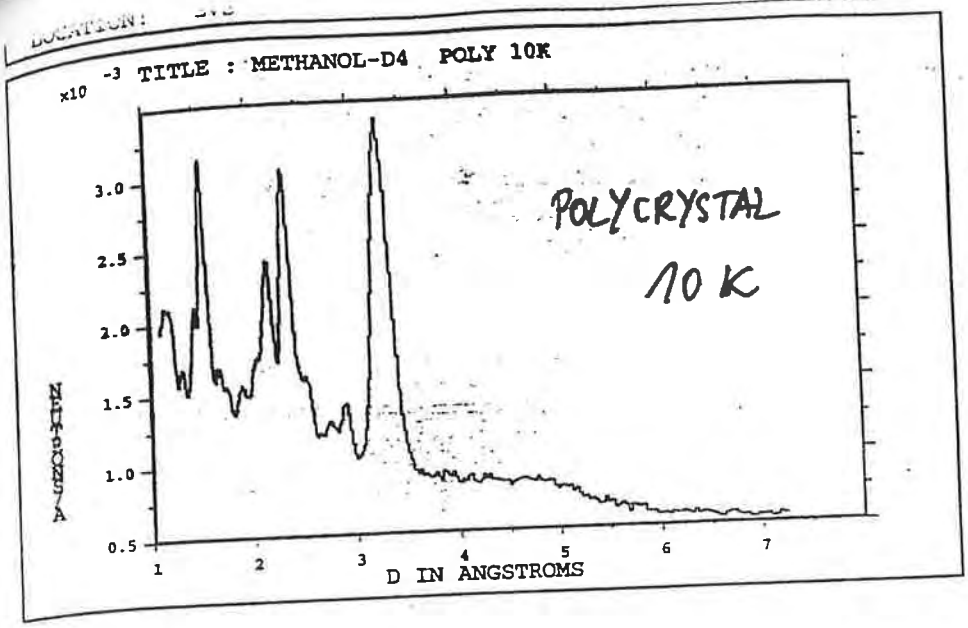
x10 -3 TITLE : METHANOL-D4 POLY 10K
3.0
2.5
2.0
1.5
1.0
0.5
1
2
3
4
5
6
7
D IN ANGSTROMS
POLYCRYSTAL
10 K

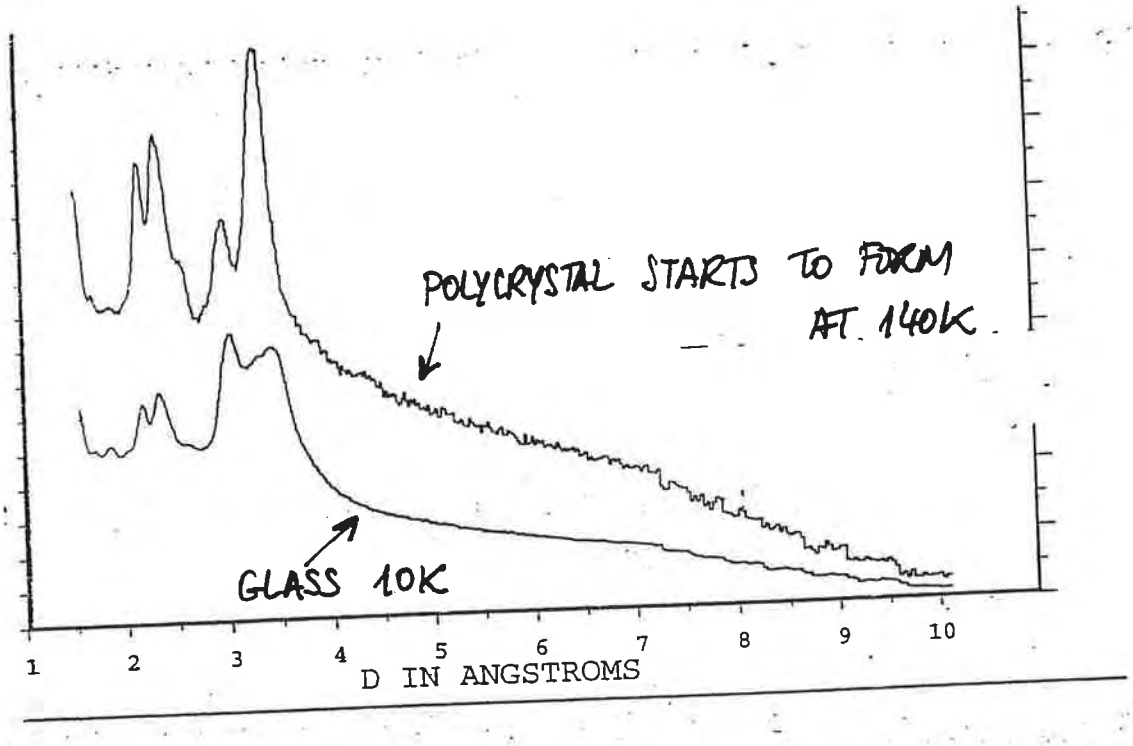
POLYCRYSTAL STARTS TO FORM
AT 140K
GLASS 10K
1
2
3
4
5
6
7
8
9
10
D IN ANGSTROMS

INSTRUMENT: EVS	USER: FM, AS/JM/ACE
RUN NUMBER: 2062	RUN START TIME: 29-OCT-199
SPECTRUM : 36	PLOT DATE: Fri 29-OCT-199
	BINNING IN GROUPS OF 4
LOCATION: DAE memory	

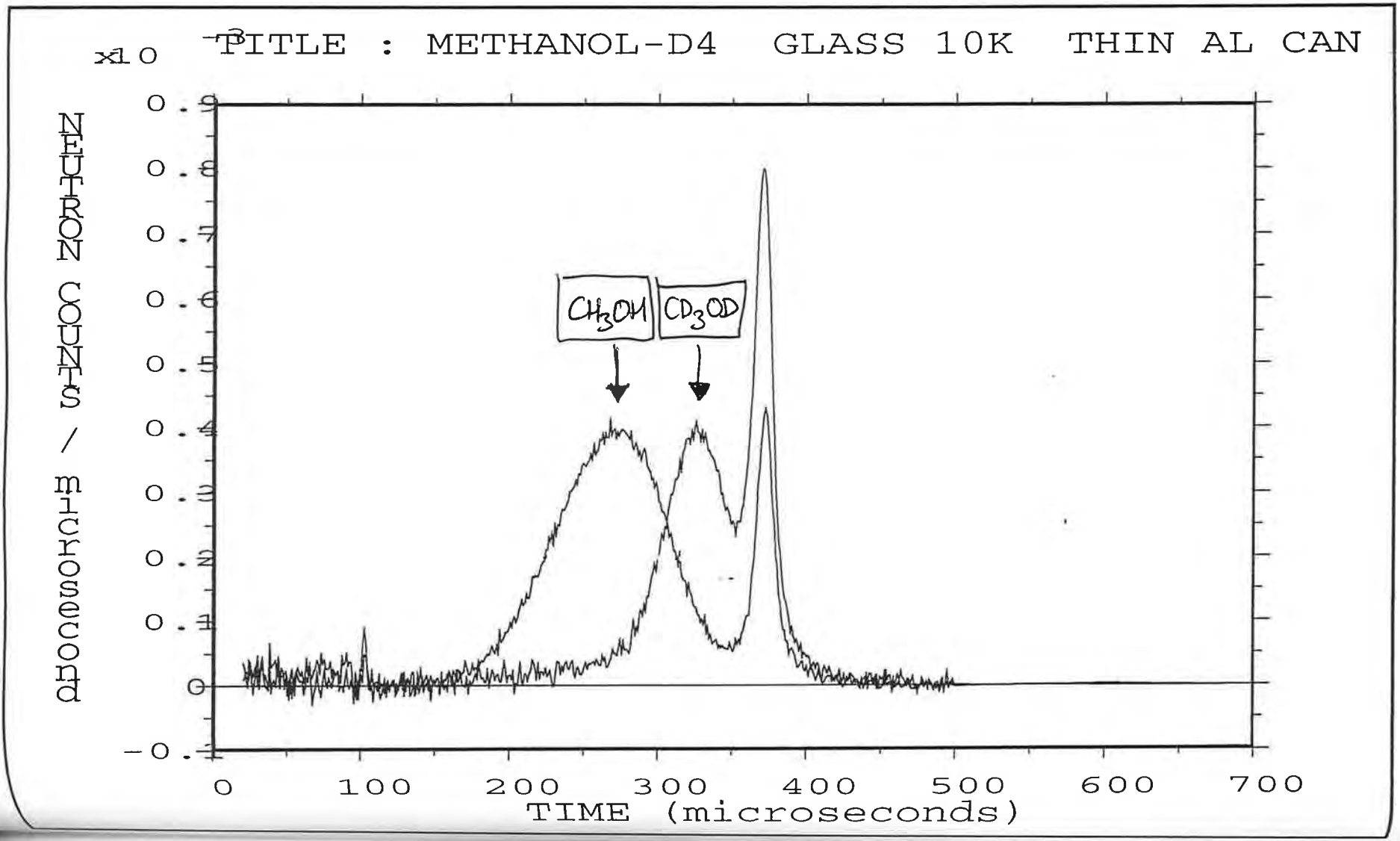

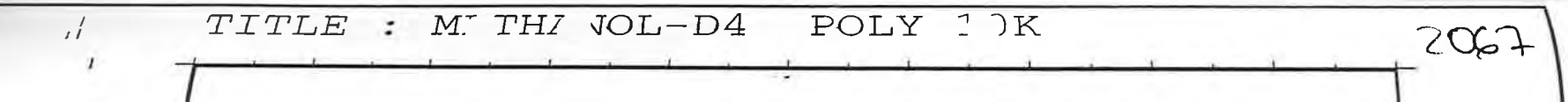

0 100 200 300 400 500 600 700
TIME (microseconds)

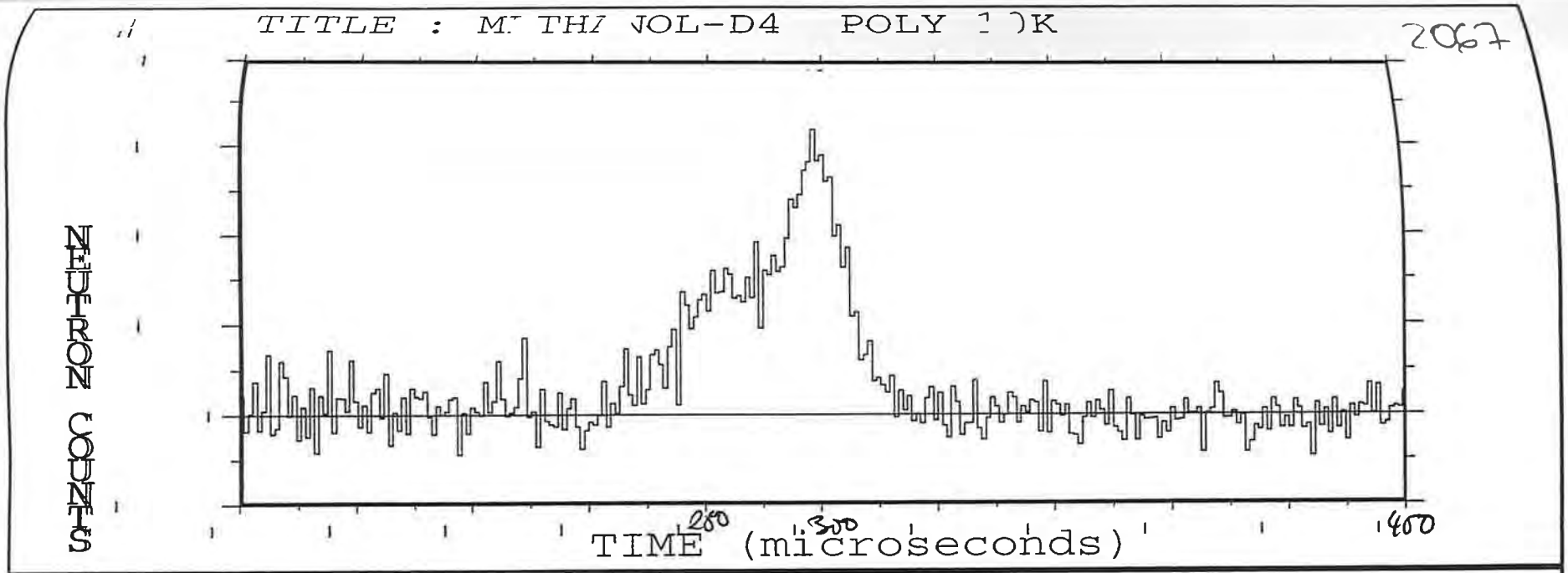

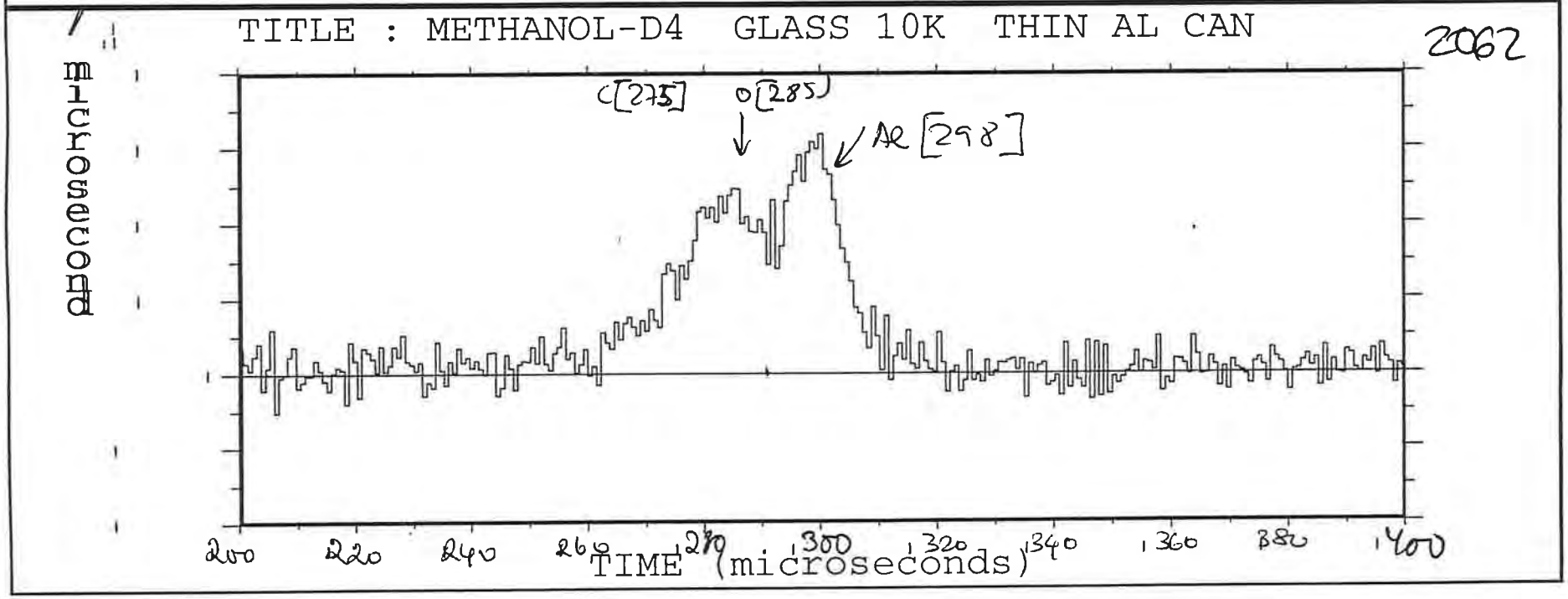

$n(p)$ for H, D

* Symmetrized y-profiles
* n_H, n_D ~ 0.5% above free atom
* weighted average over detectors for subsequent interpretations

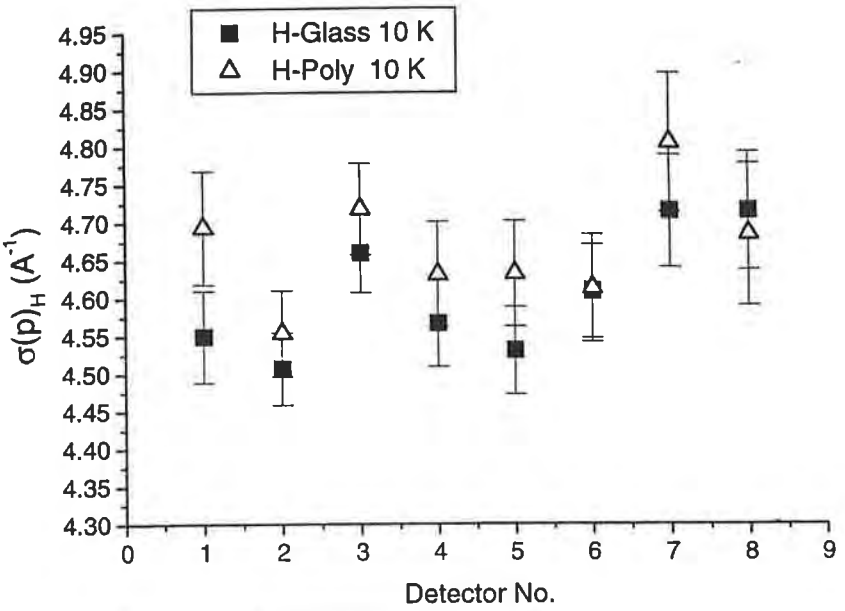
H-Glass 10 K
H-Poly 10 K
σ(p)H (A-1)
Detector No.

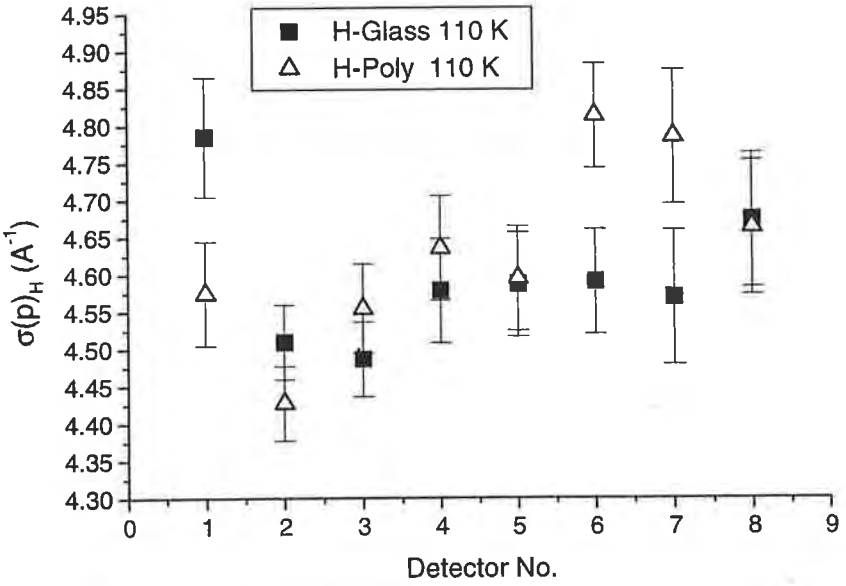
H-Glass 110 K
H-Poly 110 K
σ(p)H (A-1)
Detector No.

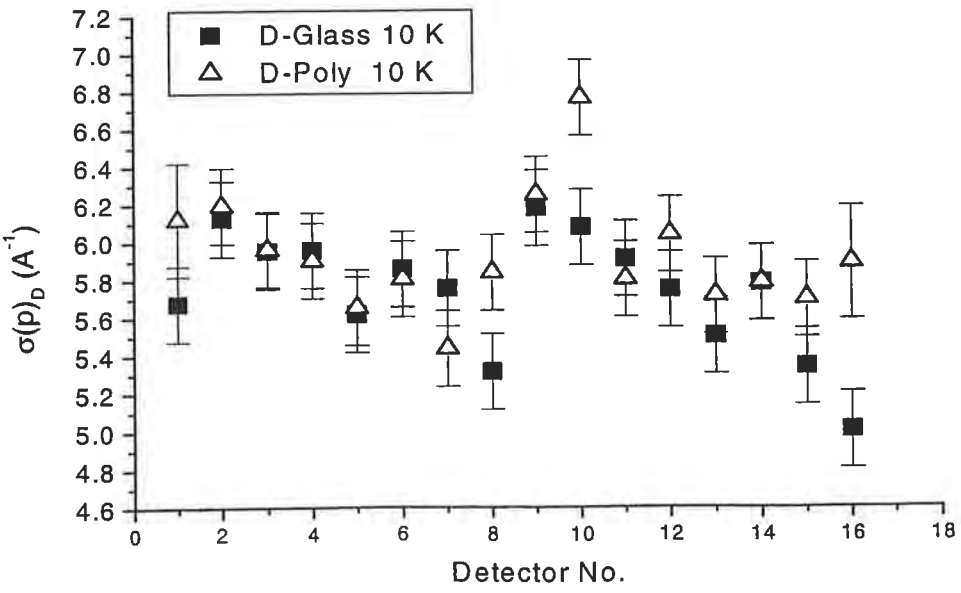
D-Glass 10 K
D-Poly 10 K
σ(p)D (A-1)
Detector No.

Model

Molecular Glass ⟹ Lattice contribution + "Molecular" contribution

$$J_{tot}(y) = \int dy' \, J_\ell(y') \, J_m(y'-y)$$

$$\sigma_\ell = \sqrt{\frac{2MK_\ell}{\hbar^2}} \quad ; \quad K_\ell = \frac{3}{4}\int_0^\infty \omega \, Z(\omega) \coth\left(\frac{\hbar\omega}{2k_B T}\right)$$

σ_ℓ ↓ different for G or C

$Z(\omega)$ ↑ INS, MD, LD.

$$\sigma_m = \frac{\hbar \coth\left(\frac{\hbar\bar{\omega}}{2k_B T}\right)}{\langle d^2(T)\rangle^{1/2}}$$

average over normal modes

σ_m ↓ assumed G = C [high resolution gas spectroscopy]

$\langle d^2(T)\rangle^{1/2}$ ↑ i) summed over all normal modes
ii) averaged over identical nuclei (H, D)

σ_{total} from convolution (σ_ℓ, σ_m

Results

($Å^{-1}$)

ple	T/K	σ_{exp}	σ_t	σ_l	σ_m
H	10	4.5_5	4.26	1.159	4.09
H	10	4.6_5	4.32	1.390	4.09
H	110	4.5_6	4.19	1.458	3.93
H	110	4.6_6	4.22	1.522	3.93
D	10	5.48	4.98	1.304	4.81
D	10	5.68	5.06	1.576	4.81

$T = 10\,K$

$$\frac{\sigma_D^2}{\sigma_H^2} = \left(\frac{m_D}{m_H}\right)^{1/2} = 1.413 \begin{cases} \nearrow 1.45 \text{ G} \\ \searrow 1.49 \text{ C} \end{cases}$$

Conclusion (Molecular glass)

* Most of the observed kinetic energy comes from intramolecular contributions but lattice contributions are measurable (indirectly) and different in the disordered and crystalline phases.

* It is of interest to study the situation when

$$\sigma_m \to 0$$

e.g. : binary metallic glass

↳

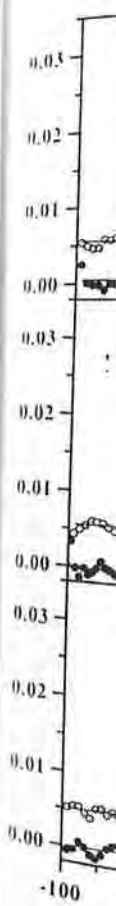

1. Experim
crystal data
s in ordinat

1.B. METALLIC GLASS

(Dawidowski et al., Phys. Lett. A, 214, 59 (1996))

$Ni_{0.83}{}^{11}B_{0.17}$ → amorphous (ribbons)
→ polycrystal

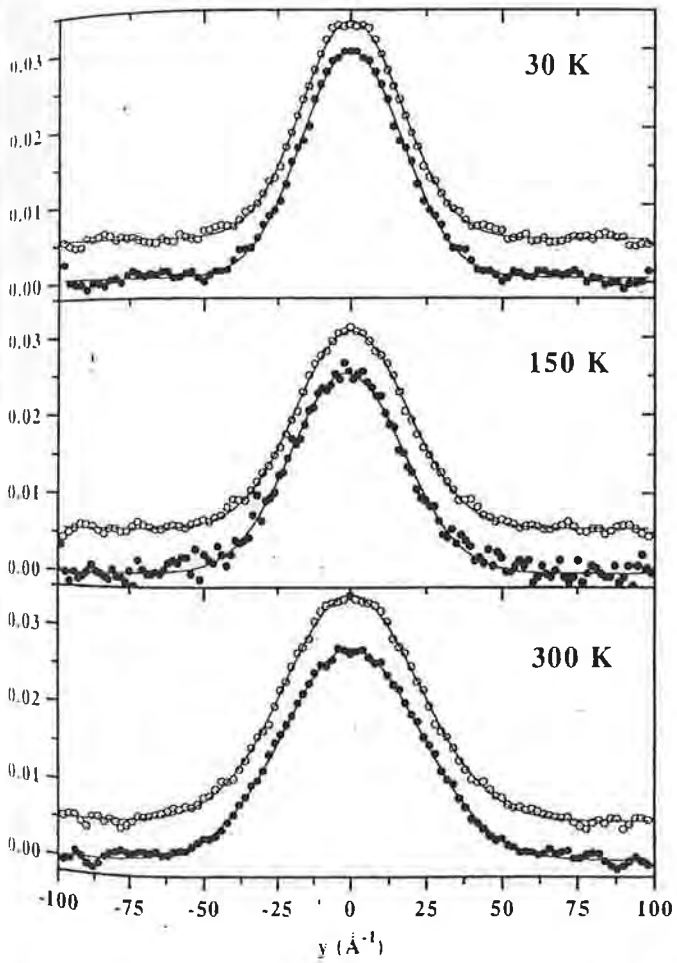

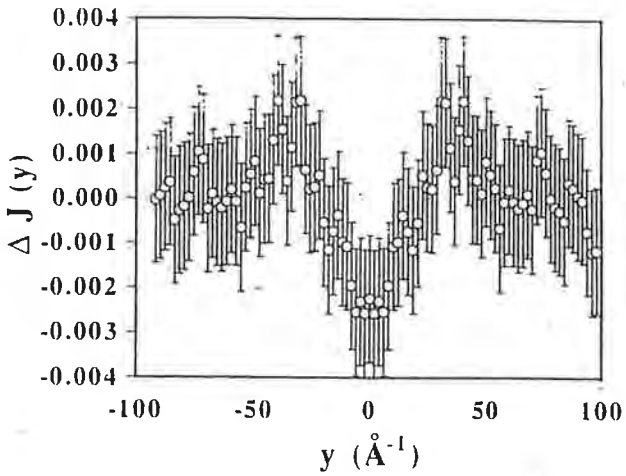

xtal - glass

1. Experimental neutron Compton profiles. Full circles indicate crystal data. The glass data (hollow circles) are shifted 0.005 s in ordinates for the sake of clarity. Fitted Gaussian profiles

Ni

Table 1
Experimental neutron Compton profile widths and calculated kinetic energies

Temp. (K)	σ_{cryst} (Å^{-1})	K_{cryst} (K)	σ_{glass} (Å^{-1})	K_{glass} (K)
30	14.04±0.17	244.4±5.9	13.88±0.15	238.8±5.2
150	16.36±0.29	331.8±11.7	15.93±0.15	314.6±5.9
300	20.97±0.19	545.1±9.9	20.49±0.15	520.4±7.6

[12]. In Table 1 we show the fitted widths, along with the corresponding kinetic energies.

magnetic contributions?

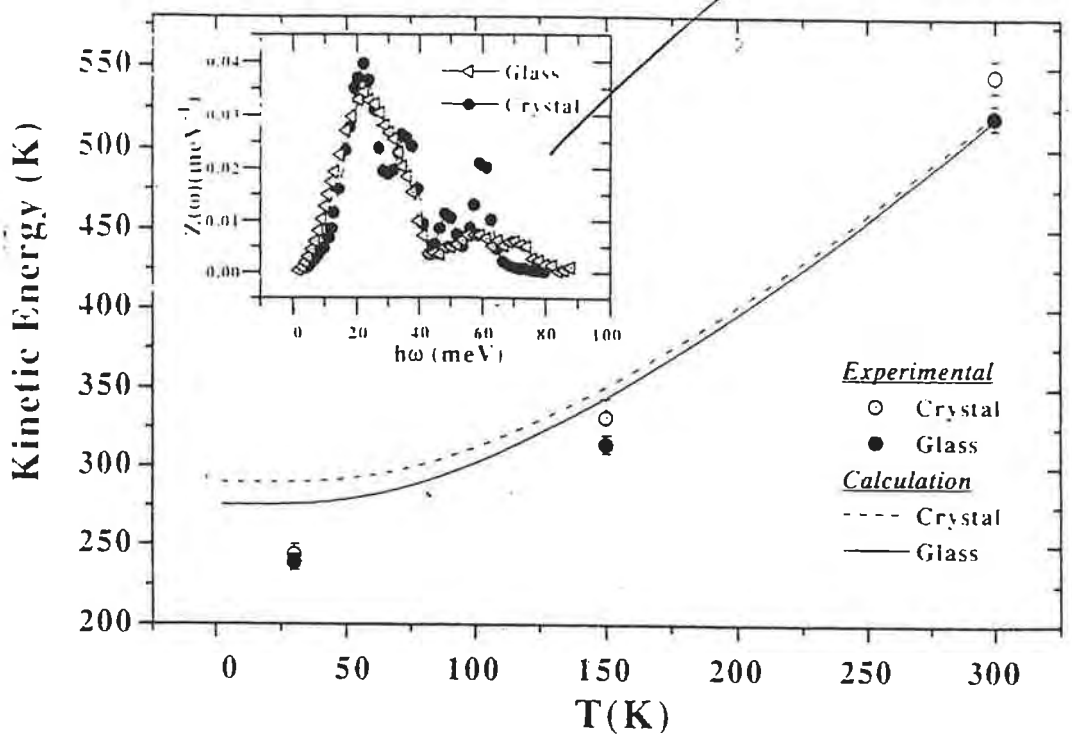

Fig. 3. Kinetic energy for the glass and crystal phase obtained from our experiment and those calculated from Eq. (6). Inset: densities of states used in the calculation (see text for details).

1. C. CONCLUSIONS

* DINS is suitable to study dynamics of glassy sistems: high frequency fingerprints appear in $n(p)$.

* A more complete picture could be obtained if the dynamics could be viewed through several types of atoms in the samples.

* Average kinetic energies of atoms in crystalline samples seem to be consistently higher than in glasses at same temperatures.

EXPERIMENT ON $PrBaFeCuO_{5+\delta}$

WHY STUDY $PrBaFeCuO_{5+\delta}$?

Related to high T_C superconductor $YBa_2Cu_3O_{7-x}$

i) charge reservoir closer to conduction layer

ii) Fe substitution increases T_{Neel}

iii) Pr substitution increases lattice volume available for extra O

iv) $\delta = 0$ & $\delta \cong 0.25$ ← softening in Mössbauer (^{57}Fe) ~ $T = 100K$

but $PrBaFeCuO_{5+\delta}$ does not become HTCS

→ Assumme lattice origin :

is it also observed on $n(p)$ for O ?

eVS : $\delta = 0$; 0.25

Figure 1: PrBaCuFe

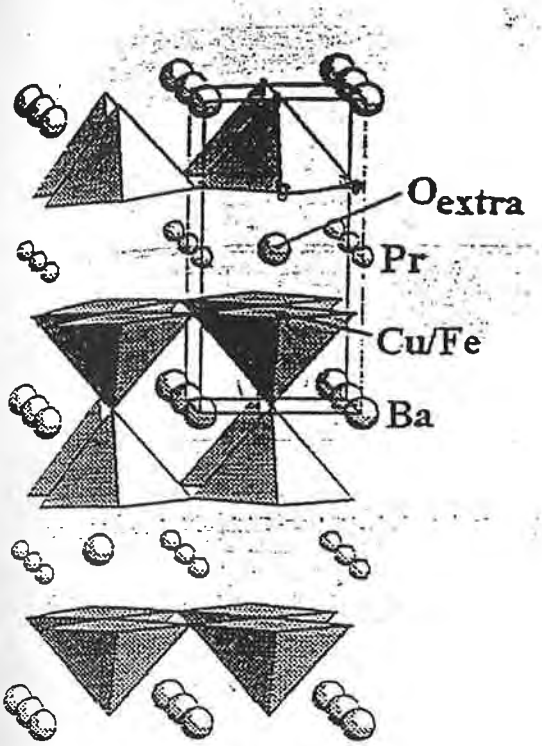

Figure 1: Schematic representation of the structure of $PrBaCuFeO_{5-\gamma}$

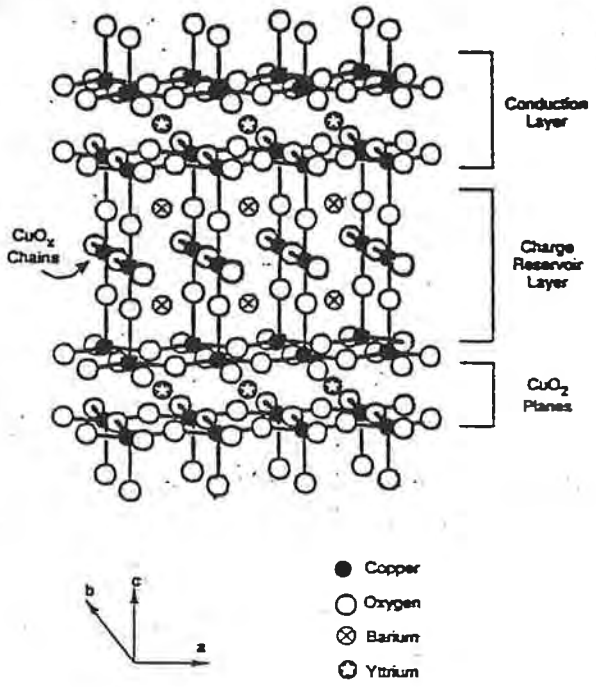

FIG. 3. Crystal structure of $YBa_2Cu_3O_{6+x}$ (taken from Jorgensen, 1991).

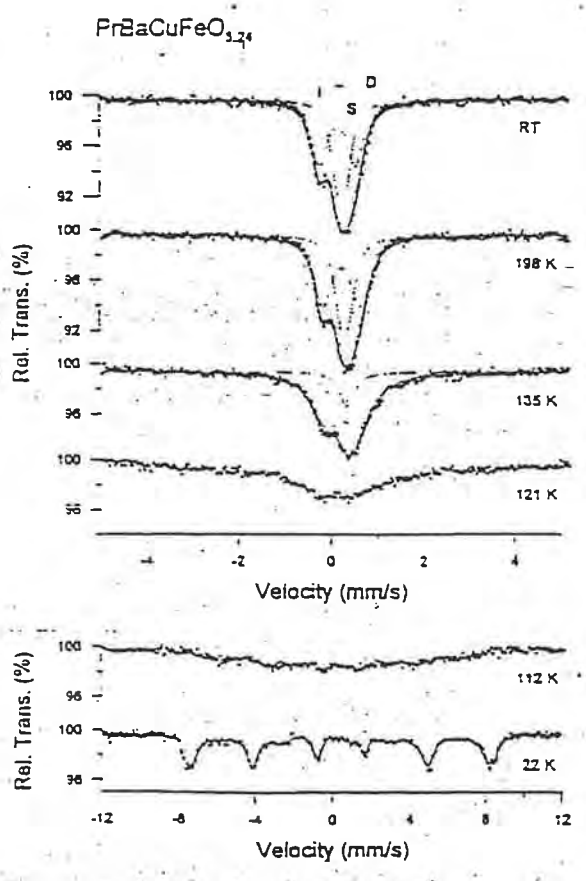

Figure 5: Mössbauer spectra at different temperatures for oxygenated $PrBaCuFeO_{5.24}$

B) ON eVS:

1st campaign 1997

2nd campaign 1998

* U foil analyzer
* TOF fits to 3 peaks:

O	M = 16 amu
Al	M = 27 amu
other atoms	M = 139 amu

INSTRUMENT: EVS
RUN NUMBER: 4168
USER: F. MOMP AN
RUN START TIME: 2-JUN-1997 00:06:

INSTRUMENT: EVS
RUN NUMBER: 4168
SPECTRUM : 42

USER: F. MOMP. AN
RUN START TIME: 2-JUN-1997 00:06:
PLOT DATE: Tue 3-JUN-1997 21:13:
BINNING IN GROUPS OF 2

LOCATION: EVS_DATA:EVS04169.RAW

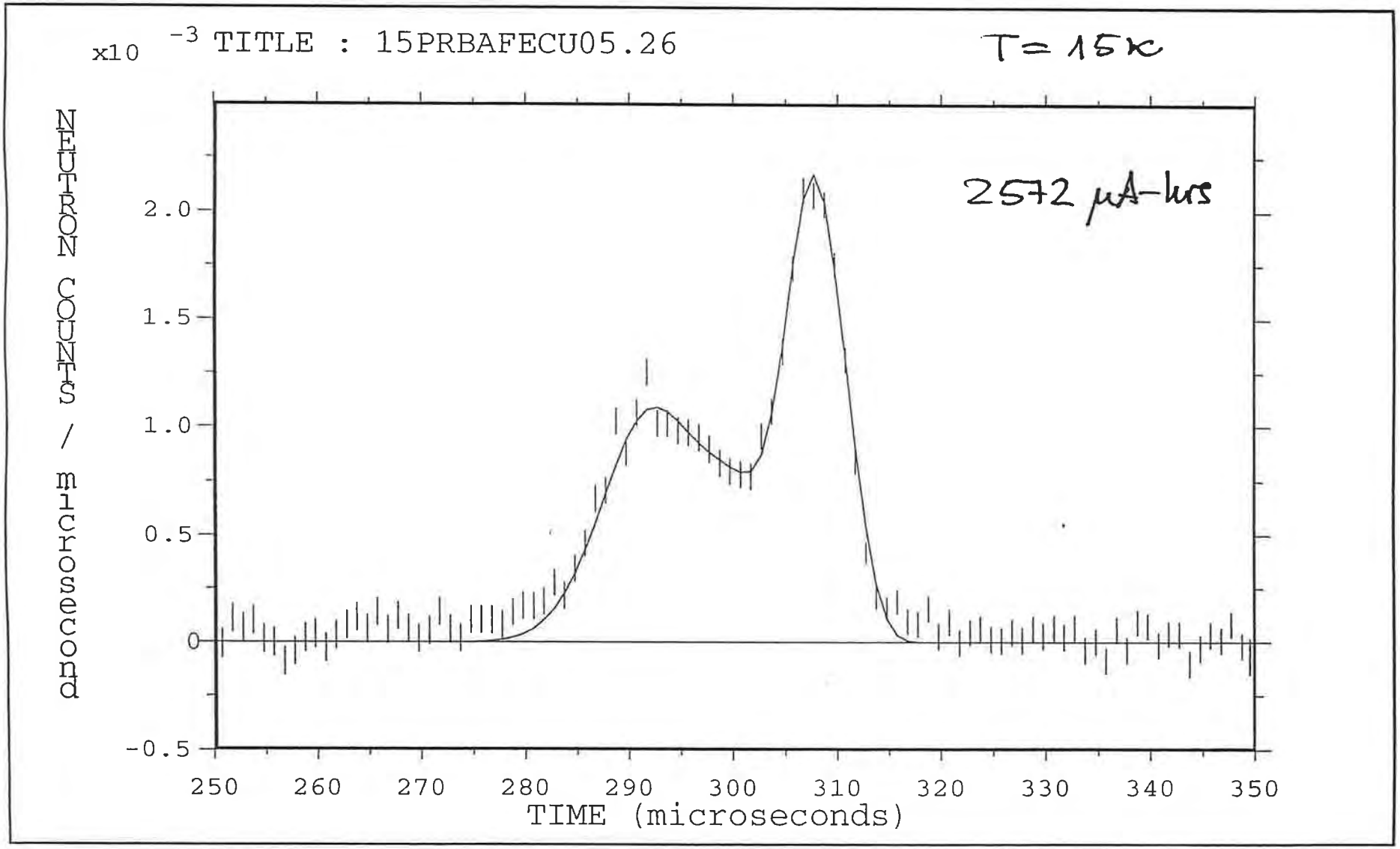

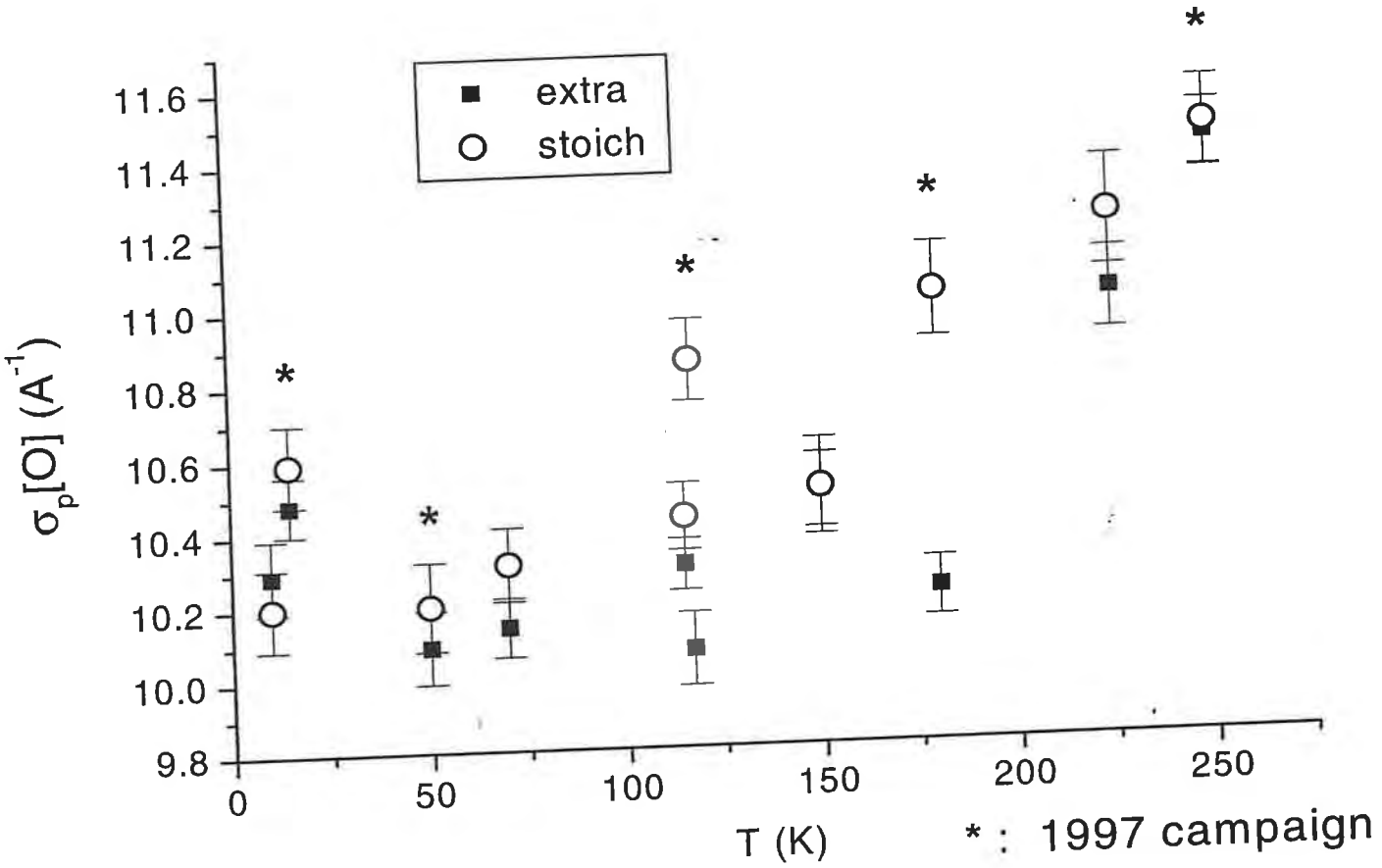
extra
stoich
11.6
11.4
11.2
11.0
10.8
10.6
10.4
10.2
10.0
9.8
$\sigma_p[O]$ (A^{-1})
0
50
100
150
200
250
T (K)
*
*
*
*
*
* : 1997 campaign

C. CONCLUSION

* $\sigma_p(0)_{\delta=0.25} < \sigma_p(0)_{\delta=0}$

(Pissas et al. Phys Rev B 55 397 (1997)

$B_{iso}(0)_{\delta=0.25} > B_{iso}(0)_{\delta=0}$

$B_{iso} \sim 8\pi^2 \langle u^2 \rangle$

* uncertainty as to systematic accidental errors in our exp?

(TGA samples after 2nd campaign did not reveal anomalies)

(* DINS vs Mößbauer : a time scale problem?

* purely magnetic disorder on Fe sites?)

3. OTHER PROBLEMS IN 'NOVEL' OXIDES

i) $CuGeO_3$

Spin-Peierls transition at 14 K

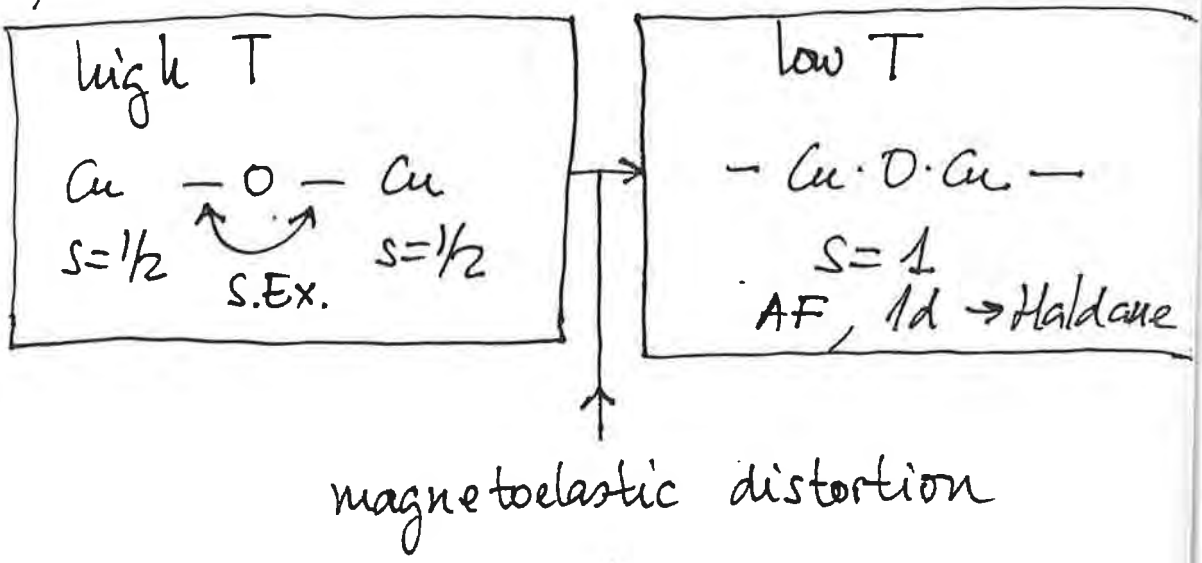

ii) CMR manganites

example $La_{1-x}Ca_xMnO_3$

- rich phase diagram, including regions with phase segregation into metallic / insulator clusters
- structural and magnetic polarons.

Deep Inelastic Neutron Scattering from H_2 and D_2: the eVS results

C. Andreani[(a)], **D. Colognesi**[(b)] & E. Pace[(c)]

(a) Dip.to Fisica and UdR INFM, Roma Torvergata (Rome, IT)

(b) GNSM-CNR (Rome, IT) and INFM, UdR Roma Torvergata (Rome, IT)

(c) Dip.to Fisica and Sez. INFN, Roma Torvergata (Rome, IT)

1) Theoretical Background

DINS from a single H_2/D_2 molecule:

$$\frac{d^2\sigma}{d\Omega dE'} = \frac{k'}{k}\sum_I p_I \sum_F \left| \left\langle \Psi_F \left| \sum_{n=1}^{2} \hat{b}_n \exp\left(i\vec{Q}\cdot\vec{r}_n\right) \right| \Psi_I \right\rangle \right|^2 \delta\left(\hbar\omega - E_F + E_I\right)$$

(*incoherence among different molecules assumed*)

Decoupling the CM motion from the internal (INT) one:

$$\frac{d^2\sigma}{d\Omega dE'} = \frac{\sigma_{TOT}}{2\pi}\frac{k'}{k} S_i^{CM}(Q,\omega) \otimes \Sigma_{INT}(Q,\omega)$$

(V. Sears, 1966; reasonable for H_2/D_2 only!)

where $S_i^{CM}(Q,\omega)$ contains the whole many-body problem. If $\hbar\omega >> \varepsilon_{coll} \approx (0\text{-}8)$ meV, the *inter-molecular impulsive regime* is reached:

$$S_i^{CM}(Q,\omega) \cong N \exp\left[-\left(\hbar\omega - \frac{\hbar^2 Q^2}{2M_m}\right)^2 \left(\frac{4\hbar^2 Q^2}{3M_m}\langle E_K \rangle_{CM}\right)^{-1}\right]$$

$\Sigma_{INT}(Q,\omega)$ contains only a two-body (*i.e.* one body) problem, but is not a structure factor:

$$\Sigma_{INT}(Q,\omega) = \frac{1}{2\sigma_T} \sum_{i,t} p_{i,t} \sum_f \sigma_{t,i,f} \left| \langle \varphi_f \left| \exp\left(i\vec{Q}\cdot\vec{r}/2\right) \pm \right. \right.$$
$$\left. \left| \exp\left(-i\vec{Q}\cdot\vec{r}/2\right) \right| \varphi_i \rangle \right|^2 \delta\left(\hbar\omega - E_f + E_i\right)$$

with $\vec{r} = \vec{r}_1 - \vec{r}_2$ and $\varphi = \varphi(\vec{r})$

However, if $Q > Q_{INC}$ with $f_{INT}(Q_{INC}) \cong 1$:

$$\Sigma_{INT}(Q,\omega) \rightarrow S_i^{INT}(Q,\omega) =$$
$$= \sum_i p_i \sum_f \left| \left\langle \varphi_f \left| \exp(i\vec{Q}\cdot\vec{r}/2) \right| \varphi_i \right\rangle \right|^2 \delta(\hbar\omega - E_f + E_i)$$

(D. Colognesi & E. Pace, 1998)

H_2/D_2: free molecular rotation $\Rightarrow$

$$\varphi_i(\vec{r}) = \frac{1}{r} u_{v(E)}(r) Y_{j,m_j}(\hat{r})$$

$\sigma_{t,i,f} = \sigma_{t,j,j'} =$

$\sigma_{e\to o}$= 159.8 b ($pH_2 \to oH_2$); 1.5 b ($oD_2 \to pD_2$)

$\sigma_{o\to e}$= 110.1 b ($oH_2 \to pH_2$); 12.2 b ($pD_2 \to oD_2$)

$\sigma_{e\to e}$= 3.6 b ($pH_2 \to pH_2$); 13.7 b ($oD_2 \to oD_2$)

$\sigma_{o\to o}$= 53.3 b ($oH_2 \to oH_2$); 3.0 b ($pD_2 \to pD_2$)

Plugging the free molecular rotation into $\Sigma_{INT}(Q,\omega)$ and assuming v=0:

$$\Sigma_{INT}(Q,\omega) = \frac{1}{\sigma_T} \sum_{t,j} p_{j,t} \sum_{j',v'(E')} \sigma_{t,j,j'} f^2{}_{j,0\to j',v'(E')}(Q)$$

$$\delta\left(\hbar\omega - E_{j',v'(E')} + E_j\right) \cong \sum_{t,j} p_{j,t} \sum_{j',v'(E')} f^2{}_{j,0\to j',v'(E')}(Q)$$

$$\delta\left(\hbar\omega - E_{j',v'(E')} + E_j\right)$$

with the *molecular structure factor* $f^2(Q)$:

$$f^2{}_{j,0\to j',v'(E')}(Q) = (2j'+1)\, C(j,j',0,0;l,0)$$
$$\sum_{l=|j-j'|}^{j+j'} \left| \int_0^\infty dr\, u_{j',v'(E')}(r)\, j_l(Qr/2) u_{j,0}(r) \right|^2$$

where the *initial state* $u_{j,0}(r)$ is reasonably described by:

$$u_{j,0}(r) \cong \sqrt{\frac{\alpha}{\sqrt{\pi}}} \exp\left[-\frac{\alpha^2}{2}(r-d)^2 \right]$$

for j=0,1 (H_2/D_2 @ T<100 K)

α=1.975 A^{-1} (H_2) and 2.349 A^{-1} (D_2)

$E_{(j=0,v=0)} \cong \hbar\omega_0/2$ =258 meV (H_2)

=186 meV (D_2)

$E_{(j=1,v=0)} \cong \hbar\omega_0/2+2B$=273 meV ($H_2$)

=193 meV (D_2)

Scattering model $\Leftrightarrow$ $f^2(Q)$ $\Leftrightarrow$ $u_{j',v'}(r)$

1. YK model (J.A.Young & J. Koppel, 1964)

$$u_{j',v'}(r) = N_{v'} \exp\left[-\frac{\alpha^2}{2}(r-d)^2\right] H_{v'}[\alpha(r-d)]$$

$$E_{j',v'} = \hbar\omega_0(v'+1/2) + Bj'(j'+1)$$

Purely harmonic vibrations - Rigid rotations

2. Intramolecular IA (J. Mayers, 1993; C. Andreani *et al.*, 1995)

$$u_{j',k'}(r) = r\, j_{j'}(k'r)$$

$$E_{j',k'} = \frac{\hbar^2 k'^2}{2\mu}$$

Freely recoiling particle

- Problems with YK (and MYK)

theoretically (D. Colognesi, 1998):

$$\lim_{\substack{Q\to\infty \\ y=const}} \Sigma_{INT}^{(YK)}(Q,\omega) \neq S_{INT}^{(IA)}(Q,\omega)$$

(i.e. $\omega=\hbar Q^2/2M_a$*)*

experimentally (W. Langel *et al.*, 1988; M. Zoppi *et al.*, 1996):

MYK works well between 5 A^{-1} < Q <30 A^{-1} but <u>not</u> on **eVS** (35 A^{-1} < Q <65 A^{-1})

- Problems with Intramolecular IA (and M Intra-IA)

When does Intra-IA apply ?

$$\frac{2}{3}Q\langle E_k\rangle_1 >> \left\langle \left(\vec{F}_1\cdot\hat{Q}\right)^2\right\rangle^{1/2} \approx 1500\, meVA^{-1}$$

(Sears, 1971)

H_2: $\langle E_k\rangle_1 \approx 70$ meV; D_2: $\langle E_k\rangle_1 \approx 50$ meV $\Rightarrow$

Intra-IA does <u>not</u> apply on **eVS**

($35\ A^{-1} < Q < 65\ A^{-1}$)

Experimental evidences on pH_2 (C. Andreani, D. Colognesi *et al.*, 1998; M. Zoppi, J. Mayers *et al.*, 1998) and oD_2 (C. Andreani, D. Colognesi *et al.*, 1999).

2) Experiments on eVS

- Samples:

1. liquid pH_2 (97.0%) at T=30 K (ρ=22.0 nm^{-3}, $\langle E_k \rangle_{CM}$=77 K)

2. gaseous eH_2 (pH_2=56.0%) at T=70 K (ρ=10.7 nm^{-3}, $\langle E_k \rangle_{CM}$=135.5 K)

3. liquid oD_2 (97.2%) at T=20.7 K (ρ=25.4 nm^{-3}, $\langle E_k \rangle_{CM}$=54.5 K)

- **Range and resolution**

H: 35 A^{-1}<Q_0<58 A^{-1} & 2.54 eV<$\hbar\omega_0$<6.97 eV
D: 31 A^{-1}<Q_0<73 A^{-1} & 0.99 eV <$\hbar\omega_0$<5.53 eV

$y=0 \Leftrightarrow \omega_0=\hbar Q_0^2/2M_a$

Voigt resolution in y

H:	$\sigma_y \approx 0.6\text{-}0.8\ A^{-1}$ & $\Gamma_y \approx 1.2\text{-}2.0\ A^{-1}$
D:	$\sigma_y \approx 0.8\text{-}1.0\ A^{-1}$ & $\Gamma_y \approx 2.4\text{-}5.2\ A^{-1}$

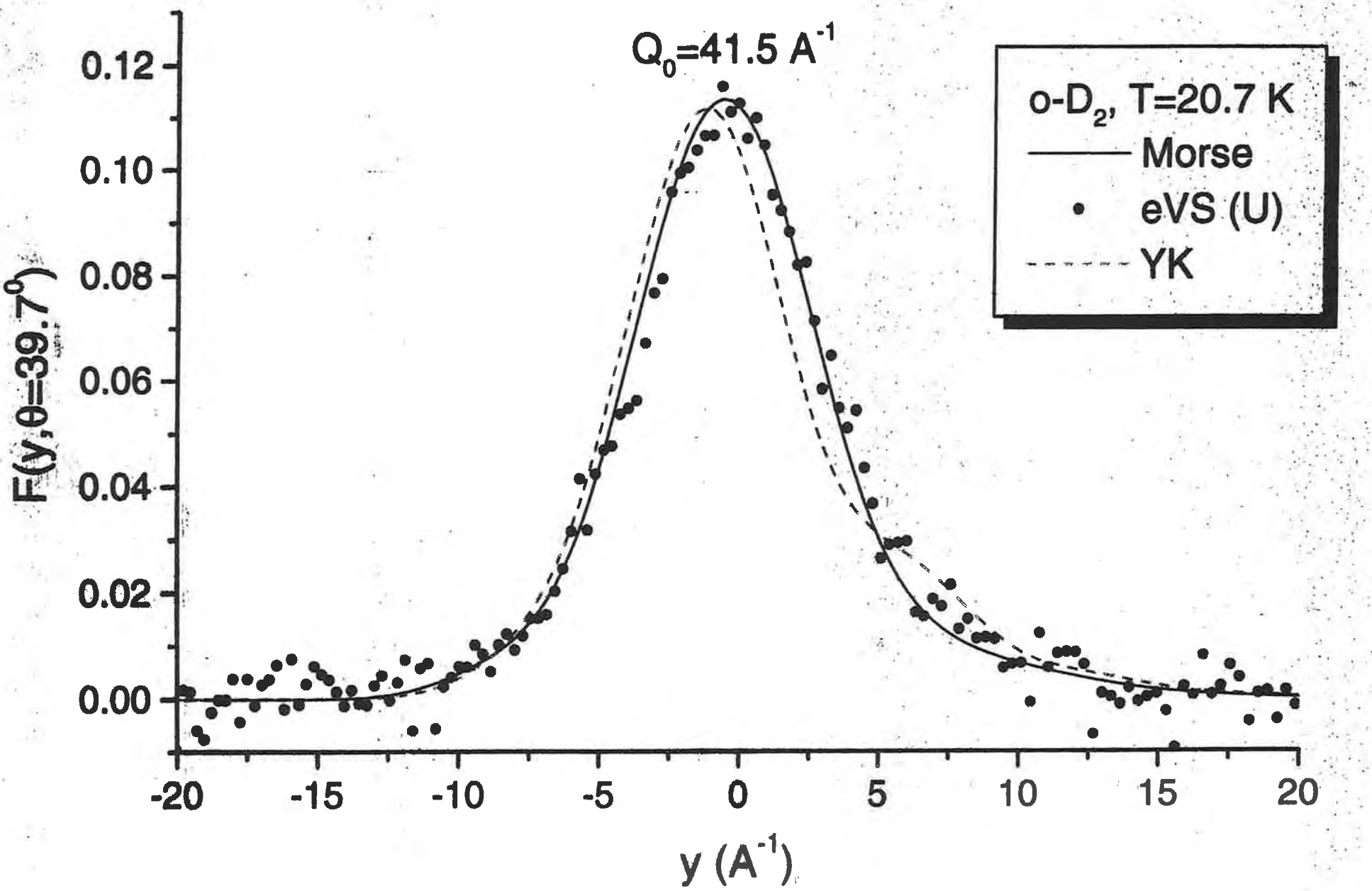
Q_0=41.5 A^{-1}
o-D_2, T=20.7 K
Morse
eVS (U)
YK
F(y,θ=39.7°)
0.12
0.10
0.08
0.06
0.04
0.02
0.00
-20
-15
-10
-5
0
5
10
15
20
y (A^{-1})

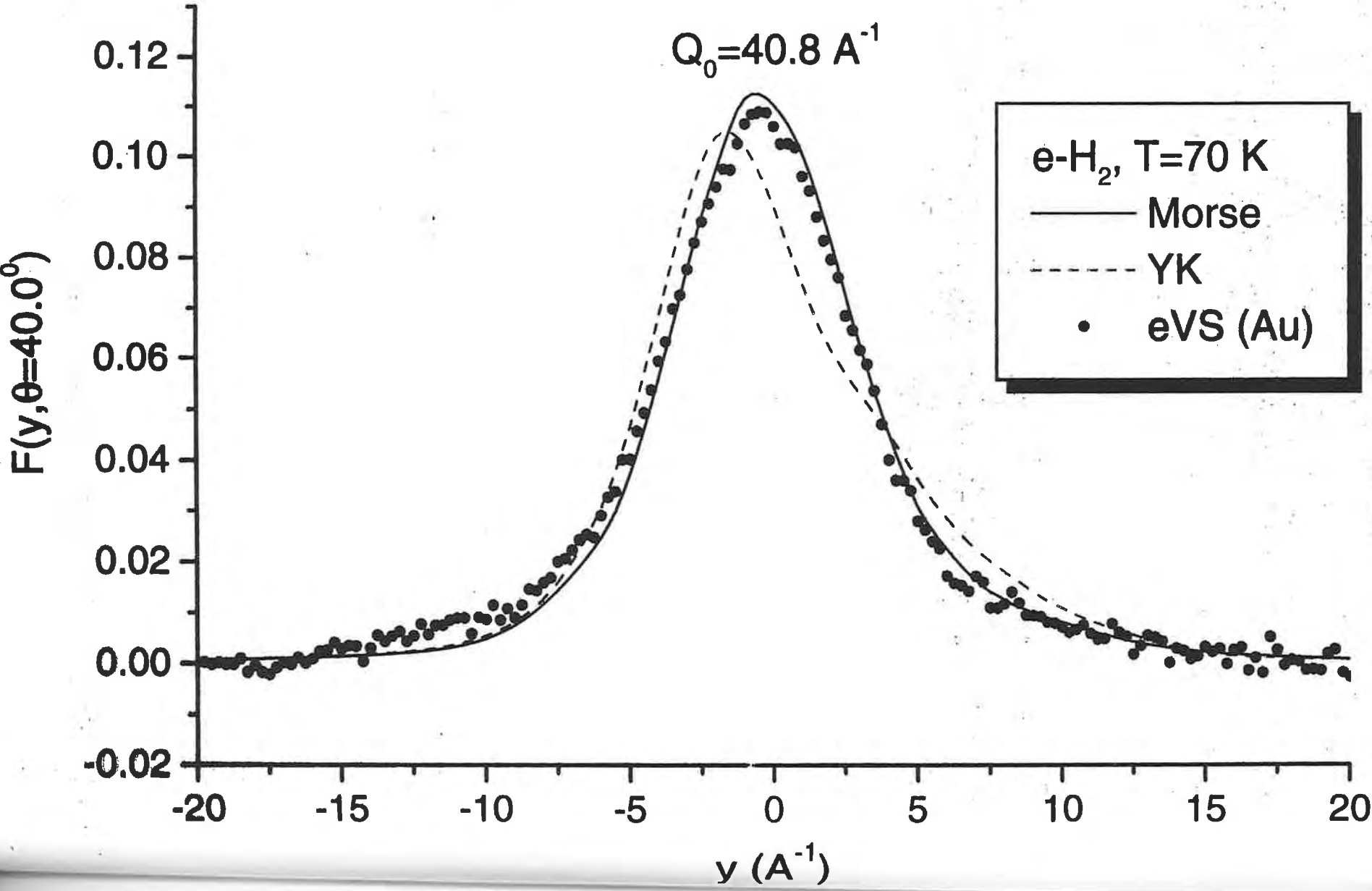
Q_0=40.8 A^{-1}
e-H_2, T=70 K
Morse
YK
eVS (Au)
F(y,θ=40.0°)
y (A^{-1})
0.12
0.10
0.08
0.06
0.04
0.02
0.00
-0.02
-20
-15
-10
-5
0
5
10
15
20

y (A^{-1})

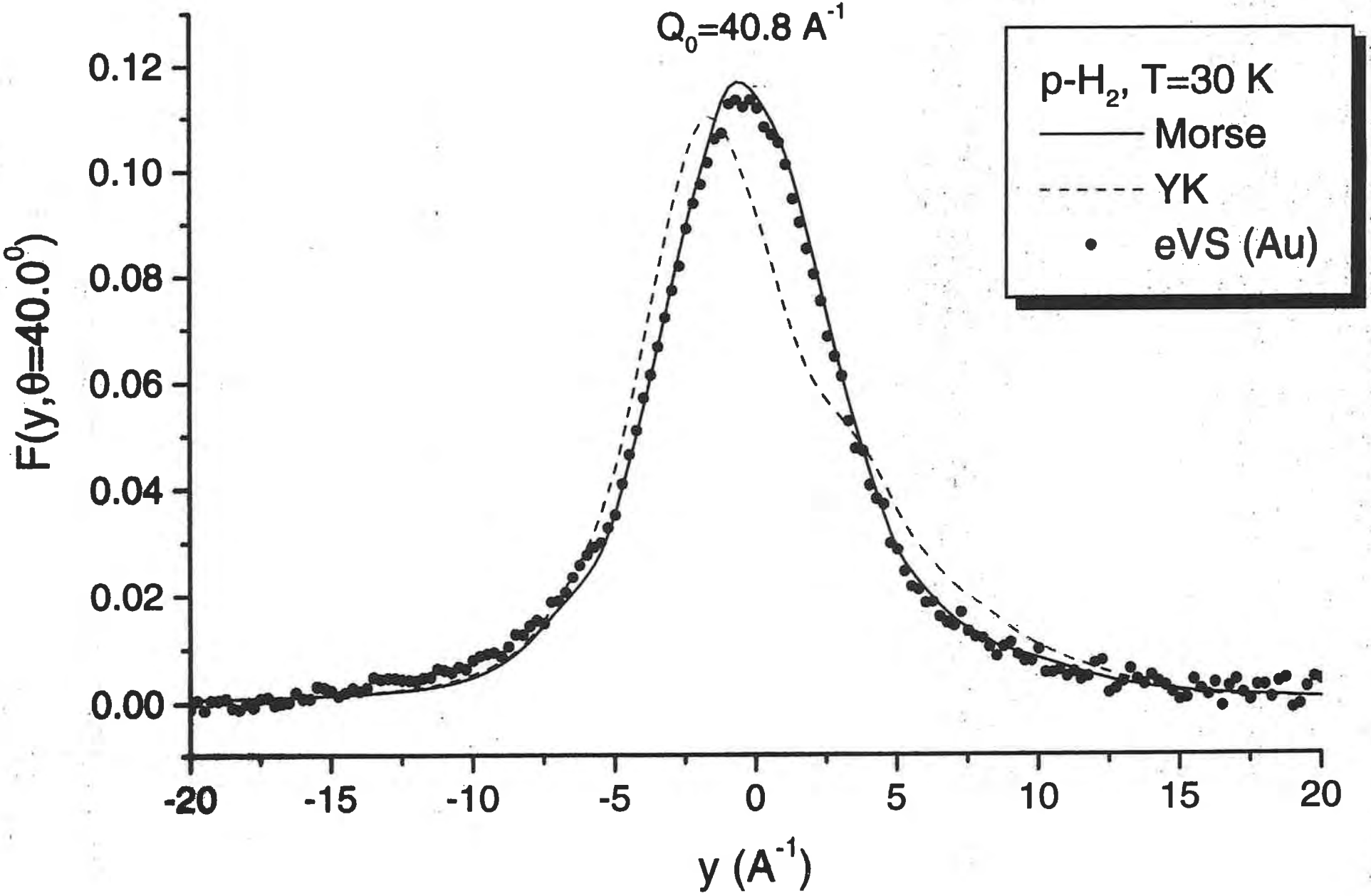
Q_0=40.8 A^{-1}
p-H_2, T=30 K
Morse
YK
eVS (Au)
F(y,θ=40.0°)
0.12
0.10
0.08
0.06
0.04
0.02
0.00
-20
-15
-10
-5
0
5
10
15
20
y (A^{-1})

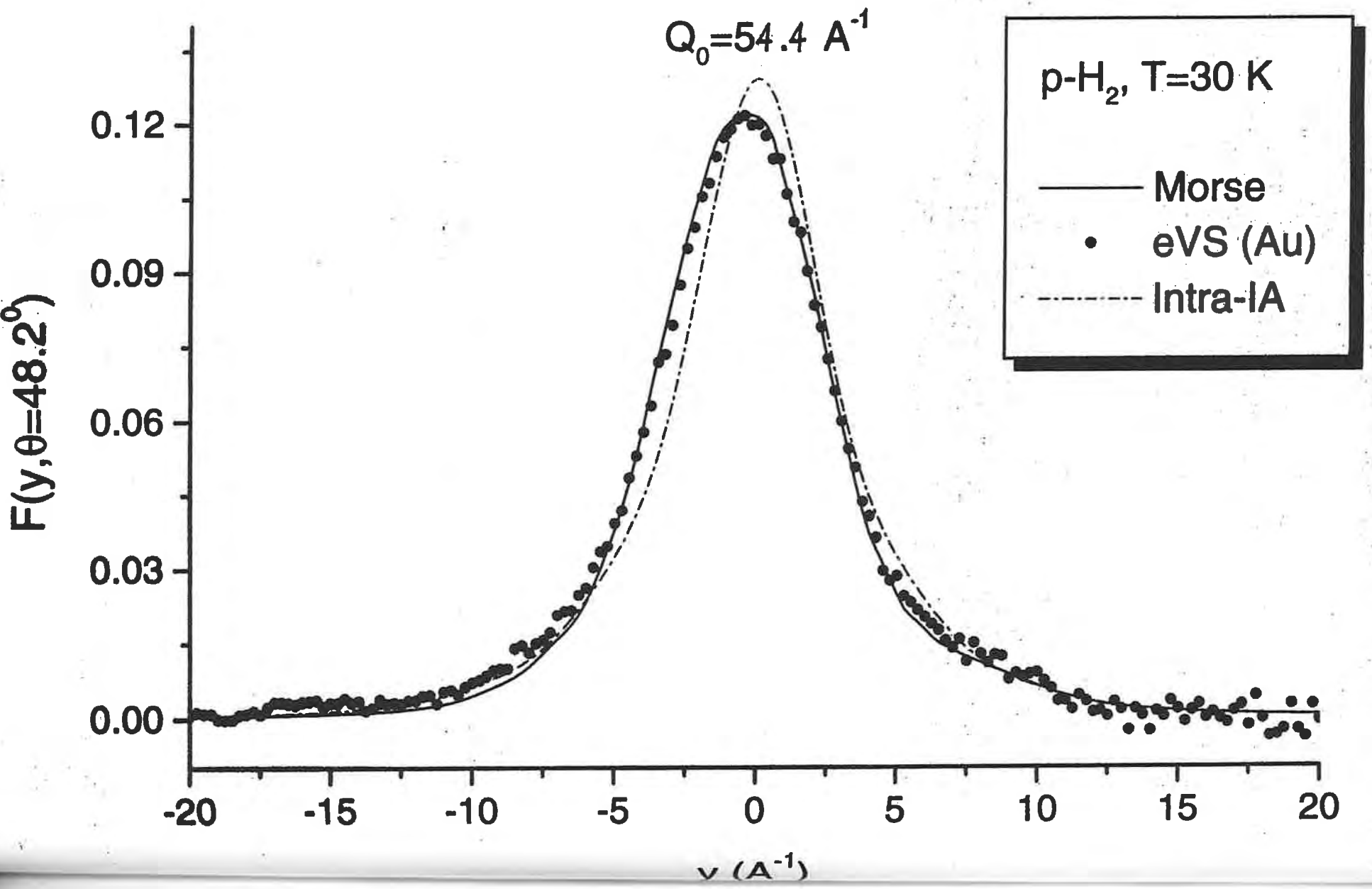
Q_0=54.4 A^{-1}
p-H_2, T=30 K
Morse
eVS (Au)
Intra-IA
F(y,θ=48.2°)
0.12
0.09
0.06
0.03
0.00
-20
-15
-10
-5
0
5
10
15
20
y (A^{-1})

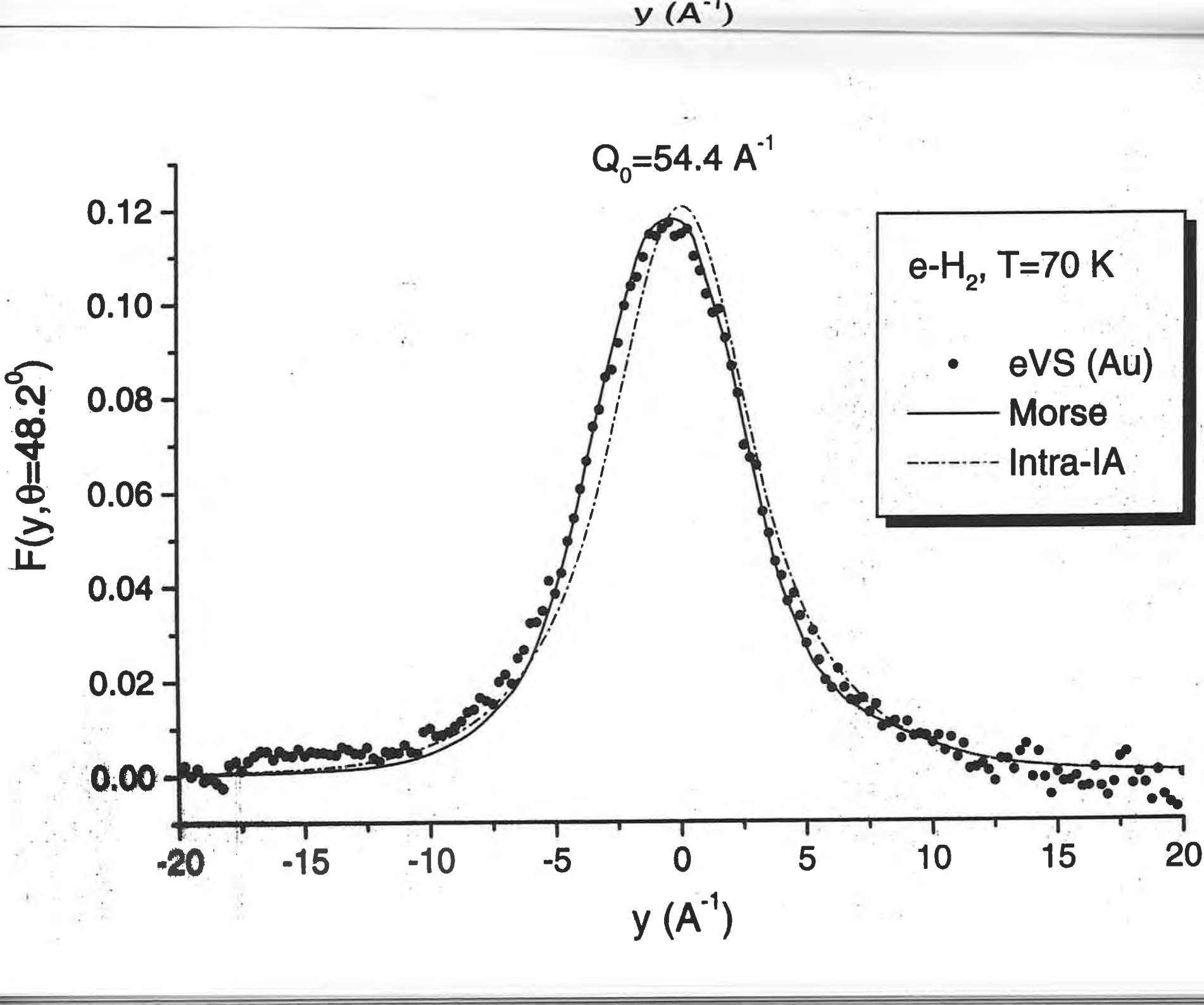
y (A-1)
Q0=54.4 A-1
e-H2, T=70 K
eVS (Au)
Morse
Intra-IA
F(y,θ=48.2°)
0.12
0.10
0.08
0.06
0.04
0.02
0.00
-20
-15
-10
-5
0
5
10
15
20
y (A-1)

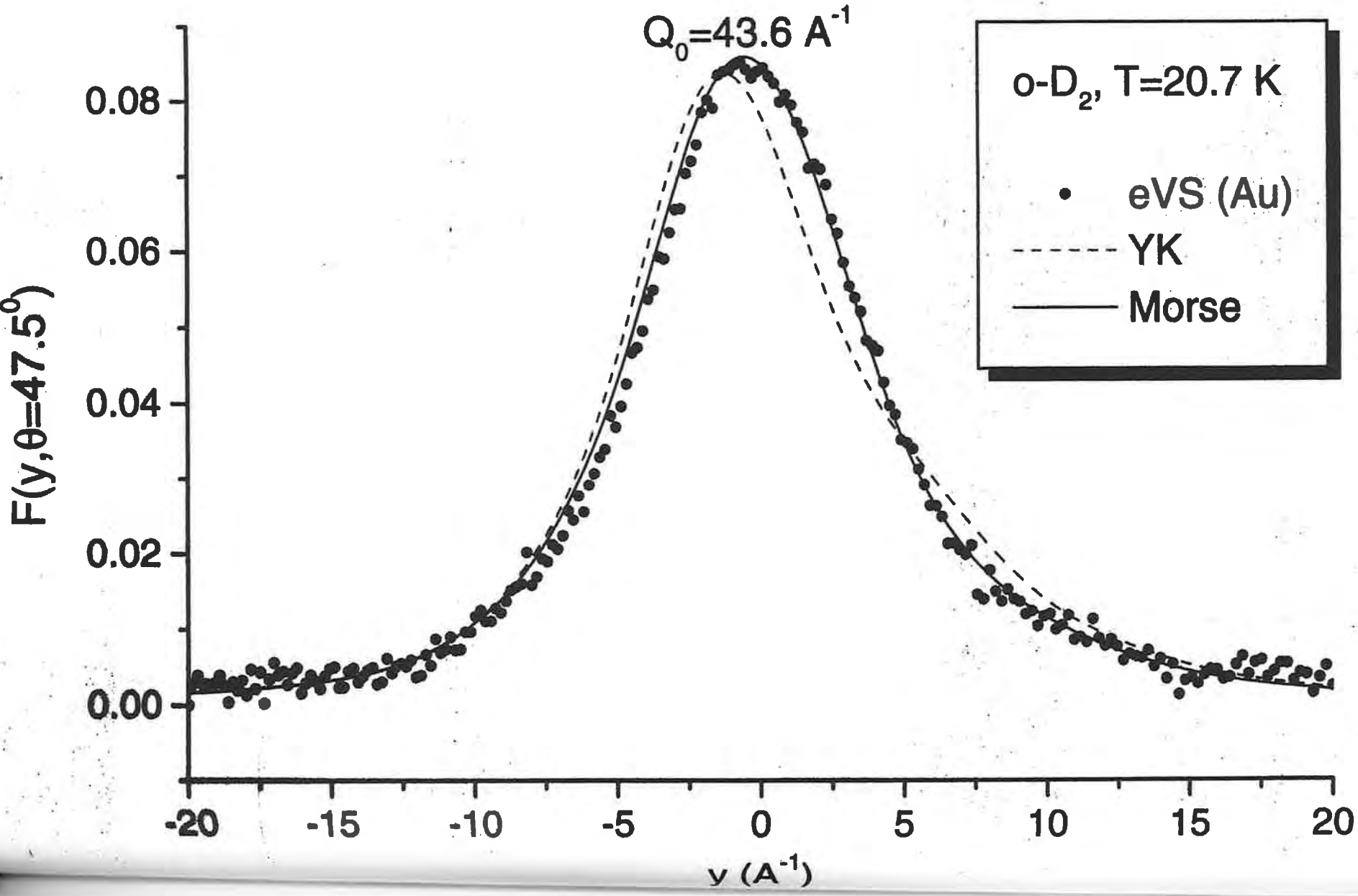
Q_0=43.6 A^{-1}
o-D_2, T=20.7 K
eVS (Au)
YK
Morse
F(y,θ=47.5°)
0.08
0.06
0.04
0.02
0.00
-20
-15
-10
-5
0
5
10
15
20
y (A^{-1})

3) New approach and conclusions

- Calculation of more reliable $f_{j,0\to j',v'(E')}(Q)$ using "real" $u_{j',v'(E')}(r)$ from the radial Schroedinger equation:

$$\frac{d}{dr}u(r) = W(r)$$

$$\frac{d}{dr}W(r) = -\frac{2\mu}{\hbar^2}\left(E - V_{j'}(r)\right)u(r)$$

- Choice of the Morse intra-molecular potential:

$$V_{j'}(r) = V_0\left(e^{-2a(r-d)} - 2e^{-a(r-d)}\right) + \frac{\hbar^2}{2\mu}\frac{j'(j'+1)}{r^2}$$

y (A^{-1})

with:

V_0=4.736 eV (H_2); 4.742 eV (D_2)

a=1.976 A^{-1} (H_2); 1.870 A^{-1} (D_2)

d=0.741 A (H_2); 0.748 A (D_2)

- Morse eigenvalue spectrum

$E_{j',v'}$<0: discrete; 330 eig., 16 at j'=0 (H_2)

720 eig., 22 at j'=0 (D_2)

$E_{j',k'}$>0: continuum & degeneracy in j'

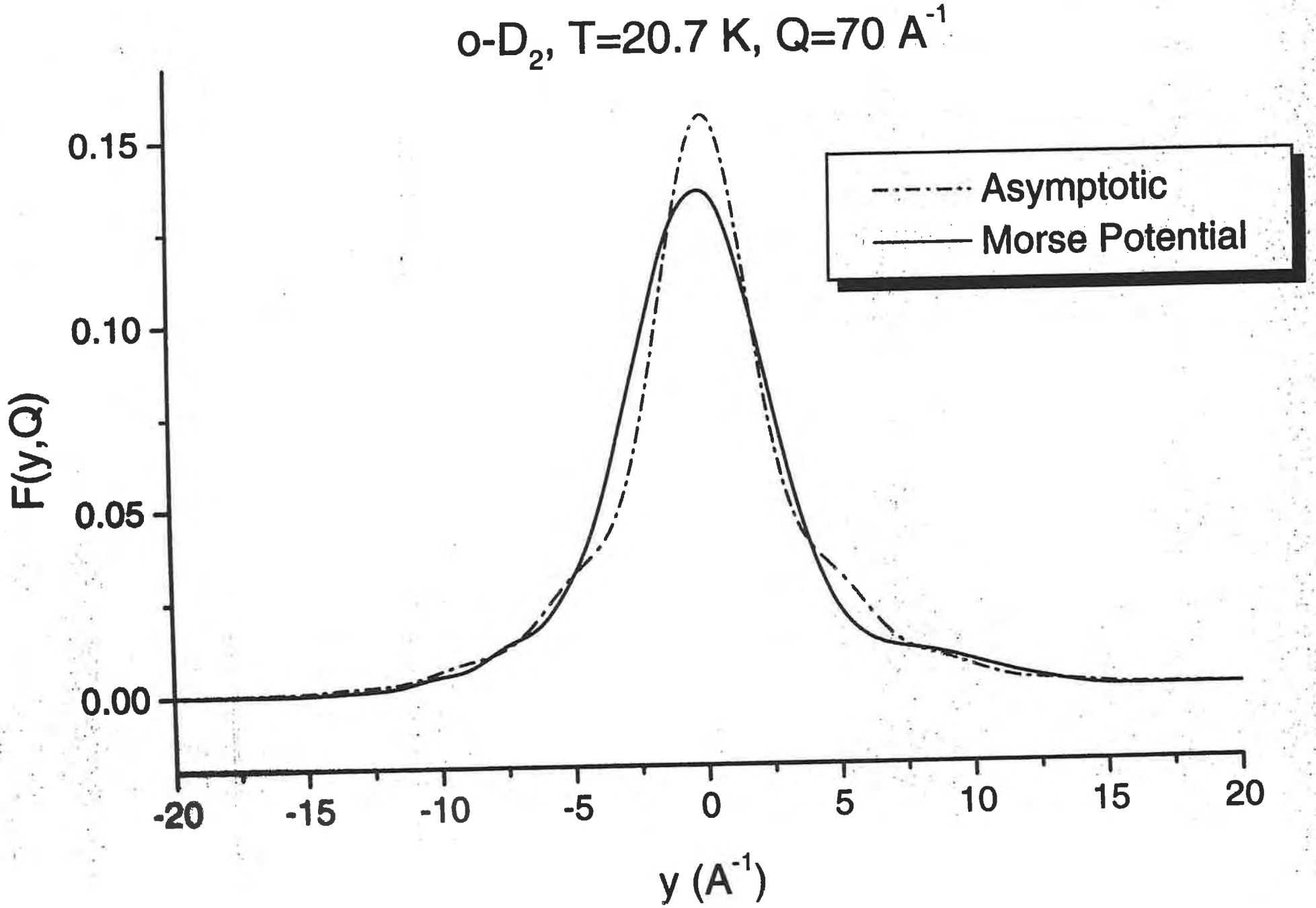
o-D2, T=20.7 K, Q=70 A-1
Asymptotic
Morse Potential
F(y,Q)
0.15
0.10
0.05
0.00
-20
-15
-10
-5
0
5
10
15
20
y (A-1)

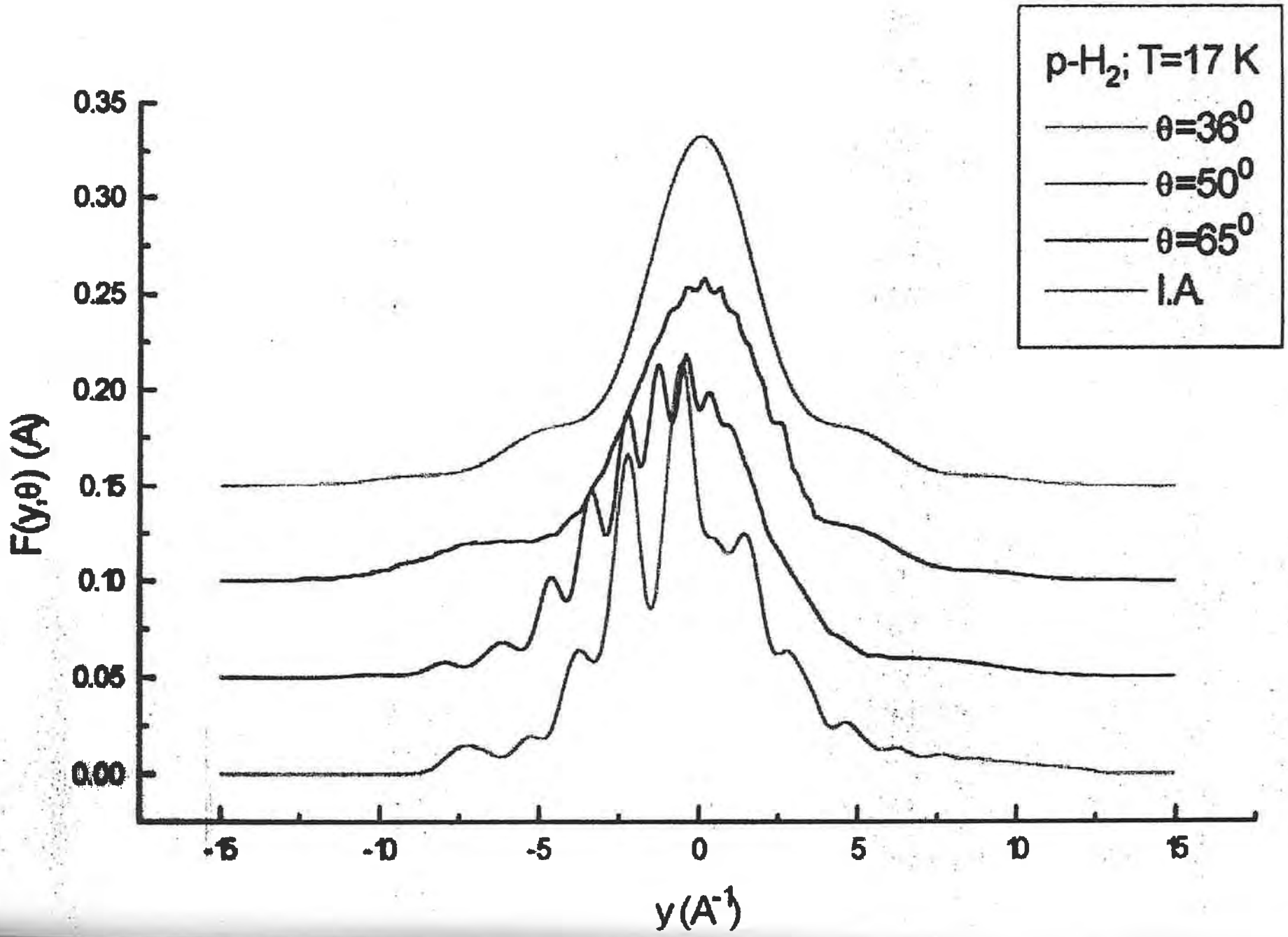

o-D_2, T=20.7, Morse simulations

y(A^{-1})

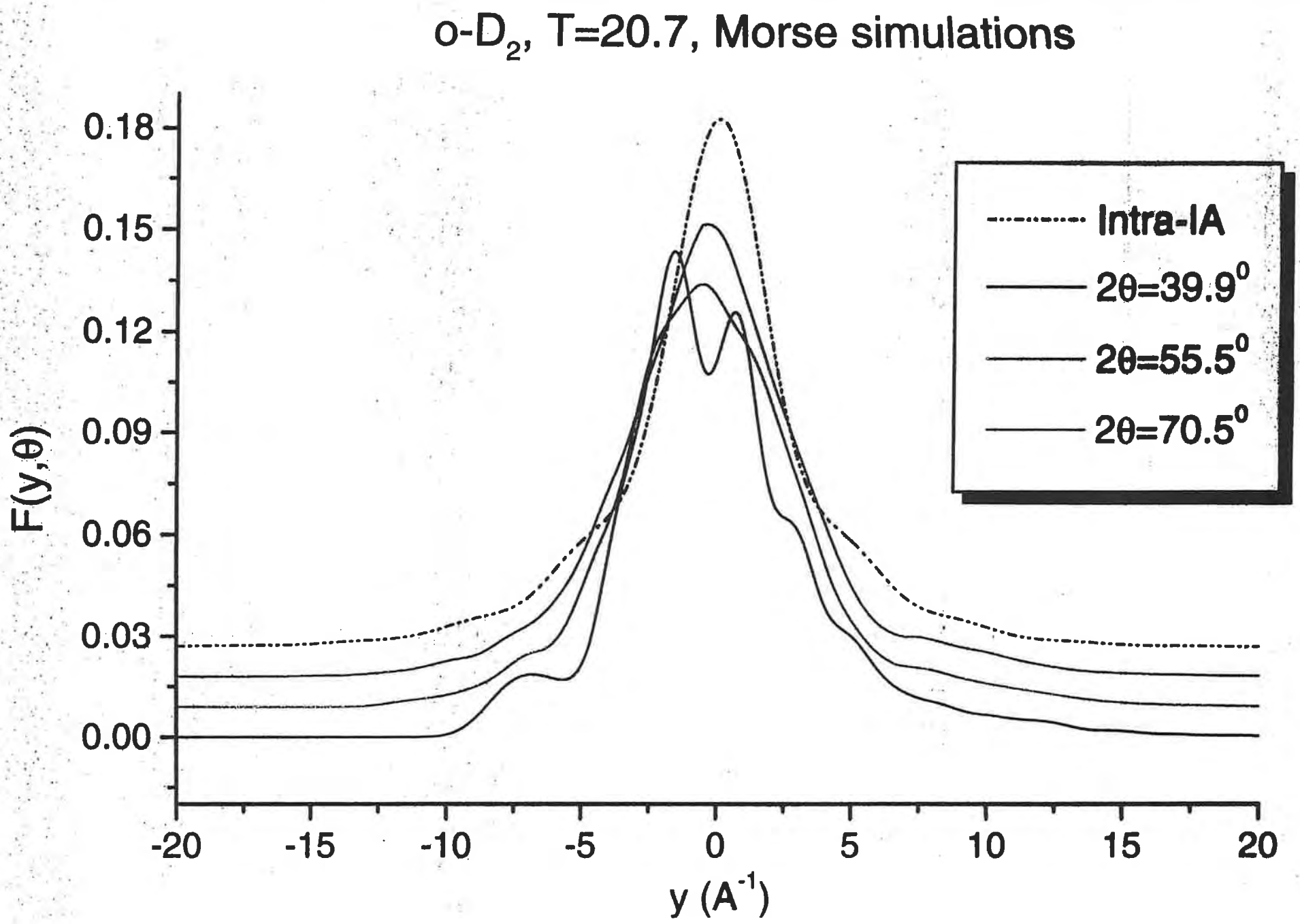
o-D2, T=20.7, Morse simulations
F(y,θ)
0.18
0.15
0.12
0.09
0.06
0.03
0.00
-20
-15
-10
-5
0
5
10
15
20
y (A-1)
Intra-IA
2θ=39.9°
2θ=55.5°
2θ=70.5°

- **Conclusions**

In DINS from condensed H_2/D_2 :

1. The internal, one-body, dynamics plays the most relevant role (little information on CM motion).

2. This INT dynamics is strongly un-harmonic and centrifugally distorted within the eVS (Q-ω) range.

3. Owing to the core of the H-H (or D-D) potential, the Intra-IA regime is not fully reached within the eVS (Q-ω) range.

Data analysis

An illustrated Bayesian view, with eVS data

D. S. Sivia
CLRC, ISIS Facility

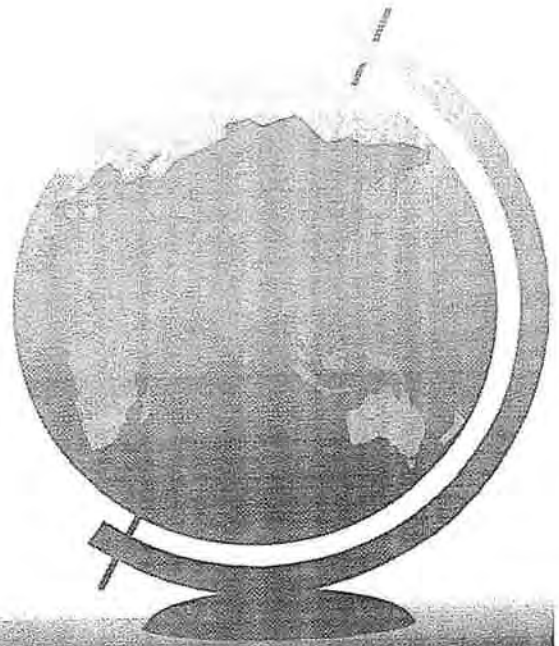

A Bayesian view

Bernoulli (1713), Bayes (1763) and Laplace (1812)

— *developed probability theory to reason in situations of uncertainty.*

- A probability encodes a state of knowledge.
- All probabilities are conditional.

"Data analysis is simply a dialogue with the data" (Gull, 1994)

What's the question?

Want prob(Peak-width | Data, I), but what is I?

Must define I, the relevent background information and assumptions, for an unambiguous question to be posed

— *different questions have different answers!*

More information

Data analysis is simply a dialogue with the data !

http://www.isis.rl.ac.uk/dataanalysis/dss.htm

Data Analysis: a Bayesian tutorial, Sivia (1996), OUP

http://bayes.wustl.edu/sivia/Sivia.html

Dealing with "outliers"

"Counts"

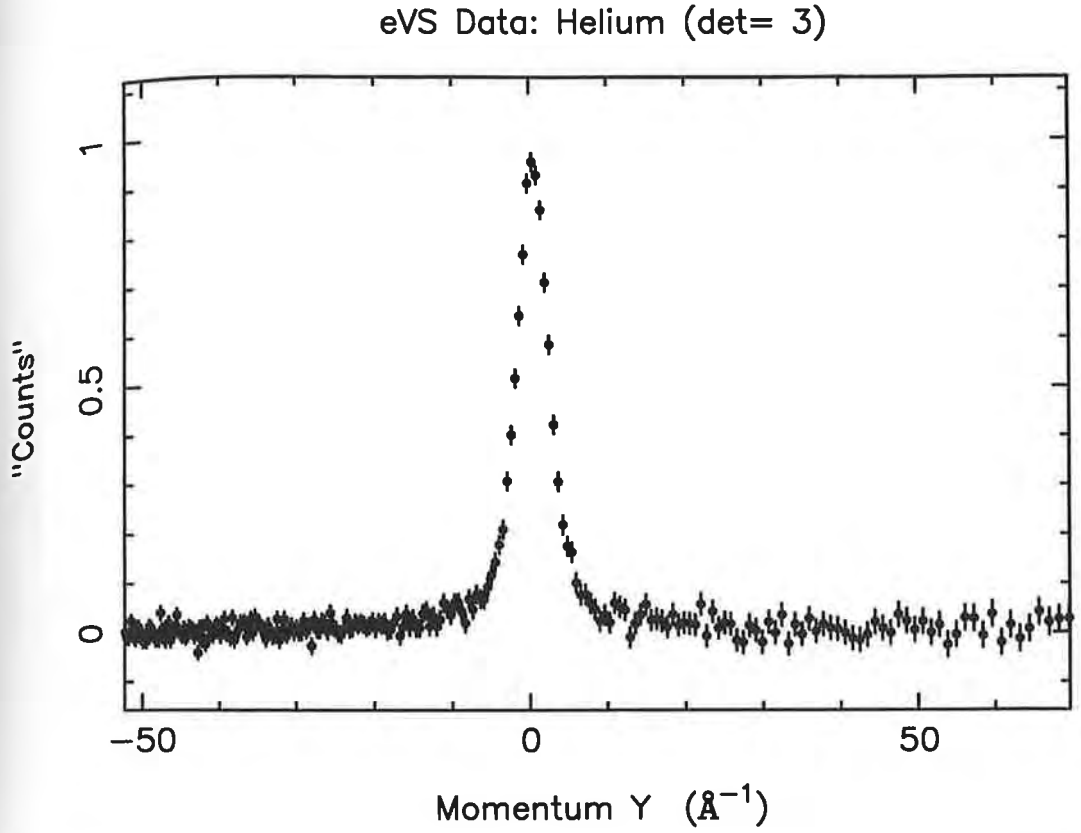
eVS Data: Helium (det= 3)
"Counts"
0
0.5
1
−50
0
50
Momentum Y (Å^{-1})

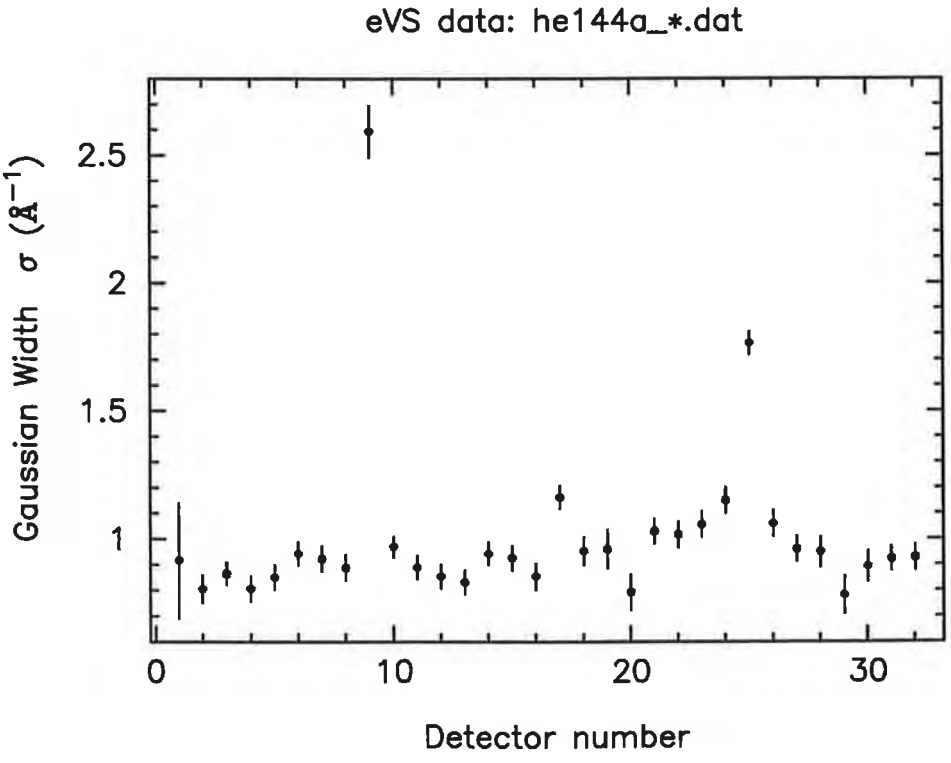
eVS data: he144a_*.dat
Gaussian Width σ (Å^{-1})
1
1.5
2
2.5
0
10
20
30
Detector number

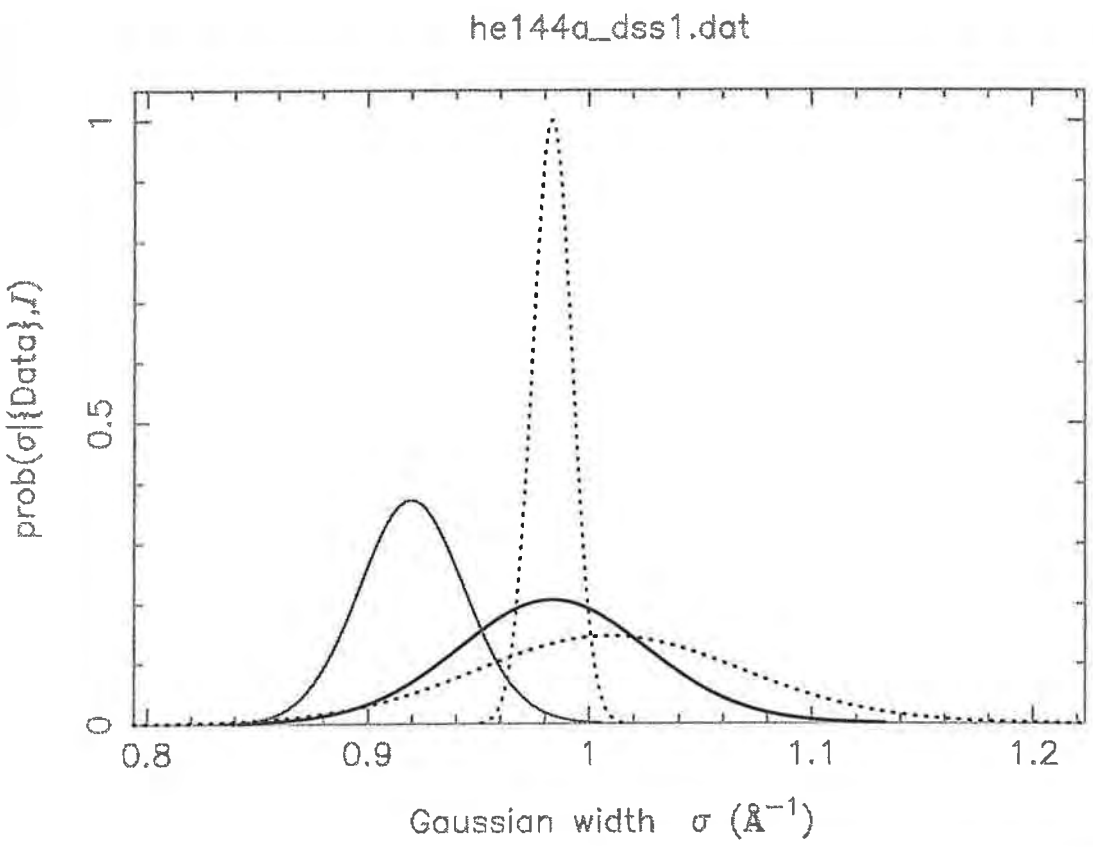
he144a_dss1.dat
prob(σ|{Data},I)
0
0.5
1
0.8
0.9
1
1.1
1.2
Gaussian width σ (Å^{-1})

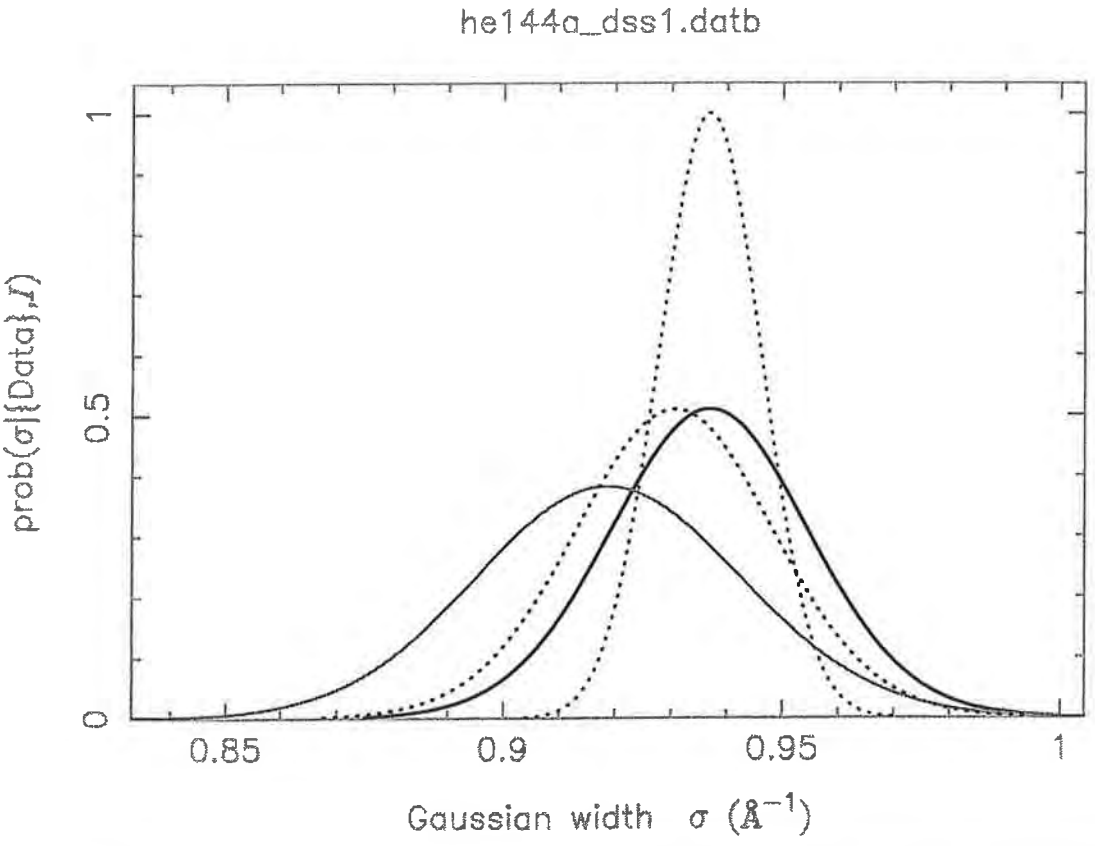
he144a_dss1.datb
prob(σ|{Data},I)
0
0.5
1
0.85
0.9
0.95
1
Gaussian width σ (Å^{-1})

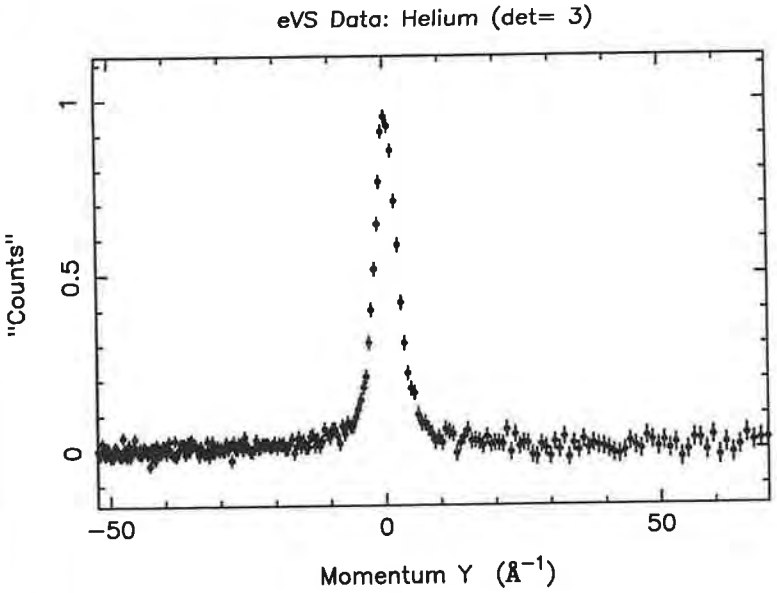
eVS Data: Helium (det= 3)
"Counts"
0
0.5
1
−50
0
50
Momentum Y (Å^{-1})

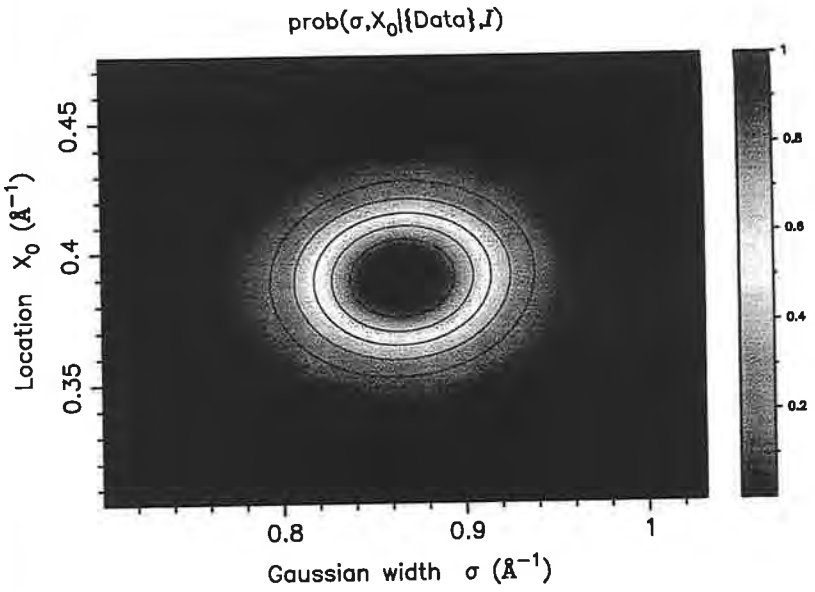
prob(σ,X$_0$|{Data},I)
Location X$_0$ (Å^{-1})
0.35
0.4
0.45
0.8
0.9
1
Gaussian width σ (Å^{-1})
0.2
0.4
0.6
0.8
1

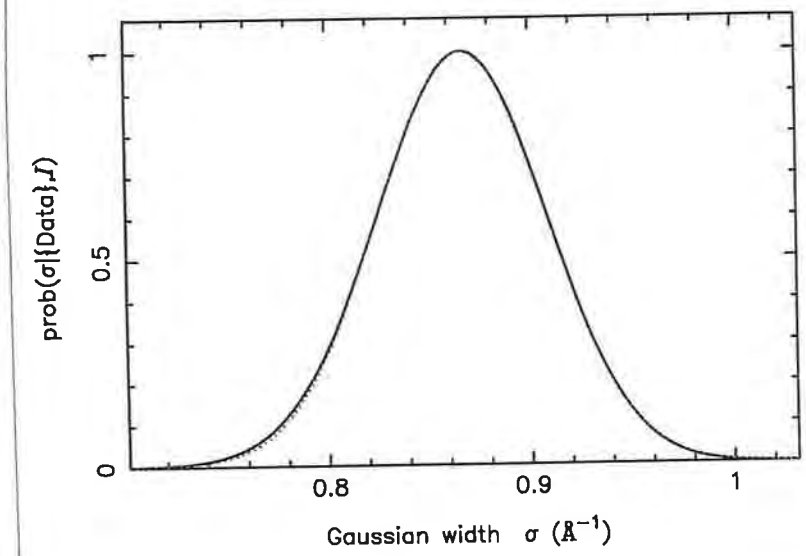
prob(σ|{Data},I)
0
0.5
1
0.8
0.9
1
Gaussian width σ (Å^{-1})

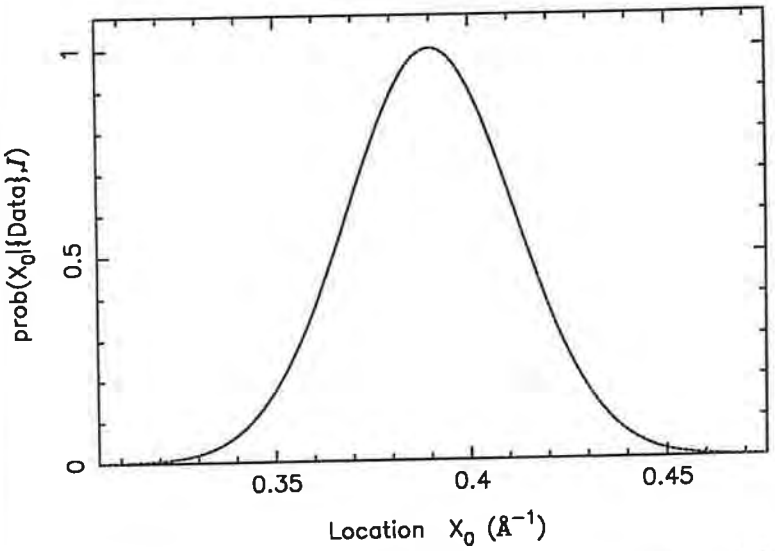
prob(X$_0$|{Data},I)
0
0.5
1
0.35
0.4
0.45
Location X$_0$ (Å^{-1})

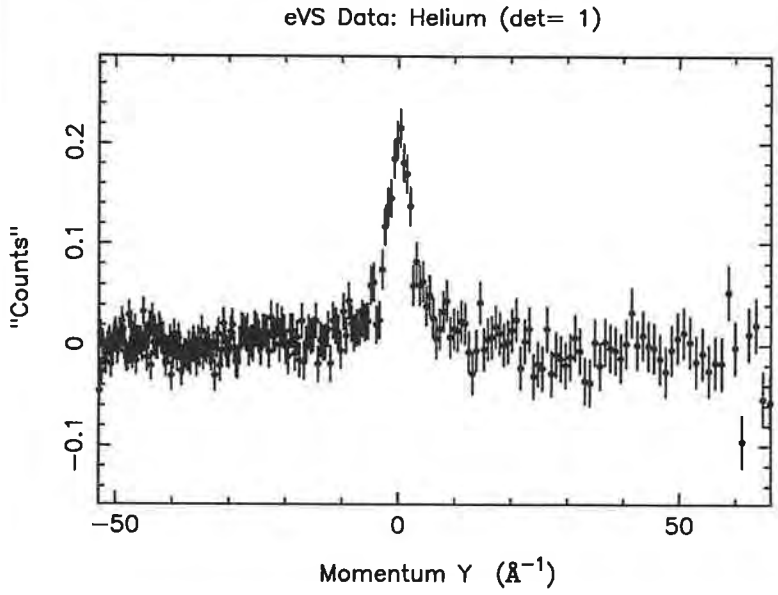
eVS Data: Helium (det= 1)
"Counts"
0.2
0.1
0
−0.1
−50
0
50
Momentum Y (Å^{-1})

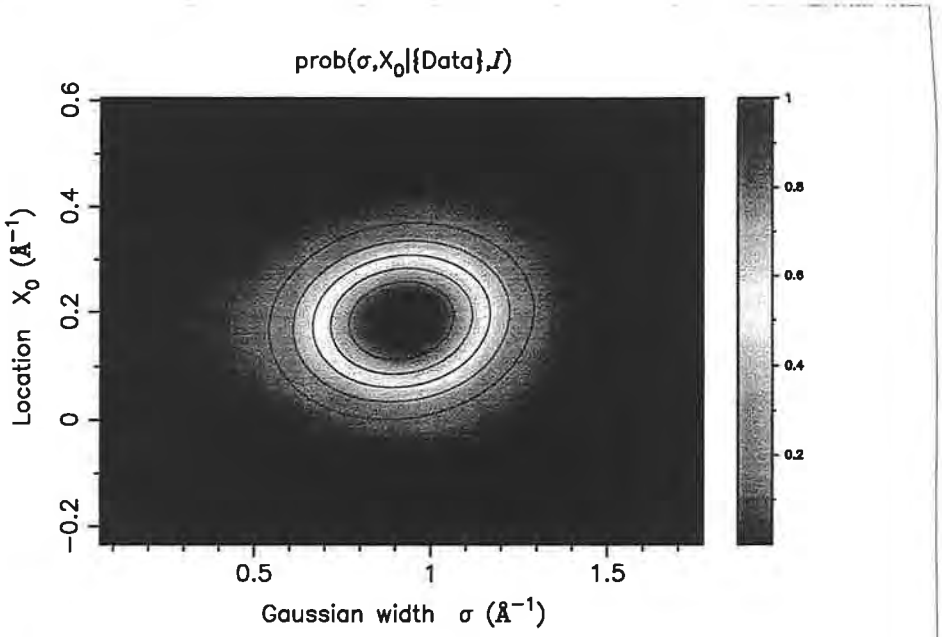
prob(σ,X$_0$|{Data},I)
Location X$_0$ (Å^{-1})
0.6
0.4
0.2
0
−0.2
0.5
1
1.5
Gaussian width σ (Å^{-1})
1
0.8
0.6
0.4
0.2

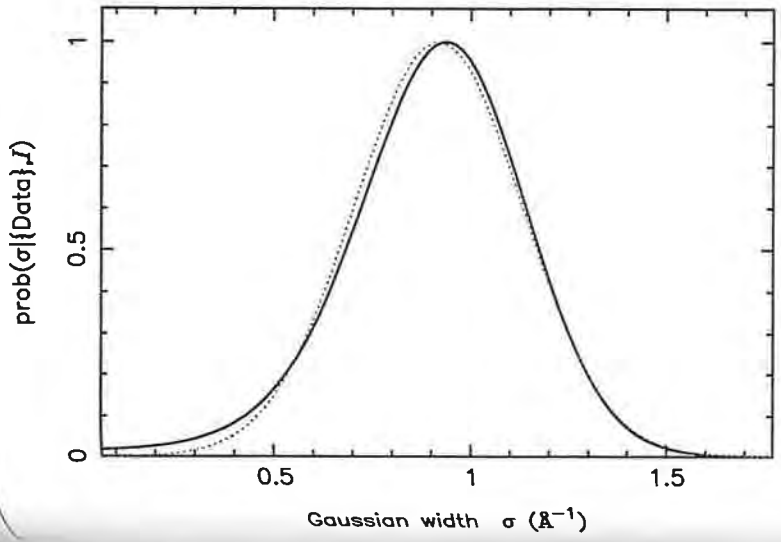
prob(σ|{Data},I)
1
0.5
0
0.5
1
1.5
Gaussian width σ (Å^{-1})

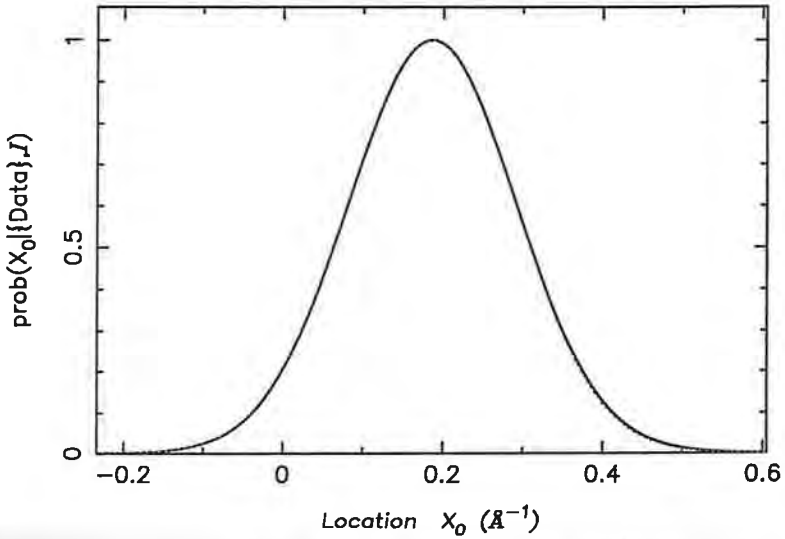
prob(X$_0$|{Data},I)
1
0.5
0
−0.2
0
0.2
0.4
0.6
Location X$_0$ (Å^{-1})

eVS Data: Helium (det= 3)

Gaussian width σ ($\AA^{-1}$)

Location X_0 ($\AA^{-1}$)

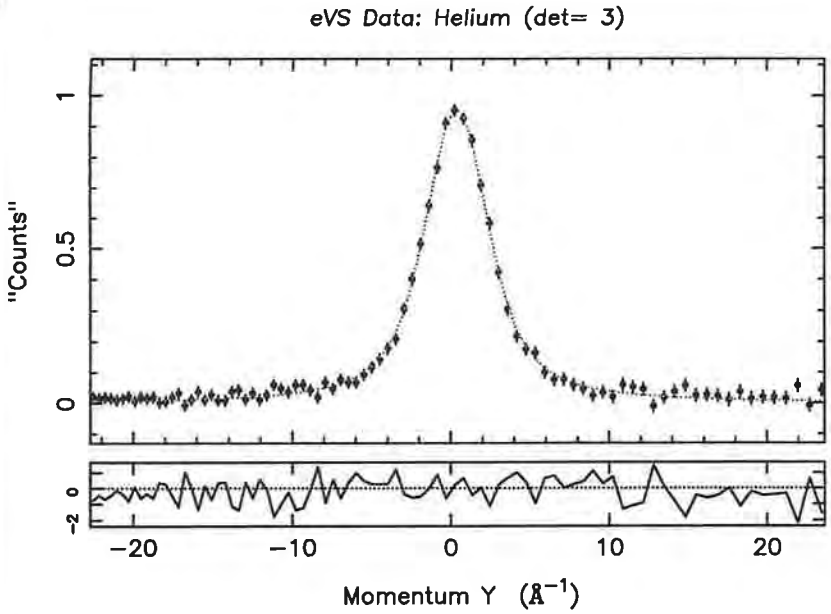

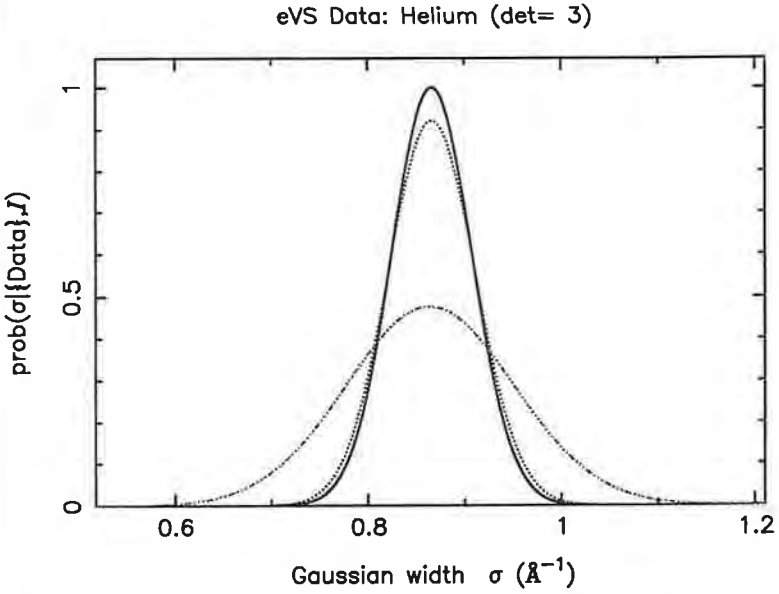

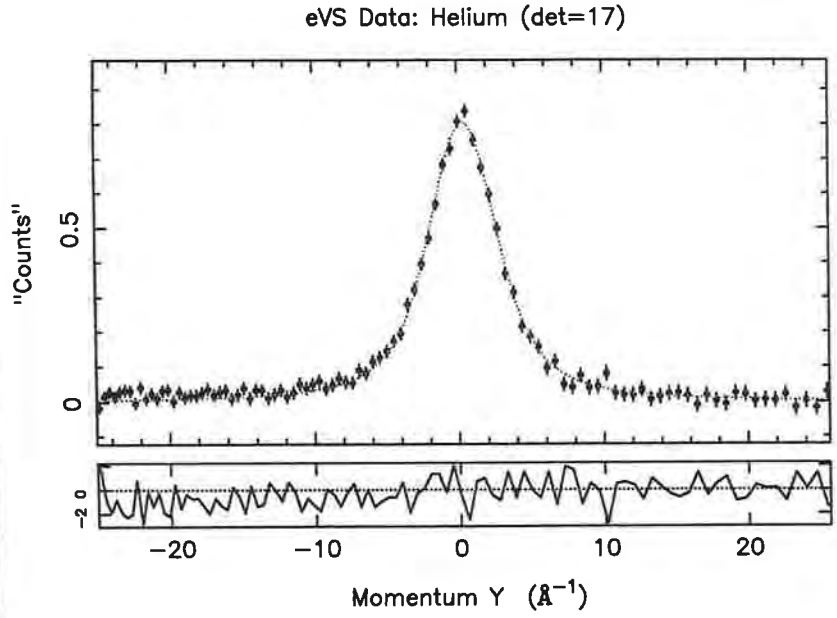

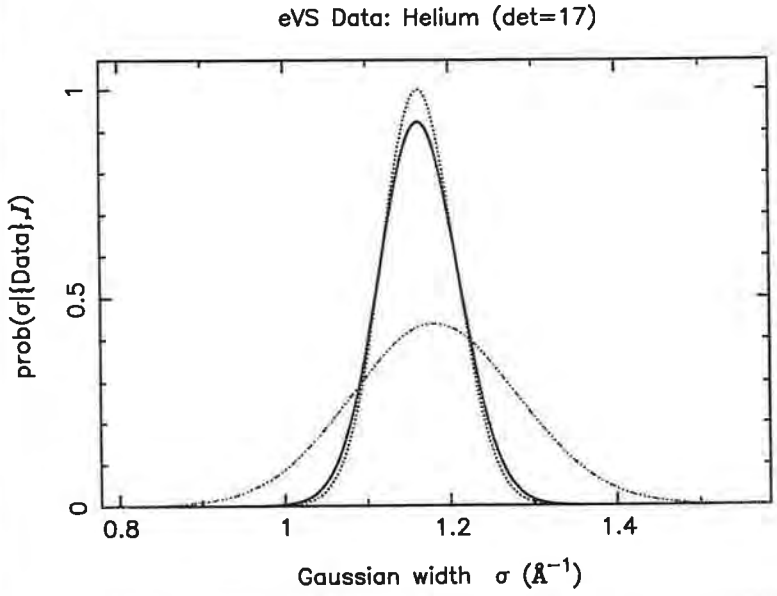

Resolution = Voigt

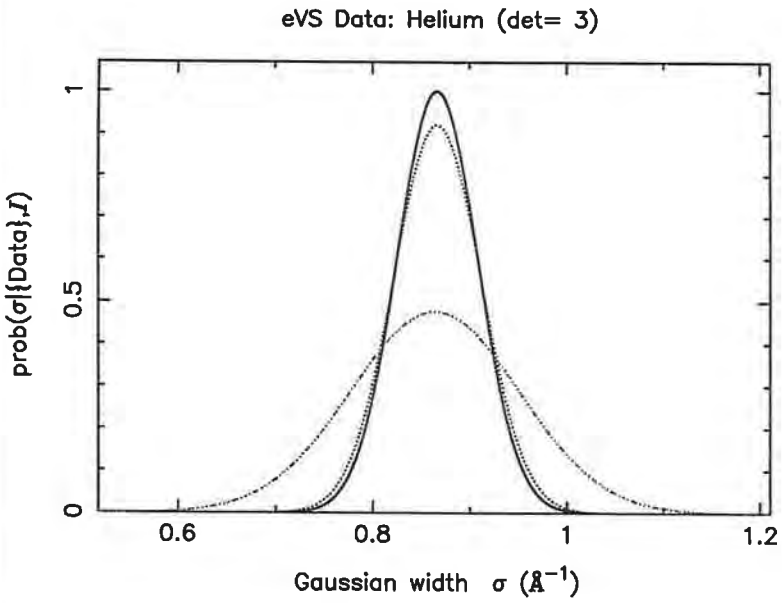

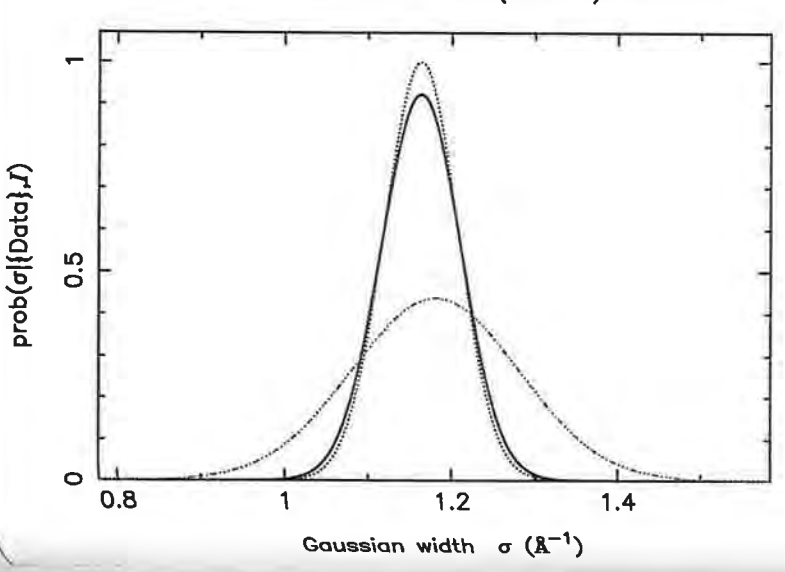

Resolution = Voight, with ±5% error on parameters

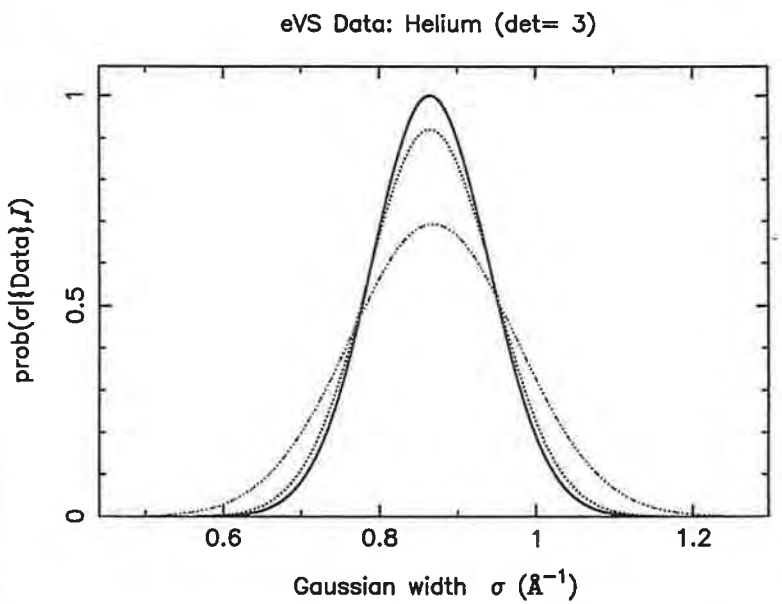

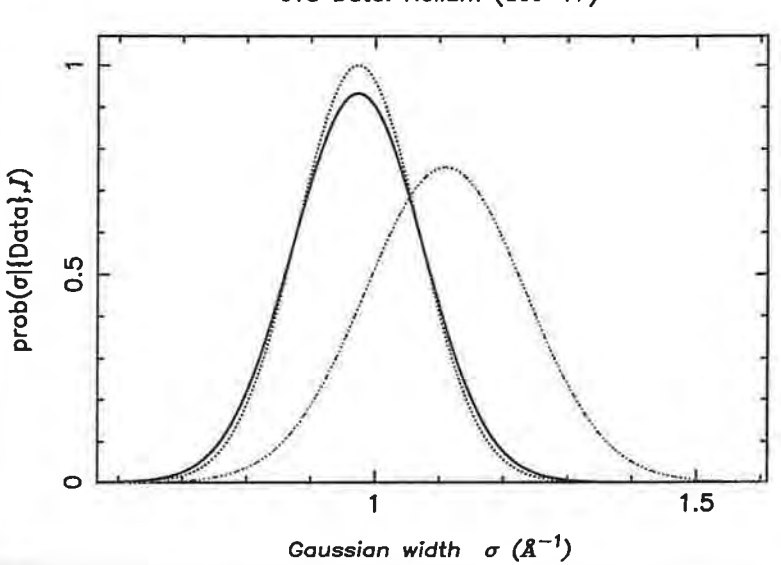

Gaussian width σ ($\AA^{-1}$)

Gaussian width σ ($\AA^{-1}$)

ISIS

Calibration of the electron Volt Spectrometer

Andrew Fielding

Department of Physics, University of Liverpool.

Calibration of the electron Volt Spectrometer

Andrew Fielding

Department of Physics, University of Liverpool.

ISIS

Overview

1. Calibration of flight paths and scattering angles
2. Calibration of resolution function
3. Energy calibration
4. Energy resolution calibration
5. eVS measurements - ZrH_2, ^4He, Sn

electron Volt Spectrometer

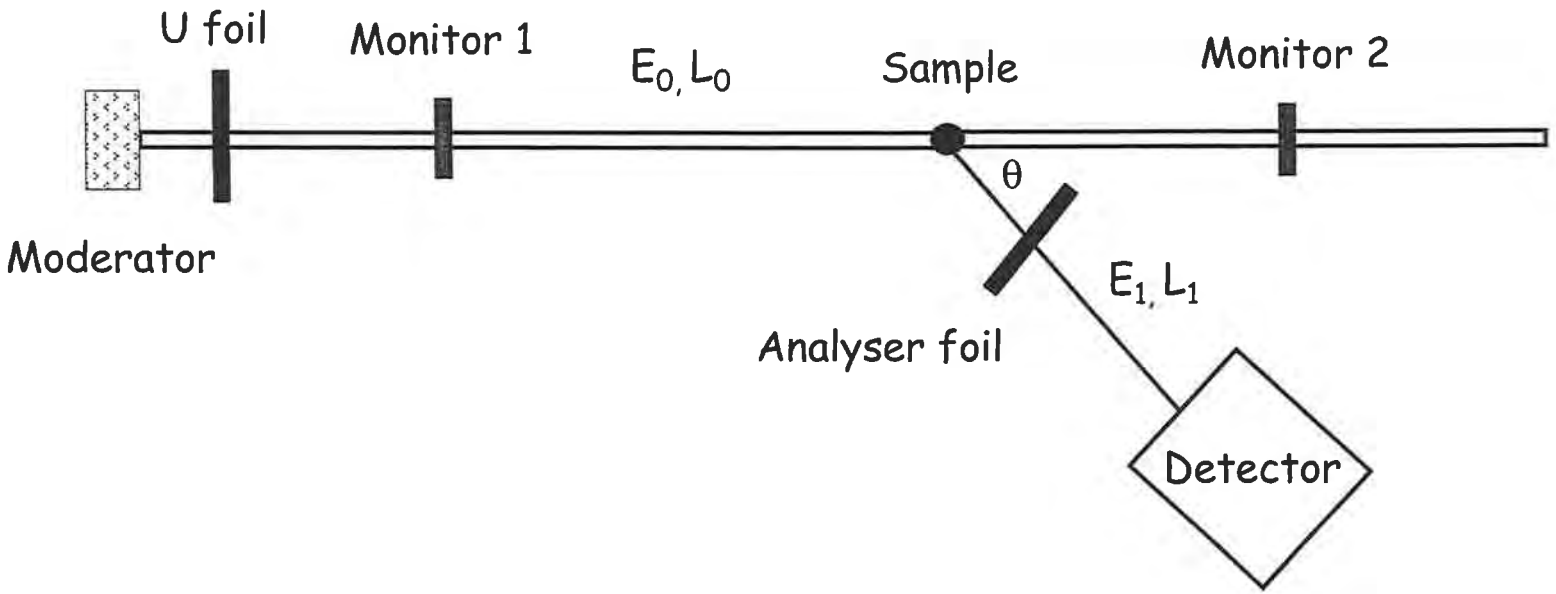

ISIS

ISIS

Calibration runs

- 2 runs performed

  U foil in the incident beam

  Pb calibration run

- Pb used for calibration

  Narrow momentum distribution (resolution dominates)

  Large mass of Pb atoms (~ elastic scattering)

  Low T_{debye} therefore classical E_K.

Flight path and angle calibration 1

Length calibration

Pb recoil scattering > 5eV : IA valid

$$\frac{v_1}{v_0} = R(\theta) = \frac{\cos\theta + \sqrt{(M/m)^2 - \sin^2\theta}}{(M/m)+1}$$

0.99 (θ=180°) < R(θ) > 1 (θ=0°)

$$t = \left(\frac{L_0 + L_1}{R(\theta)}\right)\frac{1}{v_0} + t_0$$

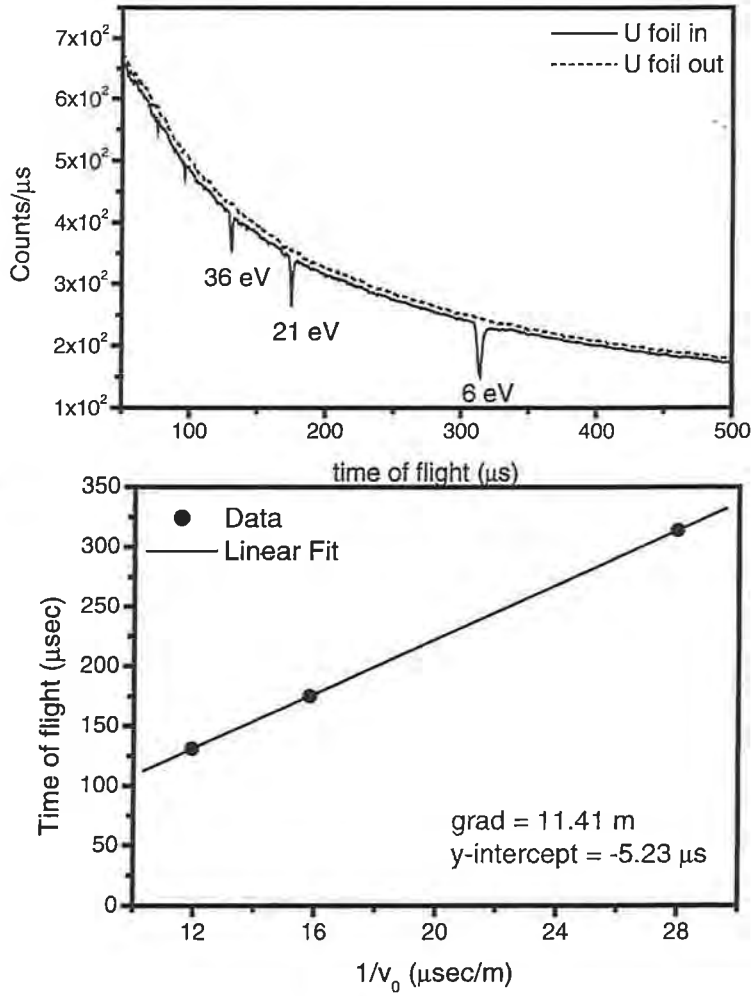

ISIS

Flight path and angle calibration 2

Bragg scattering

$$2d\sin\left(\frac{\theta}{2}\right)=\frac{n\hbar(t-t_0)}{m(L_0+L_1)}$$

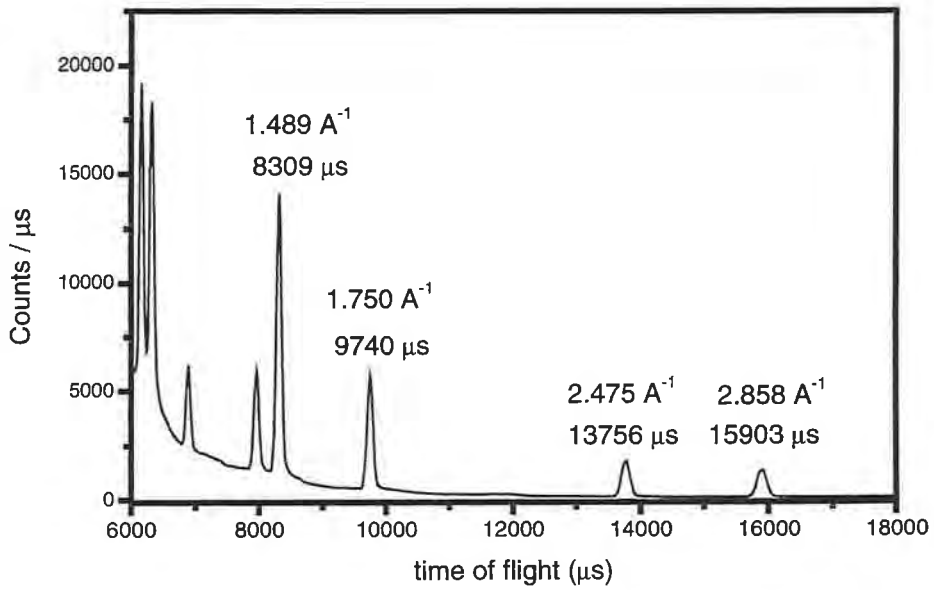

L

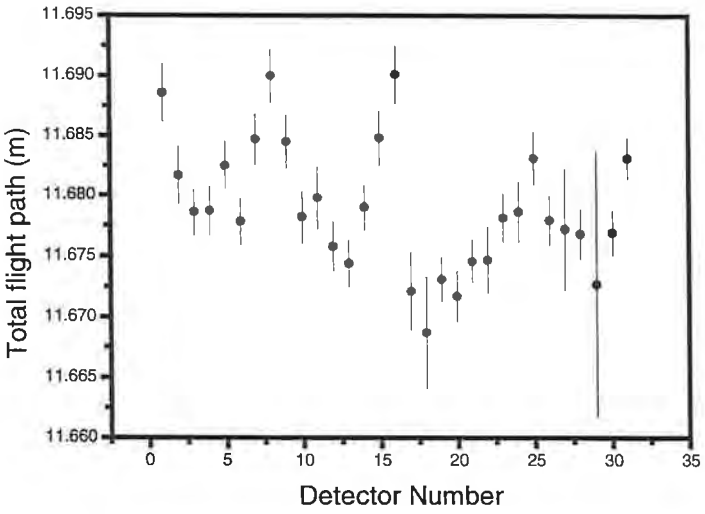
Total flight path (m)
11.695
11.690
11.685
11.680
11.675
11.670
11.665
11.660
0
5
10
15
20
25
30
35
Detector Number

t_0

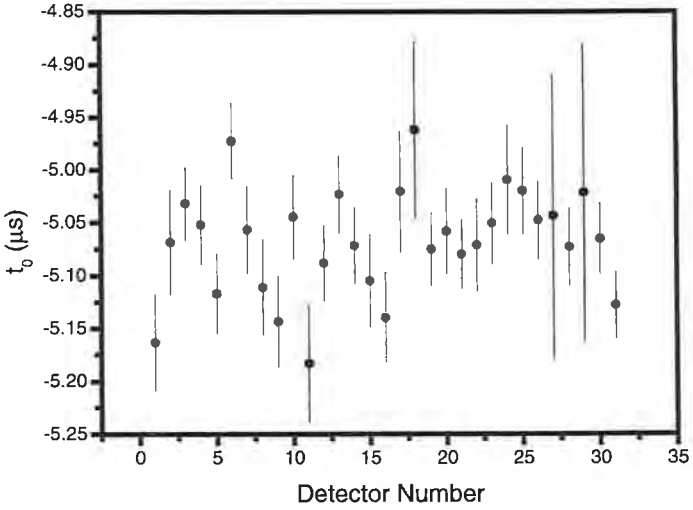
t_0 (μs)
-4.85
-4.90
-4.95
-5.00
-5.05
-5.10
-5.15
-5.20
-5.25
0
5
10
15
20
25
30
35
Detector Number

θ

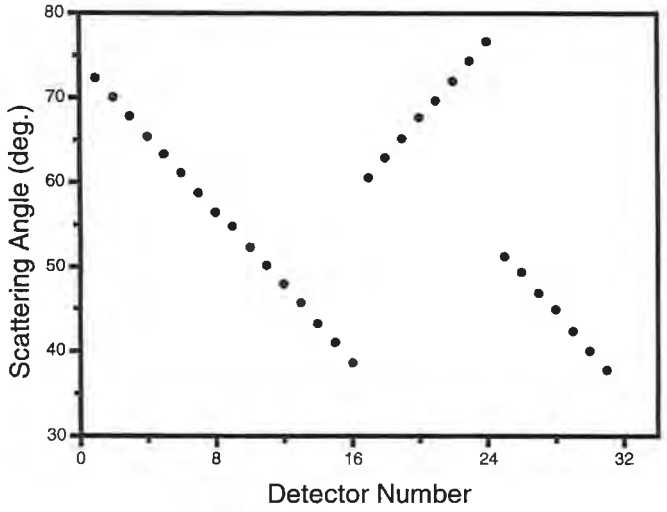
Scattering Angle (deg.)
80
70
60
50
40
30
0
8
16
24
32
Detector Number

Flight path and angle calibration 3

IP file

1	80.37120	-4.933419	11.05500	0.5797424
2	77.81760	-4.990836	11.05500	0.5783758
3	75.37700	-5.079510	11.05500	0.5795956
4	73.00400	-5.059198	11.05500	0.5791397
5	70.58200	-5.018191	11.05500	0.5732632
6	68.15860	-5.041014	11.05500	0.5782194
7	65.47750	-5.022477	11.05500	0.5789948
8	63.31930	-5.084239	11.05500	0.5837145
9	44.96050	-4.986458	11.05500	0.5738516
10	42.53810	-5.061194	11.05500	0.5697479
11	40.08190	-5.025412	11.05500	0.5645161
12	37.72390	-5.142959	11.05500	0.5685692
13	35.16310	-5.146472	11.05500	0.5684748
14	32.77440	-5.102875	11.05500	0.5661402
15	30.24410	-5.103216	11.05500	0.5680590
16	85.24810	-5.163209	11.05500	0.5980330
17	48.96270	-5.028796	11.05500	0.5988731
18	44.33560	-4.975801	11.05500	0.5772915
19	46.67050	-4.936397	11.05500	0.5891523
20	41.99750	-4.980521	11.05500	0.5801535
21	39.51330	-5.028459	11.05500	0.5800648
22	37.17790	-5.027584	11.05500	0.5768938
23	34.56990	-5.089212	11.05500	0.5820255
24	32.14390	-4.973400	11.05500	0.5744314
25	54.31170	-5.114817	11.05500	0.6061554
26	56.66620	-5.092596	11.05500	0.6075516
27	59.09530	-5.019924	11.05500	0.6033144
28	61.36500	-5.059965	11.05500	0.6059666
29	63.69470	-5.059031	11.05500	0.6100922
30	66.09250	-5.031414	11.05500	0.6088848
31	68.47270	-5.032735	11.05500	0.6158543
32	70.65400	-5.050249	11.05500	0.6245413
33	0.0000000E+00	-4.440600	11.05500	-2.4605
34	0.0000000E+00	-4.562700	11.05500	2.389000

Instrument Resolution

Contributions

Angle $\Delta\theta$

Incident flight path ΔL_0

Final flight path ΔL_1

time Δt_0

Energy ΔE_1

ISIS

Flight path and time resolution 1

- Transmission measurements with U foil in incident beam

Width of absorption 'dip' in tof

$$\sigma^2_{total} = \underbrace{\frac{\Delta L^2}{v_1^2}}_{\text{Flight path uncertainty}} + \underbrace{\frac{L^2}{v_1^2}\frac{\Delta E_1^2}{4E_1^2}}_{\text{Intrinsic energy width of U foil absorption resonance}} + \underbrace{\Delta t_0^2}_{\text{Time uncertainty}}$$

Flight path and time resolution 2

$\Delta L_0 \Rightarrow$ monitor detectors

$(\Delta L_0 + \Delta L_1) \Rightarrow$ scintillator detectors

	ΔL_0 (cm)	Δt_0 (μs)
Monitor 1	1.75 ± 0.21	0.30 ± 0.03
Monitor 2	2.16 ± 0.20	0.26 ± 0.03

Detectors	ΔL (cm)	Δt_0 (μs)
1-8	3.02 (0.07)	0.28 (0.02)
9-16	2.89 (0.09)	0.26 (0.01)
17-24	2.93 (0.11)	0.27 (0.03)
25-32	2.71 (0.11)	0.33 (0.04)
1-32	2.90 (0.05)	0.28 (0.01

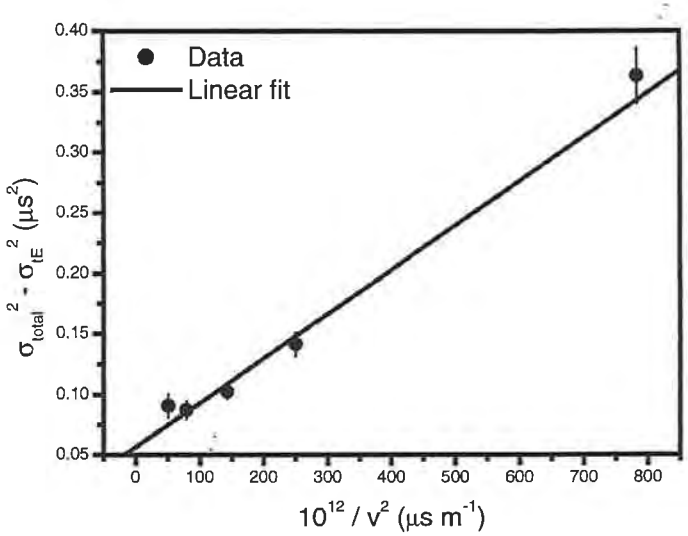

$$\Delta L_1^2 = \Delta L^2 - \Delta L_0^2$$

$$\Delta L_1 \sim 1.8 \text{ cm}$$

Angular resolution

Monte-Carlo calculation
of angular distribution

$w = 2L_1\Delta\theta$ effective detector width

w ~ 2.0 cm

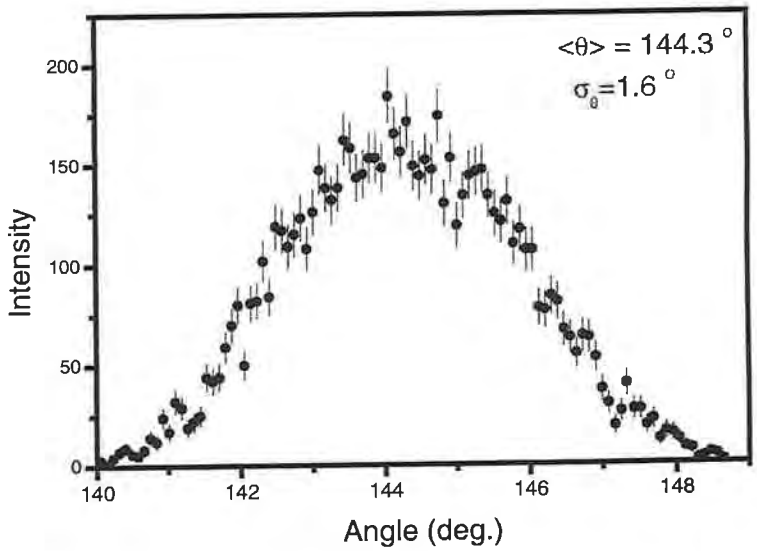

Energy calibration 1

- Analyse the recoil scattering from Pb sample
- U foils - fit Gaussian
- Au foils - fit Voigt

- Calculate RMS momentum for Pb using $3/2k_BT$. Fix width J(y)
- Fix all other resolution widths
- Fit peak position
- Fit the width of E_1 contribution

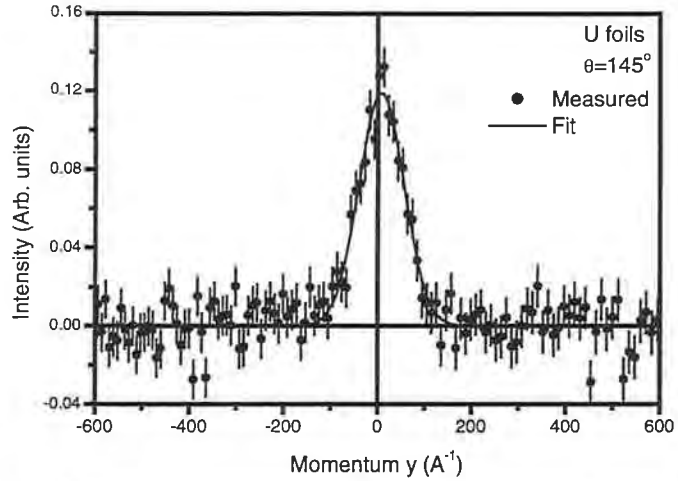

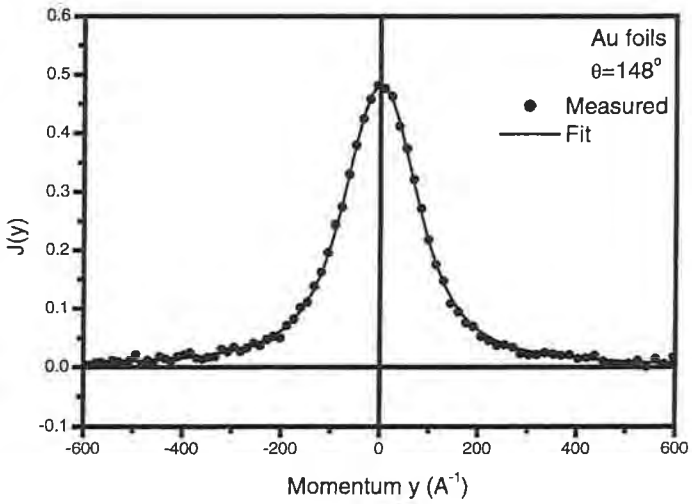

ISIS

Energy calibration 2

Calibrated energies and widths

Detectors	E_1 (meV)	ΔE_1 (meV)
1 - 8	4908.09 (2.05)	131.18 (1.91)
9 - 16	4909.55 (2.36)	136.18 (3.12)
17 - 24	4908.1 (2.84)	133.36 (6.95)
25 - 32	4909.93 (2.65)	136.93 (3.17)
1 - 32	4908.94 (2.47)	134.33 (4.67)

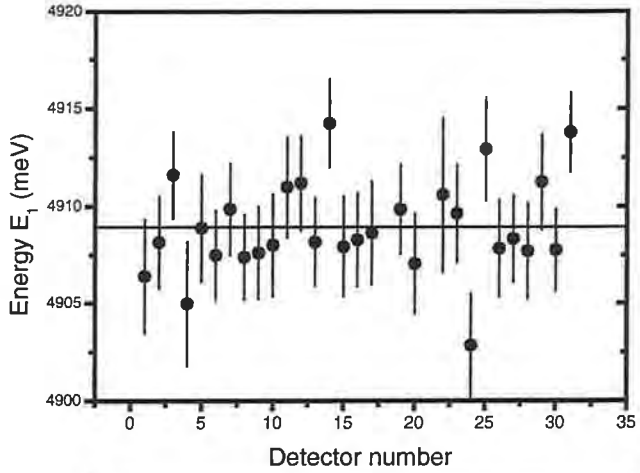

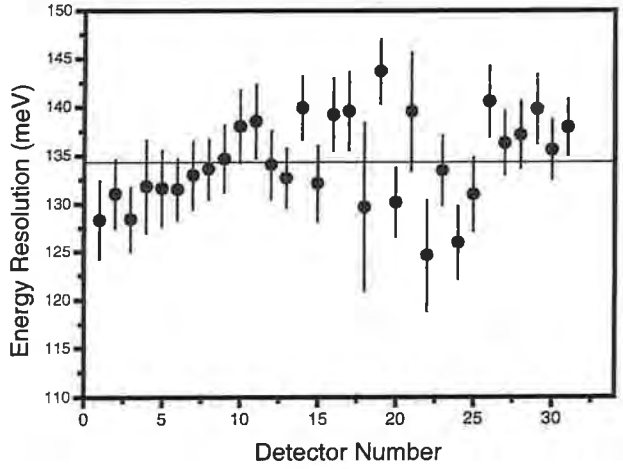

Examples of eVS measurements 1

ZrH_2

Resolution

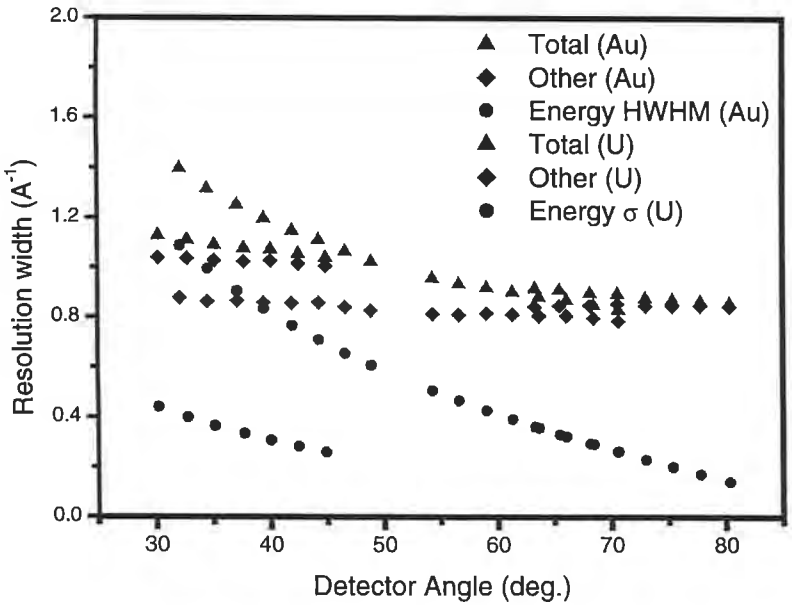

Fitted RMS momentum

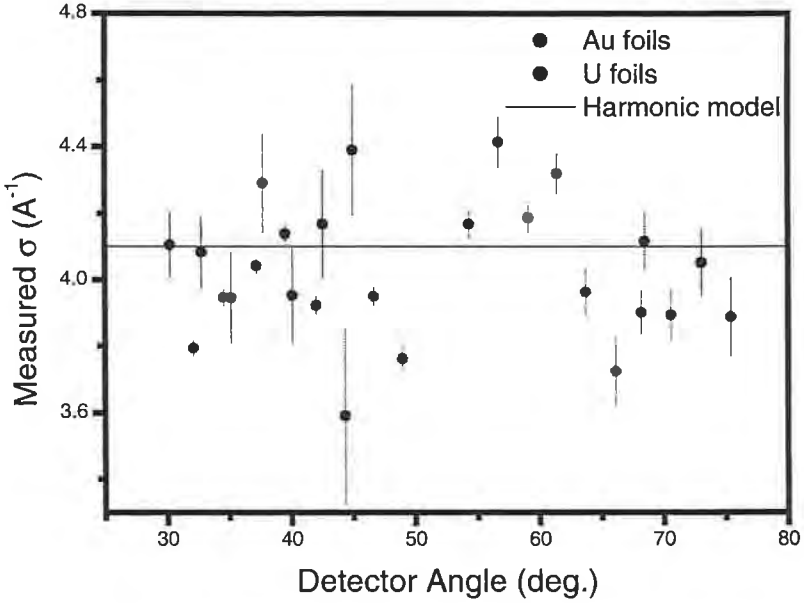

ISIS

Examples of eVS measurements 2

^{4}He

Resolution

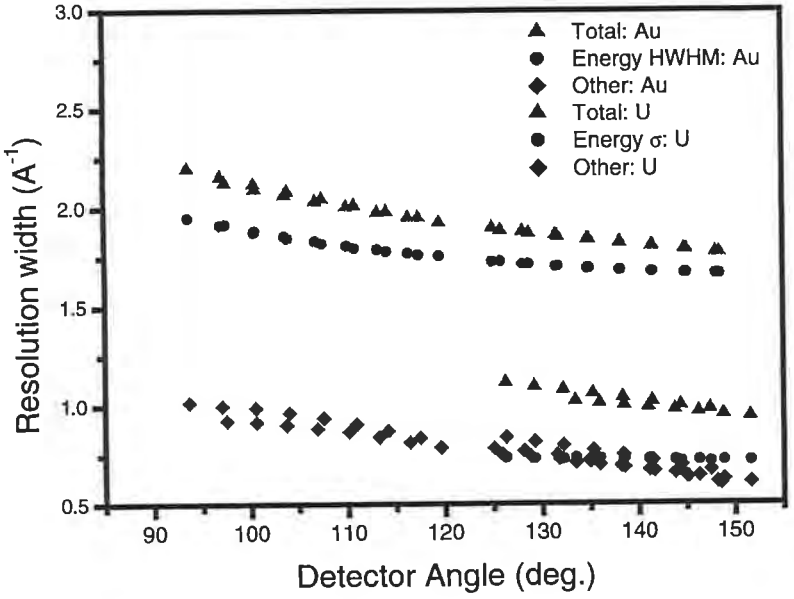

Fitted RMS momentum

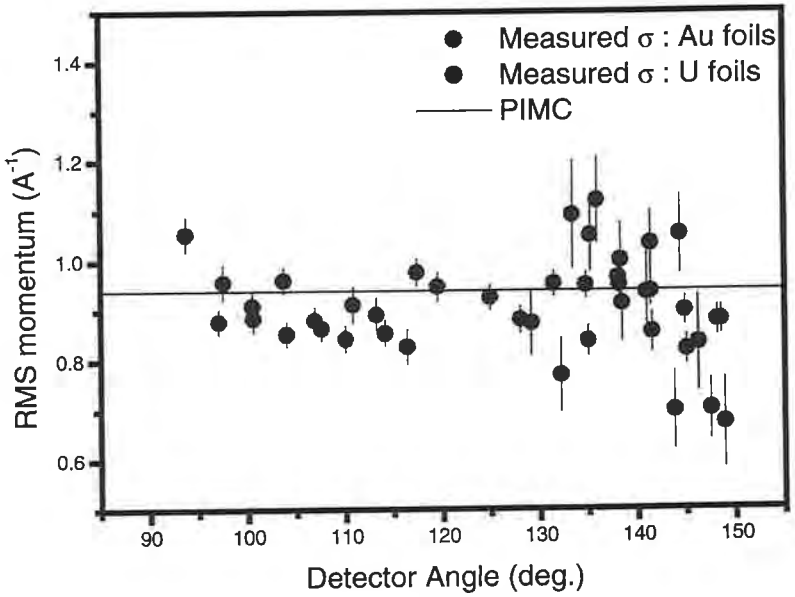

Examples of eVS measurements 3

Sn

Resolution

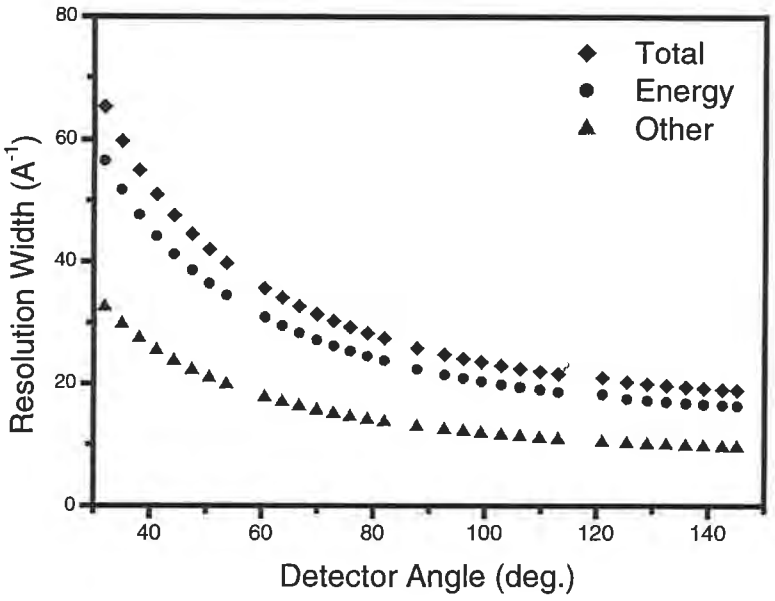

Fitted RMS momentum

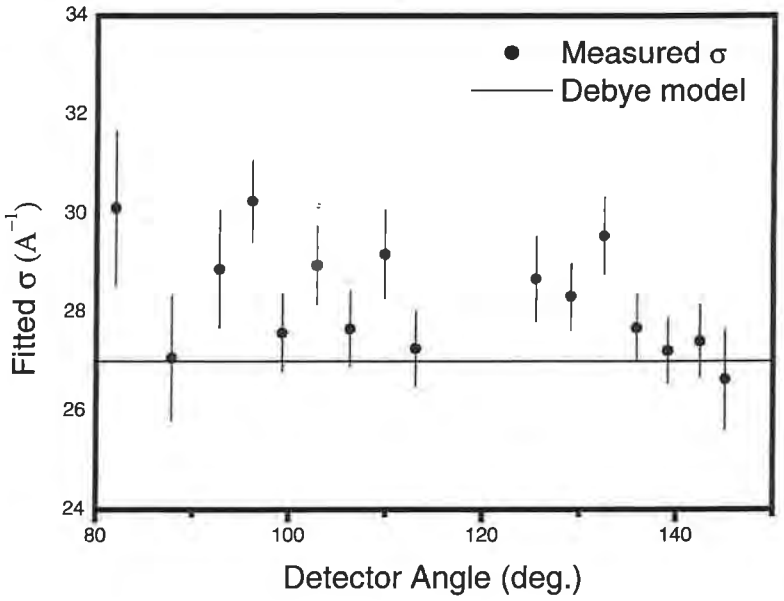

ISIS

ISIS

Summary

- Shown the calibration procedures used on eVS
- Shown how they allow successful measurements on a wide range of systems including hydrogen, the quantum fluid ^{4}He and the heavy mass of Sn

Detectors for VESUVIO

November 26^{th} 1999

*Roberto Senesi**, A.L Fielding, J. Mayers, M. Moxon, N. J. Rhodes, E. Schooneveld

*INFM Roma Tor Vergata - Rome

- Overview of neutron scintillation detectors
- Lithium glass detectors for VESUVIO
- Tests performed
- Future tests and improvements

Desired properties of neutron detectors:

- efficiency near 100%
- low gamma sensitivity
- prompt response

The best compromise for the eV range TOF neutron scattering is represented by scintillators.

Neutron-induced reactions used in scintillation detection, (all *charged particle out* type reactions):

a) $^{6}Li +^{1} n \Rightarrow^{3} H +^{4} \alpha \qquad Q - val = 4.78\, MeV$

with $E_{H} = 2.73 MeV$ and $E_{\alpha} = 2.05 MeV$

b) $^{10}B +^{1} n \Rightarrow \begin{cases} ^{7}Li +^{4} \alpha & Q - val = 2.792\, MeV \\ ^{7}Li^{*} +^{4} \alpha & Q - val = 2.310\, \mathrm{MeV} \end{cases}$

which, in the lower branch case leads to

$E_{Li^*} = 0.84\,MeV$ and $E_\alpha = 1.47\,MeV$

Scintillators based on $^6Li(n,\alpha)$ ***reaction***

cross section at 5 eV$\simeq 10^2 b$

- two choices for activation phosphor materials:

1. ZnS slower response-opaque binder-small thickness ($\sim$ 1mm)

2. Ce^{3+} faster response-transparent glass matrix-increased thickness

multiple step neutron detection mechanism for cerium activated lithium glasses:

The two charged particles produced in the reaction a) liberate ion pairs trough ionization energy loss along their tracks in the glass.

The maximum electron energies created by these particles are $\simeq$ 1keV for the α and $\simeq$ 2keV for the triton,

the triton having the higher ionization volume and being the principal responsible to the luminescence excitation.

These electrons will migrate outwards from the columnar ionization zone, and are widely scattered.

The secondary electrons created migrate through the glass and some will excite the Ce^{3+}centers to produce luminescence.

This luminescence is charachterised by an emission band centered around 400 nm, broadened by the varying energy environments in the glass host.

The 5d emitting state of cerium is split in many components depending on the site simmetry of the cerium, leading to a measured average decay time of 140 ns.

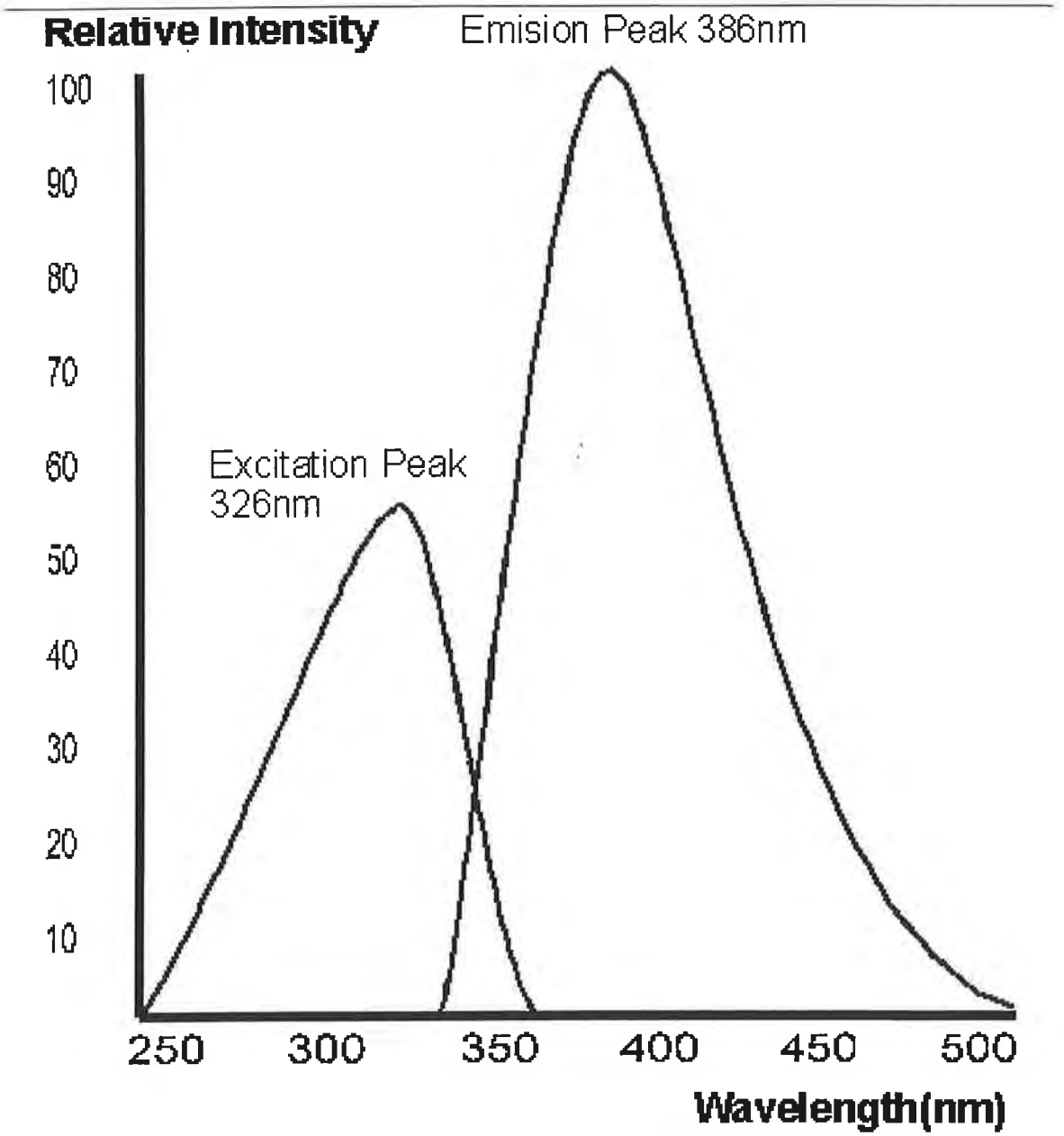

Figure 1: Excitation and emission spectra of Ce^{3+} in the scintillator glass. Luminescence decay time~ 140 ns. Negligible self-absorption.

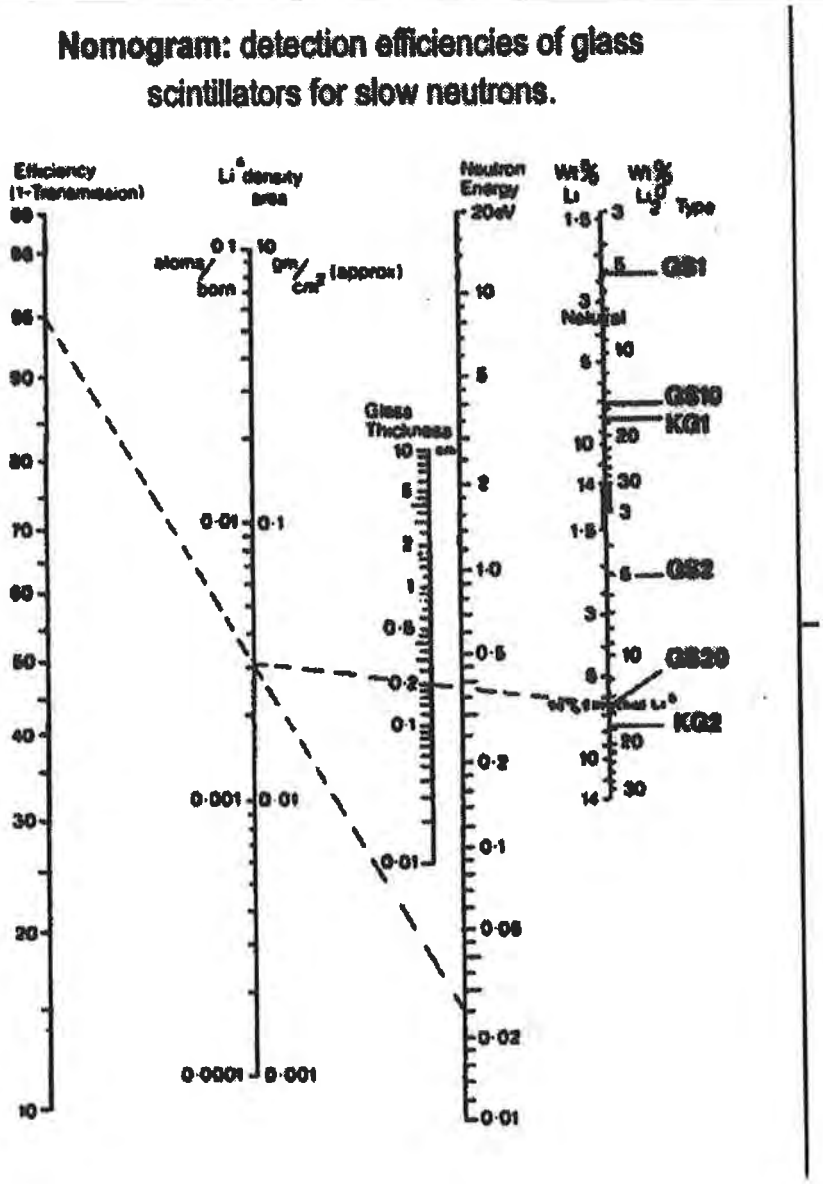

Figure 2: Detector efficiency (*1-transmission*).

Tests performed

1. Choice of thickness

2. gamma sensitivity

3. scintillator-photomultiplier optical coupling

▷ 1+2

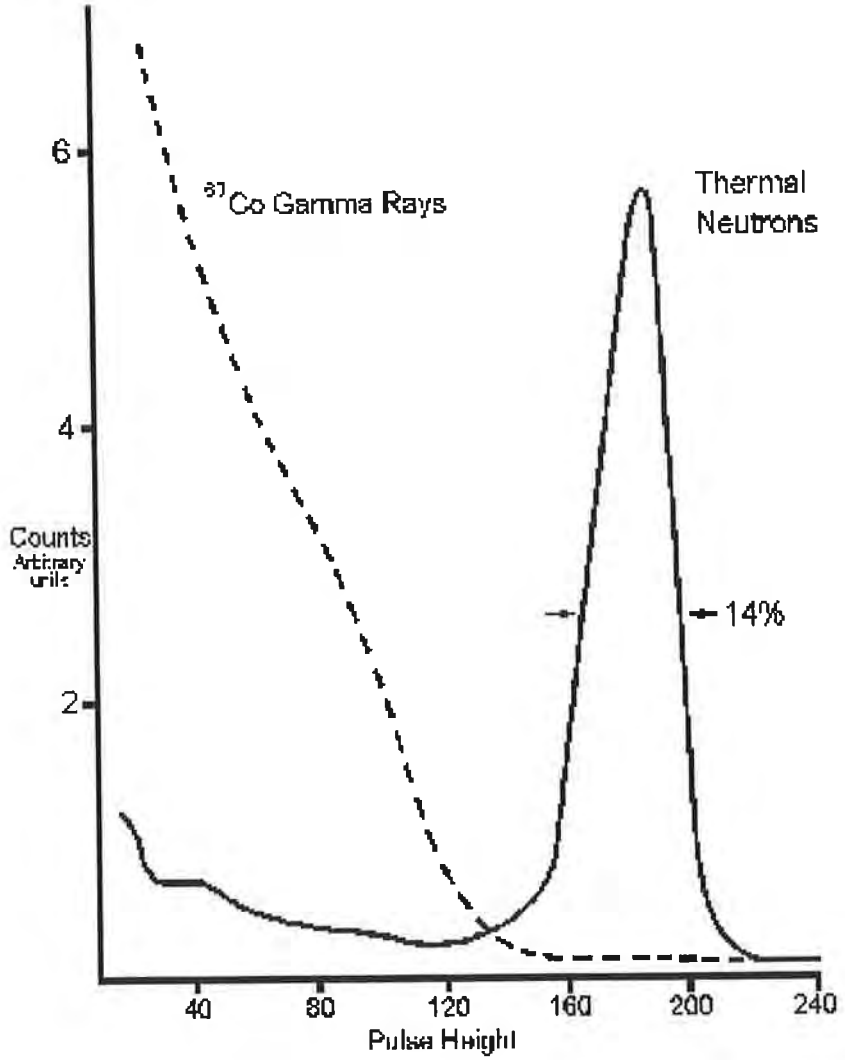

Figure 3: Pulse height responses (1mm glass) to thermal neutrons compared with ^{60}Co (1.17 and 1.33 MeV) gamma rays

Measurements using the scattering from a tin sample using currently available 2cm thick glasses:

several resonances for tin in the epithermal region leading to increased gamma sensitivity. Test for all resonating samples.

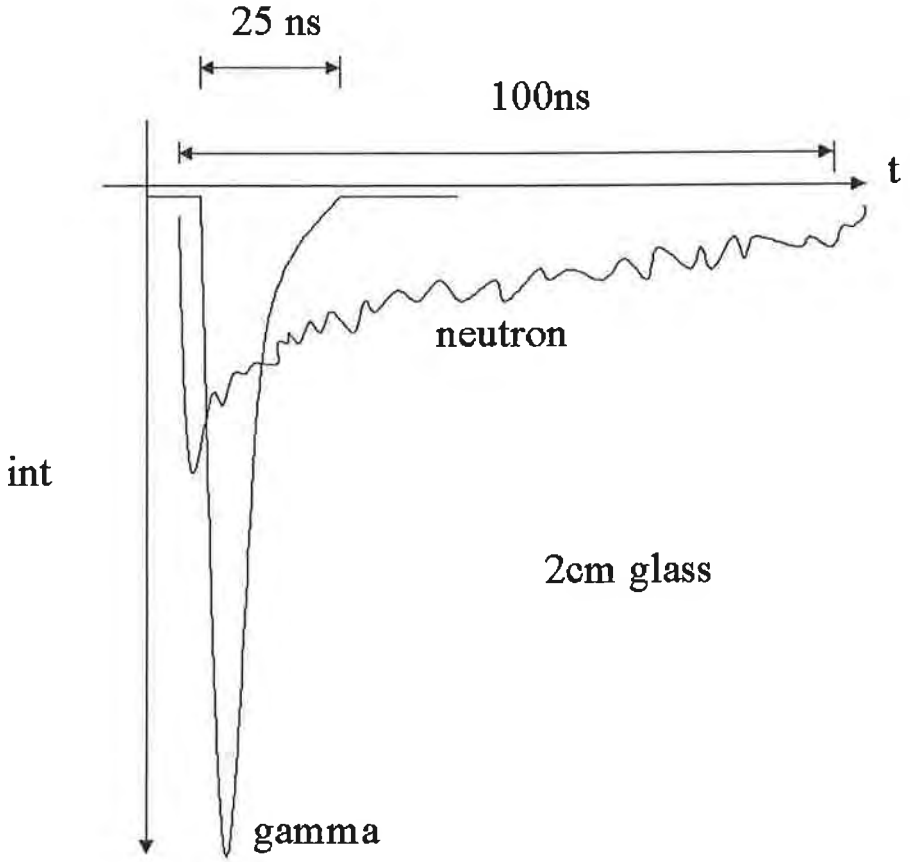

Figure 4: neutron and sample dependent (Sn) gamma pulses for a 2cm thick glass

⇒Reduce the glass thickness? Use window discrimination technique?

possible problems, already assessed in the literature,

of ^6Li leaching and inhomogeneities during glass cutting

Optical coupling

Objective: reduce and optimise the number of reflections to reach the photomultiplier window

-Ray tracing Monte Carlo simulation for different geometries (E. Schooneveld, N. Rhodes)

-Measurements with a laboratory source (E. Schooneveld, N. Rhodes)

two basic geometries: with final "light pipe" and without final "light pipe".

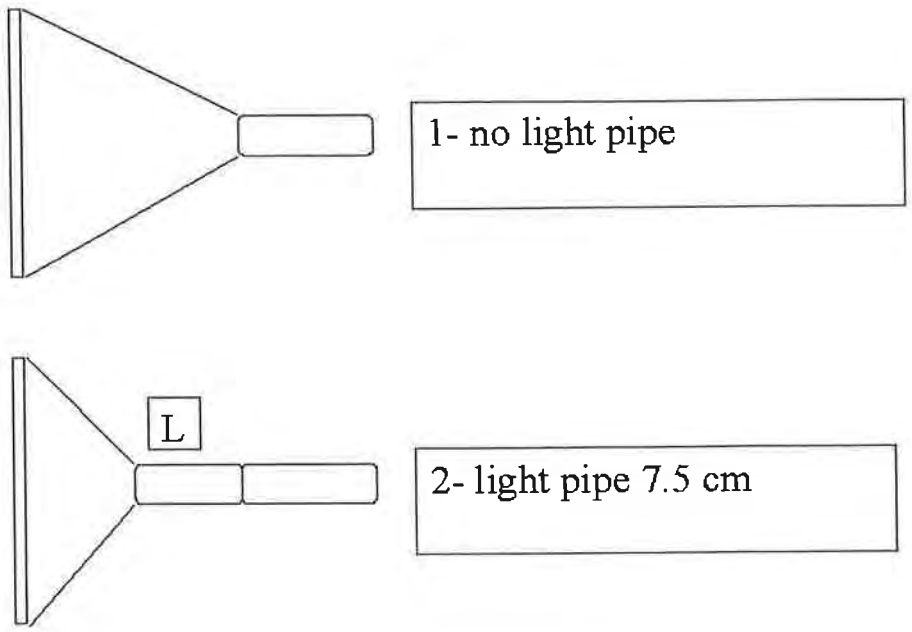

Figure 5: the two types of geometries investigated

The average number of reflection to reach the PMT tube is 50 for in type 1) geometry. The light pipe geometry allows to increase the light collection.

PH analysis on VESUVIO scinillators

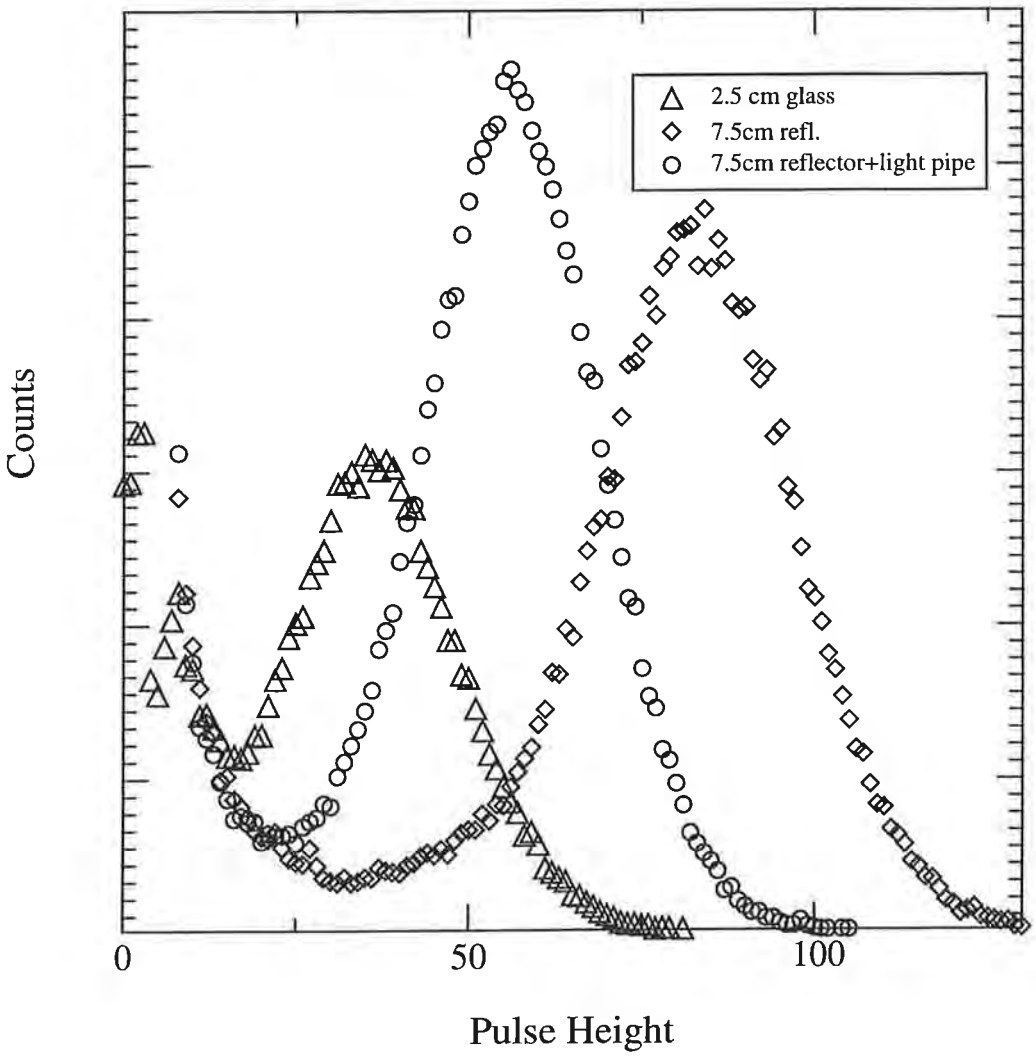

Another solution being currently investigated to prevent back reflection to the scintillator surface is to coat with a white scattering paint (magnesium oxide or aluminium oxide) to promote light to enter in the light pipe channel.

Future tests and proposed improvements

- Liquid ^{10}B scintillation module (already purchased)- gamma sensitivity ?

- Choice of Li glass thickness (thinner glass-larger area detector...). At 10 eV the comparison between 1cm and 2 cm glasses results in a reduction in count rate of $\simeq$ 25% and a factor of two for 1 MeV gamma rays

- Reduce the dead time by removing PMT amplification (down to <300 ns)

- Remove γ rays originated from the neutron source and its surroundings

Quantum effects on the THz dynamics of ^{4}He and ^{3}He probed by Inelastic X ray scattering

A. Cunsolo
I.N.F.M. Roma-Italy

measurements performed at
E.S.R.F.-Grenoble

- Introduction to IXS techniques and beamline layout
- The second moment in the classic and quantum cases
- The temperature dependence of IXS moments
- The ~~temperature~~ DENSITY dependence of IXS moments
- Conclusions

Inelastic X-ray Scattering Beamline (ID16-BL21) at the ESRF

Side view

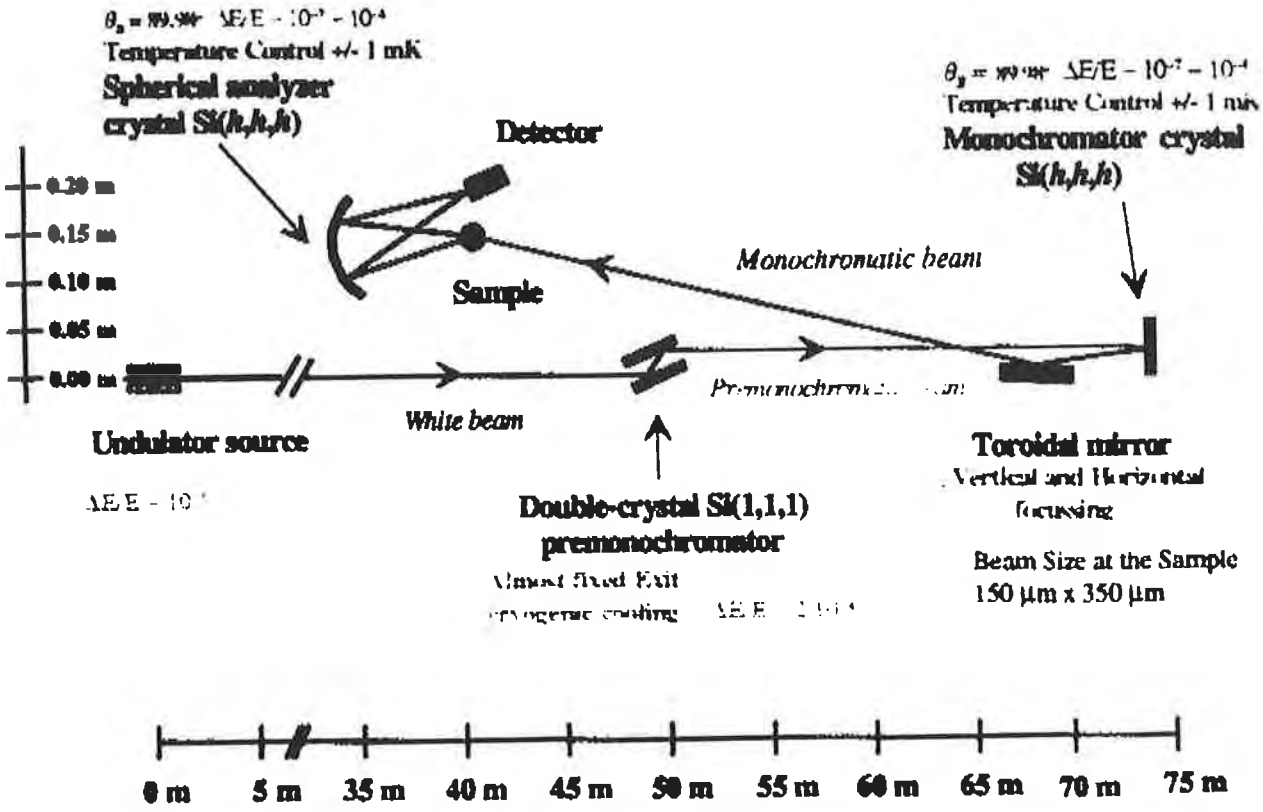

Monochromator performances for the most used Si(*h*,*h*,*h*) high order reflections

Reflections	Energy (*eV*)	Δ*E* (*meV*)	Δ*E*/*E*	Flux (*ph/s/200 mA*)
(7,7,7)	13840	5.0	$(3.6 \pm 0.3)\cdot10^{-7}$	$6\cdot10^{10}$
(9,9,9)	17793	1.84	$(1.0 \pm 0.08)\cdot10^{-7}$	$6\cdot10^{9}$
(11,11,11)	21748	0.78	$(3.6 \pm 0.3)\cdot10^{-8}$	$7\cdot10^{8}$
(13,13,13)	25702	0.51		

Inelastic X-Ray Scattering

- **X-ray** $\Rightarrow$ $$\frac{\partial^2\sigma}{\partial\Omega\partial\omega_1} = r_e^2 \left(\frac{\omega_1}{\omega_0}\right)(\varepsilon_0 \cdot \varepsilon_1)\left|f(Q)\right|^2 S(Q,\omega)$$

Advantages:

- **No kinematic limitations**
- **Coherent cross section** (isotope independent).
- **Very small source size** (extreme thermodynamical conditions).
- **Negligible multiple scattering.**

Disadvantages:

- **Very high energy resolution required** < 10 meV (i.e. $\frac{\Delta E}{E} = 10^{-7} \div 10^{-8}$), while preserving an high incident photon flux (> 10^6 photons/s)
- **Fast decay of the atomic form factor.**
- **Strong photoelectric absorption** (IXS more efficient with low Z materials).

The Impulse Approximation

$$\lim_{Q\to\infty} S(Q,\omega) = S_{IA}(Q,\omega) = \int dp\, n(p)\,\delta\left(\omega - \omega_R - \frac{\hbar p\cdot Q}{M}\right)$$

$$S_{IA}(Q,\omega) = \frac{M}{\hbar Q} J_{IA}(Q/Q, y)$$

$$J(y) = \frac{1}{\sqrt{2\pi\sigma}} exp\left(\frac{-y^2}{2\sigma^2}\right)$$

$$\langle E_K \rangle = \frac{3\hbar^2}{2M}\int_{-\infty}^{+\infty} y^2 J(y)\,dy$$

$$\langle E_K \rangle = \frac{3}{2}\frac{\hbar^2\sigma^2}{M}$$

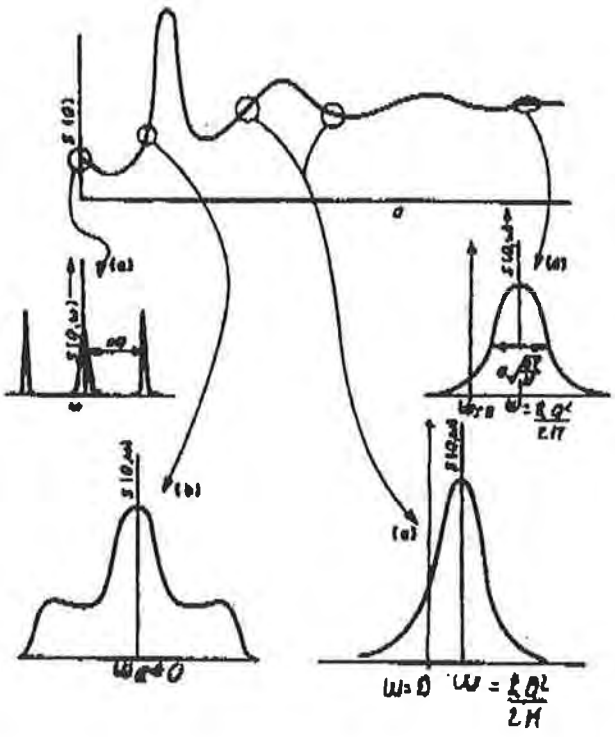

The followed thermodynamic paths

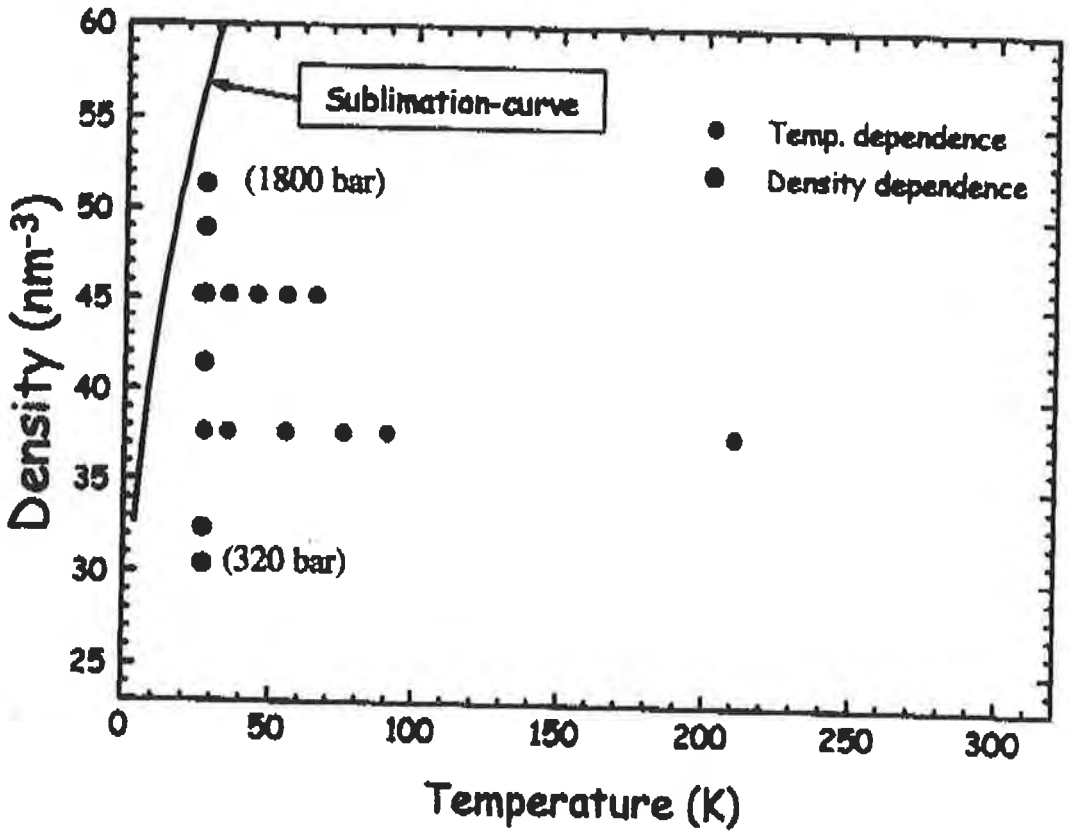

The second spectral moment of a classic fluid:

$$\langle\omega^2(Q)\rangle = \langle\omega^2(Q)\rangle_S + \langle\omega^2(Q)\rangle_D = \int_{-\infty}^{\infty}\omega^2 S(Q,\omega)d\omega = \ddot{F}(Q,t)\Big|_{t=0} = \frac{1}{N}\langle\dot{\rho}^*(Q,0)\dot{\rho}(Q,0)\rangle =$$

$$= \frac{1}{N}\sum_{i,j}\langle(\mathbf{Q}\cdot\mathbf{v}_i)(\mathbf{Q}\cdot\mathbf{v}_i)\exp(\mathbf{Q}\cdot\mathbf{r}_{ij})\rangle = \frac{1}{N}\sum_{\alpha,\beta}\sum_{i,j}Q_\alpha Q_\beta\langle(v_{i\alpha}v_{j\alpha})\rangle = \frac{1}{N}\sum_{i}\langle(\mathbf{Q}\cdot\mathbf{v}_i)^2\rangle =$$

$$= \frac{3K_BT}{2M}Q^2$$

.....and that of a quantum one:

$$\langle\omega^2(Q)\rangle = \langle\omega^2(Q)\rangle_S + \langle\omega^2(Q)\rangle_D$$

$$\Downarrow$$

$$\hbar^2\langle\omega^2(Q)\rangle_S = (\hbar^2Q^2/(2M))^2 + \hbar^2Q^2\frac{1}{N}\sum_j\langle(1/m)(\hat{Q}\cdot\hat{\mathbf{p}}_j)^2\rangle$$

$$\hbar^2\langle\omega^2(Q)\rangle_D = (\hbar^2Q^2/(2M))^2\frac{1}{N}\sum_{\substack{ij\\ i\neq j}}\langle\exp(-i\mathbf{Q}\cdot r_{ij})\rangle$$

$$+\hbar^2Q^2/(2M^2)\frac{1}{N}\sum_{\substack{ij\\ i\neq j}}\langle[\hat{Q}\cdot\hat{\mathbf{p}}_i\hat{Q}\cdot\hat{\mathbf{p}}_j\exp(-i\mathbf{Q}\cdot r_{ij})]_+\rangle$$

$$= (\hbar^2Q^2/(2M))^2\frac{1}{N}\sum_{\substack{ij\\ i\neq j}}\langle\cos\mathbf{Q}\cdot r_{ij}\rangle \quad \text{S(Q)-1}$$

$$+\hbar^2Q^2/(2M^2)\frac{1}{N}\sum_{\substack{ij\\ i\neq j}}\langle[\hat{Q}\cdot\hat{\mathbf{p}}_i\hat{Q}\cdot\hat{\mathbf{p}}_j\cos\mathbf{Q}\cdot r_{ij}]_+\rangle$$

$[\omega^2+\Gamma_L^2(Q,T)]^2$ $[\Omega_L^2(Q,T)-\omega^2)^2+\Gamma_L^2(Q,T)]$

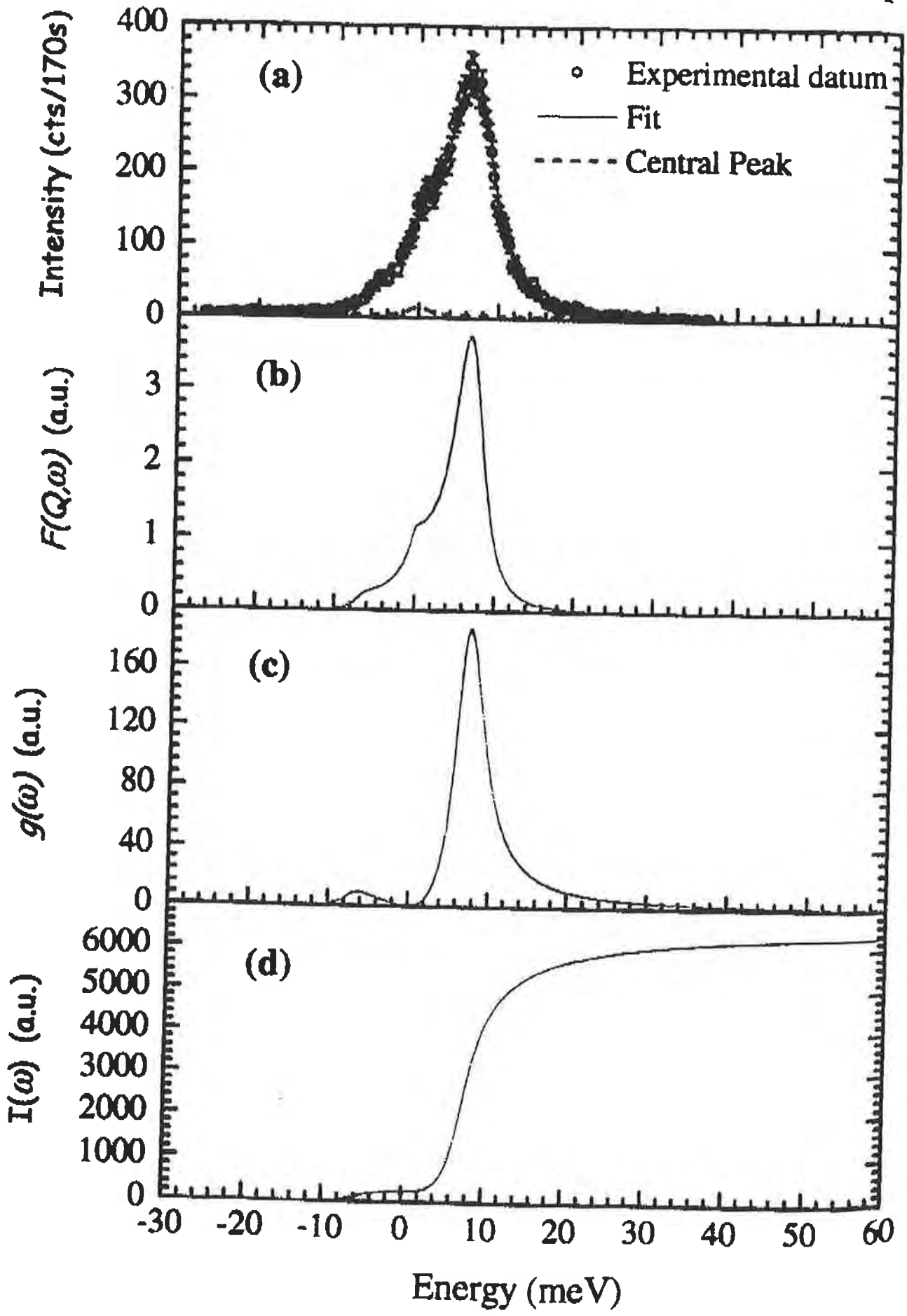

Intensity (a.u.)

Intensity (a.u.)

Intensity (a.u.)

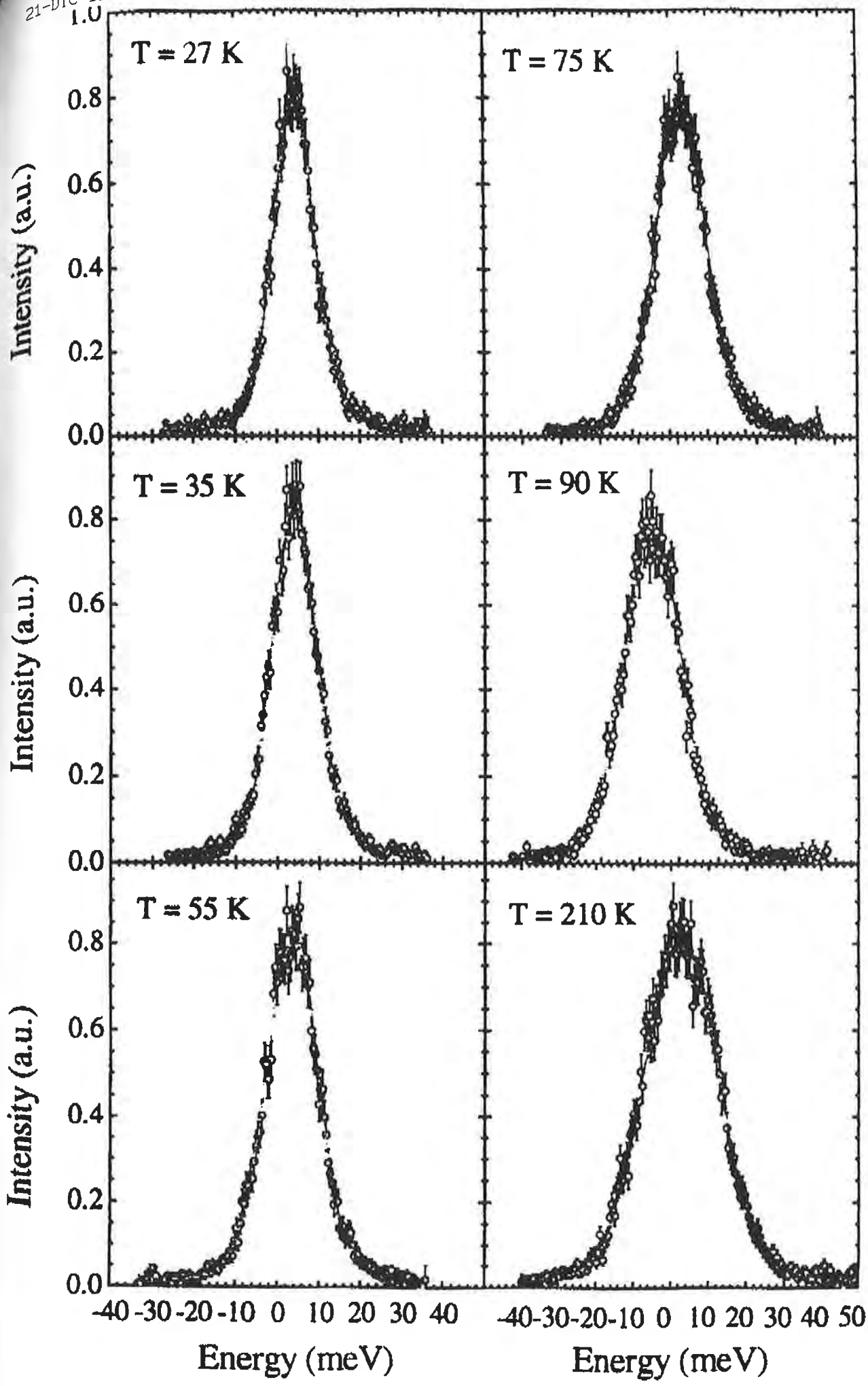
T = 27 K
T = 75 K
T = 35 K
T = 90 K
T = 55 K
T = 210 K
Intensity (a.u.)
Intensity (a.u.)
Intensity (a.u.)
0.0
0.2
0.4
0.6
0.8
1.0
-40 -30 -20 -10 0 10 20 30 40
-40 -30 -20 -10 0 10 20 30 40 50
Energy (meV)
Energy (meV)

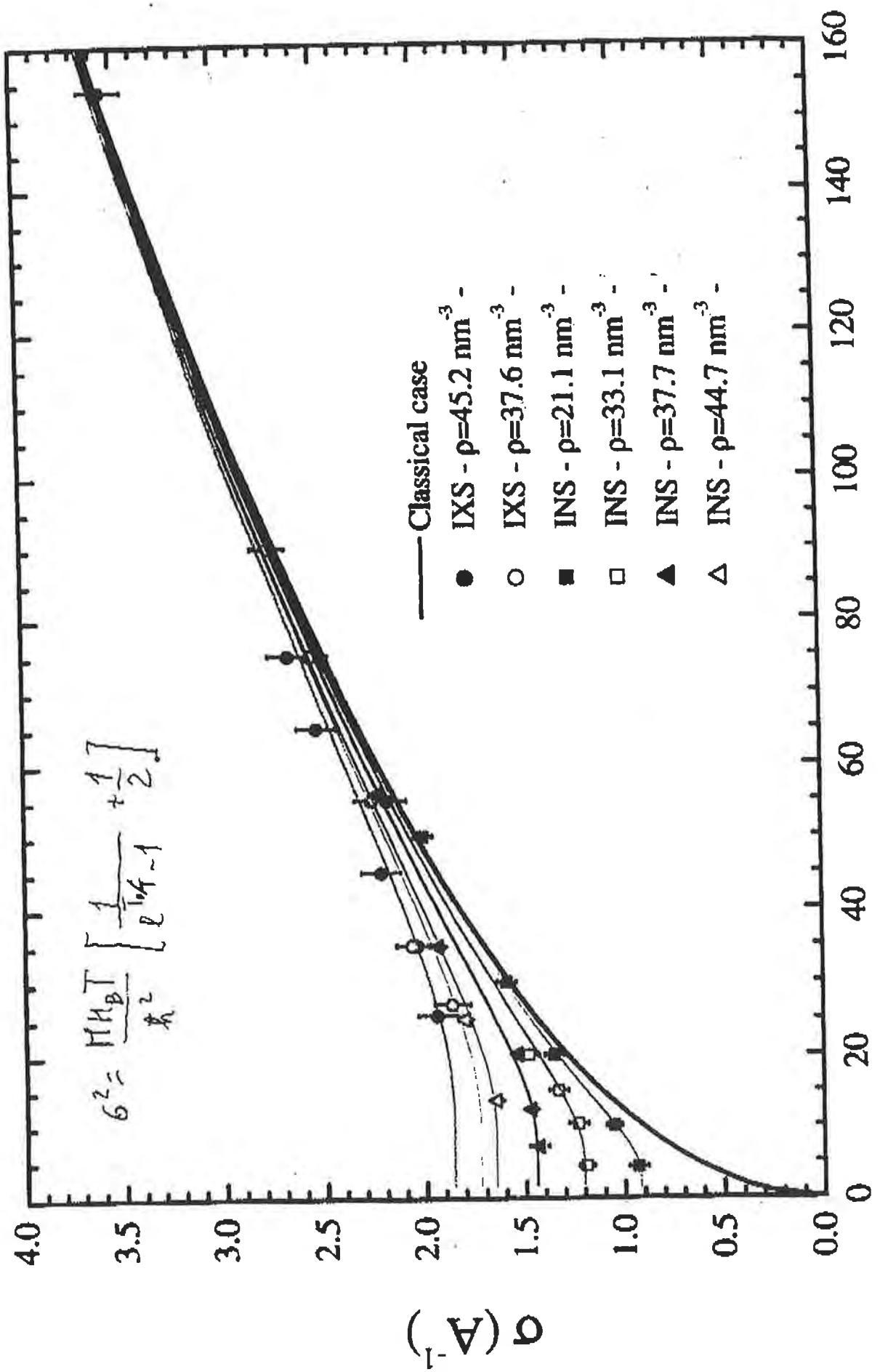
σ (Å⁻¹)
Temperature (K)
Classical case
IXS - ρ=45.2 nm⁻³ -
IXS - ρ=37.6 nm⁻³ -
INS - ρ=21.1 nm⁻³ -
INS - ρ=33.1 nm⁻³ -
INS - ρ=37.7 nm⁻³ -
INS - ρ=44.7 nm⁻³ -
σ² = ħμ_B T / k² [1/(e^{1/4} - 1) + 1/2]

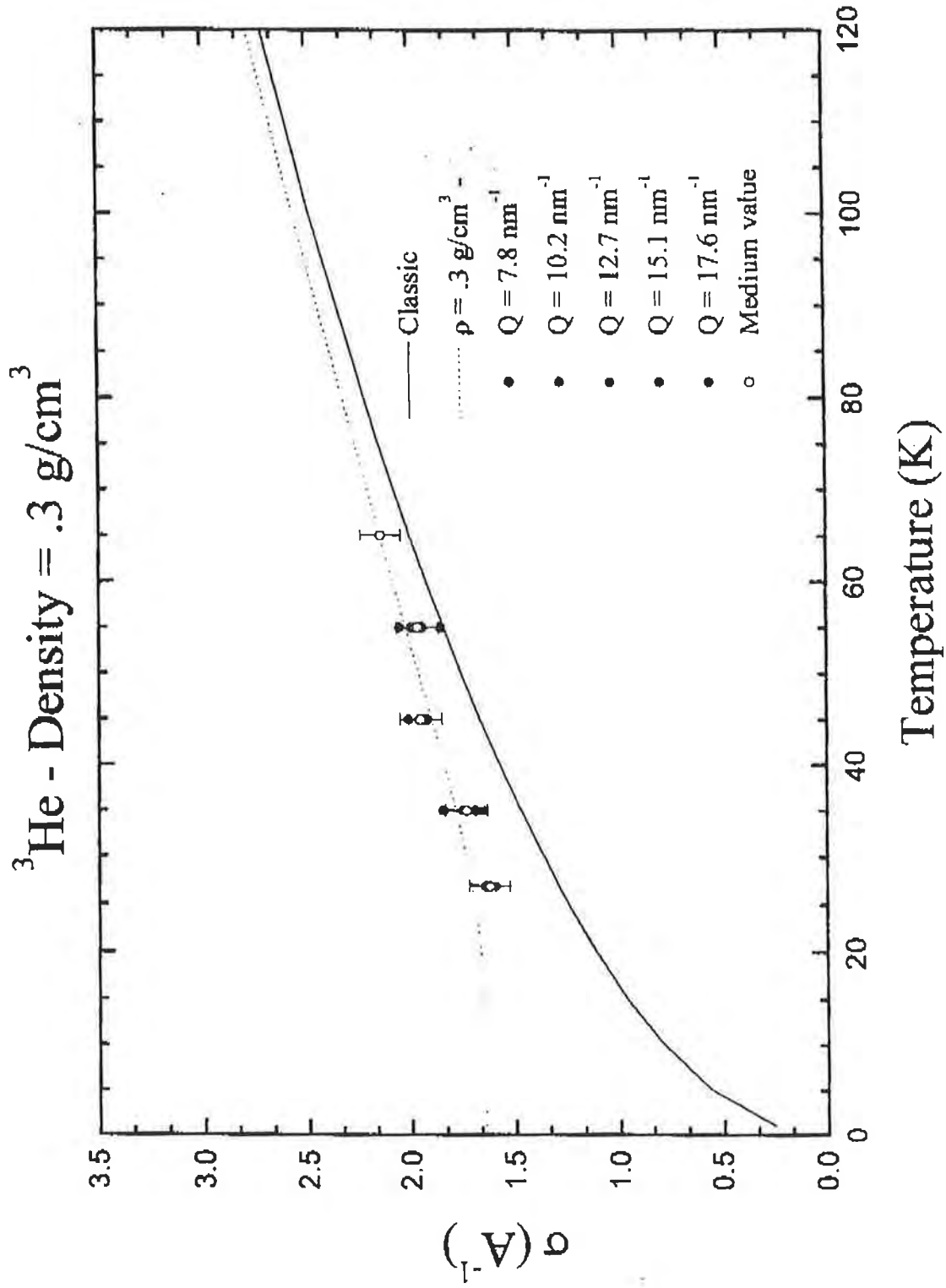
^{3}He - Density = .3 g/cm^3
Classic
ρ = .3 g/cm^3 -
Q = 7.8 nm^{-1}
Q = 10.2 nm^{-1}
Q = 12.7 nm^{-1}
Q = 15.1 nm^{-1}
Q = 17.6 nm^{-1}
Medium value
σ (Å^{-1})
Temperature (K)
0.0
0.5
1.0
1.5
2.0
2.5
3.0
3.5
0
20
40
60
80
100
120

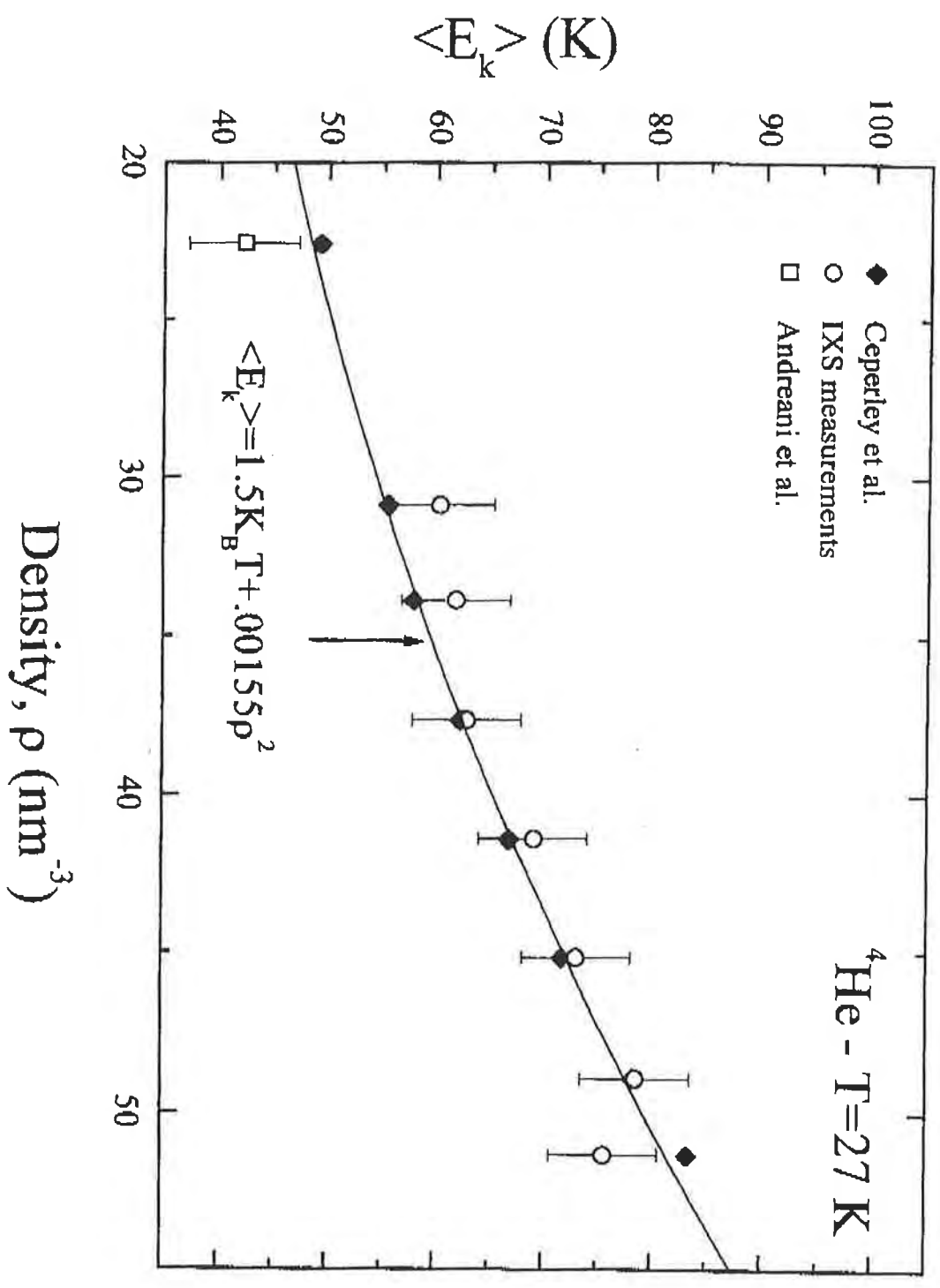
$\langle E_k \rangle$ (K)
100
90
80
70
60
50
40
20
30
40
50
Density, ρ (nm^{-3})
Ceperley et al.
IXS measurements
Andreani et al.
^{4}He - T=27 K
$\langle E_k \rangle = 1.5 K_B T + .00155 \rho^2$

Conclusions

- We have measured the second spectral moment through the best fit of IXS spectra of ^{3}He and ^{4}He as a function of both temperature and density, in a Q range extending below and around the first S(Q) maximum.
- We have observed the departure from the classic prediction at the lower temperatures.
- We have shown that the kinetic energy inferred from the computation of second spectral moments is in good agreement with PIMC computations as well as with Inelastic Neutron Scattering measurements.
- We have observed that the density evolution parallels a parabolic growth in density.

ACKNOWLEDGMENTS:

R. VERBENI, F. SETTE, C. MASCIOVECCHIO, F. ROSICA, G. RUOCCO, G. PRATESI

Erik B. Karlsson:

ANOMALOUS NEUTRON CROSS SECTIONS OBSERVED AT VERY SHORT SCATTERING TIMES

Coworkers:

C.A .Chatzidimitriou-Dreismann, T.Abdul-Redah and R.M.F. Streffer,

I.N.Stranski-Institut für Physikalische und Theoretische Chemie, Technische Universität Berlin, Str.d.17. Juni 112 , D-10623 Berlin, Germany

B. Hjörvarsson and J. Öhrmalm

Department of Physics, Royal Institute of Technology, S-10044 Stockholm, Sweden

J. Mayers,

Rutherford-Appleton Laboratory, Chilton, OX 11 0QX, England

Statement of the problem:

Anomalies have earlier been observed for σ_H/σ_D in water (both in neutron and Raman scattering)

1) **Can they be found for other substances as well?**
2) **Is σ_H or σ_D anomalous, or both?**
3) **What more can be learnt from improved experiments?**
4) **What are the possible reasons for anomalies?**

Improved experiments

Measure H and D-scattering independently

Minimize additional scattering material

Improve counting statistics

Investigate temperature dependence

and

Select a H- (or D-) containing system with

a) well-known H configuration

b) well-known H-environment

The choice is NbH_x, NbDy, or NbH_xDy ($x+y \approx 0.85$)

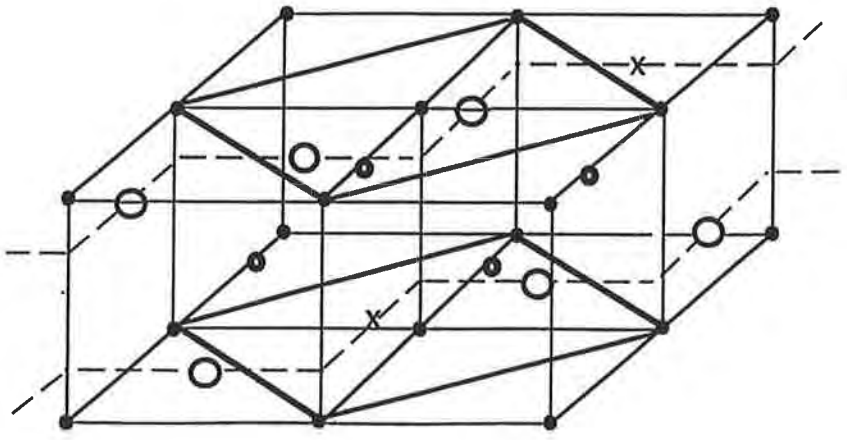

● Nb-atoms ○ H or D x Vacancy

What is neutron Compton scattering ?

(or "deep inelastic" neutron scattering)

>1 eV neutrons (instead of thermal, ≈0.01 eV)

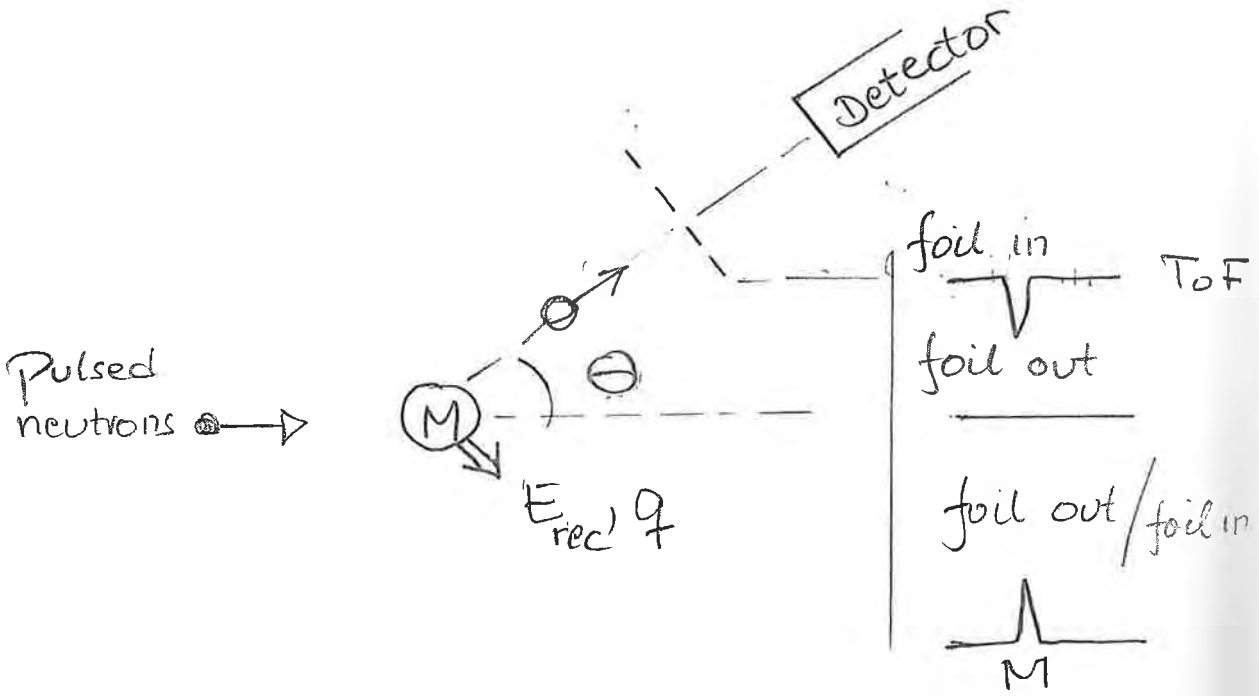

The eVS at ISIS, Rutherford-Appleton Lab., UK

is an "inverse geometry" spectrometer

(E_n of outgoing neutron selected; white spectrum ≈25–100 eV in; time-of flight analysis of events in detectors at different angles Θ)

$E_n = 4.9$ eV

ToF ⇒ E_{rec}, q for each M

+ Cross sections

From kinematics, one expects:

a)
Mass separated peaks

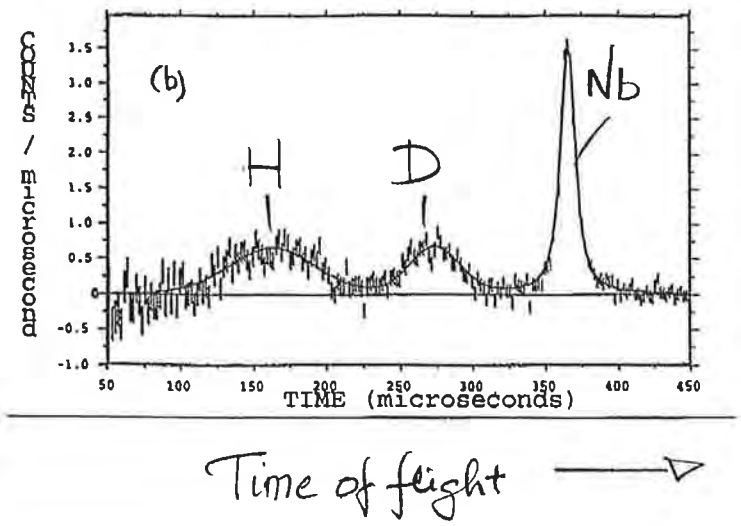

b)
For each Θ, a value of cross section ratios

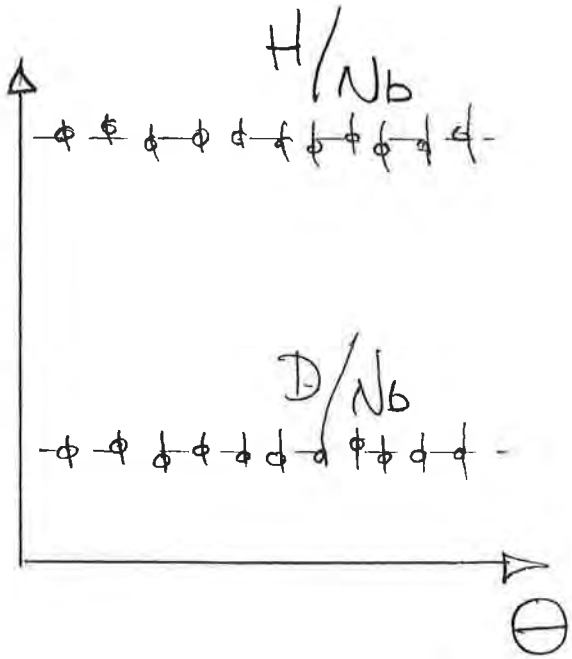

RESULTS

<u>First</u>: take averages of all data (usual procedure)

For $NbH_{0.85}$ $\sigma H/\sigma Nb \approx 11.3$ (instead of 13.1) 13.1)

For $NbH_{0.4}D_{0.45}$ $\sigma H/\sigma Nb \approx 10.0$ (instead of 13.1) 13.1)

For $NbD_{0.85}$ $\sigma D/\sigma Nb \approx 1.09$ (instead of 1.22) 1.22)

OBSERVATIONS:

1) Anomalies are there, also in metal hydrid

2) Anomalies are largest in σH

BUT THERE WAS ALSO A SURPRISE:

3) A clear Θ-dependence remained (strongest for $\sigma H/\sigma Nb$) !

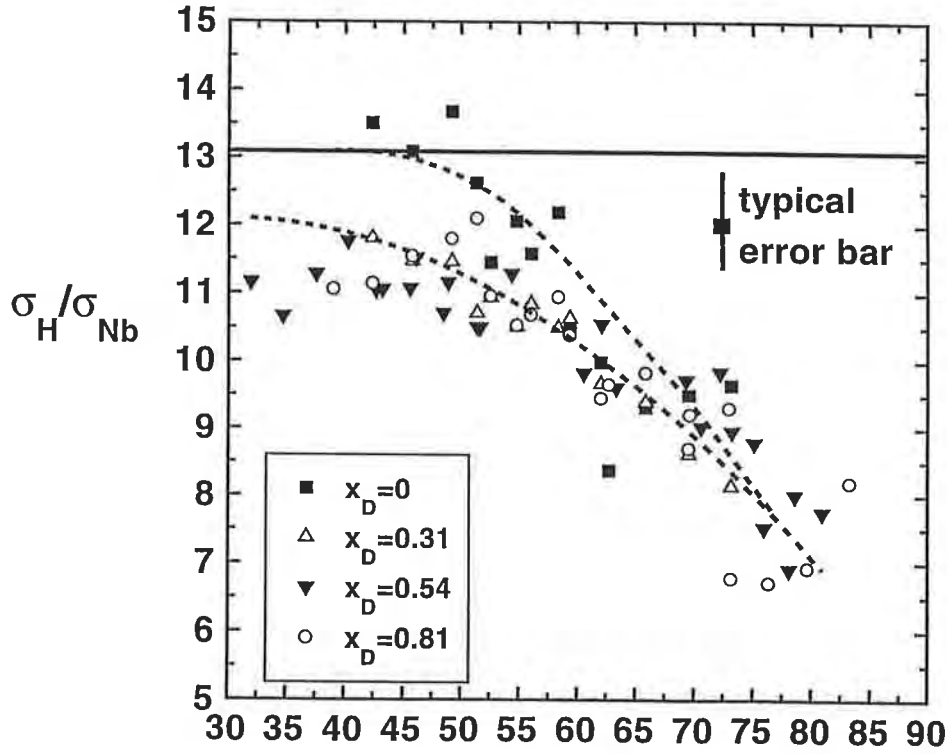

It can be traced back to a time-dependence of the anomaly (it exists only for very short observat times)

How fast is the scattering?

Order of magnitude estimate: $\tau_s \approx \hbar / \Delta E \approx 10^{-15}$ s

More detailed analysis (Watson, 1996):

$$\tau_s = \frac{M\hbar}{q\sqrt{\langle p_H^2 \rangle}}$$

transferred momentum

width on momentum distribution in vibrational state (known)

Θ-dependence ---> t-dependence:

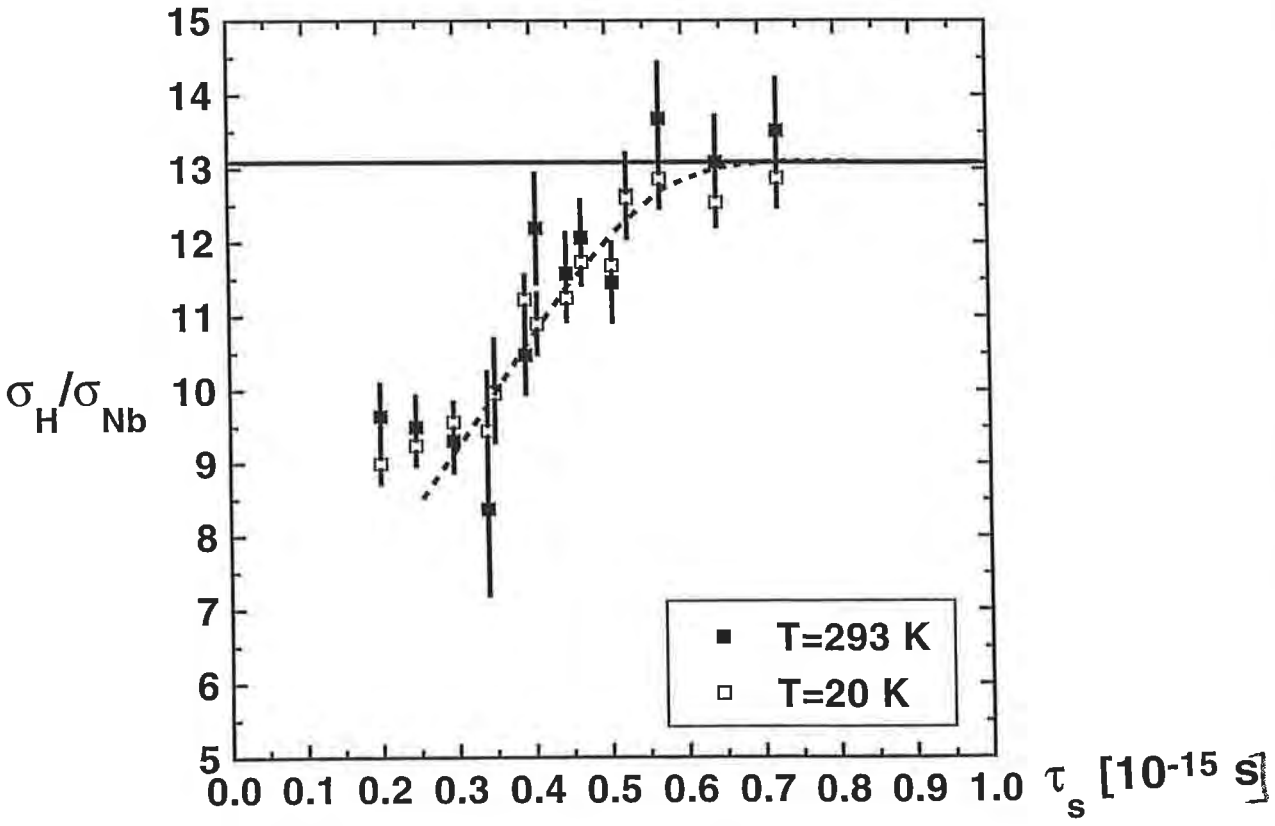

If system is observed over times > 0.6×10^{-15} there is no anomalous scattering (for $NbH_{0.85}$)

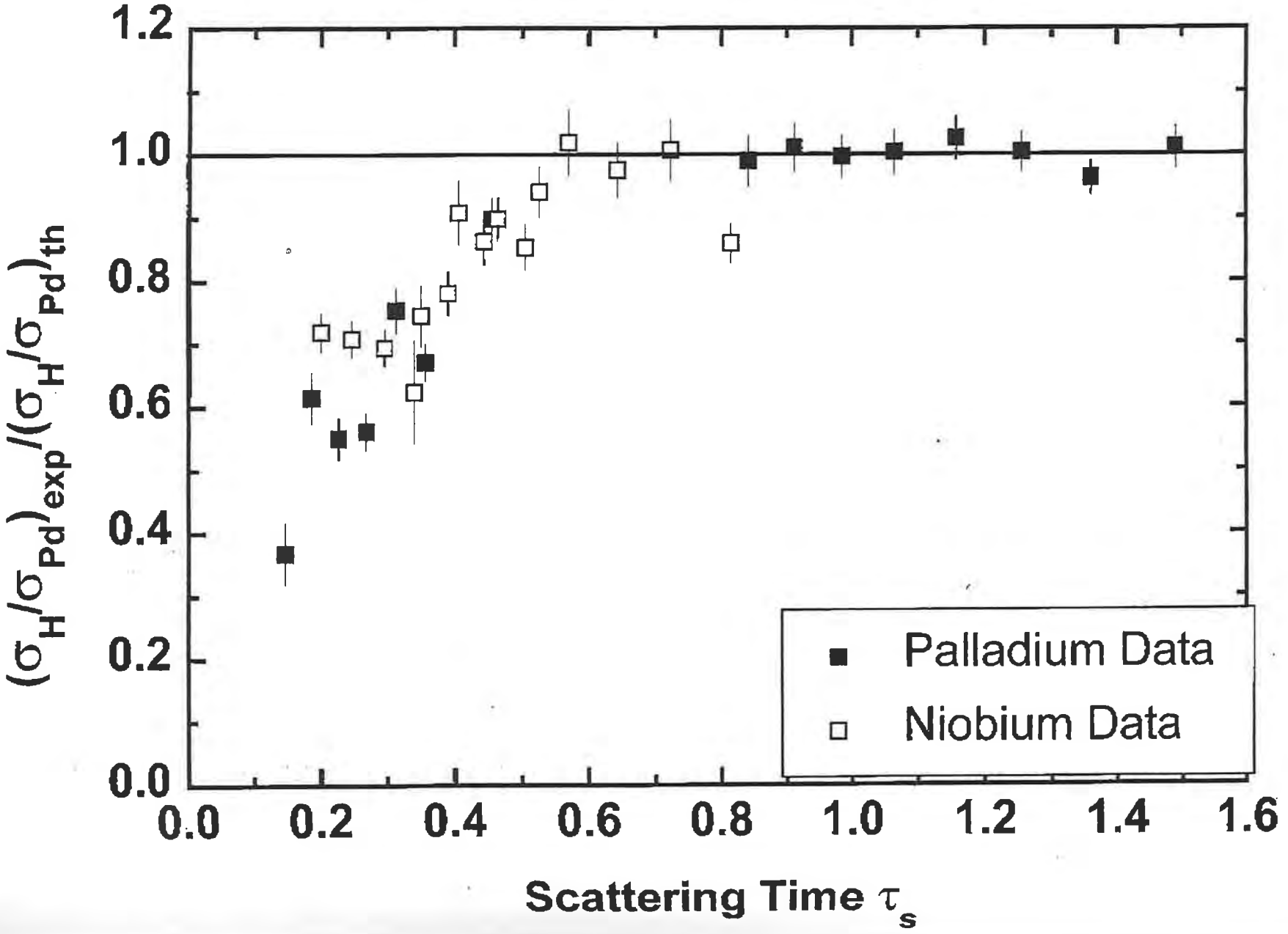
1.2
1.0
0.8
0.6
0.4
0.2
0.0
0.0
0.2
0.4
0.6
0.8
1.0
1.2
1.4
1.6
$(\sigma_H/\sigma_{Pd})_{exp}/(\sigma_H/\sigma_{Pd})_{th}$
Scattering Time τ_s
Palladium Data
Niobium Data

(fsec)

Fig. 3a

Fig. 5a

E. Karlsson

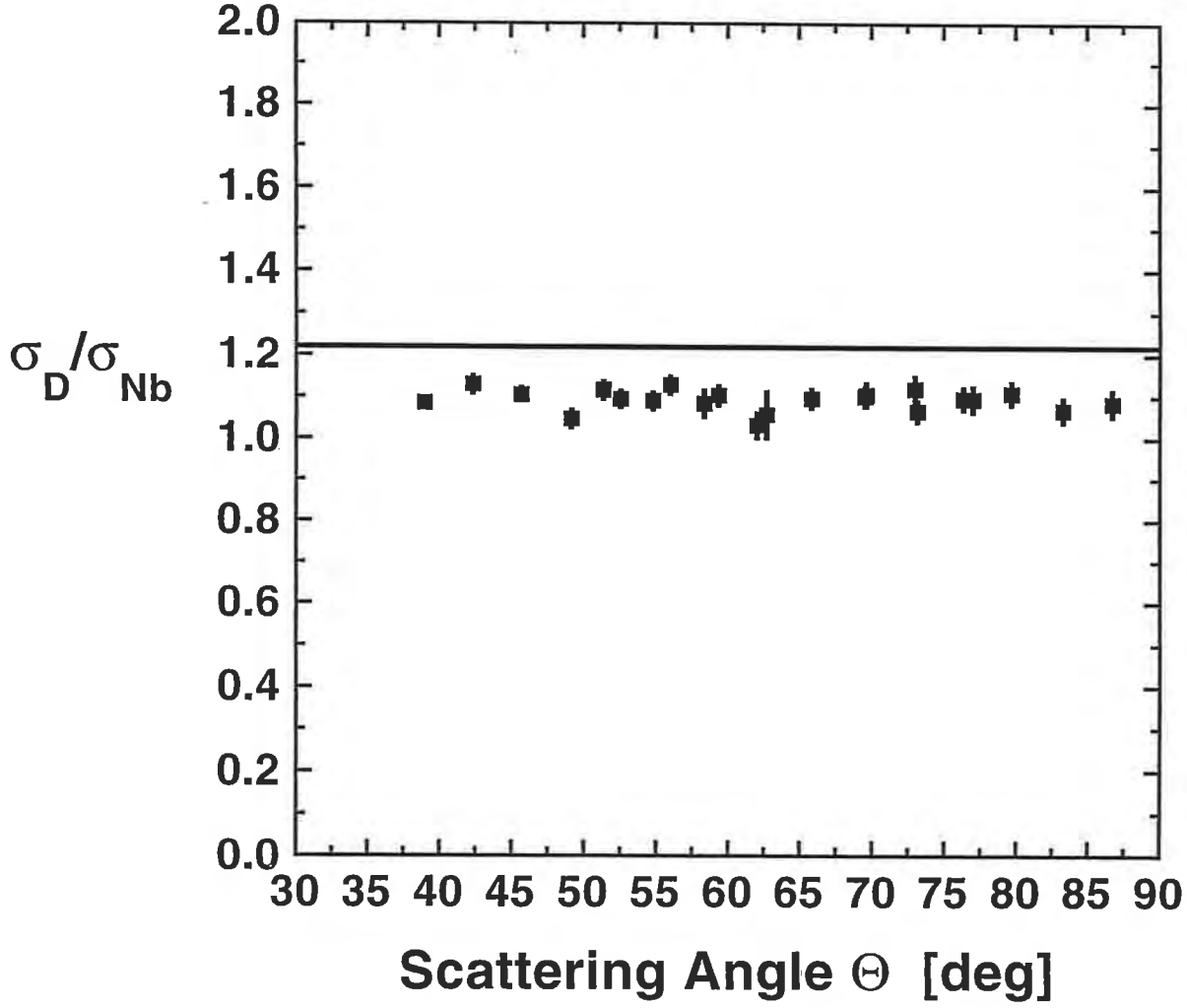

Time scales for loss of quantum coherence:

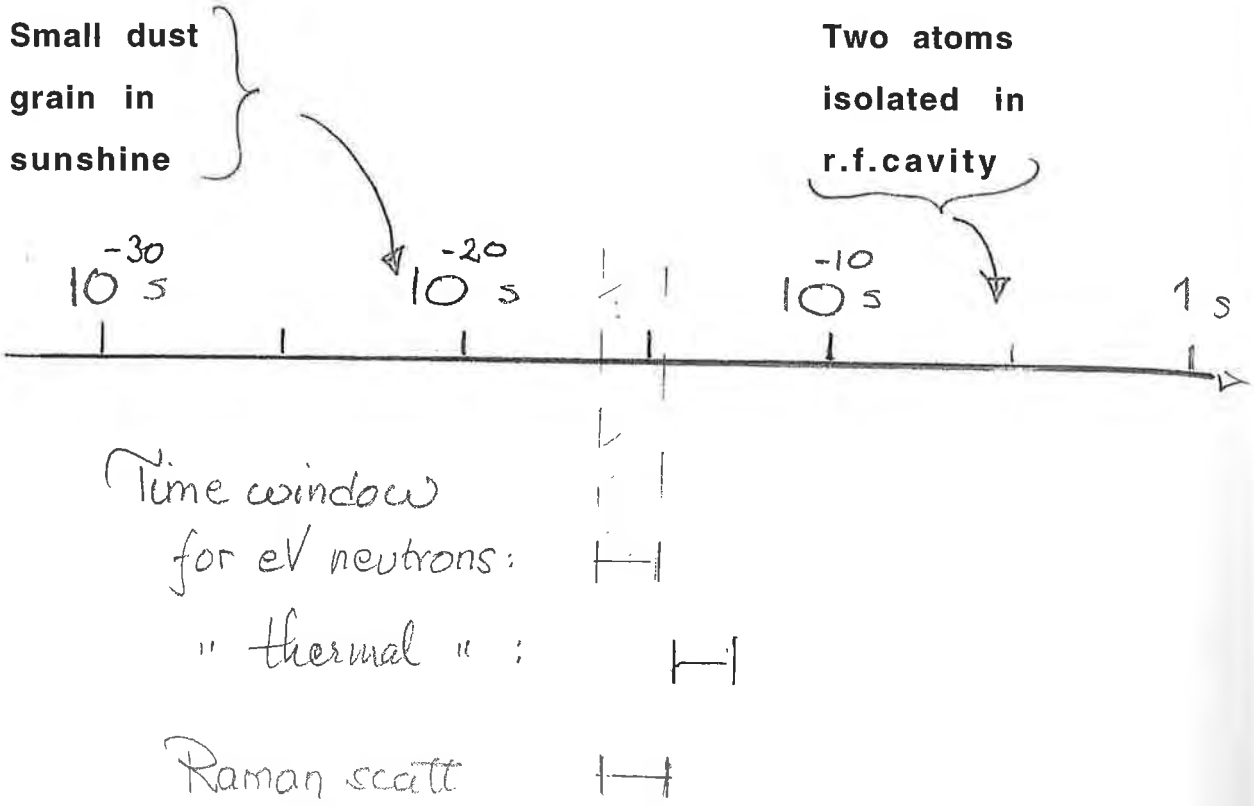

A formula by Joos and Zeh (not quite applicable, but perhaps good for an estimate):

$$\tau_{coh}^{-1} \approx n k_0^2 (x-x')^2$$

$x-x'$ linear extension of quantum object

n number of hits/s of "radiation" with

k_0 wave number

PHYSICSWATCH

We are in this time-domain (but Penrose was a bit optimistic!)

Edited by Alison Wright

Except where otherwise stated, these news items are taken from the Institute of Physics Publishing's PhysicsWatch service, which is available at "http://PhysicsWeb.org".

Quantum modelling of the mind

Some of the best minds in biophysics have been divided on the question of how to model the workings of the human brain. Mainstream research has concentrated on developing complex neural networks to perform the cognitive processes that we call consciousness. However, others, including Roger Penrose at Oxford, have argued that consciousness is in fact a quantum effect and can only reasonably be simulated by a quantum computer.

The big issue in quantum consciousness is coherence time: how long can a superposition of quantum states in the brain persist? For the brain to be a true quantum mechanical system, the coherence time must be at least 1 s. Some say that it is, while others, including Stephen Hawking, say that it isn't. Now, Mark Tegmark of Princeton has weighed in with new calculations of coherence times for two cognitive models.

The first model describes the thought process as "neuron firing", where brain impulses are caused by neurons pumping out sodium ions and absorbing potassium ions. In the quantum picture, a neuron can exist in a superposition of firing and non-firing states.

In Penrose's alternative model, consciousness resides in microtubules – hollow cylinders of protein that act as "scaffolding" to maintain the shape of brain cells. Using techniques from string theory, thoughts can be modelled as the collapse of a quantum superposition of electrical excitations propagating in a microtubule.

Whether the model involves neuron firing of charged ions or propagating excitations in microtubules, Tegmark calculated that the influence of nearby ions, by collision or coulomb interaction, will destroy the coherence of the superposed states on very short timescales (10^{-20} s for neurons and 10^{-13} s for microtubules) – too short for a quantum system.

"There is nothing fundamentally quantum mechanical about the cognitive process in the brain", said Tegmark. For the neural network community "it's business as usual". *AIP*

Only 18 clicks of hyperlink separation

Two randomly selected Web pages are on average 18 hyperlinks (or clicks) apart. So says a group of US scientists who used a technique based on power law distributions, borrowed from statistical physics, to investigate the topology of the Internet. The team also predicted that, even if the number of pages on the Web grows by 1000%, any two pages will still be only 20 clicks apart.

Symptoms of supersymmetry

Some particle physicists were excited when they heard rumours that supersymmetry had been found. The rumours were true. However, the supersymmetry in question is not the duality that boldly predicts that every known half-integer spin ("fermion") particle should have an as-yet-unseen integer spin ("boson") partner and vice versa.

A Swiss–German team has analysed in depth the energy level spectrum of gold-196, which has an odd number of protons (79) and an odd number of neutrons (117). Adding this information to their existing knowledge of neighbouring even–even and even–odd nuclei, the experimenters were able to find correlations in the energy levels that showed that nuclear forces are fermion–boson symmetric – a property known in the physics world as supersymmetry.

This is good news for nuclear physicists, who now have an additional tool to help them to understand complex nuclear spectra. However, particle physicists are still waiting for their supersymmetric day to come.

Quantum non-demolition is demonstrated on a single photon

The first repeated measurement of a single photon has been reported at Ecole Normale Supérieure, Paris. Usually light detection is a destructive process, because photons are absorbed and converted into electrical signals. However, it doesn't have to be that way – the rules of quantum mechanics do actually allow repeated measurements of a quantum object without destroying it. This is called quantum non-demolition (QND) and has been demonstrated for large photon fluxes, but never before for a single photon.

After many years of effort, the Parisian researchers have now mastered the tricky QND technique and have made repeated measurements of a single photon trapped in a niobium cavity. In the experiment, a rubidium atom is passed through the cavity and the photon causes a phase shift in the atom's wavefunction. The phase shift is detected by interferometry. Sending atoms through the cavity again and again repeats the measurement, because the photon remains undisturbed (although it does suffer a phase shift – Heisenberg's Uncertainty Principle won't let you have it every way).

This QND technique could become the basis of a quantum logic gate.

Correction

The e-mail address printed in the advertisement for VAT Vacuum Products on p12 of the July issue of *CERN Courier* was incorrect. The correct address is "uk@vatvalve.com".

SOME MAIN QUESTIONS

1) Can we find conventional explanations?

(Interference between two nearby protons impossible (if they are individual objects), because $\lambda_n << d_{H-H}$

2) Could it be quantum correlation effects?

Scattering at position (1) of an entangled pair:

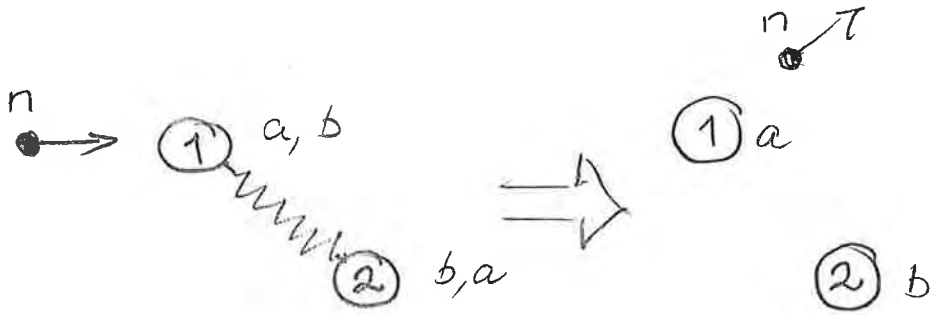

Cancellation of scattering amplitudes due to interference between *a* and *b* scattering?

3) Can quantum entanglement live for 10^{-15} s in condensed matter?

Back to NbH:

Action on H-pairs by	n =	k=
1) Nb-phonons:	$4 \times 10^{13}\ s^{-1}$	$\approx 0.5\ Å^{-1}$
2) H-phonons (local modes)	$10^{14}\ s^{-1}$	$\approx 6\ Å^{-1}$
D- -----"----------		
3) Conduction electrons: (only near E_f electrons)	effects weak	

Joos and Zeh formula gives for $x - x' = 2$ Å

$$\tau_{coh} \approx 10^{-16}\ s$$

CONCLUSIONS:

H-dynamics in condensed matter may be partly quantum controlled

Theory:

SCATTERING ON ENTANGLED PAIRS OF IDENTICAL PARTICLES

(E.K. + S.W.L.):

EXAMPLE:
Singlet (J=0) state of two entangled protons α and β:

$$\psi(J=0) \propto \left[P(\mathbf{R}_\alpha)Q(\mathbf{R}_\beta) + P(\mathbf{R}_\beta)Q(\mathbf{R}_\alpha)\right]\left[\uparrow(s_\alpha)\downarrow(s_\beta) - \uparrow(s_\beta)\downarrow(s_\alpha)\right]$$

Neutron Compton scattering on such a pair (schematic):

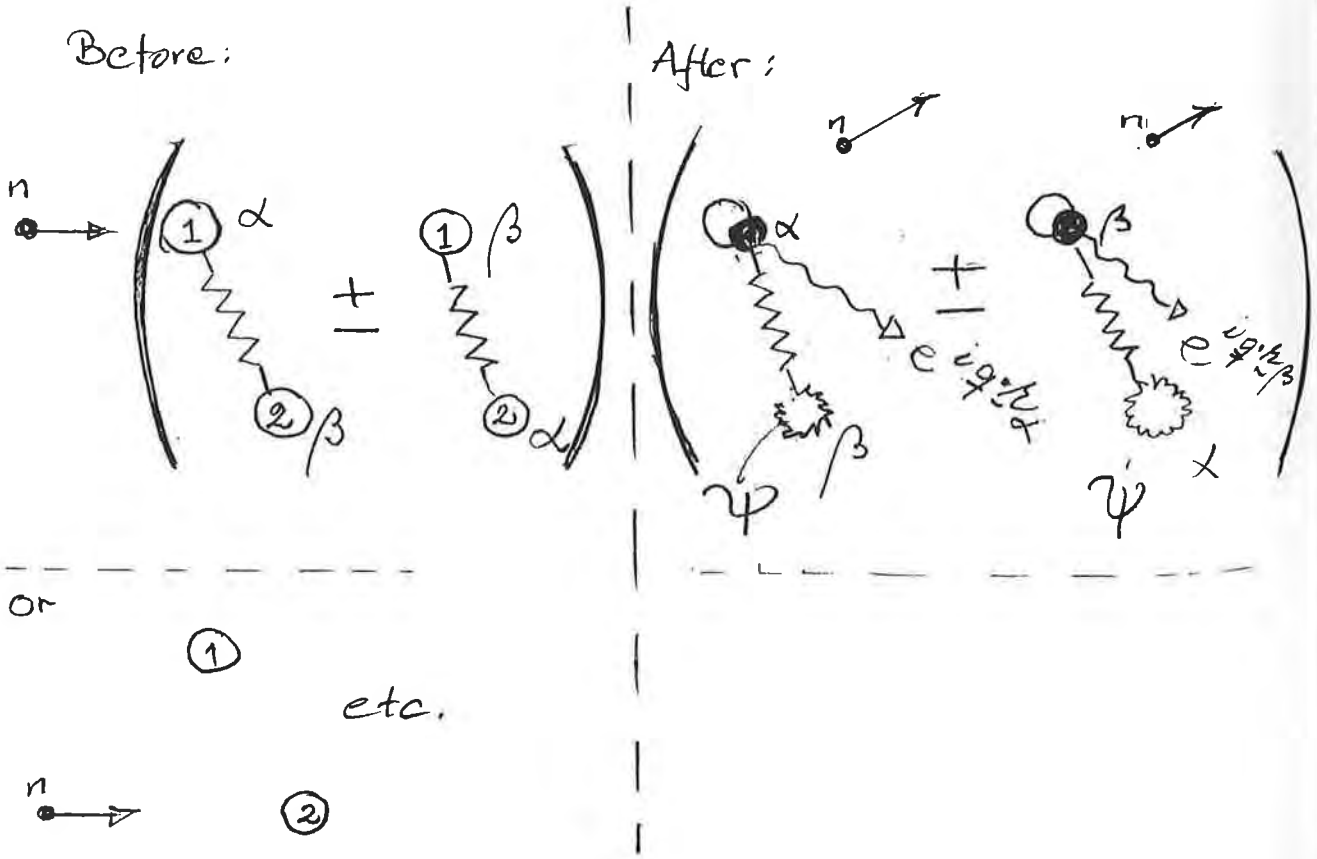

FORMULATION FOR GENERAL I (nucl.spin) AND J (pair spin)

INITIAL STATE OF TARGET

Orbital part:

$$\left\{2(1+\zeta S_{12}^2)\right\}^{-1/2}\left\{\varphi_1(\mathbf{R}_\alpha)\varphi_2(\mathbf{R}_\beta)+\zeta\varphi_1(\mathbf{R}_\beta)\varphi_2(\mathbf{R}_\alpha)\right\}\times$$

Spin part:

$$\times\chi_M^J(\alpha,\beta)=\sum_{mn}(I_\alpha m I_\beta n|JM)\left|I_\alpha m\right\rangle\left|I_\beta n\right\rangle .$$

FINAL STATE OF TARGET

$$\frac{1}{\sqrt{2\Omega}}\left\{\exp(i\mathbf{p}'\cdot\mathbf{R}_\alpha)\psi(\mathbf{R}_\beta)+\zeta'\exp(i\mathbf{p}'\cdot\mathbf{R}_\beta)\psi(\mathbf{R}_\alpha)\right\}\times$$

$$\times\chi_{M'}^{J'}(\alpha,\beta)$$

Scattering operator

$$V=b_\alpha\exp(i\mathbf{k}\cdot\mathbf{R}_\alpha)+b_\beta\exp(i\mathbf{k}\cdot\mathbf{R}_\beta),$$

$$b=A+B\mathbf{s}\cdot\mathbf{I}$$

Scattering amplitude

$$\left\langle\text{final}\left|V\right|\text{initial}\right\rangle=K(\mathbf{p})F(J',J),$$

where

$$F(J',J)=\tfrac{1}{2}\left\{\left\langle J'\left|b_\alpha\right|J\right\rangle+\zeta\zeta'\left\langle J'\left|b_\beta\right|J\right\rangle\right\}(T_2+\zeta T_1),$$

$$\left\langle J'\left|b\right|J\right\rangle=\left\{\chi_{M'}^{J'}(\alpha,\beta)\right\}^{+}b\chi_M^J(\alpha,\beta)\quad;\quad T_\nu=\int dR\,\psi^*\varphi_\nu(R)$$

For CROSS SECTIONS:

average $\langle J'|b|J\rangle^2$ **over J, J' and neutron spin projections**

$$\frac{1}{2}\sum_{m_n m_n'}\frac{1}{(2J+1)}\sum_{MM'}\left|\left\langle \tfrac{1}{2}m_n'\left|\langle J'|b_\alpha|J\rangle\right|\tfrac{1}{2}m_n\right\rangle\right|^2 =$$

$$=\delta_{J,J'}A^2+\frac{1}{4}B^2(2J'+1)I(I+1)(2I+1)\begin{Bmatrix} I & 1 & I \\ J' & I & J\end{Bmatrix}^2$$

$$=(\sigma_{inc}/4\pi)\left\{1-\frac{J(J+1)}{4I(I+1)}\right\}$$

and multiply by $|T_2+\zeta T_1|^2$ **; Assume** $T_1 = T_2$

$$\sigma_{eff} = (1/2)\sigma_{inc}(T_1)^2 = f\,\sigma_{single\ particle}$$

For $(T_1)^2 = (T_2)^2 = 1/2$

$f_{proton} = 0.245$

$f_{deuteron} = 0.065$

Note that for $\zeta' = 0$ **(broken spatial entanglement in final state):**

$$f = 1$$

Time for disentanglement set by recoiling particle (exciting lattice, etc) in neutr. compt. scatt.

WHAT INFORMATION CAN BE EXTRACTED FROM AN EVS DATA SET?

George Reiter

Jerry Mayers

Ans: **Three harmonic coefficients and a spectrum of anharmonic coefficients**

Impulse Approximation

$$S(\vec{q},\omega) = \int n(\vec{p})\delta(\omega + \frac{p^2}{2M} - \frac{\vec{p}+\hat{q})^2}{2M})d\vec{p}$$

$$\mathrm{y}=\frac{M}{q}(\omega - \frac{q^2}{2M})$$

$$S(\vec{q},\omega) = \frac{M}{q}\int n(\vec{p})\delta(y - \vec{p}.\hat{q})d\vec{p} = \frac{M}{q}J(\hat{q},y)$$

A VERY USEFUL THEORUM

If $J(\hat{q}, y)$ is expressed as

$$J(\hat{q}, y) = \frac{e^{-y^2}}{\pi^{\frac{1}{2}}} \sum_{n,l,m} a_{n,l,m} H_{2n+l}(y) Y_{lm}(\hat{q})$$

then n($\vec{p}$) is given in the related basis of Laguerre polynomials as

$$n(\vec{p}) = \frac{e^{-p^2}}{\pi^{\frac{3}{2}}} \sum_{n,l,m} 2^{2n+l} n! (-1)^n a_{n,l,m} p^l L_n^{l+\frac{1}{2}}(p^2) Y_{lm}(\hat{p})$$

FITTING PROCEDURE

For anisotropic systems

$$n(\vec{p}) = \prod_i \frac{e^{\frac{-p_i^2}{2\sigma_i^2}}}{(2\pi\sigma_i)^{\frac{1}{2}}} R(\vec{p})$$

change variables to $p_i' = p_i/\sqrt{2}\sigma_i$

)ur procedure is to expand $J'(\hat{q'}, y')$ in hermite polynomials, and least squares fit the data, $S(\vec{q}, \omega)$, to obtain the parameters, $\sigma_i, a_{n,l,m}$.

MEASUREMENT ERRORS

$$\delta n(\vec{p}) = \sum_i \frac{\delta n(\vec{p})}{\delta \rho_i} \delta \rho_i$$

$$< \delta n(\vec{p})^2 >= \sum_{i,j} \frac{\delta n(\vec{p})}{\delta \rho_i} \frac{\delta n(\vec{p})}{\delta \rho_j} < \delta \rho_i \delta \rho_j >$$

TEST CASE

$$n(p_x, p_y, p_z) = \frac{(1+r^2+2r\cos(2p_z a))}{(1+r^2+2re^{-\frac{a^2}{2\sigma_z{}^2}})} \prod_i \frac{e^{-\frac{p_i^2}{2\sigma_i^2}}}{(2\pi\sigma_i)^{\frac{1}{2}}}$$

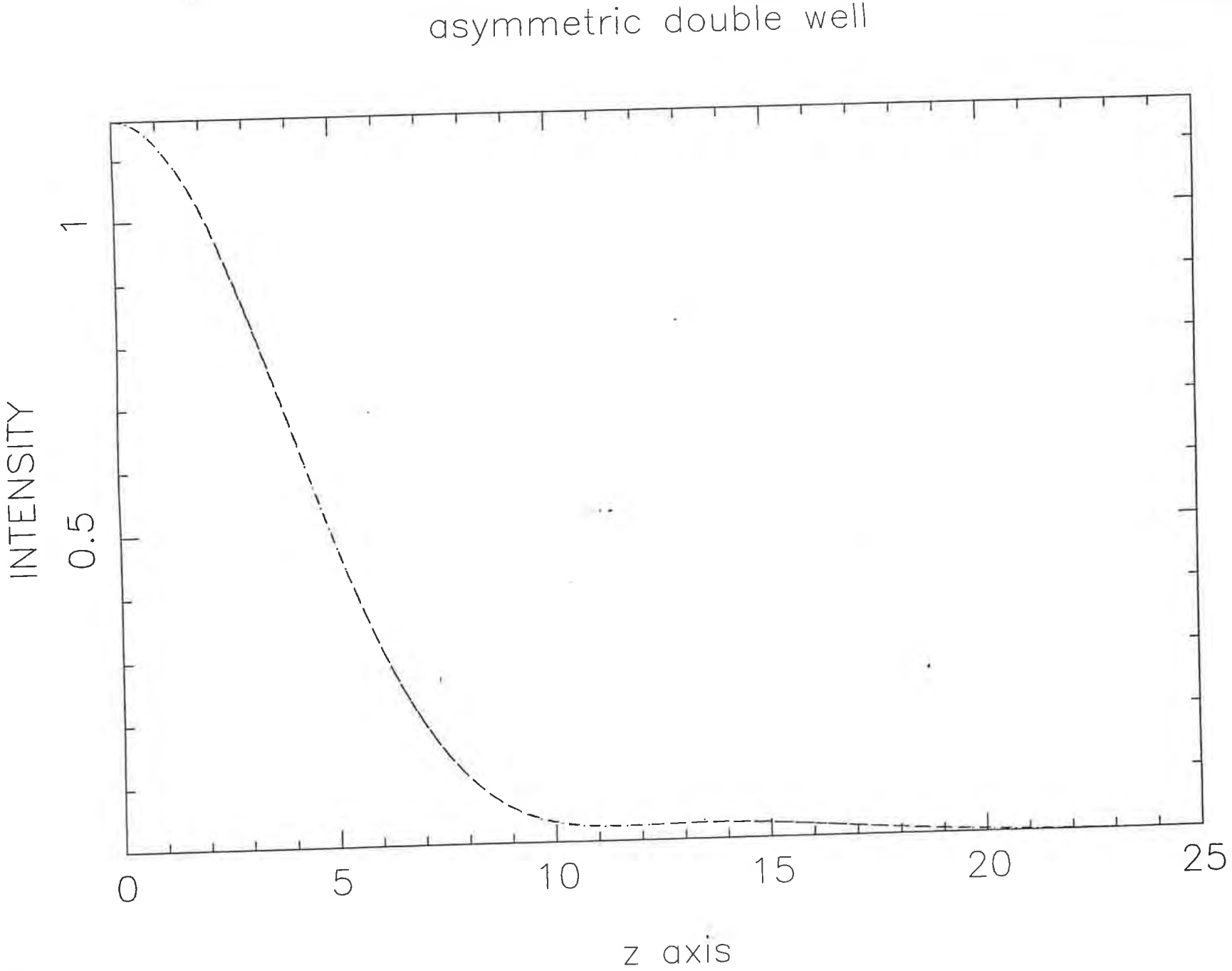
asymmetric double well
INTENSITY
1
0.5
0
5
10
15
20
25
z axis

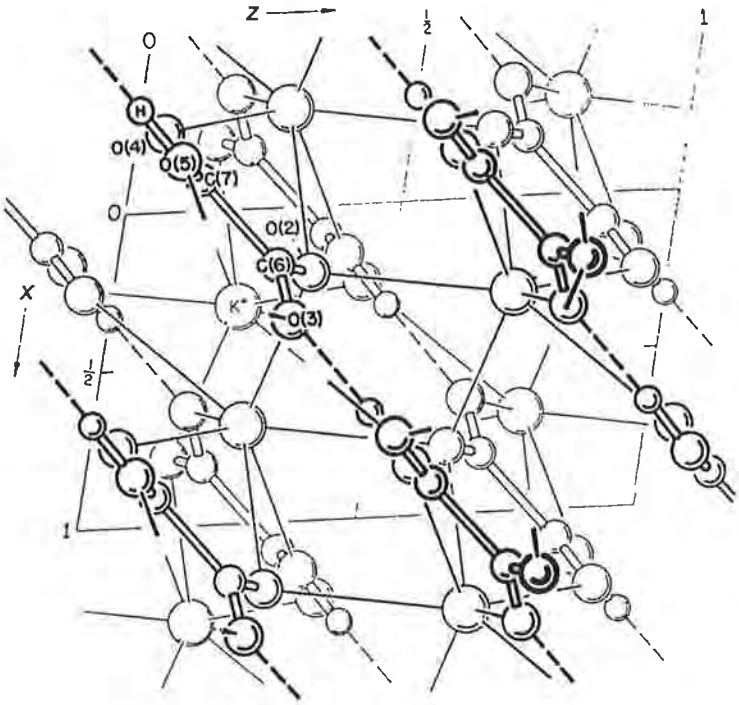

Fig. 1. The structure projected on (010).

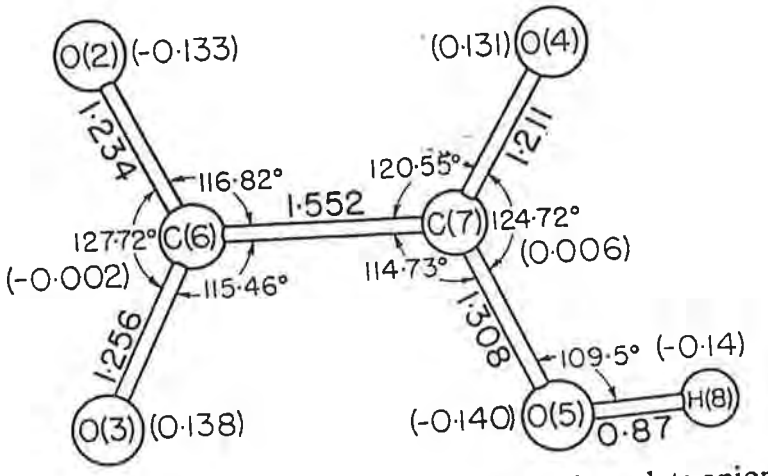

Fig. 2. Bond distances (Å) and angles for the binoxalate anion
Deviations (Å) from the mean plane are given in parentheses

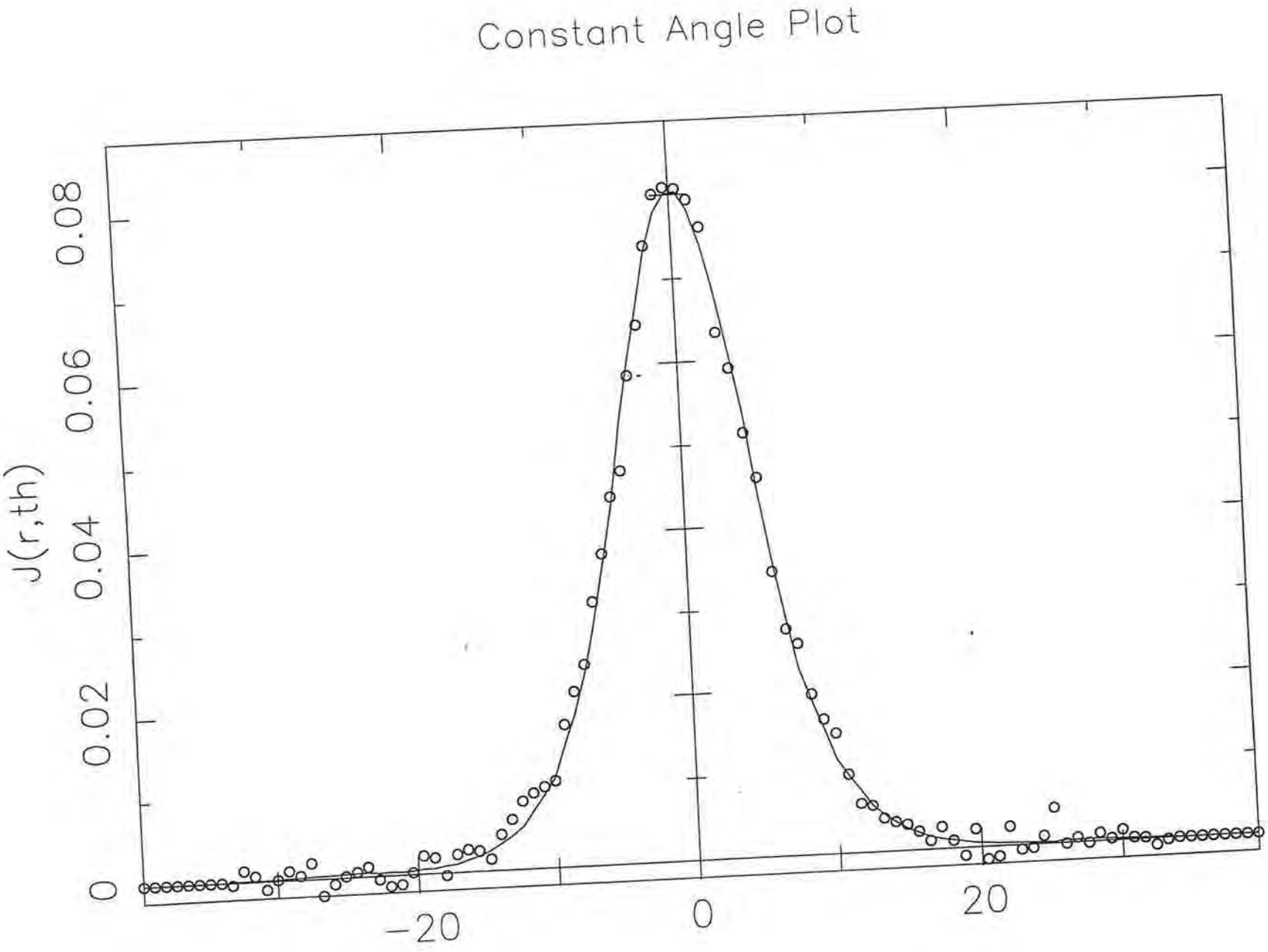
Constant Angle Plot
J(r,th)
0
0.02
0.04
0.06
0.08
−20
0
20

Potassium Binoxalate at 10K

6.1143E+00	5.6931E-02	7.	Sigma along z
4.7411E+00	1.9793E-02	8.	Sigma along x
5.0176E+00	1.1136E-02	9.	Sigma along y
5.2736E-01	3.4125E-02	10.	h4*y00
1.1849E-01	4.4028E-02	11.	h4*y20
0.0000E+00	0.0000E+00	12.	h4*y22
4.0404E-02	1.4792E-02	13.	h4*y40
-6.2650E-02	8.5612E-03	14.	h4*y42
-3.8376E-02	1.9155E-02	15.	h4*y44
0.0000E+00	0.0000E+00	16.	h6*y00
7.4833E-02	1.8913E-02	17.	h6*y20
-3.7964E-02	9.0737E-03	18.	h6*y22
0.0000E+00	0.0000E+00	19.	h6*y40
0.0000E+00	0.0000E+00	20.	h6*y42
0.0000E+00	0.0000E+00	21.	h6*y44
-9.9588E-03	3.3713E-03	22.	h6*y60
0.0000E+00	0.0000E+00	23.	h6*y62
-2.2904E-02	1.9198E-02	24.	h6*y64
4.0179E-03	3.2155E-03	25.	h6*y66
3.6860E-03	1.8732E-03	26.	h8*y00
1.5114E-02	2.8540E-03	27.	h8*y20
-4.5407E-03	2.2607E-03	28.	h8*y22
-5.2963E-03	1.4356E-03	29.	h8*y40
4.0880E-03	1.2409E-03	30.	h8*y42
0.0000E+00	0.0000E+00	31.	h8*y44
0.0000E+00	0.0000E+00	32.	h8*y60
0.0000E+00	0.0000E+00	33.	h8*y62
-9.8087E-03	4.0978E-03	34.	h8*y64
0.0000E+00	0.0000E+00	35.	h8*y66
0.0000E+00	0.0000E+00	36.	h8*y80
-1.4945E-03	8.0680E-04	37.	h8*y82
0.0000E+00	0.0000E+00	38.	h8*y84
0.0000E+00	0.0000E+00	39.	h8*y86
-1.2717E-02	3.0058E-03	40.	h8*y88

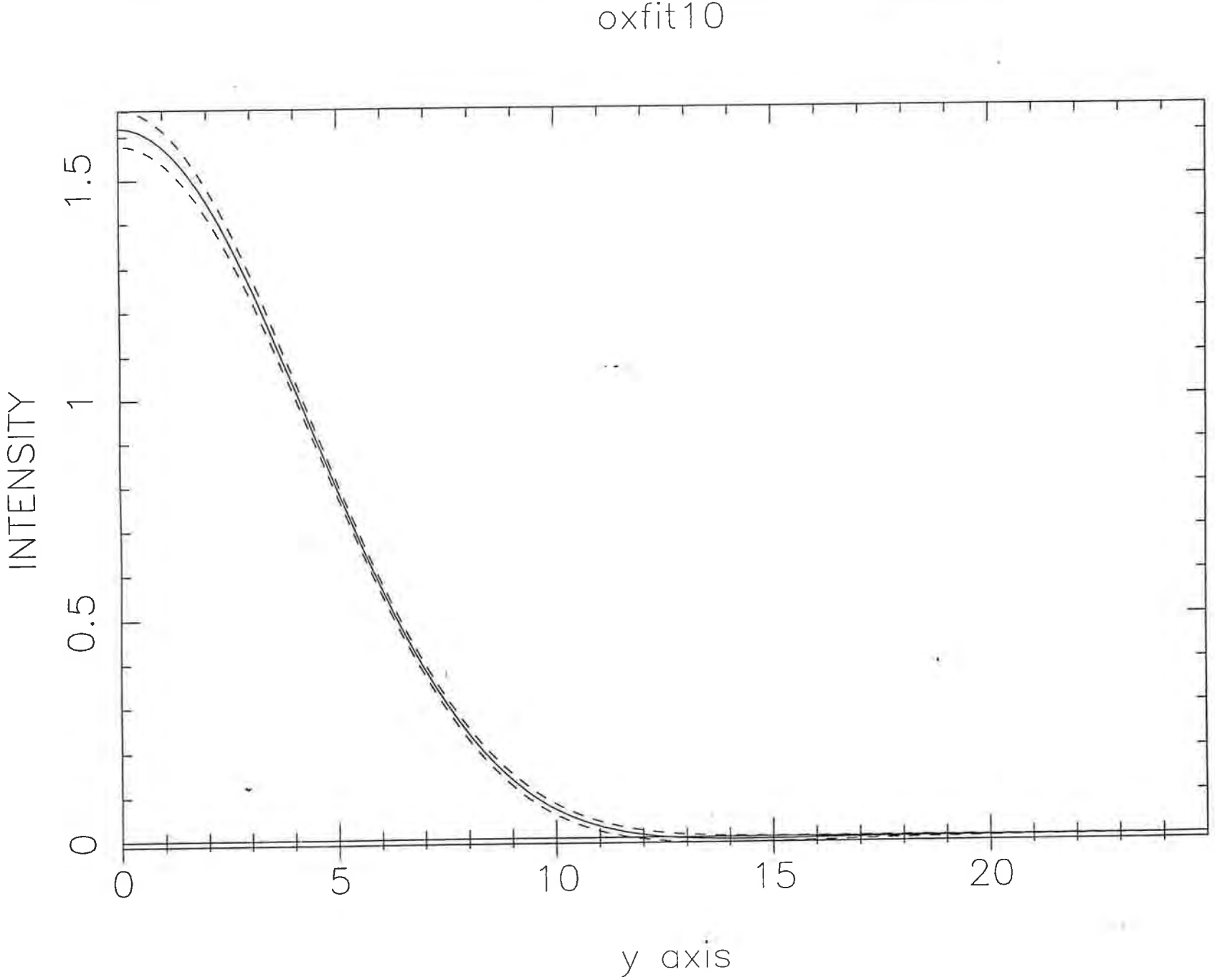
oxfit10
INTENSITY
0
0.5
1
1.5
0
5
10
15
20
y axis

INTENSITY
0.5
1
1.5
0
5
10
15
20
z axis
oxfit10

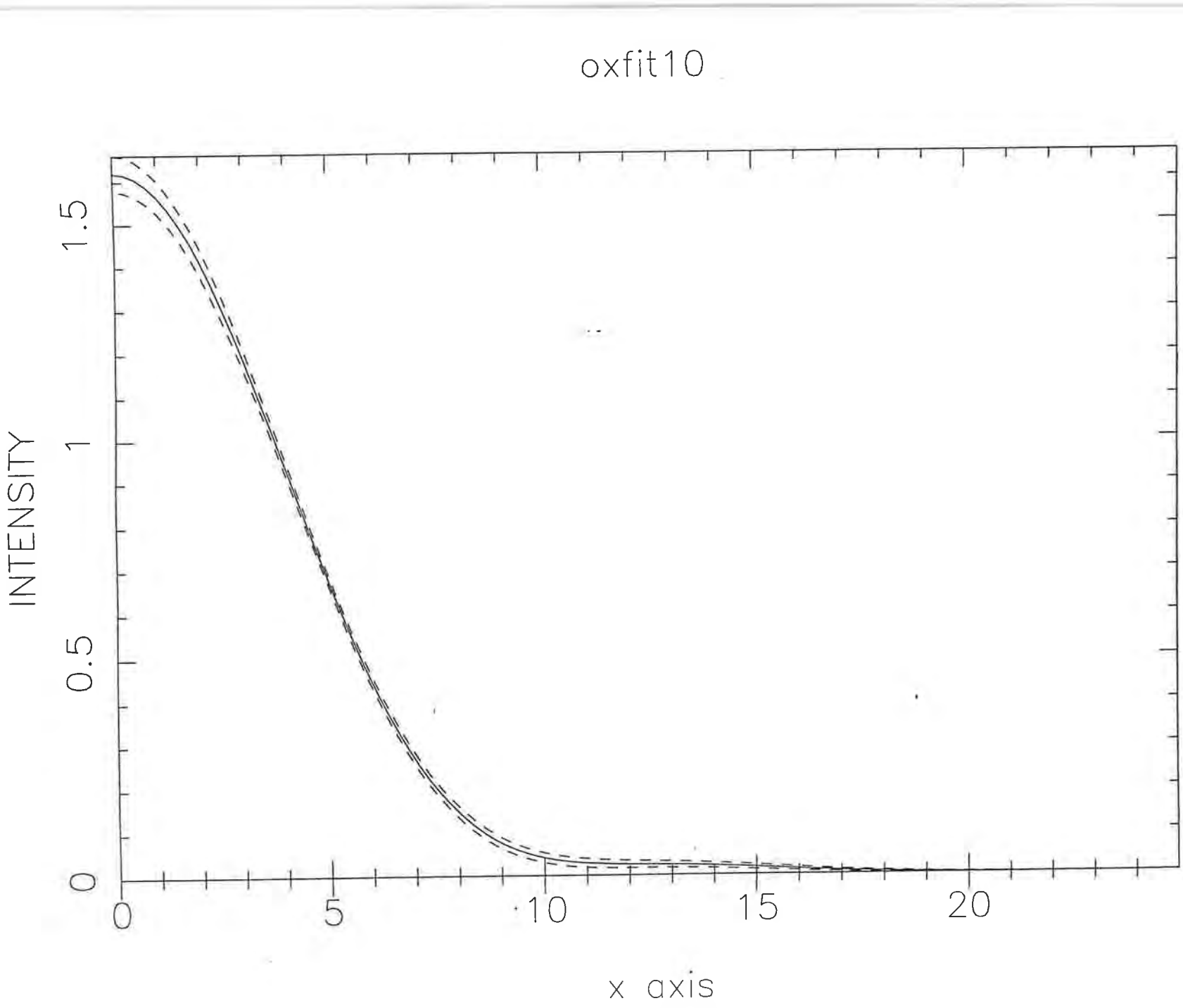
oxfit10
INTENSITY
0
0.5
1
1.5
0
5
10
15
20
x axis

H2O at 290K

7.	Sigma along z	=	5.624899	+-	4.5988556E-02
8.	Sigma along x	=	5.000000	+-	0.0000000E+00
9.	Sigma along y	=	5.000000	+-	0.0000000E+00
10.	h4*y00	=	1.411400	+-	5.8656756E-02
11.	h4*y20	=	0.0000000E+00	+-	0.0000000E+00
12.	h4*y22	=	0.0000000E+00	+-	0.0000000E+00
13.	h4*y40	=	0.0000000E+00	+-	0.0000000E+00
14.	h4*y42	=	0.0000000E+00	+-	0.0000000E+00
15.	h4*y44	=	0.0000000E+00	+-	0.0000000E+00
16.	h6*y00	=	0.6284000	+-	7.4494243E-02
17.	h6*y20	=	0.0000000E+00	+-	0.0000000E+00
18.	h6*y22	=	0.0000000E+00	+-	0.0000000E+00
19.	h6*y40	=	0.0000000E+00	+-	0.0000000E+00
20.	h6*y42	=	0.0000000E+00	+-	0.0000000E+00
21.	h6*y44	=	0.0000000E+00	+-	0.0000000E+00
22.	h6*y60	=	0.0000000E+00	+-	0.0000000E+00
23.	h6*y62	=	0.0000000E+00	+-	0.0000000E+00
24.	h6*y64	=	0.0000000E+00	+-	0.0000000E+00
25.	h6*y66	=	0.0000000E+00	+-	0.0000000E+00
26.	h8*y00	=	0.1749000	+-	2.3568094E-02
27.	h8*y20	=	0.0000000E+00	+-	0.0000000E+00
28.	h8*y22	=	0.0000000E+00	+-	0.0000000E+00
29.	h8*y40	=	0.0000000E+00	+-	0.0000000E+00
30.	h8*y42	=	0.0000000E+00	+-	0.0000000E+00
31.	h8*y44	=	0.0000000E+00	+-	0.0000000E+00
32.	h8*y60	=	0.0000000E+00	+-	0.0000000E+00
33.	h8*y62	=	0.0000000E+00	+-	0.0000000E+00
34.	h8*y64	=	0.0000000E+00	+-	0.0000000E+00
35.	h8*y66	=	0.0000000E+00	+-	0.0000000E+00
36.	h8*y80	=	0.0000000E+00	+-	0.0000000E+00
37.	h8*y82	=	0.0000000E+00	+-	0.0000000E+00
38.	h8*y84	=	0.0000000E+00	+-	0.0000000E+00
39.	h8*y86	=	0.0000000E+00	+-	0.0000000E+00
40.	h8*y88	=	0.0000000E+00	+-	0.0000000E+00
41.	h10*y00	=	1.2900000E-02	+-	1.9080538E-03

^D

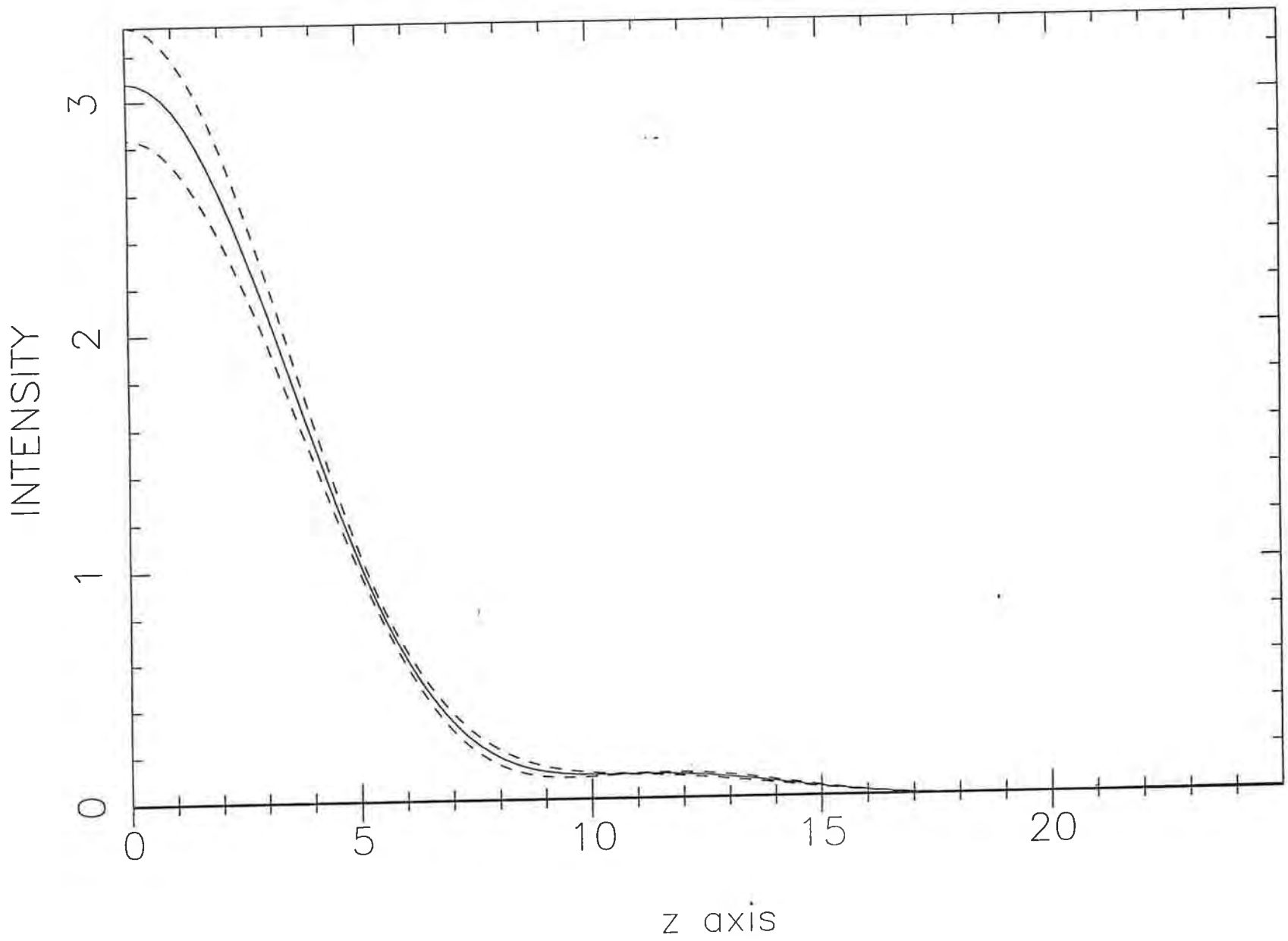
h2opar
INTENSITY
0
1
2
3
0
5
10
15
20
z axis

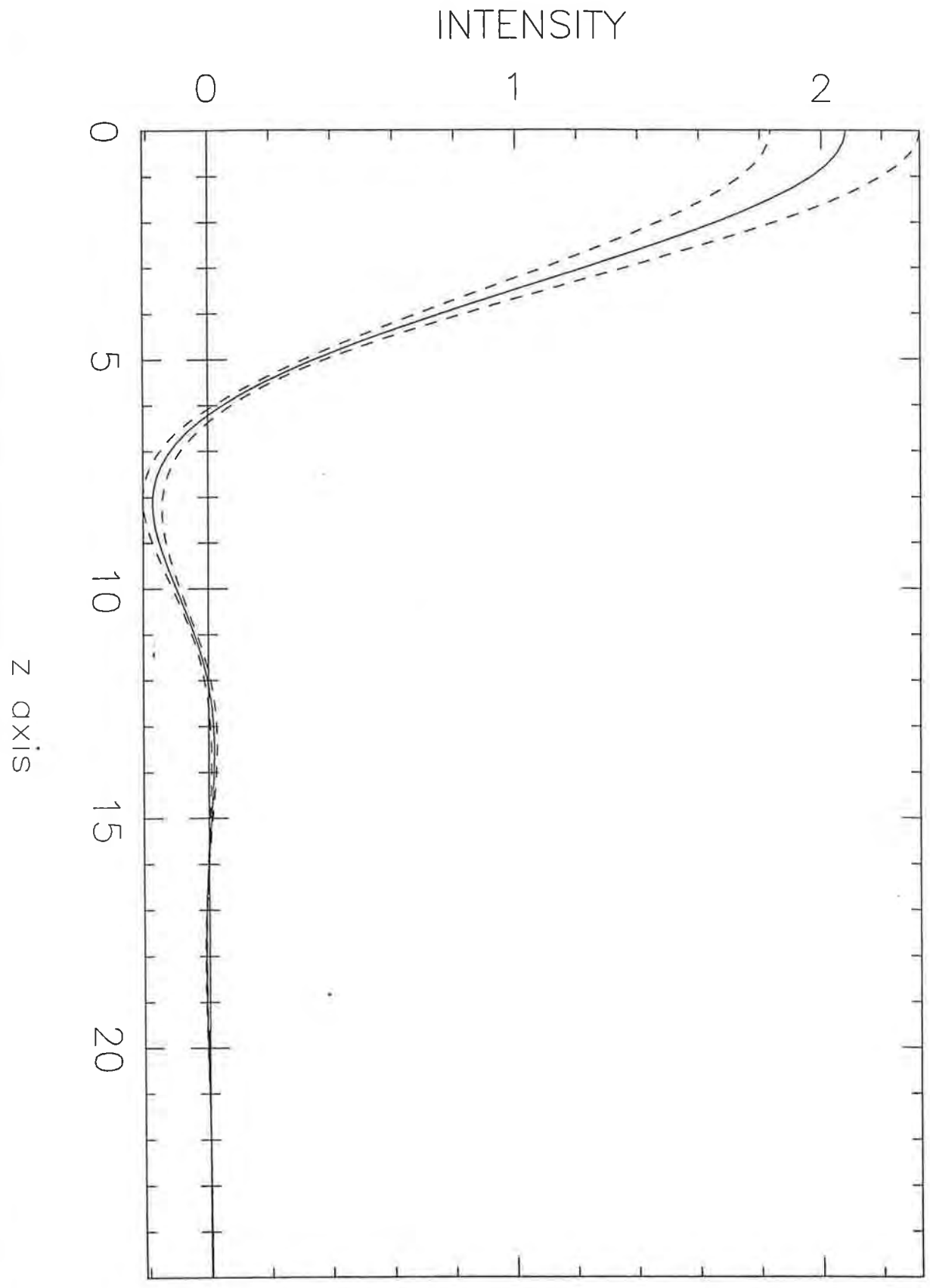
INTENSITY
0
1
2
0
5
10
15
20
z axis

$$\frac{1}{\sqrt{1+a}} e^{-\frac{Y^2}{1+a}} = \sum_{n=0}^{\infty} \frac{a^n}{n!} H_{2n}(Y) e^{-Y^2}$$

$$a = \sum_i \frac{\sigma_i^2}{\bar{\sigma}^2} (\cos^2 \alpha_i - 1/3)$$

$$\bar{\sigma}^2 = 1/3 \sum \sigma_i^2$$

$$\left\langle \frac{1}{\sqrt{1+a}} e^{-Y^2/1+a} \right\rangle = e^{-Y^2} \left(1 + \left\langle \frac{a^2}{2!} \right\rangle H_4(Y) + \left\langle \frac{a^3}{3!} \right\rangle H_6(Y) + \cdots \right)$$

$$\langle a^2 \rangle = \frac{4}{45} \left(\sum_i \frac{\sigma_i^4}{\bar{\sigma}^4} - \sum_{i \neq j} \frac{\sigma_i^2 \sigma_j^2}{\bar{\sigma}^4} \right)$$

IF $\sigma_x = \sigma_y \neq \sigma_z$

$$= \frac{4}{45} \frac{(\sigma_z^2 - \sigma_x^2)^2}{\bar{\sigma}^4}$$

Z axis